

# **Overcoming the Blue-Green gap: Engineering tools for cyanobacteria as photoautotrophic chassis organisms**

Inaugural-Dissertation

zur Erlangung des Doktorgrades  
der Mathematisch-Naturwissenschaftlichen Fakultät  
der Heinrich-Heine-Universität Düsseldorf

vorgelegt von

**Anna Behle**  
aus Herrenberg

Amsterdam, May 2022

aus dem Institut für Synthetische Mikrobiologie  
der Heinrich-Heine-Universität Düsseldorf

Gedruckt mit der Genehmigung der  
Mathematisch-Naturwissenschaftlichen Fakultät der  
Heinrich-Heine-Universität Düsseldorf

Berichtersteller:

1. Prof. Dr. Ilka M. Axmann  
Institut für Synthetische Mikrobiologie  
Heinrich-Heine-Universität Düsseldorf

2. Prof. Dr. Julia Frunzke  
Institut für Populationsheterogenität und Signaltransduktion  
Forschungszentrum Jülich

Tag der mündlichen Prüfung:

## Eidesstattliche Erklärung

Hiermit versichere ich an Eides statt, dass die eingereichte Dissertation selbständig und ohne unzulässige fremde Hilfe unter Beachtung der "Ordnung über die Grundsätze zur Sicherung guter wissenschaftlicher Praxis an der Heinrich-Heine-Universität Düsseldorf" verfasst worden ist. Weiter versichere ich andere als die in der Dissertation angegebene Literatur nicht benutzt zu haben und dass ich alle ganz oder annähernd übernommenen Textstellen sowie verwendete Grafiken, Tabellen und Auswertungsprogramme kenntlich gemacht habe. Außerdem versichere ich, dass die vorgelegte elektronische mit der schriftlichen Version der Dissertation übereinstimmt und die Abhandlung in dieser oder ähnlicher Form noch nicht anderweitig als Promotionsleistung vorgelegt und bewertet wurde.

## Declaration of academic honesty

I hereby declare an oath that the submitted dissertation has been written independently and without undue assistance, considering the "Rules and Principles for Safeguarding and Good Scientific Practice at HHU". Further, I assure that I did not use other references than the ones specified in the dissertation and that I have highlighted complete or partially adopted texts as well as graphics, tables, and analysis programs used in this work. Furthermore, I assure that the submitted electronic version is in accordance with the written version of the dissertation and that the dissertation in this or similar form has not yet been presented and evaluated as a doctoral thesis.

---

Amsterdam,

Anna Behle

# Table of Contents

<b>Abstract</b>	<b>1</b>
<b>Zusammenfassung</b>	<b>2</b>
<b>1 Introduction and Scientific Context</b>	<b>3</b>
1.1 Synthetic Biology in new chassis: The need for genetic tools	3
1.2 Cyanobacteria: A promising group of organisms	6
1.2.1 Promoters in cyanobacteria	8
1.3 Biotechnological interest in cyanobacteria	11
1.4 DNA topology and bacterial gene regulation	13
1.4.1 The role of DNA topology in the regulation of gene expression	13
1.4.2 Homeostatic control of DNA-supercoiling	15
1.5 Aim of this thesis	17
1.6 Key results	18
1.6.1 Analysis of established and newly designed promoters in a comparative manner	18
1.6.2 Successful application of multiple inducible promoters for titratable production of the sesquiterpenoid valencene	18
1.6.3 Unraveling DNA-supercoiling in a cyanobacterial chassis	19
<b>2 Manuscript I</b>	<b>20</b>
2.1 Author's contributions	20
2.2 Comparative dose-response analysis of inducible promoters in cyanobacteria	21
2.3 Supplementary Material	35
<b>3 Manuscript II</b>	<b>47</b>
3.1 Author's contributions	47
3.2 Metabolic engineering of <i>Synechocystis</i> sp. PCC 6803 for the photoproduction of the sesquiterpene valencene	48
3.3 Supplementary Material	57
<b>4 Manuscript III</b>	<b>63</b>
4.1 Author's contributions	63
4.2 Uncoupling of the Diurnal Growth Program by Artificial Genome Relaxation in <i>Synechocystis</i> sp. PCC 6803	64
4.3 Supplementary Material	88
<b>5 Conclusions and Future Perspectives</b>	<b>112</b>
<b>6 References from Chapters 1. and 5.</b>	<b>114</b>
<b>7 List of scientific contributions</b>	<b>122</b>
<b>8 Acknowledgements</b>	<b>123</b>

# Abstract

In a rapidly changing world, we are faced with new challenges to overcome every day. Currently, climate change, as well as the limited availability of finite resources is pushing industries towards the development of technologies that can make use of renewable energy sources. At the same time, the need to feed an ever-growing and -developing world is overshadowed by the limited availability of land suitable for our crops. Photoautotrophic organisms such as cyanobacteria offer promising qualities to mitigate some of these challenges. However, they are still lagging behind compared to heterotrophic model organisms, some of which have already been successfully applied in large scale in the biotechnological industry. To pave the way for innovative biotechnological applications involving cyanobacteria, as well as foundational research that can aid in research of photosynthetic organisms, more well-characterized and well-functioning genetic tools need to be developed and improved. In this work, new tools were established, and existing ones were improved. The three inducible promoters  $P_{rha}$ ,  $P_{vanCC}$ , and  $P_{L03}$  were characterized in terms of overall strength, dose-dependent response, orthogonality, and behavior over time. After assessing these tools for their robustness, two of them were further applied towards engineering the model cyanobacterium *Synechocystis* sp. PCC 6803 for the heterologous production of the plant sesquiterpene valencene. Use of inducible CRISPR interference enabled rewiring of a significant portion of the precursor pool from the carotenoids towards the desired product, yielding a production strain capable of producing 17.6 mg/L valencene. In a second project, the inducible promoters were used for targeted removal of global DNA-supercoiling by either downregulating gyrase or overexpressing topoisomerase I, enabling the extensive physiological and molecular characterization of a strain with reduced supercoiling capabilities over a period of ten days. This includes an RNA-Seq time-series with high temporal resolution. Reduction of supercoiling resulted in elevated glycogen and ATP levels for the *topA* overexpression, as well as blockage of cell division, which resulted in an increased cell volume. RNA-Seq analysis revealed functional clusters closely related to the circadian program, suggesting a cooperative role of DNA-supercoiling during the transition between darkness and light.

This work is an important contribution to the cyanobacterial research community. The identification and successful application of robust regulatory genetic tools will influence future work on these fascinating organisms and pave the way for a biotechnological revolution.

# Zusammenfassung

In einer sich schnell verändernden Welt sind wir fast täglich mit neuen Herausforderungen konfrontiert. Aktuell sind der Klimawandel, sowie die limitierte Verfügbarkeit von endlichen Rohstoffen, dafür verantwortlich, dass neue Technologien für die Nutzbarkeit von erneuerbaren Energien entwickelt werden. Gleichzeitig wird die Aufgabe, eine ständig wachsende und sich entwickelnde Welt zu ernähren, von der limitierten Nutzbarkeit unserer Agrarflächen für Nutzpflanzen überschattet. Photoautotrophe Organismen wie Cyanobakterien besitzen vielversprechende Qualitäten, die sich für die Lösung einiger dieser Herausforderungen eignen. Allerdings befinden sie sich, verglichen mit bereits im bioindustriellen Markt angewandten heterotrophen Modellorganismen, noch im Anfangsstadium. Damit der Weg hin zu innovativen biotechnologischen Anwendungen mit Cyanobakterien, sowie grundlegender Forschung, geebnet werden kann, müssen gut charakterisierte und vor allem funktionierende genetische Werkzeuge für Cyanobakterien weiterentwickelt und verbessert werden.

In dieser Arbeit wurden neue Werkzeuge etabliert, und bereits vorhandene wurden verbessert. Die drei induzierbaren Promotoren,  $P_{rha}$ ,  $P_{vanCC}$ , und  $P_{L03}$ , wurden im Hinblick auf ihre Stärke, Dosis-abhängige Antwort, Orthogonalität und Verhalten über die Zeit charakterisiert. Desweiteren wurden die zwei robusteren in einem Projekt zur Produktion des Sesquiterpens Valencen verwendet. Durch induzierbares CRISPRi konnte ein großer Teil der Vorläufermoleküle von den Carotinoiden zum gewollten Produkt gelenkt werden. Dies resultierte in einem Stamm, der in der Lage war 17.6 mg/L Valencen zu produzieren. In einem zweiten Projekt wurden die induzierbaren Promotoren eingesetzt, um gezielt globales DNA-Supercoiling zu entfernen, entweder durch die Herunterregulierung der Gyrase, oder der Überexpression der Topoisomerase I. Dies ermöglichte eine detaillierte Analyse auf molekularer und physiologischer Ebene, sowie eine RNA-Seq Analyse über einen Zeitraum von 10 Tagen, mit hoher zeitlicher Auflösung. Verringerung von Supercoiling resultierte in erhöhten Glykogen- und ATP Werten im Fall der *topA* Überexpression, sowie Blockierung der Zellteilung, was zu erhöhtem Zellvolumen führte. Mithilfe von RNA-Seq Analyse konnten diverse funktionelle cluster identifiziert werden, die im engen Zusammenhang mit dem zirkadianen Programm stehen, und eine kooperative Rolle von DNA-Supercoiling während des Übergangs von Dunkelheit ins Licht wird vermutet.

Diese Arbeit ist ein wertvoller Beitrag zum cyanobakteriellen Wissenschaftsverband. Die Identifizierung und erfolgreiche Anwendung robuster regulatorischer Werkzeuge wird einen nachhaltigen Einfluss auf zukünftige Arbeiten mit diesen faszinierenden Organismen haben und den Weg für eine neue biotechnologische Revolution ebnen.

# 1 Introduction and Scientific Context

## 1.1 Synthetic Biology in new chassis: The need for genetic tools

From the early beginnings of scientific discoveries in biology to the modern day, the field of biology has changed immensely, over and over again. Starting with Charles Darwin's "On the origin of species", to Gregor Mendel, whose work contributed to the first discoveries in genetics, to Louis Pasteur's works, which led to the formulation of germ theory - while these were major discoveries, they were not confirmed on a molecular level up until quite recently. Much more work had to be done to approach the point at which biology is today. Many of the scientific discoveries could not properly be explained until the discovery of DNA in the 1950's. During this time, the field transitioned from a more classical approach. Industrialization led to the discovery of the vast potential that biological processes, and more importantly, control thereof, held. Starting with industrialized fermentation, as well as progress in agriculture which led to the green revolution, the field of biology continuously developed towards more molecular and genetic tools. This resulted in large breakthroughs like recombinant DNA technology, Sanger sequencing, the invention of PCR, and *de novo* DNA synthesis. Towards the turn of the century, with the progress of the Human Genome Project, the era of synthetic biology started. Opposed to a more classical approach mostly on a trial-and-error basis, this field aimed to approach real world problems in a rational, computer-aided, standardized fashion.

One important characteristic of synthetic biology is its interdisciplinary and collaborative nature, with biologists, mathematicians, bioinformaticians, physicists, chemists and engineers working alongside one another. This has resulted in concept designs based on engineering principles, which are iterative and involve four different steps: 1.) Design, 2.) Build, 3.) Test, 4.) Learn/Iterate. Based on this engineering cycle, other interdisciplinary aspects of synthetic biology quickly become apparent. For example, during the design phase, mathematical modeling is often the basis for the design of more complex regulatory or metabolic networks. This may also be combined with computer-aided rational design, which involves extensive literature research and is extremely facilitated by an open science environment, such as the iGEM registry of standard biological parts<sup>1</sup>.

During the build phase, the availability of standardized and modular biological parts is extremely important. It not only ensures comparability within a project itself, but also facilitates collaborative efforts to build complex systems, as well as ensure reproducibility<sup>2</sup>. This is also an important aspect during the test phase, since biological systems highly depend on their abiotic environments, i.e., temperature, media composition, or pH, and one ultimate goal in synthetic biology is to develop systems that perform robustly despite changes in the environment, or, alternatively, to be able to predict and control fluctuating behavior. During the test phase, many new methods and techniques that were recently developed have led to more systematic approaches, for example NGS-based analyses, microfluidics, or large-scale screening platforms. While these types of systems are still expensive, they have largely influenced progress in the field and aided in quantitative data. As mentioned before, an open science environment can be of great value, because the data obtained from the test phase can then be integrated by working groups across the world and either used to build new circuits or fed back into the cycle to improve past projects.

By far the most work has been done in a select few model organisms such as *Escherichia coli* or *Saccharomyces cerevisiae*. This is mostly due to the fact that during the rise of molecular biology, these organisms were found to be extremely fast-growing, genetically tractable, and very well adapted to laboratory conditions. Especially in the case of *E. coli*, one of the main advantages was its fast doubling-time, making it an attractive host for molecular cloning and amplification of plasmids. Over time, this resulted in many engineered substrains suitable for various functions, such as cloning, protein production or biosensing. In addition, many of the regulatory systems used in molecular biology nowadays were actually discovered in *E. coli*, making it an obvious choice for further applications.

One of the first demonstrations of a synthetic biology approach in *E. coli* was published as early as 1999, when the so-called repressilator was introduced<sup>3</sup>. In this setup, a three-component circuit was designed, resulting in an oscillating output. This was closely followed by the first synthetic toggle switch<sup>4</sup>. In both cases, the basic function of a multiple-input genetic construct was investigated regarding mainly its output in the form of fluorescence signal, showing first proof-of-concept that a network with a desired output can be designed based on naturally existing biological parts.

Compared with these initial designs, research has progressed much further. One of the first major breakthroughs in terms of application was engineering the synthetic

production of artemisinin, an antimalarial drug, in *E. coli*. This involved a number of different alterations. First, the heterologous mevalonate pathway from yeast was introduced in *E. coli* to favor production of additional terpene precursors, followed by the introduction of further heterologous biosynthetic enzymes for the production of amorphadiene, the direct precursor of artemisinin. After initial trials, this was further optimized via rational selection of more efficient enzymes and finally, the entire process was optimized by changing the media composition as well as the cultivation technique.

Since moving towards this new biotechnological frontier, some limitations of model heterotrophs, and, more importantly, some advantages of alternative hosts, have become quite apparent. For example, *Vibrio natriegens* was recently modified towards an alternative cloning host<sup>5</sup>. Due to its extremely fast doubling time of only seven minutes under optimal conditions, it could be shown that a standard cloning procedure, starting with assembly of a plasmid in vitro, up until the recovery of the desired plasmid from a cell culture, could be done within 24 hours, accelerating and reducing the preliminary cloning work to a third compared with *E. coli*<sup>6,7</sup>.

Generally, the main reason why it is so challenging to adapt a synthetic biology approach to a new organism is because it requires extensive knowledge of said organism. This is not only limited to knowledge on the single gene basis, but also includes the metabolism, protocols for modification and analysis, growth media and conditions, or different regulatory systems that may play a role. Computer-aided metabolic modeling requires extensive knowledge of the metabolic network of the organism. Finally, even if all these requirements are fulfilled, genetic tools often do not translate well from one organism to another, even though an intuitive approach is to choose a well-functioning genetic part, such as an inducible promoter, from one model organism and transferring it to an unrelated new chassis.

One recent, sophisticated approach to this problem was to screen for many different small molecule sensors across a wide variety of species<sup>8</sup>, and to optimize these for the organism of interest, in this case, *E. coli*<sup>9</sup>. Initial measurements showed weak dose-dependent response, often associated with leaky expression. An additional problem was cross-reactivity between chemical inducers. In a highly iterative, biphasic directed evolution approach, promoter and regulator sequences were alternately screened for repression at uninduced conditions or addition of a non-specific chemical, and strong induction upon induction with specific inducer. This resulted in 12 highly

optimized and dose-responsive inducible promoters, tailor-made for *E. coli*. Again, an engineering approach of this extent required extensive knowledge of the organism, and the ability and tools to implement the aforementioned design concept. Ideally, this or a similar approach could also lead to similarly optimized inducible promoters in other species; unfortunately, in many cases, there are limitations stemming from sparse knowledge about their genetic systems. In many cases, broad host-range shuttle vectors are used, which require conjugative transfer via *E. coli*, with relatively low transfer efficiencies depending on the organism, while *E. coli* is easily transformable with very high efficiencies, e.g., by using electroporation. Another advantage of *E. coli* is that there are multiple compatible vector systems available, which can be used in parallel.

Next to the genetic requirements, there are other aspects when working with a new chassis that need to be considered, such as the optimal growth conditions. Many species cannot even be cultured under standard laboratory conditions, making it especially challenging to narrow it down towards the right conditions. Apart from that, there are many factors to consider, namely pH, temperature, mineral requirements, or carbon source, and in the case of photoautotrophs, light intensity.

As previously mentioned, after selecting and successfully cultivating an organism, genetic tractability is the first and most important prerequisite for any stable alteration. In some cases, genetically intractable organisms were successfully altered towards tractability, for example by incorporating parts from related organisms, leading to progress with some extremely fast-growing relatives from established hosts<sup>10,11</sup>.

Thus, the current approach for new chassis is a combination of rational design, computational prediction, and the use of native systems.

## 1.2 Cyanobacteria: A promising group of organisms

As the interest in photoautotrophic organisms has continuously grown lately, cyanobacterial research has gained more and more popularity. In terms of genetic tractability, many cyanobacteria are already naturally competent, and are able to incorporate foreign DNA into their genome via homologous recombination, as well as accept conjugative plasmids via conjugation. Genetic modification using CRISPR technology has also been successfully demonstrated in various cyanobacterial species. Since they are photoautotrophic organisms, they only require light and CO<sub>2</sub>

as energy and carbon sources, as opposed to heterotrophic organisms, which require an organic carbon source. As they are already significantly involved in global carbon fixation in the ocean<sup>12</sup>, their potential to contribute in today's challenges of reducing net carbon emissions has not gone unnoticed.

In contrast to land plants, cyanobacteria are able to grow under various conditions. Some species are especially tolerant to high salt, high pH, or high temperatures<sup>13,14</sup>. Additionally, they do not require the use of arable land, and therefore do not compete with crops. Due to their faster growth and easier cultivation along with their ancestral relationship to plants<sup>15</sup>, cyanobacteria are the obvious choice for biotechnological production of plant-derived compounds, which are costly to extract from plants and require the use of land otherwise usable for crops. Compared to eukaryotic microalgae, they have been shown to perform photosynthesis more efficiently<sup>16</sup>, and contain complex antenna proteins called phycobilisomes, enabling them to absorb a wider spectrum of light<sup>17</sup>. In contrast to plants, they make use of a unique carbon-concentrating strategy by using carboxysomes, intracellular microcompartments that enrich CO<sub>2</sub> around the major CO<sub>2</sub>-fixing enzyme Rubisco. All of these findings have had implications on using cyanobacteria as model organisms to improve photosynthesis<sup>18</sup>, as well as engineering plants to perform more efficiently by adapting cyanobacterial components<sup>19</sup>.

One of the major challenges, optimal culturing techniques for optimal usage of light and CO<sub>2</sub>, remains to be overcome.

Despite their vast potential, only a few select strains have been used more extensively so far. This is mostly due to the lack of availability of genetic tools, but also, due to the morphological difference between species, differences in genetic tractability. Nevertheless, some important groundwork has been laid.

The most comprehensively studied cyanobacterium to date is *Synechocystis* sp. PCC 6803, *Synechocystis* hereafter. First isolated in California in 1968<sup>20</sup>, the species has since been subdivided into multiple substrains with different phenotypes, such as glucose-tolerance along with the ability to grow heterotrophically, as well as phototactic motility. *Synechocystis* was the first phototrophic organism to be sequenced<sup>21</sup>, and the fourth in total<sup>22</sup>. Since then, it has served as a model organism for studying photosynthesis, nitrogen assimilation and metabolism, as well as extensive regulatory networks such as circadian rhythms. During the past 25 years, important distinctions between cyanobacteria and other model organisms have been

identified, i.e., a divergent RNA-Polymerase and, accordingly, regulatory components such as promoters and sigma factors<sup>23</sup>.

More recently, *Synechocystis*, and cyanobacteria in general, have been proposed as the new, “green *E. coli*”<sup>16,24</sup>. Indeed, many genetic tools have been developed or adapted for standardized use in *Synechocystis*, and have led to some impressive works in synthetic biology and metabolic engineering.

As mentioned, a common problem is the limited adaptability of genetic components between species. At the basis of genetic tools are the promoters, which have been extensively analyzed and engineered in *E. coli*. The current state-of-the-art for promoters in cyanobacteria will be summarized in the following chapter.

### 1.2.1 Promoters in cyanobacteria

As mentioned, promoters make up one of the most basic and fundamental type of building blocks, as they control the first step of the central dogma of biology, transcription of DNA to RNA. The textbook structure of a minimal prokaryotic promoter consists of a -10 and a -35 region, which are often highly conserved, since the sigma-factor of the RNA-Polymerase is recognized in this region. Depending on which sigma factor is recognized, the structural components and their distance can vary. For example, the alternative sigma factor  $\sigma^{54}$ , which plays an important role in the regulation of nitrogen fixation in some species, has conserved -12/-24 regions instead. The promoter ends with the transcription start site (TSS), which is often referred to as +1. A common characteristic of the core promoter sequence is that it is AT-rich. Next to the basic requirements of a promoter, it can also include regulatory elements. The most prominent example is the *lac*-operon from *E. coli*, which includes an operator site for the repressor *lacI*, which binds to the operator in the absence of lactose, and blocks transcription. In the presence of lactose, *lacI* undergoes a conformational change and frees the promoter for transcription initiation. Another common element is the upstream element, which can bind to regulatory proteins which may act as transcription enhancers or repressors.

The vast majority of research on promoters has been done in *E. coli*. In contrast, the work done in cyanobacterial species has mostly focused on native systems, such as metal-inducible promoters or promoters related to metabolism, such as nitrogen- or light-responsive promoters. One very prominent example is the nickel-inducible

promoter in *Synechocystis*, which was thoroughly investigated in terms of transcriptional response to Ni<sup>2+</sup> and Co<sup>2+</sup>, as well as metal toxicity. While the authors discussed its use in biotechnological applications and demonstrated production of ethanol as proof-of-concept, it remained quite clear that the application was limited, in part due to increased toxicity at relevant concentrations, but also due to general lack of orthogonality. In the same study, the Ni<sup>2+</sup>-inducible promoter was also compared to various other promoters native to *Synechocystis*, either other metal-inducible promoters with weak responses, or constitutive promoters with varying strength. Apart from this study, there have been only few comparative studies, making it difficult to choose between available constructs without additional assays.

In other studies, heterologous promoters were rationally designed for use in cyanobacteria, with the main focus being on sequence variations of a single construct. For example, *lacI*-regulated, IPTG-inducible promoters have been extensively investigated. In one study, effects of different spacer lengths between the -10 and -35 region were tested in *Synechocystis*<sup>25</sup>. Interestingly, within the range of promoter constructs showing any response, there was little variation between the different spacer sizes for *Synechocystis*, in contrast to *E. coli*, which showed much stronger variation.

In general, *lacI*-based systems have been reported to work well as inducible promoters in *Synechococcus* species, such as *Synechococcus elongatus* PCC 7942<sup>26</sup>, *Synechococcus* sp. PCC 7002<sup>27</sup>, or *Synechococcus* UTEX 2973<sup>10</sup>, and even filamentous species such as *Leptolyngbya* sp.<sup>28</sup>. In contrast, various attempts at establishing these systems in *Synechocystis* have been mostly unsuccessful. Another study focused on different placements of the operator region *lacO*, arguing that interaction between two *lacO*-bound *lacI* proteins promoted repression via DNA-loop formation. Despite extensive investigation and multiple different constructs, there was almost no discernible difference between uninduced and induced conditions. While the authors argued possible effects of intracellular *lacI* titers, they proposed that the main reason might be due to differences in RNA-polymerase architecture. It remains unclear why *lacI*-based systems work well in *Synechococcus* species, but not *Synechocystis*.

For *Synechocystis*, there was more success with *tetR*-based promoters. In 2013, a library of different synthetic anhydrotetracycline (aTc)-inducible promoters was constructed and analyzed<sup>29</sup>. By altering the base composition of the -10 region as well

as the downstream spacer, they were able to show an induction fold of up to 230, and tight repression in the absence of the inducer. Moreover, they were able to construct a variety of promoter strengths, ranging from native physiological strengths up to 2-fold stronger than the strongest observed native type I *Synechocystis* promoter. One limitation of this promoter system, unfortunately, is the light sensitivity of the inducer aTc, which led to a decrease in signal over time under standard light conditions. Nevertheless, this was an important first step for orthogonal inducible promoters in cyanobacteria, and has led to many follow-up works, including the application of these promoters in other cyanobacterial species<sup>30</sup> and the development of an extensive CRISPRi screening platform<sup>31</sup>.

Another group of promoters, based on the induction with arabinose or rhamnose, has been used as a protein production system in *E. coli* in a standardized fashion<sup>32</sup>. Both systems originated from *E. coli* and were based on the *araBAD* and *rhaBAD* operons, respectively. The physiological function is to sense and metabolize the respective sugar, and therefore underlies a number of feedback-regulatory levels, such as catabolite repression via glucose, or autoregulation of the regulatory proteins, AraC and RhaS. A major disadvantage in using these inducers in heterotrophs is that they are metabolized by the host. For this purpose, it is necessary to engineer specific strains incapable of metabolizing the inducer, which was done for example in the case of the *E. coli* strain DH10B. Nevertheless, the regulation of this system is extremely well-studied and provides yet another compatible genetic tool. In an effort to construct new optogenetic tools, *araC* was recently engineered to respond to light instead of arabinose, thereby creating a blue light-inducible expression system<sup>33</sup>.

In cyanobacteria, the *araBAD* and *rhaBAD* systems pose an attractive option, since they do not metabolize sugar as a primary carbon source. The *araBAD* system was successfully tested in both *S. elongatus*<sup>34</sup> and *Synechocystis* and even engineered towards increased sensitivity of arabinose, resulting in a construct capable of twice the maximum fluorescence output as the original *araBAD*<sup>35</sup>. The *rhaBAD* system was successfully demonstrated for *Synechocystis*, with tight repression in the absence of rhamnose, nice titratability, and a fold induction of up to 15x<sup>36</sup>. In both cases, there was neither evidence of changes in cellular growth, nor in loss of signal over time, further supporting the fact that the sugars are in fact not metabolized. Catabolite repression through glucose, which strongly affects regulation in hosts such as *E. coli*, was absent in cyanobacterial hosts. One drawback of the P<sub>BAD</sub> promoters is that for

full induction, they require quite a high concentration of the inducers, leading to similar high costs per volume of culture as IPTG and aTc<sup>37</sup>.

### 1.3 Biotechnological interest in cyanobacteria

The biotechnological use of living organisms for industrial fermentation, bioremediation, agricultural and medical use, as well as food production, has been continuously developing for decades. With more and more technology being developed for the genetic engineering of organisms, as well as fermentation technology for large-scale cultivation, the field is also expanding from established chassis organisms like *E. coli*, *Corynebacterium*, or *Saccharomyces* towards other promising chassis.

In recent years, there have been numerous academic publications discussing and developing cyanobacteria for the industrial production of various different compounds. The list of applications for which cyanobacteria have been successfully used on a small scale is long, and includes, but is not limited to, production of biofuels such as ethanol or 2,3 butanediol<sup>38–40</sup>, bioplastics such as PHB<sup>41,42</sup>, species used for bioremediation in crude oil degradation<sup>43</sup>, food additives<sup>44</sup>, production and secretion of sucrose<sup>45</sup> and fatty acids<sup>46</sup>, various organic acids<sup>47–49</sup>, natural products with bioactive properties<sup>50,51</sup>, terpenes/isoprene<sup>52–55</sup> and pigments<sup>56,57</sup>. While most of these small-scale approaches have yet to be applied to large-scale industrial biotechnology, they demonstrate the versatile nature of cyanobacterial hosts. In some cases, years of gradual improvement of strains using multiple different approaches has led to industrially relevant production titers<sup>58</sup>.

A general challenge in industrial biotechnology is the large-scale cultivation of the host organism, while maintaining productivity, viability and genetic stability<sup>59</sup>. One approach is the cultivation in open pond systems, however, this requires species capable of growing at high pH or in saline environments to prevent contamination<sup>60</sup>. Since cyanobacteria harness their energy from light, a major challenge to overcome is light limitation to maximize photosynthetic productivity, especially at higher cell densities, at which self-shading becomes an issue<sup>61</sup>. On the other hand, higher light intensities can lead to photoinhibition, which reduces overall productivity and damages the cell<sup>62</sup>. The development of large-scale bioreactors for the precise control of the optimal environmental conditions is therefore vital.

Along the same lines, the correct media composition is of importance to enable fast growth. In an exponentially growing culture, nitrogen and phosphorus quickly become limiting factors, and the sources need to be carefully selected for application and cost-effectiveness<sup>63,64</sup>.

Finally, a general challenge associated with industrial fermentation not only for cyanobacterial, but also heterotrophic hosts, is the recovery and purification of the product. Downstream processing of a product that needs to be extracted is extremely costly and often renders the bioproduction uneconomical. Unsurprisingly, a lot of research has focused on volatile compounds easily removable from the culture headspace<sup>65</sup>. Another approach is the secretion of the product in question to the media, which still necessitates recovery from the media, but eliminates the necessity of lysing the cells. Secretion of a product or intermediate also enables engineered co-cultures, with a heterotrophic production host included in the culture, which can use the secreted compound as a carbon source. Such a stable co-culture has already been demonstrated with various heterotrophic hosts using cyanobacteria capable of secreting sucrose<sup>66,67</sup>.

While the production of bulk chemicals might not be feasible in cyanobacteria just yet, high-value chemicals such as terpenoids have gained more attention recently. Terpenoids are derived from isoprene and are generally classified by how many isoprene-units they contain, as well as chemical groups they are decorated with. There are more than 50,000 substances that have been identified thus far<sup>68</sup>, and many of them have bioactive properties, making them attractive for the medical and pharmaceutical industry. In plants and animals, signaling molecules such as sterols and steroids are derived from the terpene biosynthesis pathway.

The terpenoids are subdivided in different groups, such as the monoterpenoids (C<sub>10</sub>), many of which are naturally volatile, can be found in essential oils and are responsible for taste and flavor<sup>69</sup>. Triterpenoids (C<sub>30</sub>) include compounds such as squalene, which is a precursor for steroids and plays an important role as a component in vaccines. Many triterpenoids have been shown to exhibit antiviral or antifungal properties<sup>68</sup>.

Finally, tetraterpenoids (C<sub>40</sub>) include carotenoids, which are present in plants as well in cyanobacteria. They play an important role in both light-harvesting and protection from high light stress<sup>70</sup>, and are generated through the MEP-pathway. For this reason, cyanobacteria offer especially suitable hosts in the biotechnological production of various types of terpenoids.

For cyanobacteria, there have been continuous efforts to engineer production hosts for various terpenoids. One strategy, which focuses on enhancing the titer of isoprene, the direct precursor for all terpenes, led to an increase of intracellular isoprene by 60-fold in *Synechocystis*<sup>71</sup>, and up to 1.26 g/L in *S. elongatus*<sup>72</sup>. Building on that, strains producing limonene<sup>73</sup>, bisabolene<sup>74</sup> or beta-phellandrene<sup>75</sup> have been successfully engineered, though only at relatively low yields of around 0.5-10 mg/L under standard shake flask conditions. Even under cultivation conditions with much higher culture densities, the productivity remained similar, although the final yield was much higher than under standard conditions, reaching up to 180 mg/L<sup>54</sup>. This, alongside some other publications focusing on media composition<sup>76</sup> and cultivation conditions<sup>77,78</sup>, suggests further possibilities of optimization apart from genetic modification.

## 1.4 DNA topology and bacterial gene regulation

### 1.4.1 The role of DNA topology in the regulation of gene expression

Many areas of bacterial gene regulation have been generally well-understood for quite a while. Transcription factor-based regulation of gene expression was investigated as early as the 1960's, yielding extensive knowledge of feedback-regulated resource allocation, the most prominent example of which, the *lac*-operon, was introduced in an earlier chapter. Systems like this are usually specialized for few genes, and quite specific in their regulatory role. Other linear gene regulatory mechanisms include transcriptional and translational control via small RNAs, which can be either cis-encoded at the same locus as their target or encoded in trans elsewhere in the genome. In the latter case, many examples have been demonstrated for *Synechocystis*, in which a single trans-encoded sRNA was able to regulate multiple downstream targets<sup>79,80</sup>.

Another example for a more global regulatory mechanism in *Synechocystis* is the circadian clock. In cyanobacteria, three core clock proteins, KaiA -B and -C, function together as an oscillatory protein complex, promoting phosphorylation or dephosphorylation of KaiC in a 24 h rhythm. Depending on the phosphorylation state of KaiC, downstream global transcriptional regulators are activated or repressed, resulting in a distinct, time-dependent transcriptional pattern. The regulation is directly based on the energy state of the cell<sup>81</sup>, resulting in distinct transcriptional and metabolic patterns depending on whether the cell is able to photosynthesize or not.

Finally, one of the most basic forms of regulation is encoded in the DNA structure itself. In addition to its natural helical conformation, the circular chromosome of growing bacteria is in an underwound state, which is referred to as negative supercoiling. This is necessary in order to package the DNA into the cell, as it would not be able to fit in a relaxed state. In eukaryotes, this process is facilitated by the nucleosomes.

Next to chromosome compaction, however, supercoiling of DNA is highly relevant to all metabolic processes involving it, such as DNA replication and transcription. Due to the torsional stress introduced by underwinding the DNA, melting of the double-stranded DNA in local areas where the DNA is especially underwound is facilitated. This is further dependent on the GC-content of the DNA – high GC content takes more energy to separate the DNA into single strands. Following that logic, GC-rich regions require more negative supercoiling for transcriptional bubble formation, while more relaxed DNA is sufficient for AT-rich regions. Structurally, over- or underwound DNA can undergo distinct conformational changes, resulting in toroidal or plectonemic structures<sup>82</sup>. Especially the formation of plectonemes can bring regions encoded at a large distance from each other in closer proximity. One example in which this has been demonstrated is the lac-operon in *E. coli*. Next to the core operator O1, there are two auxiliary operators, located upstream (O2) or downstream (O3) of the promoter, either of which can cooperatively bind a single lacI tetramer, thereby forming a DNA loop. Formation of this plectonemic structure was shown to increase repression of transcription by 50-fold<sup>83</sup>.

Formation of DNA-supercoils also occurs during transcription. Upon opening of the transcriptional bubble and subsequent progression of the RNA-polymerase, the upstream DNA is underwound, while the downstream DNA is overwound<sup>84,85</sup>. Highly expressed genes rely on the activity of topoisomerases to relieve supercoiling, which can otherwise lead to stalling of the polymerase, as well as R-loop formation. This process has been described in the literature as early as the 80's, and is referred to as the twin-domain model of supercoiling-dependent transcription<sup>86</sup>. It has been shown to have an impact especially at high rates of transcription, as this requires highly active topoisomerases. In bacteria, where multiple RNA-polymerases often transcribe a gene simultaneously, this can further facilitate speedy transcription, as one downstream positive supercoil can cancel out the next upstream negative supercoil. At the same time, as the promoter is repressed, i.e. through environmental stimuli, transcription

slows down due to the formation of supercoils which cannot be cancelled out anymore. This also has implications on genomic context in terms of positioning of genes and their arrangement, i.e. when two promoters are transcribed convergently or divergently, effectively doubling torsional stress.

The level of DNA-supercoiling is carefully regulated by an enzyme class called topoisomerases, which will be covered in detail in the following chapter.

#### 1.4.2 Homeostatic control of DNA-supercoiling

Regulation of DNA topology in bacteria is mediated by a protein family called topoisomerases. While type I topoisomerases are involved in relaxing negatively supercoiled DNA, Type II topoisomerases, also referred to as DNA gyrases, actively introduce negative supercoils by hydrolyzing ATP. These two main players involved in the global and local regulation of DNA supercoiling are themselves regulated intrinsically by the state of supercoiling; while the gyrase genes are preferentially expressed from relaxed DNA, topoisomerase I genes are expressed from negatively supercoiled DNA, leading to DNA topology homeostasis. Topoisomerase I activity is highly dependent on the state of DNA supercoiling, with the highest activity in the presence of highly negatively supercoiled DNA. In contrast, gyrase depends on the availability of ATP. Since this also reflects the energy state of the cell, negative supercoiling and actively growing cells are highly correlated. In fact, genes involved in growth and anabolic processes in general are preferentially expressed from negatively supercoiled DNA and are often GC-rich, while genes involved in catabolism (i.e., the production of ATP) are more often expressed from relaxed DNA and are often AT-rich. This has also been shown for cyanobacteria, albeit in a circadian oscillatory pattern, where the anabolic “growth” genes are expressed during the day, and the catabolic genes are expressed at night. Moreover, this circadian pattern of gene expression has been shown to correlate with DNA supercoiling in other works, with a more relaxed topological state during the night, and negative supercoiling during the day.

Disruption of this global regulatory mechanism has been attempted in *E. coli*. A comprehensive model of supercoiling homeostasis was developed by replacing the wild-type copy of *gyrA* in the genome with an IPTG-inducible operon-structured *gyrB/gyrA*, with subsequent deletion of the *gyrB* copy. This resulted in precise analysis of gyrase protein level dependent change in both superhelical status, as well as

ATP/ADP ratio. Interestingly, ATP/ADP ratio increased as a result of lower gyrase concentration in vivo, indicating reduced consumption of ATP in strains with reduced supercoiling. Simultaneously, the growth rate decreased with decreasing levels of gyrase. Homeostatic control was demonstrated by quantifying the *gyrB* promoter activity, which increased with decreasing intracellular gyrase.

Since then, this type of control has been shown in a wide variety of heterotrophic organisms, such as the pathogenic bacteria *M. tuberculosis*<sup>87</sup>, gram-positive species like *B. subtilis*<sup>88</sup>, and even species with high GC content such as *S. coelicolor*<sup>89</sup>. In contrast, direct manipulation of DNA-supercoiling in cyanobacteria has only been attempted via the gyrase-inhibitory antibiotic novobiocin, which acts on the ATPase domain of gyrase. An extensive study of the effect of different environmental stresses on *Synechocystis* in combination with disruption of supercoiling revealed that a significant portion of gene expression was affected by the superhelical status of the genome<sup>90</sup>. In *S. elongatus*, the model cyanobacterium for studies on the circadian clock, a direct link between oscillations in superhelicity and circadian gene expression output was shown, as well as significant decrease of the core clock protein KaiC after gyrase inhibition<sup>91</sup>.

It will be interesting to further dissect the many roles supercoiling might have in cyanobacteria, specifically the distinct regulatory aspects involving growth, light-response, nutrient availability, and the circadian clock.

## 1.5 Aim of this thesis

Cyanobacteria are becoming important players in current and future biotechnological applications, due to their excellent characteristics – great genetic tractability, robustness in diverse environments, fast growth and photoautotrophic CO<sub>2</sub> fixation. In an effort to bring cyanobacterial species more up to speed, there have been many toolboxes and studies published. While there are very standardized, well-working tools available for established chassis, there is still limited knowledge for cyanobacterial species, with many systems still relying on non-orthologous methods, such as metal-inducible promoters, which interfere with native systems. On top of that, gene regulation is distinct from chassis such as *E. coli*, requiring more extensive design and testing instead of simple plug-and-play.

With the intention to contribute to the numerous efforts of advancing *Synechocystis* sp. PCC 6803 as a chassis organism, this thesis focuses on chemically inducible genetic systems for controlled gene expression. Mainly, the following aspects are tackled:

- a) Identification, standardization and comparative testing of different inducible and constitutive promoters in *Synechocystis* – **Manuscript I**
- b) Application of inducible promoters for titrated gene expression of different native and heterologous components, and targeted conversion of carotenoid precursors towards the sesquiterpenoid valencene – **Manuscript II**
- c) Application of inducible promoters in basic research – targeted disruption of global DNA supercoiling and analysis of the transcriptional output over time – **Manuscript III**

## 1.6 Key results

### 1.6.1 Analysis of established and newly designed promoters in a comparative manner

Promoters, especially inducible ones, are key components for the engineering of genetic systems, but cyanobacteria were lacking well-characterized inducible promoters. Literature analysis revealed three promising inducible promoters, namely  $P_{\text{vanCC}}$ ,  $P_{\text{rha}}$  and  $P_{\text{L03}}$ , of which the latter two had already been validated in *Synechocystis* before. The three promoters and their respective regulatory transcription factors were optimized for *Synechocystis* and constructed in a comparative manner, alongside constitutive native and heterologous minimal promoters. Measurement of activity showed a wide range of promoter strength, with the inducible systems showing tight repression without inducer. Moreover, all three responded in a dose-dependent manner with increasing inducer. Their inducer specificity was confirmed, i.e., they only responded to their respective inducer, but not the others, rendering them orthogonal. Finally, their response in cultures of different cell densities was assessed, showing a reduced response at higher densities for  $P_{\text{vanCC}}$  and  $P_{\text{L03}}$ , but not for  $P_{\text{rha}}$ . Overall, these results contribute to a more extensive repertoire of tools for *Synechocystis* and pave the way for many further applications.

### 1.6.2 Successful application of multiple inducible promoters for titratable production of the sesquiterpenoid valencene

One of the applications made possible by inducible promoters is testing the limits of a system by exploring the effects of conditionally switching off essential genes. This work focused on developing an engineering strategy to boost the heterologous production of the plant sesquiterpene valencene, which is derived from the central precursor FPP, which, in cyanobacteria, is also further converted towards carotenoids. A number of strategies were combined to achieve this. First, markerless genomic deletions of the genes *shc* and *sqs* were introduced to remove undesirable downstream reactions. In addition to traditional heterologous expression of the biosynthetic gene required for valencene synthesis, CnVS, which were controlled from the strong rhamnose-inducible promoter, CRISPRi was successfully applied for downregulating *crtE*, the first gene in the carotenoid synthesis pathway. Since this

gene is also responsible for the stepwise elongation of the isoprenoid chain towards FPP, it was additionally substituted with the *E. coli* homolog *ispA*, which only performs the reaction up to FPP. By using the aTc-inducible promoter for CRISPRi and the rhamnose-inducible promoter for FPP and valencene biosynthesis, both strategies could be titrated and assessed independently in the same strain. CnVS and *ispA* were assessed both in an operon and as a fusion protein, the operon strategy yielding better results. While strains expressing only the valencene biosynthesis pathway already were able to accumulate a substantial amount of valencene, the combination of the two strategies resulted in more than 5-fold higher valencene yield, with a maximum of 17.6 mg/L in the best-producing strain.

### 1.6.3 Unraveling DNA-supercoiling in a cyanobacterial chassis

The second application of inducible promoters was demonstrated by using them for the manipulation of global supercoiling. Since the genes encoding gyrase, the key enzyme responsible for introducing negative supercoils, are essential and therefore cannot be inactivated, inducible CRISPRi was applied to downregulate gyrase A or B subunits (*gyrA* or *-B*), which resulted in loss of supercoiling. Additionally, topoisomerase I (*topA*) was overexpressed, which led to active removal of negative supercoils. The goal was to analyze the short- and long-term transcriptional response of *Synechocystis*, as well as phenotypical and metabolic changes associated with loss of supercoiling. While cell growth still proceeded, cell division was blocked, resulting in a cell volume about 4x compared to the wild type. Glycogen levels were increased by 4-fold, but only in *topA* overexpressing strains, while ATP levels were increased both in gyrase-knockdown and *topA* overexpressing strains.

The transcriptional response was investigated by an extensive 10-day RNA-Seq time series, with a high temporal resolution during the first 24 h. Data analysis revealed distinct clusters of supercoiling-activated and -repressed genes, either high in GC or AT-content, respectively. In addition, distinct coexpression clusters related to the diurnal light-dark rhythm could be identified, suggesting an important role of supercoiling in the diurnal transcription program.

Finally, we were able to confirm that homeostatic control of the key enzymes involved in supercoiling also applies to *Synechocystis*.

## 2 Manuscript I

### 2.1 Author's contributions

A. Behle, P. Saake, A. T. Germann, D. Dienst, and I. M. Axmann, "Comparative Dose–Response Analysis of Inducible Promoters in Cyanobacteria," *ACS Synth. Biol.*, vol. 9, no. 4, pp. 843–855, Apr. 2020, doi: 10.1021/acssynbio.9b00505

A.B. and I.M.A. designed and conceived the study. A.B. and P.S. performed the experiments and analyzed the data. ATG performed modeling of the data and wrote the corresponding methodology section (SI File 3). A.B. and D.D. wrote the manuscript with input from all authors. All authors read and approved the manuscript.

Study design: 80%

Experimental contribution: 50%

Data analysis: 50%

Manuscript preparation: 90%

## 2.2 Comparative dose-response analysis of inducible promoters in cyanobacteria

# Comparative Dose–Response Analysis of Inducible Promoters in Cyanobacteria

Anna Behle, Pia Saake, Anna T. Germann, Dennis Dienst, and Ilka M. Axmann\*

Cite This: *ACS Synth. Biol.* 2020, 9, 843–855

Read Online

ACCESS |

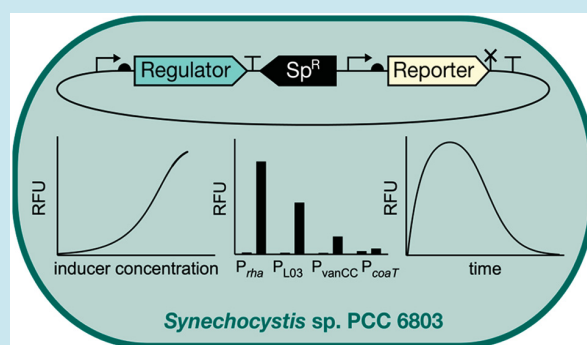
Metrics &amp; More

Article Recommendations

Supporting Information

**ABSTRACT:** Design and implementation of synthetic biological circuits highly depends on well-characterized, robust promoters with predictable input–output responses. While great progress has been made with heterotrophic model organisms such as *Escherichia coli*, the available variety of tunable promoter parts for phototrophic cyanobacteria is still limited. Commonly used synthetic and semisynthetic promoters show weak dynamic ranges or no regulation at all in cyanobacterial models. Well-controlled alternatives such as native metal-responsive promoters, however, pose the problems of inducer toxicity and lacking orthogonality. Here, we present the comparative assessment of dose–response functions of four different inducible promoter systems in the model cyanobacterium *Synechocystis* sp. PCC 6803. Using the novel bimodular reporter plasmid pSHDY, dose–response dynamics of the re-established vanillate-inducible promoter  $P_{\text{vanCC}}$  was compared to the previously described rhamnose-inducible  $P_{\text{rha}}$ , the anhydrotetracycline-inducible  $P_{\text{L03}}$ , and the  $\text{Co}^{2+}$ -inducible  $P_{\text{coaT}}$ . We estimate individual advantages and disadvantages regarding dynamic range and strength of each promoter, also in comparison with well-established constitutive systems. We observed a delicate balance between transcription factor toxicity and sufficient expression to obtain a dose-dependent response to the inducer. In summary, we expand the current understanding and employability of inducible promoters in cyanobacteria, facilitating the scalability and robustness of synthetic regulatory network designs and of complex metabolic pathway engineering strategies.

**KEYWORDS:** *Synechocystis*, inducible promoter, vanillate, synthetic biology, cyanobacteria, pSHDY



Cyanobacteria are versatile photoautotrophic organisms that are becoming more and more interesting for various research applications. Due to their ability to fix carbon photosynthetically, they are promising candidates for the biotechnological production of various compounds, including biofuels<sup>1</sup> and more complex, industrially relevant chemicals.<sup>2</sup> Their ancestral relation to today's plant chloroplasts makes them important model organisms in the field of basic and applied photosynthesis research.<sup>3</sup> Many cyanobacteria are naturally competent and possess the ability to incorporate free DNA into their genomes as well as receive and replicate conjugative plasmids, making them attractive from a genetic engineering perspective.<sup>4</sup>

In recent years, an increasing number of genetic and synthetic tools, including promoters and ribosomal binding sites, have been developed and characterized for diverse cyanobacterial species.<sup>5</sup> This includes well-studied model organisms such as *Synechocystis* sp. PCC 6803<sup>6</sup> (referred to as *Synechocystis* hereafter), *Synechococcus elongatus* PCC 7942<sup>7,8</sup> (referred to as *S. elongatus* hereafter), and *Anabaena* sp. PCC 7120,<sup>9</sup> as well as fast-growing strains like *Synechococcus* sp. PCC 7002<sup>10</sup> and the more recently discovered *Synechococcus elongatus* UTEX 2973.<sup>11</sup> Particularly for *Synechocystis*, a set of

native metal-responsive promoters has been previously established and evaluated in a comparative fashion.<sup>12,13</sup> While metal-responsive promoters facilitate robust induction of gene expression with suitable dynamic ranges, they are not orthogonal, and toxicity of excessive inducer concentrations may compromise cell physiology. Alternatively, a number of synthetic, non-native promoters previously established in *Escherichia coli* are currently available. One challenging aspect when applying non-native promoters is the difference in RNA polymerase architecture, which results in different binding affinities and overall responses to promoter and operator regions.<sup>14</sup> Nevertheless, a range of synthetic promoters, both constitutive<sup>6,11</sup> and inducible,<sup>12</sup> has been engineered and successfully implemented in *Synechocystis*. These publications tend to either focus on a single promoter construct with

Received: December 11, 2019

Published: March 5, 2020



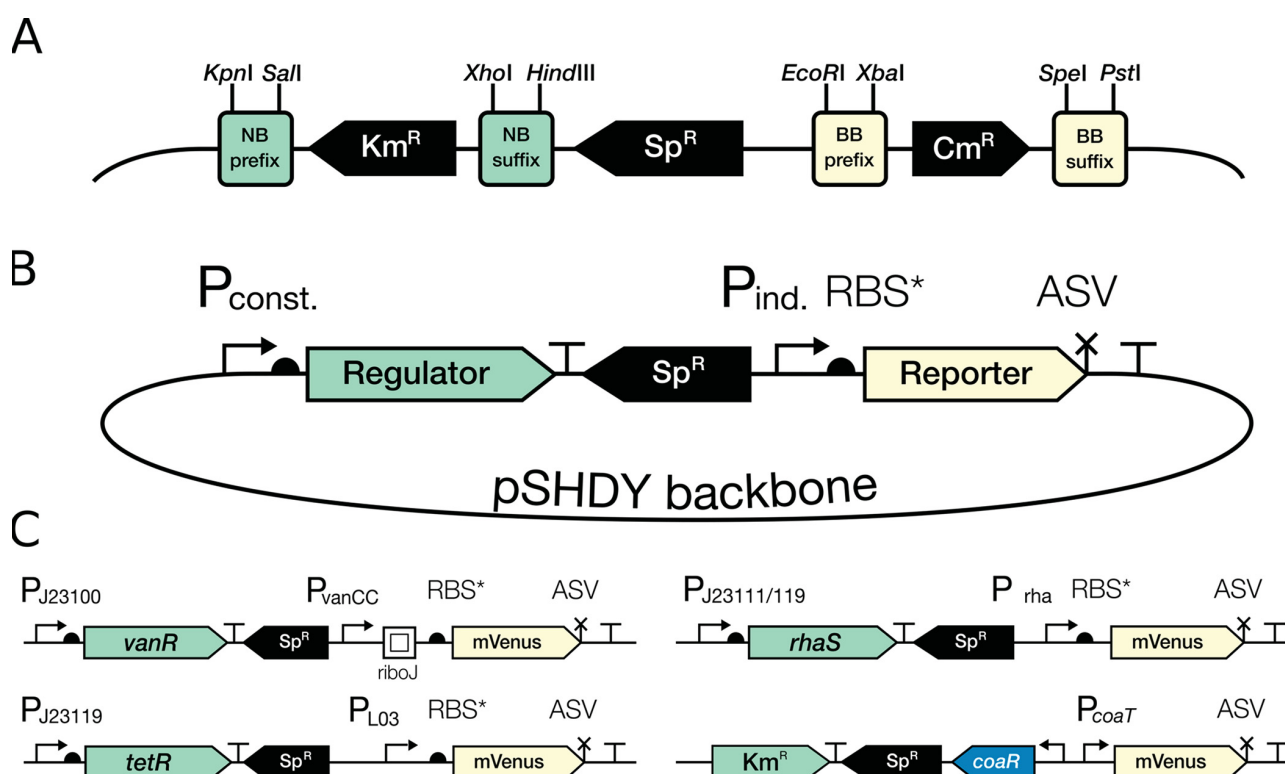


**Figure 1.** Genetic composition of the different promoter and sensor constructs measured in this work. A: Detailed overview of the two modular cloning sites, the NeoBrick (NB) shown in green and the BioBrick (BB) sites shown in yellow. B: Overview of the plasmid composition of reporter constructs used in this work.  $P_{const}$ : Constitutive promoter.  $Sp^R$ : Spectinomycin resistance.  $P_{ind}$ : inducible promoter. ASV: *ssrA*-based ASV-degradation tag. C: Overview of genetic composition of the four inducible promoter constructs tested in this work. Upper left:  $P_{vanCC}$ ; Upper right:  $P_{rha}$ ; Lower left:  $P_{L03}$ ; Lower right:  $P_{coaT}$ .

detailed work on sequence variations or have a different core angle such as metabolic engineering.

For the purpose of engineering more extensive synthetic regulatory networks, the availability of multiple differentially regulated promoters or regulatory building blocks is essential; for comparability, they should be characterized in a way that one can easily choose from depending on the application. In order to efficiently fine-tune and optimize more complex systems which combine transcriptional and translational output, fundamental evaluation of precise expression dynamics and strength in the context of a range of constitutive promoters is highly desirable.

One of the most standard inducible promoter systems, which is based on the *lac*-operon from *E. coli* and is inducible by the lactose analog IPTG, has been tested and implemented in some cyanobacterial species. The  $P_{trc}$  promoter, for example, performs well in *S. elongatus* and is commonly used in many applications.<sup>15</sup> However, efforts to implement similar constructs in *Synechocystis* have mostly failed, resulting in either extremely leaky expression under noninduced conditions or little to no regulation at all.<sup>16</sup> For example, Camsund et al. investigated sequence-specific repression patterns in *Synechocystis*.<sup>17</sup> They reported a 2.3-fold induction ratio for the original  $P_{trc}$  promoter, arguing that this was likely due to insufficient cellular levels of the repressor protein LacI, pointing at presumably higher expression levels of the *lacI* gene in *S. elongatus*. Albers et al. investigated different IPTG-inducible constructs by modification of the gap between the sigma factor binding sites.<sup>18</sup> They placed *lacI* under the control

of  $P_{sigA}$ , which promotes expression of the housekeeping sigma factor *sigA* and therefore assures stable, strong expression of the repressor. For their promoter construct  $P_{sca6-2}$ , they were able to show approximately 10-fold induction ratios.

Another well-characterized promoter in *Synechocystis* is the aTc (anhydrotetracycline)-inducible, *tetR*-regulated system. Huang et al. constructed a library by altering the region downstream of the  $-10$  promoter region.<sup>19</sup> They reported induction ratios of up to 239 for their best performing promoter,  $P_{L03}$ , under LAHG (light-activated heterotrophic growth) conditions. This promoter suite was also successfully implemented by Yao et al. for dCas9-mediated gene repression, although they reported better results with the weaker, more tightly repressed  $P_{L22}$  due to leaky expression of dCas9 from  $P_{L03}$ .<sup>20</sup> A general issue with aTc is the fact that it is light-degradable, making its activity difficult to predict under photoautotrophic growth conditions, particularly when stable and sustained induction is desired.

A third system, which was established for *Synechocystis* by Kelly et al. is the L-rhamnose-inducible promoter  $P_{rha}$  which is regulated by the transcriptional activator *rhaS*.<sup>21</sup> This promoter was thoroughly investigated under different light and nutrient conditions, demonstrating tight repression under noninduced conditions, with a linear response upon induction and a good dynamic range. In addition, L-rhamnose is nontoxic to and nonmetabolizable by the cells. To date, this is the most robust promoter system in *Synechocystis* in terms of orthogonality, performance, and inducer characteristics.

Table 1. Overview of Promoter Constructs Tested in This Work<sup>a</sup>

Name	Full genotype of construct	Addgene ID	inducer	regulator	5'UTR	Source of promoter
EVC (pSHDY)	NB_Km <sup>R</sup> _NB BB_Cm <sup>R</sup> _BB	137661	-	-	-	This work
P <sub>vanCC</sub>	NB_P <sub>J23100</sub> :vanR_NB BB_P <sub>vanCC</sub> :riboJ- RBS*:mVenus_BB	137664	vanillic acid	VanR	riboJ + RBS*	<sup>27</sup>
P <sub>rha</sub> (111)	NB_P <sub>J23111</sub> :rhaS_NB	-	L-rhamnose	RhaS	RBS*	<sup>21</sup>
P <sub>rha</sub> (119)	NB_P <sub>J23119</sub> :rhaS_NB BB_P <sub>rha</sub> :RBS*:mVenus_BB	137662	-	(Arg218Leu)	-	-
P <sub>L03</sub> (tetR-mut5)	NB_P <sub>J23119</sub> -mut5:rhaS_NB	137663	aTc	TetR	RBS*	<sup>19</sup>
P <sub>L03</sub> (tetR-mut8)	NB_P <sub>J23119</sub> -mut8:rhaS_NB BB_P <sub>L03</sub> :RBS*:mVenus_BB	-	-	-	-	-
P <sub>coaT</sub>	BB_ <sub>coaR</sub> :P <sub>coaT</sub> :mVenus_BB	-	CoCl <sub>2</sub>	CoaR	native	<i>Synechocystis</i>
P <sub>mpB</sub>	BB_P <sub>mpB</sub> :RBS*:mVenus_BB	-	-	-	RBS*	<i>Synechocystis</i>
P <sub>cpc560</sub>	BB_P <sub>cpc560</sub> :mVenus_BB	-	-	-	native	<i>Synechocystis</i> <sup>33</sup>
P <sub>J23119</sub>	BB_P <sub>J23119</sub> :RBS*:mVenus_BB	-	-	-	RBS*	BioBrick
P <sub>J23100</sub>	BB_P <sub>J23100</sub> :RBS*:mVenus_BB	-	-	-	RBS*	BioBrick
P <sub>rbcL</sub>	BB_P <sub>rbcL</sub> :RBS*:mVenus_BB	-	-	-	131 bp native +RBS*	<i>Synechocystis</i>

<sup>a</sup>Inducible promoters are shown above, and constitutive promoters below the double line.

A general issue when selecting promoters for different applications is the data reproducibility. Depending on factors like the choice of measurement methods, (reporter) genes, RBS/5'UTR<sup>22</sup> or growth conditions, effects on mRNA stability, fold activation, or promoter strength may strongly differ between laboratories and publications.<sup>23–25</sup> While each lab should replicate measurements under their own conditions to ensure reproducibility, an evaluation of constructs in a side-by-side manner using comparable genetic elements and culturing conditions can be helpful in choosing a suitable promoter to begin with.

In contrast to cyanobacteria, there has been ongoing, successful work published for more accessible model organisms such as *E. coli*. For example, Ruegg et al. reported the optimization of a promoter system in *E. coli*, previously identified in *Enterobacter lignolyticus*,<sup>26</sup> which responds to a variety of cationic dyes at very low, nontoxic concentrations, including the cheap inducer compound crystal violet, for which they report a dynamic range of 4 orders of magnitude.

A recent publication introducing the *E. coli* "Marionette" strains focused on optimization of selected parameters using a two-phase directed evolution approach:<sup>27</sup> (i) binding of the transcription factor to the operator, (ii) full repression under noninduced conditions, and (iii) elimination of cross-talk.<sup>27</sup> The positive selection process involving expression of DNA polymerase was combined with a negative selection involving the toxic expression of a mutant aminoacyl tRNA-synthetase. This yielded 12 highly optimized promoter/sensor pairs, including a vanillate-inducible system originating from *Caulobacter crescentus*.

In this work, we constructed and investigated a comparative library of different inducible promoters by adapting and evaluating them using the same genetic architecture in the bimodular plasmid pSHDY, which was designed for this work. Alongside established aTc, L-rhamnose-, and Co<sup>2+</sup>-inducible

systems, we also present the newly tested vanillate-inducible promoter system.

Finally, we estimated individual promoter performance in a controlled setting for various downstream applications.

## RESULTS AND DISCUSSION

**Design Framework of All Promoter Constructs Tested in *Synechocystis*.** In order to assay each promoter while ensuring comparability/reproducibility, a suitable reporter system was required. We considered a vector with two spatially separated cloning sites, in which the reporter construct comprising promoter, RBS, and reporter CDS could be located distantly from the repressor/activator and could easily be switched out. For this reason, we constructed pSHDY, a conjugative shuttle vector based on pVZ321,<sup>28</sup> but much more suitable for cloning due to multiple restriction sites flanking the antibiotic resistance cassettes (Figure S4A). In addition, pSHDY also contains the mobAY25F point mutation investigated by Taton et al., which leads to an increase in supercoiled plasmid and therefore more efficient downstream cloning applications such as restriction digest.<sup>29</sup>

The basic pSHDY cloning vector contains a total of three antibiotic resistance cassettes, chloramphenicol and kanamycin, which are flanked by two independent cloning sites termed the BioBrick and the NeoBrick site, respectively, and a spectinomycin resistance separating the two (Figure 1A). For the purpose of comparability, we cloned each promoter/reporter construct into the BioBrick site, while keeping the corresponding repressor constructs in the NeoBrick site (Figure 1B,C).

The promoter/reporter devices were constructed in a comparable manner. For the reporter, we chose mVenus, an eYFP variant with enhanced brightness.<sup>30</sup> The CDS was codon-optimized for *Synechocystis*, and an *ssrA*-based ASV degradation tag for moderate protein turnover<sup>31</sup> was added to the C-terminus to minimize effects from stable protein

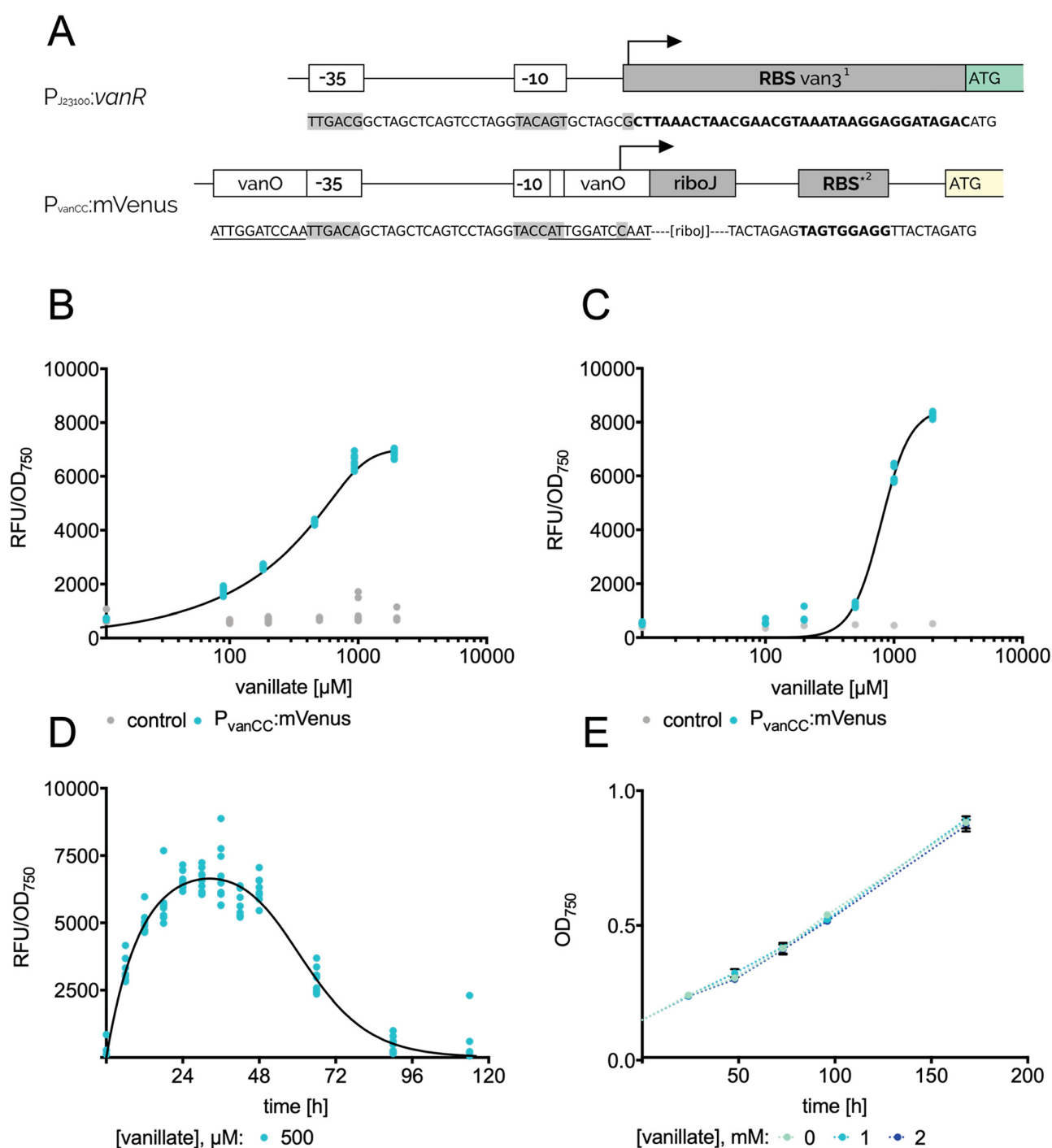


**Figure 2.** Dose-dependent response of the vanillate-inducible promoter in *Synechocystis*. **A:** Schematic overview of genetic construct used. Top: Genetic composition of regulator expression cassette. Bottom: Genetic composition of regulated promoter. Promoter regions  $-10$ ,  $-35$ , and TSS + 1 are highlighted in gray; RBS is shown in bold. Operator regions are underlined. <sup>1</sup> $van3$  RBS; <sup>2</sup>RBS\*. **B:** Dose-response of the vanillate-inducible promoter  $P_{vanCC}$  to different concentrations of vanillate after 24 h. The x-axis is shown in logarithmic scale ( $\log_{10}$ ). A control (empty vector only) is shown in gray. **C:** Dose-response of the vanillate-inducible promoter  $P_{vanCC}$  to different concentrations of vanillate after 48 h. The x-axis is shown in logarithmic scale ( $\log_{10}$ ). A control (empty vector only) is shown in gray. **D:** Response of  $P_{vanCC}:mVenus$  to 500  $\mu$ M vanillate over time. **E:** Growth of WT *Synechocystis* in different vanillate concentrations.

accumulation that might interfere with the inducer-dependent expression readout. As 5'UTR, we used the established synthetic RBS\*,<sup>32</sup> which was shown to perform well in *Synechocystis* on multiple occasions, except in the native promoter constructs,  $P_{coaT}$ , as well as  $P_{cpc560}$ , which has been

reported to require its native RBS for maximum strength.<sup>11</sup> In the case of  $P_{vanCC}$ , the RiboJ insulator was added to the 5'UTR as was constructed in the original publication.<sup>27</sup>

Table 1 contains a basic description of all promoters tested in this work, while detailed descriptions and sequences of each

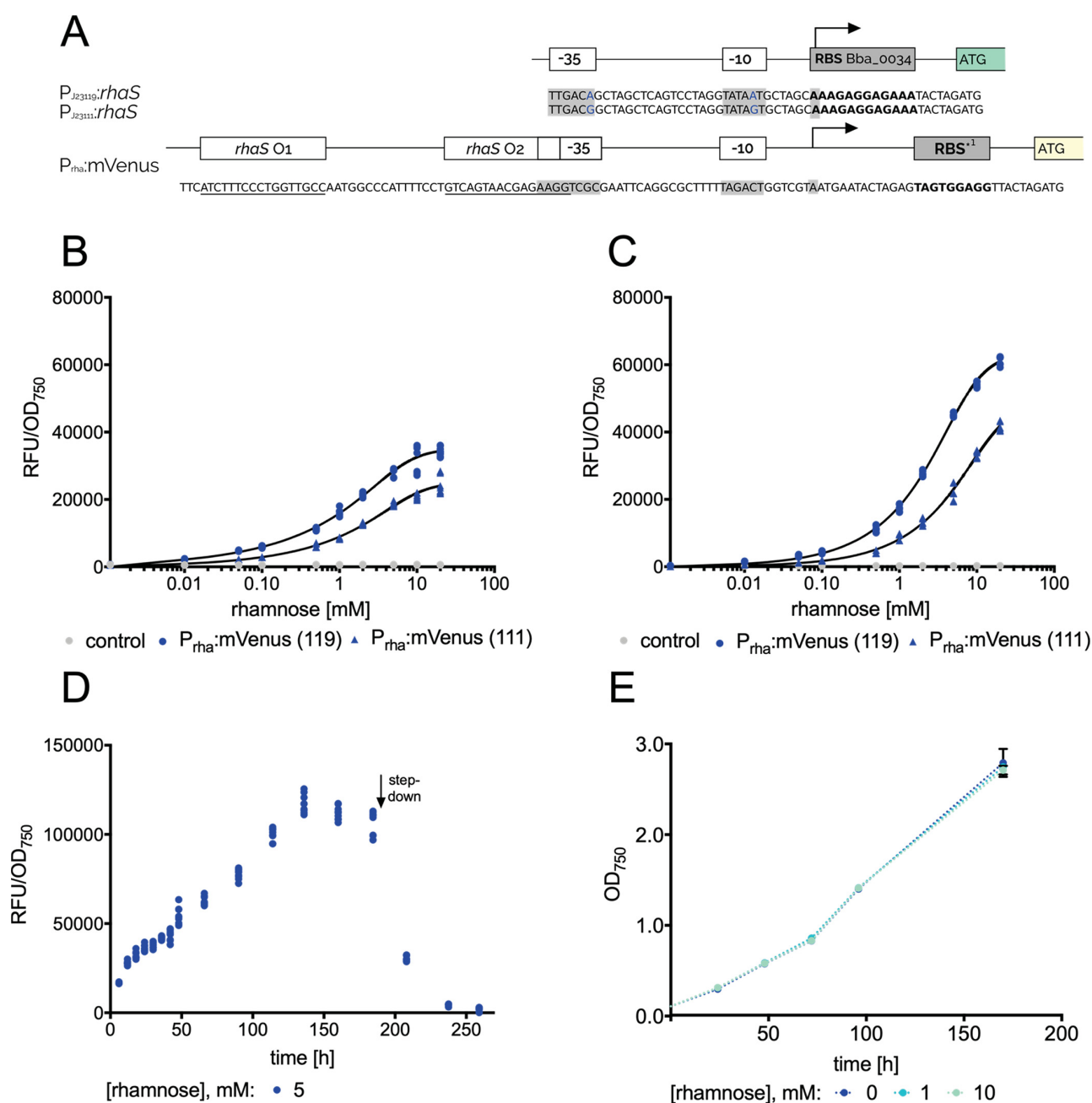


**Figure 3.** Dose-dependent response of the rhamnose-inducible promoter  $P_{rha}$  in *Synechocystis*. **A:** Schematic overview of genetic constructs used. Top: Genetic composition of regulator. Bottom: Genetic composition of regulated promoter.  $-10$ ,  $-35$ , and  $+1$  are highlighted in gray; RBS is shown in bold. Operator regions are underlined.  $^1$ RBS\* from ref 32. **B:** Dose-response of the rhamnose-inducible promoter  $P_{rha}$  to different concentrations of L-rhamnose after 24 h. The x-axis is shown logarithmic ( $\log_{10}$ ). A control (empty vector only) is shown in gray. **C:** Dose-response of the rhamnose-inducible promoter  $P_{rha}$  to different concentrations of L-rhamnose after 72 h. The x-axis is shown logarithmic ( $\log_{10}$ ). A control (empty vector only) is shown in gray. **D:** Response of  $P_{rha}::mVenus(119)$  to 5 mM rhamnose over time. OD<sub>750</sub> of each sample was adjusted to 0.25 prior to fluorescence measurement. **E:** Growth of WT *Synechocystis* in different rhamnose concentrations. Three biological replicates were cultured in BG11 + inducer and fluorescence and OD<sub>750</sub> was monitored in a microplate reader in three technical replicates each. The dose-response data was fitted to the modeled function eq 2 (SI File 3). The time course data could not be fitted, due to the step-down.

promoter construct can be found in the Supporting Information (Table S1).

**Introducing the Vanillate-Inducible Promoter  $P_{vanCC}$  in *Synechocystis*.** While there have been publications on vanillate inducible systems, mainly in  $\alpha$ -proteobacteria,<sup>34</sup> but also in *E. coli*,<sup>27</sup> to the best of our knowledge, this is the first

detailed, dose-dependent vanillate-responsive promoter study in *Synechocystis*. One publication focusing on its applicability for implementing logic circuits in *S. elongatus* PCC 7942 used the promoter/repressor pair  $vanR/P_{vanA}$  from *Corynebacter glutamicum*.<sup>35</sup> There, the regulation of the promoter-sensor pair was successfully implemented independently of the

inducer vanillate. However, vanillate-dependent induction was not further investigated.

We ultimately chose to evaluate the *vanR*/ $P_{\text{vanCC}}$  system from the recent publication by Meyer et al.<sup>27</sup> in *Synechocystis*. The authors rationally designed the promoter/repressor pair *vanR*/ $P_{\text{vanCC}}$  from *Caulobacter crescentus* and then further optimized it via directed evolution for *E. coli*. This approach resulted in a vanillate sensor with both improved dynamic range as well as lower cross-reactivity.

We chose the weak constitutive promoter  $P_{J23100}$  from the Anderson library (Registry of standard biological parts, iGEM) and the published *van3* RBS to control *vanR*, shown schematically in Figure 2A. The *van3-vanR* fusion was amplified from sAJM.1504, the Marionette-Clo strain (addgene ID 108251). For  $P_{\text{vanCC}}$ , we amplified the original promoter construct, including the RiboJ insulator in the 5'UTR, from pAJM.714 (addgene ID 108515), but replaced the RBS with the synthetic RBS\*. Detailed descriptions and sequences are provided in the Supporting Information (Table S1).

The conjugative plasmid containing  $P_{J23100}::\textit{vanR}$  and  $P_{\text{vanCC}}::\textit{mVenus}$  (Figure S4B) was transferred to *Synechocystis* via conjugation. Transconjugants were validated, cultured, and induced, and *mVenus* fluorescence, as well as the optical density at 750 nm, was monitored. An empty vector control was included for each concentration.

We observed a linear dose–response to vanillate 24 h post-induction, which saturated at 1 mM (Figure 2B). Furthermore, under noninduced conditions, the promoter remained tightly repressed, reaching the same autofluorescence levels observed in the control.

Three biological replicates were cultured in BG11 + vanillate and fluorescence and  $OD_{750}$  was monitored (three technical replicates each). The dose–response data as well as the time course data was fitted to the modeled function eq 2 and eq 6, respectively (SI File 3).

After 48 h, a decrease in fluorescence to 30% of that after 24 h could be observed at lower concentrations (100–500  $\mu\text{M}$ ), while fluorescence increased or remained at a similar level at saturating concentrations of 1–2 mM (Figure 2C). While there is no evidence of light-mediated degradation of vanillate, it is an intermediate in the biochemical degradation of lignin,<sup>36</sup> so we hypothesized that vanillate might be degraded or otherwise converted by *Synechocystis* after longer periods of time by an unknown mechanism. We therefore investigated vanillate-induced *mVenus* fluorescence in a higher time resolution and over an extended period. To minimize possible inducer degradation, we chose a vanillate concentration of 500  $\mu\text{M}$ , which was below saturation of expression and at which concentration a temporal decrease of the fluorescence readout was observed (Figure 2B,C).

After induction, cultures were measured every 6 h. To account for cell density-related effects, an aliquot of each culture was sampled and cell density was adjusted to the start  $OD_{750}$  of 0.25 prior to each measurement.

$P_{\text{vanCC}}$  rapidly responded to vanillate induction, reaching a fluorescence maximum after approximately 24 h. This level was maintained until 48 h post-induction, after which fluorescence gradually decreased in a linear fashion, reaching autofluorescence levels after 90 h in total (Figure 2D).

Since the signal resulting from vanillate induction appears to be completely lost in *Synechocystis* after 90 h, we chose to investigate whether it had any effect on its growth. Wild-type

cultures of *Synechocystis* were treated with different concentrations of vanillate, and  $OD_{750}$  was monitored over 7 days (Figure 2E). Interestingly, vanillate had no positive or negative influence on the growth of *Synechocystis*. However, a change in the characteristic absorption spectrum of vanillate could be observed after 24–48 h when added to *Synechocystis* cultures (Figure S5). While vanillate does not seem to contribute significantly to growth, it remains to be investigated whether it is in fact utilized within the *Synechocystis* metabolism, or converted nonspecifically, e.g., by promiscuous enzymes.

Overall,  $P_{\text{vanCC}}$  performs well in *Synechocystis* in a dose-dependent manner, showing no toxicity, tight repression, and wide dynamic range, with a maximum fold induction of 16 $\times$  (2 mM vanillate, 48 h post-induction).

**The Strong Rhamnose-Inducible Promoter  $P_{\text{rha}}$  Can Be Fine-Tuned via Activator Expression.** While the temporal induction pattern shown for  $P_{\text{vanCC}}$  can be positive for certain applications, it can also be a drawback if long-term expression is desired.

Since the  $P_{\text{rha}}$  promoter published by Kelly et al.<sup>21</sup> exhibited very promising characteristics regarding its dynamic range and stability over time, we aimed to reproduce the data under our lab conditions. In accordance with our design framework, which allows for modular exchange of genetic parts, we chose to investigate whether L-rhamnose response could be further tuned by fusing two different minimal constitutive promoters upstream of the activator gene *rhaS*.  $P_{J23119}$ , containing the *E. coli* consensus core elements and reportedly the strongest of the Anderson promoter library, and  $P_{J23111}$ , which was shown to be approximately half as strong as  $P_{J23119}$  in *Synechocystis*,<sup>11</sup> were used (Figure 3A). Plasmids containing these fusions, as well as  $P_{\text{rha}}::\textit{mVenus}$ , were transferred into *Synechocystis* via conjugation. The strains were termed  $P_{\text{rha}}::\textit{mVenus}$ (119) and  $P_{\text{rha}}::\textit{mVenus}$ (111), respectively, with the number in parentheses corresponding to the respective Anderson promoter number.

A typical dose-dependent response can be observed in both reporter constructs 24 h post-induction, saturating at approximately 10 mM L-rhamnose (Figure 3B). A maximum fold induction of 55 $\times$  and 39 $\times$  is achieved for  $P_{\text{rha}}::\textit{mVenus}$ (119) and  $P_{\text{rha}}::\textit{mVenus}$ (111) at this concentration, respectively. While Kelly et al. do not specify fold changes, a 15 $\times$  increase under similar conditions can be roughly estimated from their data. Within our setup, we show that this promoter can achieve even higher induction responses. We hypothesize that this can be attributed to both an increase of cellular activator levels and the use of the well-established RBS\* instead of the native *E. coli* RBS, which may increase the maximal expression achievable with  $P_{\text{rha}}$ .

When growing induced cultures over a longer time period, the general dose-dependent pattern remained the same for both strains. However, both overall fluorescence intensity and fold induction at 10 mM appeared to further increase over time, up to 165 $\times$  and 143 $\times$  after 76 h for  $P_{\text{rha}}::\textit{mVenus}$ (119) and  $P_{\text{rha}}::\textit{mVenus}$ (111), respectively (Figure 3C). Therefore, we decided to also evaluate the short- and long-term temporal expression dynamics. To account for possible inducer degradation and reliably assert expression dynamics, we chose a rhamnose concentration of 5 mM, which was below saturation of expression.

After induction, cultures were measured every 6 h. To minimize effects caused by cell density, an aliquot of each culture was sampled and cell density was adjusted to the start

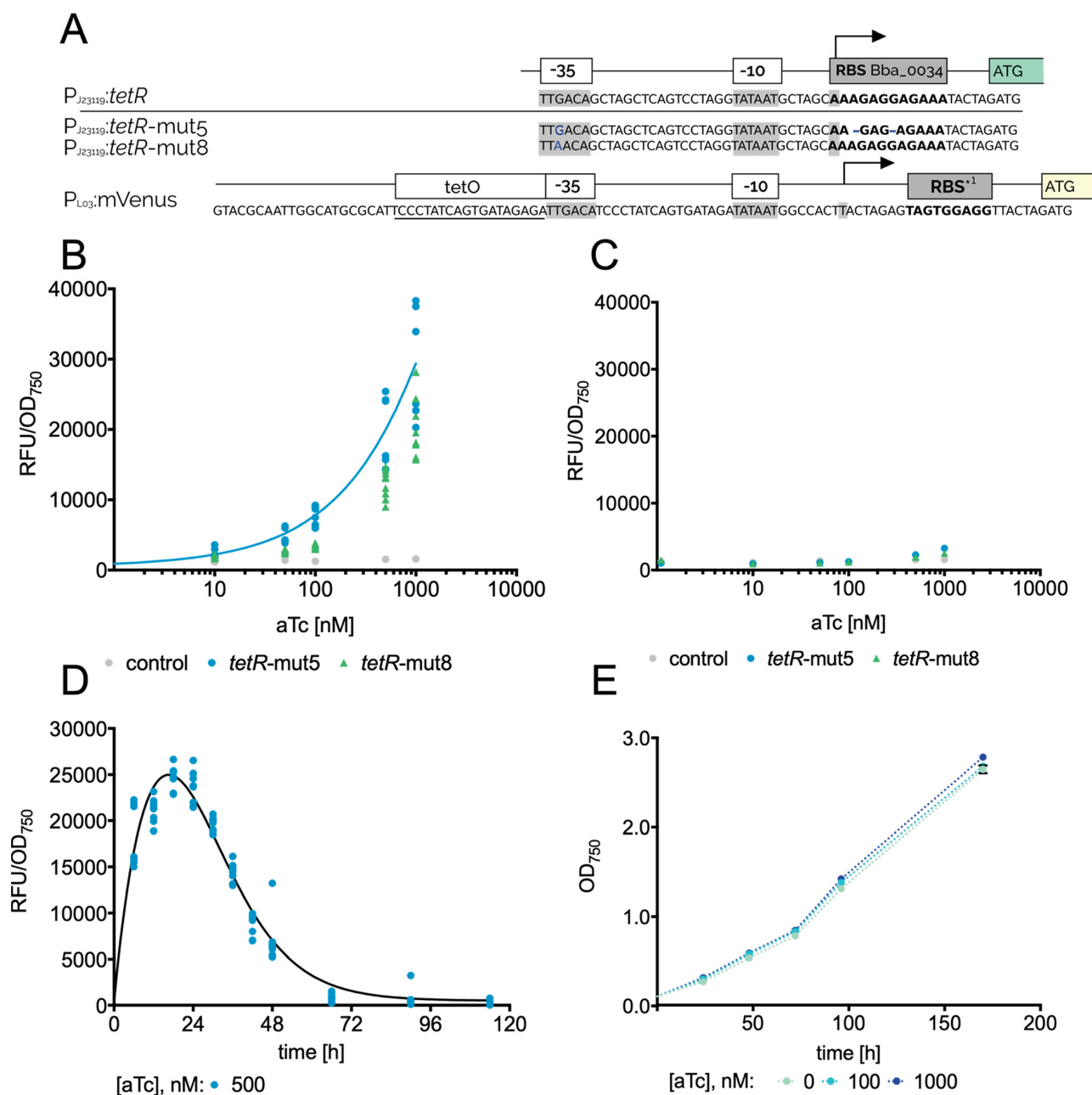


**Figure 4.** Dose-dependent response of the aTc-inducible promoter  $P_{L03}$  in *Synechocystis*. **A:** Schematic overview of the mutant variants with the intended construct ( $P_{J23119}::tetR$ ) as a reference. Top: Genetic composition of regulator. Bottom: Genetic composition of the regulated promoter  $P_{L03}$ . -10, -35, and +1 are highlighted in gray; RBS is shown in bold. Point mutations/deletions are shown in blue. <sup>1</sup>RBS\* from ref 32. **B:** Dose-response of the aTc inducible promoter  $P_{L03}$  to different concentrations of aTc after 24 h. The  $x$ -axis is shown logarithmic ( $\log_{10}$ ). A control (empty vector only) is shown in gray. **C:** Dose-response of the aTc inducible promoter  $P_{L03}$  to different concentrations of aTc after 48 h. The  $x$ -axis is shown logarithmic ( $\log_{10}$ ). A control (empty vector only) is shown in gray. **D:** Growth of *Synechocystis* WT supplemented with different concentrations of aTc. Three biological replicates each were cultured in BG11 and measured in the spectrophotometer. **E:** Response of  $P_{L03}(tetR\text{-mut5})$  to 500 nM aTc over time. OD<sub>750</sub> of each sample was adjusted to 0.25 prior to fluorescence measurement. Two and three biological replicates for *tetR*-mut5 and *tetR*-mut8, respectively, were cultured in BG11 + inducer and fluorescence and optical density was monitored. The dose-response data as well as the time course data were fitted to the modeled function eq 2 and eq 6, respectively (SI File 3).

OD<sub>750</sub> of 0.25 prior to each measurement. Fluorescence rapidly increased directly after induction. Eighteen hours post-induction, this increase became linear. Fluorescence continued to increase linearly until 136 h post-induction, after which fluorescence levels remained stable for three more days (Figure 3D). To investigate whether this was reversible, we performed

a step-down by washing the cells twice with BG11 to remove all L-rhamnose from the media. OD<sub>750</sub> was adjusted to 1.0. Fluorescence rapidly decreased after step-down, reaching preinduction autofluorescence levels after 3 days.

Finally, we investigated whether L-rhamnose had any effects on *Synechocystis* growth, since some of the concentrations used

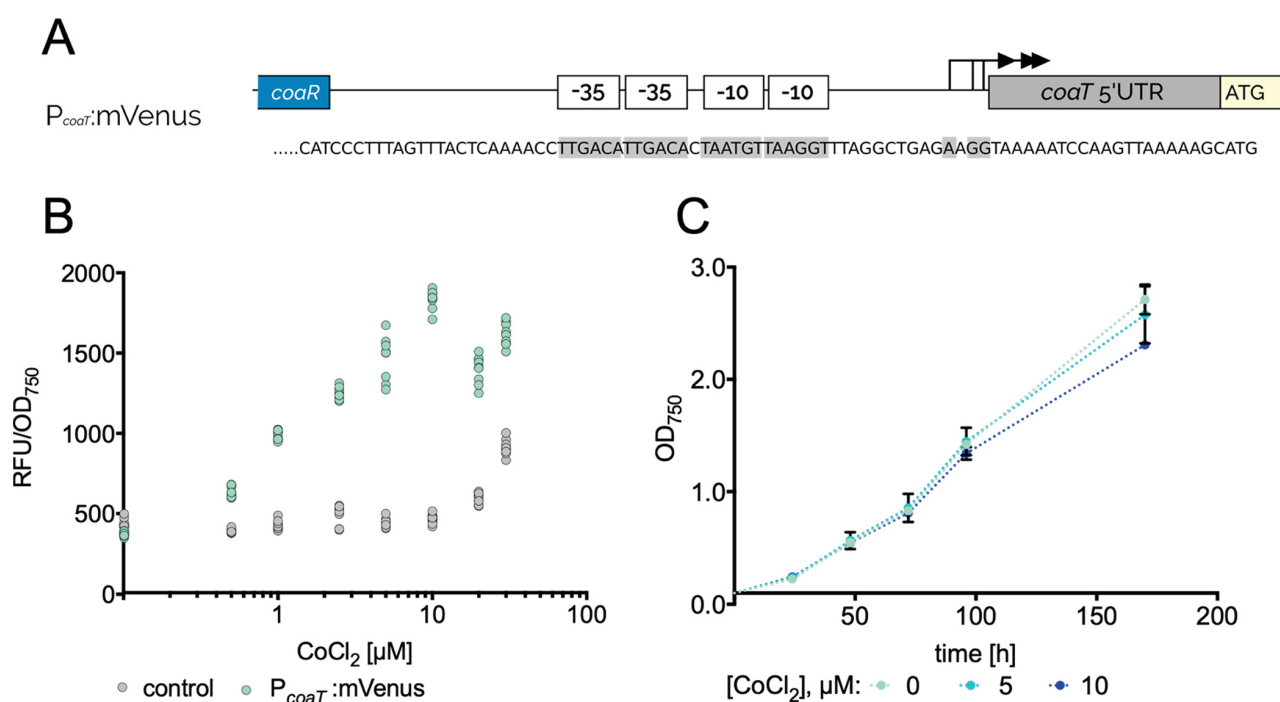


**Figure 5.** Dose-dependent response of *Synechocystis* to cobalt. **A:** Schematic overview of genetic construct used. Putative  $-10$ ,  $-35$ , and  $+1$  are highlighted in gray. **B:** Dose–response of  $P_{coaT}:mVenus$  to different concentrations of  $CoCl_2$  after 48 h. A control (empty vector only) is shown in gray. **C:** Cobalt-dependent growth behavior of WT *Synechocystis* over time. Optical density was measured at 750 nm. Three biological replicates were cultured in BG11 + inducer and fluorescence and optical density was measured in a microplate reader.

were higher than those previously tested by Kelly et al. WT *Synechocystis* cells were treated with different concentrations of L-rhamnose, and  $OD_{750}$  was monitored over 7 days (Figure 3E). Consistent with previous results, L-rhamnose had neither a positive nor a negative effect on *Synechocystis* growth. Moreover, the fluorescence time-course results further support the hypothesis that *Synechocystis* is unable to use L-rhamnose as a carbon source.

As already stated by Kelly et al.,  $P_{rha}$  performs exceptionally well as an inducible promoter, with a high dynamic range, tight repression, stable expression over at least 7 days, and no toxic effects or metabolization of the inducer.

**The aTc-Inducible Promoter  $P_{L03}$  Shows Improved Function by Increasing the Protein Levels of the *tetR* Repressor.** Next, we chose to evaluate the  $P_{L03}$  promoter published by Huang and Lindblad.<sup>19</sup> Despite their promising results of 300-fold induction, this promoter was also reported to lead to leaky expression of dCas9 by Yao et al.<sup>20</sup> For these reasons, we implemented a set of different design strategies to possibly reduce leakiness. First, we removed the *ssrA*-based LVA degradation tag from the *tetR* cassette to overcome rapid degradation of the repressor protein. Second, we chose the strong promoter  $P_{J23119}$  in place of  $P_{J23101}$  to further increase intracellular TetR. Finally, we applied the same plasmid-based design strategy used for the other promoters to be able to compare the results later on.

Interestingly, we were unable to obtain clones with the expected regulatory sequences upstream of *tetR* planned *in silico*. Instead, each sequenced clone showed point mutations either in the promoter or RBS sequence, suggesting toxicity resulting from excessive expression of *tetR*. Since we preselected clones that showed no fluorescence in *E. coli* for sequencing, indicating tight repression of  $P_{L03}$  in *E. coli*, we

decided to investigate two of them despite the point mutations. We termed them *tetR*-mut5 and *tetR*-mut8. Figure 4A highlights the genetic composition of the two mutants compared to the desired construct.

Cultures containing the plasmid constructs were treated identically to the ones containing the  $P_{vanCC}$  and  $P_{rha}$  promoter constructs. For the purpose of employing this promoter in broad, standard applications, we limited our experimental setup to photoautotrophic growth conditions (see the Method section for details), despite Huang et al. reporting better results for cultures grown in red light and LAHG.

Figure 4B shows the dose response of the two mutant constructs 24 h post-induction. Interestingly, the dose–response assay shows the expected linear aTc-dependent increase of relative fluorescence. The fold change at 1000 nM aTc was lower than for rhamnose with 16-fold and 11-fold for *tetR*-mut5 and *tetR*-mut8, respectively. While the *tetR*-mut8 strain outperforms *tetR*-mut5 both in dynamic range and in maximum promoter strength, it also shows minimally higher leaky expression under uninduced conditions (Figure 4B).

The dynamic range of mVenus expression decreased over time; by 48 h post-induction, fluorescence had significantly decreased to a fraction of what was measured before (Figure 4C). We therefore decided to also evaluate the short- and long-term temporal expression dynamics.

To account for possible inducer degradation, we chose an aTc concentration of 500 nM, which was below saturation of expression. After induction, cultures were measured every 6 h. To account for effects caused by cell density, an aliquot of each culture was sampled and cell density was adjusted to the start  $OD_{750}$  of 0.25 prior to each measurement.

Consistent with the results observed for  $P_{vanCC}$  and  $P_{rha}$ , fluorescence rapidly increased, reaching a maximum after 18 h

(Figure 4D). However, in contrast to  $P_{\text{vanCC}}$ , fluorescence decreased again just as rapidly, reaching autofluorescence levels after 66 h. In accordance with published literature, the rapid decrease in fluorescence is most likely a result of light-mediated degradation of aTc. Since aTc is a derivative of the antibiotic tetracycline, there have been reports on its toxicity in *E. coli* at high concentrations.<sup>37</sup> Thus, we were interested in its effects on the growth of *Synechocystis* WT at the relevant concentrations used for induction of  $P_{\text{L03}}$ .

Interestingly, aTc-treated cells show slightly improved growth compared to untreated cells (Figure 4E). We attribute this effect to hormesis, a positive effect on growth often observed in bacteria as a result of a global stress response to sublethal concentrations of antibiotics.<sup>38</sup> At concentrations relevant for the induction of  $P_{\text{L03}}$ , aTc appears to have no growth-inhibiting effect on *Synechocystis*.

As previously shown by Huang et al.,  $P_{\text{L03}}$  performs well as an inducible promoter. By providing a suitable intracellular amount of TetR, it shows minimal leakiness and a wide dynamic range. Especially during the first 24 h, it shows rapid, strong induction, making it a suitable tool for applications within this time frame. Due to the light-sensitive properties of aTc, this promoter may be better suited under red light or darkness for longer-term induction experiments.<sup>19</sup> It also may be beneficial for the half-life of aTc to adjust the culture conditions to a higher cell density, thereby preserving the aTc due to shading.

**Evaluating the Native  $\text{Co}^{2+}$ -Responsive Promoter  $P_{\text{coaT}}$  as an Inducible Promoter.** Next, we decided to investigate a commonly used metal-inducible promoter. Since the highly efficient and commonly used  $\text{Ni}^{2+}$ -responsive promoter  $P_{\text{nrsB}}$  has already been investigated in detail elsewhere,<sup>12</sup> we chose  $P_{\text{coaT}}$ . This promoter was successfully used toward small-scale biotechnological production of plant terpenoids<sup>39</sup> and ethylene<sup>40</sup> in *Synechocystis*, as well as for mimicking a null mutant in the filamentous cyanobacterium *Anabaena* sp. by selectively removing  $\text{Co}^{2+}$  and  $\text{Zn}^{2+}$  from the media.<sup>41</sup>

Since the TSS of  $P_{\text{coaT}}$  has, to the best of our knowledge, not been mapped previously, we performed 5'RACE (rapid amplification of cDNA ends) to determine the TSS of  $P_{\text{coaT}}$ . Our results indicate at least 3 putative TSS for  $P_{\text{coaT}}$  (Figure 5A, Figure S1). We therefore decided to maintain the native promoter+5'UTR architecture, and fused the entire 1195 bp upstream of *coaT*, including the *coaR* repressor, upstream of mVenus.

Upon induction with different concentrations of  $\text{CoCl}_2$ , a linear response could be observed up to a concentration of 10  $\mu\text{M}$  (Figure 5B). For higher concentrations, the values measured became erratic for both  $P_{\text{coaT}}$ :mVenus and the control. This is likely due to toxic effects of  $\text{Co}^{2+}$  ions under these experimental conditions.

Upon investigating effects of relevant  $\text{CoCl}_2$  concentrations on the growth of WT *Synechocystis*, a slight defect in growth was observed at 10  $\mu\text{M}$  (Figure 5C). This effect was even stronger in  $P_{\text{coaT}}$ :mVenus (Figure S2). This increased sensitivity to  $\text{Co}^{2+}$  was also observed previously in a *coaT* deletion mutant.<sup>42</sup> Increasing the amount of CoaR repressor in the cell, as done in this work by expression of an additional copy from a plasmid, might have the same effect. Moreover, the maximum working concentration of  $\text{Co}^{2+}$  reported throughout the literature for the  $P_{\text{coaT}}$  promoter is 6  $\mu\text{M}$ ,<sup>43</sup> indicating toxic effects at higher concentrations.

More importantly, for complete repression of  $P_{\text{coaT}}$ , it is necessary to culture strains in  $\text{Co}^{2+}$ -depleted BG11. Since  $\text{Co}^{2+}$  ions are required for the synthesis of coenzyme  $\text{B}_{12}$  in diverse cyanobacteria,<sup>44</sup> this means that complete repression of the promoter may require a defect in growth as a result of nutrient limitation (Figure S2). When looking into temporal expression dynamics, Englund et al. could show a decrease of fluorescence for  $P_{\text{nrsB}}$  due to  $\text{Ni}^{2+}$  actively being pumped out of the cells.<sup>12</sup> We hypothesize that this is also the case for  $\text{Co}^{2+}$ , since *coaT* encodes an efflux pump.  $P_{\text{coaT}}$  specifically as well as metal-inducible promoters in general are rather unsuitable as switches in synthetic biology. They lack orthogonality, require laborious alteration of standard culture media, show inducer toxicity at higher concentrations, and are outperformed by all three inducible systems shown in this work, in terms of both dynamic range and maximum strength.

**Different Inducible Promoters Cover a Wide Range of Expression Levels.** Finally, we measured the performance of each promoter alongside one another, either uninduced or induced. In order to categorize each promoter within a broader range, we included the native promoter constructs  $P_{\text{cpc560}}$ ,  $P_{\text{mpB}}$  and  $P_{\text{rbcL}}$ , as well as the minimal constitutive promoters  $P_{\text{J23100}}$  and  $P_{\text{J23119}}$ .

All strains were cultured in accordance with the dose–response assays shown previously. Transconjugants were validated and cultured, and mVenus fluorescence, as well as the optical density at 750 nm, was measured in a microplate reader after 24 h. For all four inducible promoters, cultures both uninduced and induced with 10 mM L-rhamnose, 1  $\mu\text{M}$  aTc, 1 mM vanillate, or 10  $\mu\text{M}$   $\text{CoCl}_2$ , were grown and measured. Consistent with the previous results, the fluorescence of  $P_{\text{rha}}$  is the strongest of the inducible promoters, closely followed by  $P_{\text{L03}}$  and  $P_{\text{vanCC}}$  (Figure 6A). While these three show promise in terms of both dynamic range and strength,  $P_{\text{coaT}}$  is by far the weakest of the four. The uninduced control, which was cultured in regular BG11 instead of BG11 lacking  $\text{CoCl}_2$ , shows leaky induction, leading of a fold change of only 2X for  $P_{\text{coaT}}$ .

The strongest inducible promoter,  $P_{\text{rha}}$  is still weaker than  $P_{\text{cpc560}}$ , the “super-strong” promoter published by Zhou et al.<sup>13</sup> This promoter enabled expression of heterologous proteins leading up to 15% of total soluble protein. However, the data shown in Figure 6A was measured 24 h post-induction, and  $P_{\text{rha}}$  shows a steady and strong increase in fluorescence over 7 days (Figure 3D). It could be assumed that  $P_{\text{rha}}$  is able to reach levels similar to  $P_{\text{cpc560}}$  after a sufficient induction time.

To evaluate the importance of cell density at the time of induction, fluorescence response of each inducible promoter at fixed, nonsaturating concentrations of inducer was measured for three different starting  $\text{OD}_{750}$  values, namely, 0.1, 0.5, and 1.0. Specifically, cultures were maintained at the respective  $\text{OD}_{750}$  for 3 days by semicontinuous back-dilution, after which they were induced with 500  $\mu\text{M}$  vanillate, 500 nM aTc, or 5 mM L-rhamnose, respectively. Fluorescence was measured 24 h after induction (Figure 6B).

For vanillate- and aTc-specific induction, fluorescence response decreases with increasing  $\text{OD}_{750}$ . This effect is especially strong for induction of  $P_{\text{L03}}$ :mVenus, which is 6-fold reduced at a starting  $\text{OD}_{750} = 0.5$  compared to 0.1. When inducing at  $\text{OD}_{750} = 1.0$ , both  $P_{\text{vanCC}}$ :mVenus and  $P_{\text{L03}}$ :mVenus showed only a small fraction of residual fluorescence. This further reinforces the hypothesis of cellular vanillate conversion. In contrast,  $P_{\text{rha}}$  response appeared only

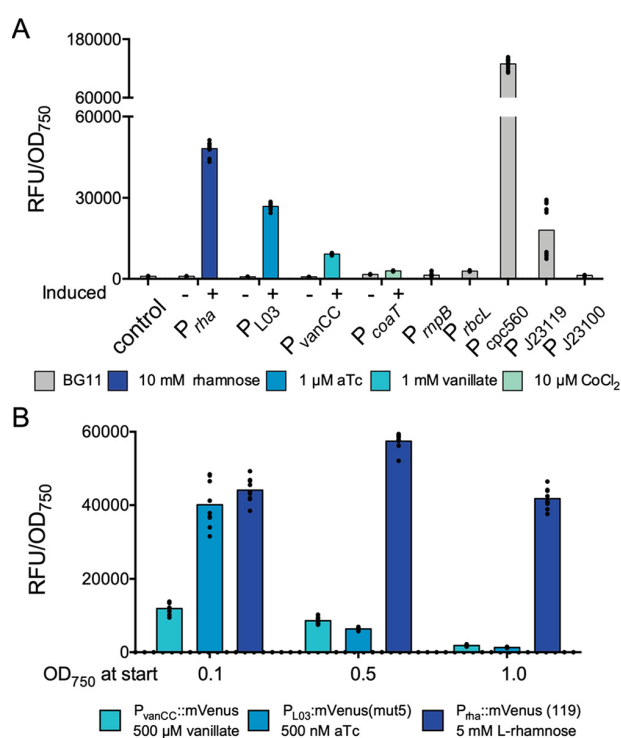


**Figure 6.** Comparison of established constitutive promoter and inducible promoters. A: Comparison of inducible with constitutive promoters. Control: Empty vector control. P<sub>rha</sub>::P<sub>rha</sub>:mVenus(119). P<sub>L03</sub>::P<sub>L03</sub>:mVenus (*tetR*-mut5). B: Cell density dependent response of inducible promoters. Three biological replicates each, including an EVC, were precultured in BG11 to an OD<sub>750</sub> of 0.1, 0.5, or 1.0, after which an inducer (10 mM rhamnose, 1 mM vanillate, or 1 μM aTc) was added. Then, fluorescence and optical density at OD<sub>750</sub> were measured in a microplate reader after 24 h. The RFU/OD<sub>750</sub> values of the EVC were subtracted.

slightly higher at an induction density of 0.5, but remained relatively stable at all three cell densities. Finally, in order to investigate inducer specificity, each single promoter construct was also induced with all possible combinations of inducers. Cultures were induced with 10 mM L-rhamnose, 1 μM aTc or 1 mM vanillate, or a combination thereof. If left uninduced, the corresponding volume of solvent (H<sub>2</sub>O or ethanol) was added.

All promoters show specific induction only in the presence of the respective inducer molecule (Figure S3). The level of fluorescence appears to be the same regardless of the presence or absence of the other inducers for each promoter. In terms of inducer specificity, the promoter constructs are therefore compatible with one another.

It remains to be investigated whether they are truly orthogonal to each other in terms of transcription factor binding specificity, i.e., whether the transcriptional regulators are able to bind to unspecific operator sequences and activate or repress gene expression.

## CONCLUSIONS AND OUTLOOK

In this work, we constructed and evaluated the dose–response function of a library of different inducible promoters in a way that enables a useful comparison for later selection of a suitable promoter in *Synechocystis*. Using the pSHDY plasmid facilitated efficient exchange of parts to build this library, as well as comparable conditions.

We observed a delicate balance between transcription factor toxicity and sufficient expression to obtain a dose-dependent response to the inducer. This observation should be kept in mind for future work, as it might significantly improve the performance of other promoters. Next to the established aTc- and rhamnose-inducible promoters P<sub>L03</sub> and P<sub>rha</sub> we report the vanillate inducible promoter P<sub>vanCC</sub> as a new tool for *Synechocystis*. All three promoters show a linear induction over a range of inducer concentrations, as well as little to no leakiness in the absence of the inducer. Interestingly, they show different strengths of expression, as well as different temporal expression patterns, with the potential for a wide range of biological applications. Thus, our promoter library allows moving away from metal-inducible promoters and toward well-characterized, defined, and orthogonal parts, a key requirement of synthetic biology.

The genetic sequence suggests two operator sites for the vanillate inducible promoters and one for the aTc-inducible promoter. While developing our model, to find a proper fit for both promoters, a Hill coefficient of 4 and 2, respectively, was necessary. This may be an indication that the corresponding transcription factors *vanR* and *tetR* form functional dimers. Since this is already well-known for *tetR*,<sup>45</sup> this model-based approach may be a useful method to determine possible structural properties such as dimerization.

An initial consideration when designing this study was encoding the repressor constructs on the chromosome and the promoter constructs on a plasmid, but we decided against it for two reasons. First, the copy number of the *Synechocystis* genome can fluctuate depending on different conditions such as growth phase, light intensity, or nutrient availability, potentially resulting in different repressor copy numbers and subsequent strength of gene repression.<sup>46,47</sup> In contrast, the plasmid copy number is more stringently regulated within the cell, leading to more consistent results.<sup>48</sup> This also relates to the fact that expression may vary depending on the genomic context.<sup>49</sup> Since different working groups have been using different genomic integration sites, data may not be directly reproducible. Second, it takes longer to generate fully segregated chromosomal mutants, extending the amount of time between conceiving a project and measuring the data, further complicating rapid genetic screens.

Therefore, we determined a plasmid-encoded reporter system to be the most reasonable option for this study. However, the next step in applying the three inducible promoters for future works would be evaluating their performance in a strain chromosomally encoding the transcriptional regulators. Ultimately, encoding the regulators on the chromosome using a markerless genomic manipulation strategy would facilitate working with cyanobacteria, since it would free available space on the plasmid, as well as antibiotic resistance. This strategy has proven successful in the past in *E. coli*,<sup>50</sup> resulting in many expression strains for different applications.

Another emerging area of research that should be taken into account in the future is the analysis of each promoter on the single-cell level. This would yield a more complete understanding of the cellular expression dynamics and ultimately enable a statement regarding the robustness of the expression system.

Finally, all three promoters should be combined with different reporter genes each and encoded in one strain to evaluate whether they are truly orthogonal and whether they

can be used in combination to control multiple genes or operons, enabling the scalability of synthetic networks or metabolic engineering strategies.

## MATERIAL AND METHODS

**Plasmid and Strain Construction.** A detailed list of all relevant genetic modules and information regarding their origin, as well as plasmids constructed from them, is provided in the Supporting Information (Table S1).

All parts were amplified and fused using overlap extension PCR ([dx.doi.org/10.17504/protocols.io.psndnde](https://doi.org/10.17504/protocols.io.psndnde)) and integrated into the pSHDY backbone via Gibson assembly ([dx.doi.org/10.17504/protocols.io.n9xdh7n](https://doi.org/10.17504/protocols.io.n9xdh7n)). Plasmids were transferred to *Synechocystis* sp. PCC 6803 wild-type using triparental mating ([dx.doi.org/10.17504/protocols.io.psndnde](https://doi.org/10.17504/protocols.io.psndnde)). Clones were verified via colony PCR ([dx.doi.org/10.17504/protocols.io.mk5c4y6](https://doi.org/10.17504/protocols.io.mk5c4y6)). An overview of all relevant plasmid maps is shown in Figure S4.

**Culture Conditions.** All strains were maintained on BG11 plates containing 40  $\mu\text{g}/\text{mL}$  spectinomycin. Recipe for BG11 media  $\rightarrow$  [dx.doi.org/10.17504/protocols.io.7kmhku6](https://doi.org/10.17504/protocols.io.7kmhku6). Prior to each assay, BG11 + 20  $\mu\text{g}/\text{mL}$  spectinomycin were inoculated with the strain of interest, grown for 5 days, diluted to an  $\text{OD}_{750}$  of 0.2, grown for 3 more days, and diluted again to the desired  $\text{OD}_{750}$  (specified in each assay) prior to starting the experiment. Liquid cultures were grown in constant white light ( $80 \mu\text{mol}\cdot\text{m}^{-2}\cdot\text{s}^{-1}$ , 16% intensity setting in the Infors HT multitron) at 30  $^{\circ}\text{C}$  and 75% humidity with constant agitation at 150 rpm without added  $\text{CO}_2$ .

Detailed protocols for each assay can be found on protocols.io: Dose response assay  $\rightarrow$  [dx.doi.org/10.17504/protocols.io.55wg87e](https://doi.org/10.17504/protocols.io.55wg87e). Toxicity assay  $\rightarrow$  [dx.doi.org/10.17504/protocols.io.6tgejw](https://doi.org/10.17504/protocols.io.6tgejw). Fluorescence time course assay  $\rightarrow$  [dx.doi.org/10.17504/protocols.io.6tkhek](https://doi.org/10.17504/protocols.io.6tkhek).

**Measurements and Settings.** To determine cell density, absorbance of cells was measured in a Specord 200 Plus spectrophotometer (Analytik Jena) at 750 nm after blanking with BG11. Fluorescence measurements were performed using a BMG Clariostar. Absorbance at 750 nm, as well as fluorescence at  $\lambda^{\text{ex}}/\lambda^{\text{em}}$  511/552, was measured every time. Prior to each measurement, the plate was shaken at 500 rpm for 30 s. The exact protocol for the BMG measurements can be found in SI File 1.

**Data Analysis and Treatment.** For dose response assays, fluorescence values were divided by  $\text{OD}_{750}$ . For fluorescence time course assays, fluorescence values were divided by  $\text{OD}_{750}$ . Then, the mean of the values measured for the uninduced control culture was subtracted from each individual value measured for the induced culture. For the fluorescence time courses, all raw fluorescence values were normalized to  $\text{OD}_{750}$ , then, the mean fluorescence of the uninduced control was subtracted from each value of the induced culture.

**Mathematical Modeling.** In order to infer additional information from the experimental data, a model describing inducible promoters was derived. The dose response assays, as well as the time course assays, were fitted to eq 2 and eq 6 (see SI File 3), respectively. All fits were performed with R (v 3.5.2) and Wolfram Mathematica (v 12.0.0). See SI File 3 for the fitted parameters (Table 1 SI File 3) and detailed information about the derivation of the mathematical model. The plasmid pAJM.714, as well as the strain sAJM.1504 were a gift from Christopher Voigt (Addgene plasmid ID 108515; Bacterial strain ID 108251).

## ASSOCIATED CONTENT

### Supporting Information

The Supporting Information is available free of charge at <https://pubs.acs.org/doi/10.1021/acssynbio.9b00505>.

SI File 1: BMG ClarioStar protocol for measurement of mVenus fluorescence in *Synechocystis* sp. PCC 6803 (TXT)

SI File 2: Supporting Tables and Figures for this work (PDF)

SI File 3: Mathematical modeling of induced gene expression (PDF)

## AUTHOR INFORMATION

### Corresponding Author

Ilka M. Axmann – Institute for Synthetic Microbiology, Heinrich Heine University Duesseldorf, 40225 Duesseldorf, Germany; [orcid.org/0000-0002-0856-8667](https://orcid.org/0000-0002-0856-8667); Email: [Ilka.Axmann@hhu.de](mailto:Ilka.Axmann@hhu.de)

### Authors

Anna Behle – Institute for Synthetic Microbiology, Heinrich Heine University Duesseldorf, 40225 Duesseldorf, Germany; [orcid.org/0000-0002-0244-0312](https://orcid.org/0000-0002-0244-0312)

Pia Saake – Institute for Synthetic Microbiology, Heinrich Heine University Duesseldorf, 40225 Duesseldorf, Germany

Anna T. Germann – Institute for Synthetic Microbiology, Heinrich Heine University Duesseldorf, 40225 Duesseldorf, Germany

Dennis Dienst – Department of Chemistry – Ångström, Uppsala University, 75120 Uppsala, Sweden

Complete contact information is available at: <https://pubs.acs.org/10.1021/acssynbio.9b00505>

### Author Contributions

A.B. and I.M.A. designed and conceived the study. A.B. and P.S. performed the experiments and analyzed the data. ATG performed modeling of the data and wrote the corresponding methodology section (SI File 3). A.B. and D.D. wrote the manuscript with input from all authors. All authors read and approved the manuscript.

### Funding

This work was supported by the Deutsche Forschungsgemeinschaft (DFG, project ID 391465903/GRK 2466) to ATG and IMA.

### Notes

The authors declare no competing financial interest.

## ACKNOWLEDGMENTS

We thank Nicolas Schmelling, Michelle Schulz, and Trevor Powell for assistance with cloning and measurements. We would like to thank Rainer Machné for helpful discussions on fluorescence measurements and mathematical modeling. We would also like to thank Dr. Vladislav Zinchenko (Dept. of Genetics, Moscow State University) for his permission to use the pVZ vector as a backbone for our newly designed vector named pSHDY and its derivatives.

## ABBREVIATIONS

aTc, anhydrotetracycline; CDS, coding sequence; *E. coli*, *Escherichia coli*; LAHG, light-activated heterotrophic growth; RBS, ribosome binding site; *S. elongatus*, *Synechococcus*

*elongatus* PCC 7942; *Synechocystis*, *Synechocystis* sp. PCC 6803; WT, wild type; OD<sub>750</sub>, Optical density at 750 nm; TSS, Transcription start site

## REFERENCES

- (1) Oliver, N. J., Rabinovitch-Deere, C. A., Carroll, A. L., Nozzi, N. E., Case, A. E., and Atsumi, S. (2016) Cyanobacterial metabolic engineering for biofuel and chemical production. *Curr. Opin. Chem. Biol.* 35, 43–50.
- (2) Ducat, D. C., Way, J. C., and Silver, P. A. (2011) Engineering cyanobacteria to generate high-value products. *Trends Biotechnol.* 29, 95–103.
- (3) Zarzycki, J., Axen, S. D., Kinney, J. N., and Kerfeld, C. A. (2013) Cyanobacterial-based approaches to improving photosynthesis in plants. *J. Exp. Bot.* 64, 787–798.
- (4) Ramey, C. J., Barón-Sola, Á., Aucoin, H. R., and Boyle, N. R. (2015) Genome Engineering in Cyanobacteria: Where We Are and Where We Need To Go. *ACS Synth. Biol.* 4, 1186–1196.
- (5) Huang, H.-H., Camsund, D., Lindblad, P., and Heidorn, T. (2010) Design and characterization of molecular tools for a synthetic biology approach towards developing cyanobacterial biotechnology. *Nucleic Acids Res.* 38, 2577–2593.
- (6) Wang, B., Eckert, C., Maness, P.-C., and Yu, J. (2018) A Genetic Toolbox for Modulating the Expression of Heterologous Genes in the Cyanobacterium *Synechocystis* sp. PCC 6803. *ACS Synth. Biol.* 7, 276–286.
- (7) Kim, W. J., Lee, S.-M., Um, Y., Sim, S. J., and Woo, H. M. (2017) Development of SyneBrick Vectors As a Synthetic Biology Platform for Gene Expression in *Synechococcus elongatus* PCC 7942. *Front. Plant Sci.* 8, 1–9.
- (8) Santos-Merino, M., Singh, A. K., and Ducat, D. C. (2019) New Applications of Synthetic Biology Tools for Cyanobacterial Metabolic Engineering. *Front. Bioeng. Biotechnol.* 7, 273.
- (9) Higo, A., and Ehira, S. (2019) Spatiotemporal Gene Repression System in the Heterocyst-Forming Multicellular Cyanobacterium *Anabaena* sp. PCC 7120. *ACS Synth. Biol.* 8, 641–646.
- (10) Markley, A. L., Begemann, M. B., Clarke, R. E., Gordon, G. C., and Pfeleger, B. F. (2015) Synthetic Biology Toolbox for Controlling Gene Expression in the Cyanobacterium *Synechococcus* sp. strain PCC 7002. *ACS Synth. Biol.* 4, 595–603.
- (11) Vasudevan, R., Gale, G. A. R., Schiavon, A. A., Puzorjov, A., Malin, J., Gillespie, M. D., Vavitsas, K., Zulkower, V., Wang, B., Howe, C. J., Lea-Smith, D. J., and McCormick, A. J. (2019) CyanoGate: A Modular Cloning Suite for Engineering Cyanobacteria Based on the Plant MoClo Syntax. *Plant Physiol.* 180, 39–55.
- (12) Englund, E., Liang, F., and Lindberg, P. (2016) Evaluation of promoters and ribosome binding sites for biotechnological applications in the unicellular cyanobacterium *Synechocystis* sp. PCC 6803. *Sci. Rep.* 6, 36640.
- (13) Peca, L., Kós, P. B., Máté, Z., Farsang, A., and Vass, I. (2008) Construction of bioluminescent cyanobacterial reporter strains for detection of nickel, cobalt and zinc. *FEMS Microbiol. Lett.* 289, 258–264.
- (14) Imamura, S., and Asayama, M. (2009) Sigma Factors for Cyanobacterial Transcription. *Gene Regul. Syst. Biol.* 3, 1–23.
- (15) Geerts, D., Bovy, A., De Vrieze, G., Borrias, M., and Weisbeek, P. (1995) Inducible expression of heterologous genes targeted to a chromosomal platform in the cyanobacterium *Synechococcus* sp. PCC 7942. *Microbiology* 141, 831–841.
- (16) Ferreira, E. A., Pacheco, C. C., Pinto, F., Pereira, J., et al. (2018) Expanding the toolbox for *Synechocystis* sp. PCC 6803: validation of replicative vectors and characterization of a novel set of promoters. *Synth. Biol. (Oxford, U. K.)* 3, 1.
- (17) Camsund, D., Heidorn, T., and Lindblad, P. (2014) Design and analysis of LacI-repressed promoters and DNA-looping in a cyanobacterium. *J. Biol. Eng.* 8, 1–23.
- (18) Albers, S. C., Gallegos, V. A., and Peebles, C. A. M. (2015) Engineering of genetic control tools in *Synechocystis* sp. PCC 6803 using rational design techniques. *J. Biotechnol.* 216, 36–46.
- (19) Huang, H.-H., and Lindblad, P. (2013) Wide-dynamic-range promoters engineered for cyanobacteria. *J. Biol. Eng.* 7, 10.
- (20) Yao, L., Cengic, I., Anfelt, J., and Hudson, E. P. (2016) Multiple Gene Repression in Cyanobacteria Using CRISPRi. *ACS Synth. Biol.* 5, 207–212.
- (21) Kelly, C. L., Taylor, G. M., Hitchcock, A., Torres-Méndez, A., and Heap, J. T. (2018) A Rhamnose-Inducible System for Precise and Temporal Control of Gene Expression in Cyanobacteria. *ACS Synth. Biol.* 7, 1056–1066.
- (22) Cambray, G., Guimaraes, J. C., and Arkin, A. P. (2018) Evaluation of 244,000 synthetic sequences reveals design principles to optimize translation in *Escherichia coli*. *Nat. Biotechnol.* 36, 1005–1015.
- (23) Thiel, K., Mulaku, E., Dandapani, H., Nagy, C., Aro, E.-M., and Kallio, P. (2018) Translation efficiency of heterologous proteins is significantly affected by the genetic context of RBS sequences in engineered cyanobacterium *Synechocystis* sp. PCC 6803. *Microb. Cell Fact.* 17, 1–12.
- (24) Cho, S. H., Haning, K., Shen, W., Blome, C., Li, R., Yang, S., and Contreras, L. M. (2017) Identification and Characterization of 5' Untranslated Regions (5'UTRs) in *Zymomonas mobilis* as Regulatory Biological Parts. *Front. Microbiol.* 8, 233.
- (25) Los, D. A., Zorina, A., Sinetova, M., Kryazhov, S., Mironov, K., and Zinchenko, V. V. (2010) Stress Sensors and Signal Transducers in Cyanobacteria. *Sensors* 10, 2386–2415.
- (26) Ruegg, T. L., Pereira, J. H., Chen, J. C., and Nature, A. D. (2018) Jungle Express is a versatile repressor system for tight transcriptional control. *Nat. Commun.*, 1 DOI: 10.1038/s41467-018-05857-3.
- (27) Meyer, A. J., Segall-Shapiro, T. H., Glassey, E., Zhang, J., and Voigt, C. A. (2019) *Escherichia coli* “Marionette” strains with 12 highly optimized small-molecule sensors. *Nat. Chem. Biol.* 15, 196–204.
- (28) Zinchenko, V. V., Piven, I. V., Melnik, V. A., and Shestakov, S. V. (1999) Vectors for the Complementation Analysis of Cyanobacterial Mutants. *Russian Journal of Genetics* 35, 228–232.
- (29) Taton, A., Unglaub, F., Wright, N. E., Zeng, W. Y., Paz-Yepes, J., Brahmsha, B., Palenik, B., Peterson, T. C., Haerizadeh, F., Golden, S. S., and Golden, J. W. (2014) Broad-host-range vector system for synthetic biology and biotechnology in cyanobacteria. *Nucleic Acids Res.* 42, No. e136.
- (30) Kremers, G.-J., Goedhart, J., van Munster, E. B., and Gadella, T. W. J. (2006) Cyan and yellow super fluorescent proteins with improved brightness, protein folding, and FRET Förster radius. *Biochemistry* 45, 6570–6580.
- (31) Andersen, J. B., Sternberg, C., Poulsen, L. K., Bjorn, S. P., Givskov, M., and Molin, S. (1998) New unstable variants of green fluorescent protein for studies of transient gene expression in bacteria. *Appl. Environ. Microbiol.* 64, 2240–2246.
- (32) Heidorn, T., Camsund, D., Huang, H.-H., Lindberg, P., Oliveira, P., Stensjö, K., and Lindblad, P. (2011) Synthetic biology in cyanobacteria engineering and analyzing novel functions. *Methods Enzymol.* 497, 539–579.
- (33) Zhou, J., Zhang, H., Meng, H., Zhu, Y., Bao, G., Zhang, Y., Li, Y., and Ma, Y. (2015) Discovery of a super-strong promoter enables efficient production of heterologous proteins in cyanobacteria. *Sci. Rep.* 4, 235–6.
- (34) Kaczmarczyk, A., Vorholt, J. A., and Francez-Charlot, A. (2015) Synthetic vanillate-regulated promoter for graded gene expression in *Sphingomonas*. *Sci. Rep.* 4, 6453.
- (35) Taton, A., Ma, A. T., Ota, M., Golden, S. S., and Golden, J. W. (2017) NOT Gate Genetic Circuits to Control Gene Expression in Cyanobacteria. *ACS Synth. Biol.* 6, 2175–2182.
- (36) Kamimura, N., Takahashi, K., Mori, K., Araki, T., Fujita, M., Higuchi, Y., and Masai, E. (2017) Bacterial catabolism of lignin-derived aromatics: New findings in a recent decade: Update on bacterial lignin catabolism. *Environ. Microbiol. Rep.* 9, 679–705.

- (37) Oliva, B., Gordon, G., McNicholas, P., Ellestad, G., and Chopra, I. (1992) Evidence that tetracycline analogs whose primary target is not the bacterial ribosome cause lysis of *Escherichia coli*. *Antimicrob. Agents Chemother.* 36, 913–919.
- (38) Mathieu, A., Fleurier, S., Frénoy, A., Dairou, J., Bredeche, M.-F., Sanchez-Vizuete, P., Song, X., and Matic, I. (2016) Discovery and Function of a General Core Hormetic Stress Response in *E. coli* Induced by Sublethal Concentrations of Antibiotics. *Cell Rep.* 17, 46–57.
- (39) Loeschcke, A., Dienst, D., Wewer, V., Hage-Hülsmann, J., Dietsch, M., Kranz-Finger, S., Hüren, V., Metzger, S., Urlacher, V. B., Gigolashvili, T., Kopriva, S., Axmann, I. M., Drepper, T., and Jaeger, K.-E. (2017) The photosynthetic bacteria *Rhodobacter capsulatus* and *Synechocystis* sp. PCC 6803 as new hosts for cyclic plant triterpene biosynthesis. *PLoS One* 12, No. e0189816.
- (40) Guerrero, F., Carbonell, V., Cossu, M., Correddu, D., and Jones, P. R. (2012) Ethylene Synthesis and Regulated Expression of Recombinant Protein in *Synechocystis* sp. PCC 6803. *PLoS One* 7, e50470.
- (41) González, A., Bes, M. T., Peleato, M. L., and Fillat, M. F. (2016) Expanding the Role of FurA as Essential Global Regulator in Cyanobacteria. *PLoS One* 11, e0151384.
- (42) Cavet, J. S., Borrelly, G. P. M., and Robinson, N. J. (2003) Zn, Cu and Co in cyanobacteria: selective control of metal availability. *FEMS Microbiol. Rev.* 27, 165–181.
- (43) Berla, B. M., Saha, R., Immethun, C. M., Maranas, C. D., Moon, T. S., and Pakrasi, H. (2013) Synthetic biology of cyanobacteria: unique challenges and opportunities. *Front. Microbiol.* 4, 4.
- (44) Holm Hansen, O., Gerloff, G. C., and Skoog, F. (1954) Cobalt as an Essential Element for Blue-Green Algae. *Physiol. Plant.* 7, 665–675.
- (45) Cuthbertson, L., and Nodwell, J. R. (2013) The TetR family of regulators. *Microbiol. Mol. Biol. Rev.* 77, 440–475.
- (46) Griese, M., Lange, C., and Soppa, J. (2011) Ploidy in cyanobacteria. *FEMS Microbiol. Lett.* 323, 124–131.
- (47) Labarre, J., Chauvat, F., and Thuriaux, P. (1989) Insertional mutagenesis by random cloning of antibiotic resistance genes into the genome of the cyanobacterium *Synechocystis* strain PCC 6803. *J. Bacteriol.* 171, 3449–3457.
- (48) Rawlings, D. E., and Tietze, E. (2001) Comparative Biology of IncQ and IncQ-Like Plasmids. *Microbiol. Mol. Biol. Rev.* 65, 481–496.
- (49) Pinto, F., Pacheco, C. C., Oliveira, P., Montagud, A., Landels, A., Couto, N., Wright, P. C., Urchueguía, J. F., and Tamagnini, P. (2015) Improving a *Synechocystis*-based photoautotrophic chassis through systematic genome mapping and validation of neutral sites. *DNA Res.* 22, 425–437.
- (50) Daegelen, P., Studier, F. W., Lenski, R. E., Cure, S., and Kim, J. F. (2009) Tracing Ancestors and Relatives of *Escherichia coli* B, and the Derivation of B Strains REL606 and BL21(DE3). *J. Mol. Biol.* 394, 634–643.

# Comparative dose-response analysis of inducible promoters in cyanobacteria.

Anna Behle<sup>1</sup>, Pia Saake<sup>1</sup>, Anna T. Germann<sup>1</sup>, Dennis Dienst<sup>2</sup>, Ilka M. Axmann<sup>1\*</sup>

<sup>1</sup>Institute for Synthetic Microbiology, Heinrich Heine University Duesseldorf, Duesseldorf, Germany

<sup>2</sup>Department of Chemistry – Ångström, Uppsala University, Uppsala, Sweden

\*E-Mail: [Ilka.Axmann@hhu.de](mailto:Ilka.Axmann@hhu.de) | Website: <http://www.synmikrobiologie.hhu.de>

## Supporting Information

Supplementary File 1: BMG ClarioStar protocol for measurement of mVenus fluorescence in *Synechocystis* sp. PCC 6803

Supplementary File 2: Supporting Tables and Figures for this work.

Table S1: Detailed descriptions and sequences of all relevant genetic modules used in this work

Fig. S1: 5'RACE results from TSS-mapping of  $P_{coaT}$ .

Fig. S2: Growth of control strain and  $P_{coaT}$ :mVenus strain in different  $Co^{2+}$  concentrations.

Fig. S3: Evaluation of chemical crosstalk between different promoter constructs and inducers.

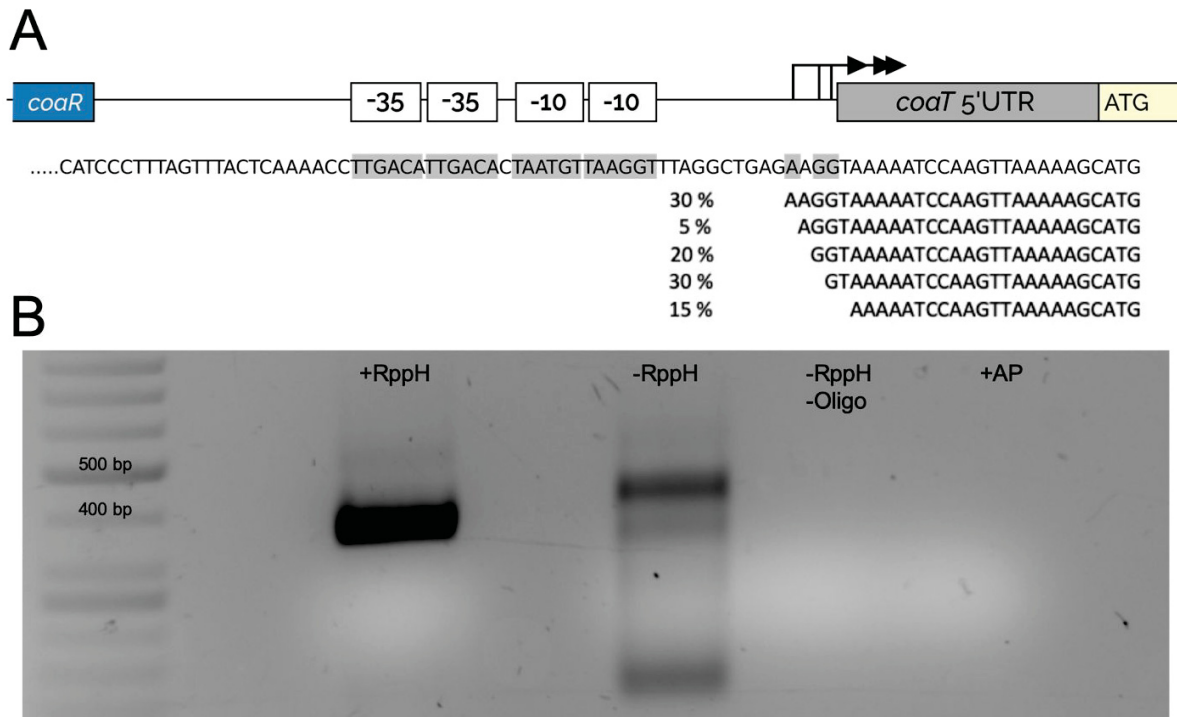
Fig. S4: Maps of vectors used.

Fig. S5: Absorption spectra of culture supernatants supplemented with different concentrations of vanillate.

Supplementary File 3: Mathematical modeling of induced gene expression.

### 5'RACE of the $Co^{2+}$ -inducible promoter $P_{coaT}$

To map the transcription start site (TSS) of  $P_{coaT}$ , we performed 5'RACE, as described in detail on [protocols.io](https://protocols.io) ([dx.doi.org/10.17504/protocols.io.jk7ckzn](https://doi.org/10.17504/protocols.io.jk7ckzn)). Five putative TSS were discovered, three of which occurred at a higher frequency (Fig. S1 A).



**Fig. S1: 5'RACE results from TSS-mapping of  $P_{coaT}$ .**

A: Top: Schematic overview of genetic construct used. Putative -10, -35 and +1 are highlighted in grey. Bottom: Putative transcription start sites based on sequencing results from 5'RACE. The percentages indicate the frequency of each individual start site as determined by sequencing. A total of 20 clones were sequenced.

B: 1% agarose gel electrophoresis of PCRs on *coaT*-specific *Synechocystis* cDNA using adapter-specific and gene-specific, nested primer. +RppH: RNA was treated with RppH (pyrophosphohydrolase), ligated to RNA-linker, then, cDNA synthesis was performed with gene specific primer. -RppH: untreated RNA was ligated to RNA-linker, then, cDNA synthesis was performed with gene specific primer. -RppH -Oligo: cDNA from untreated RNA control without ligated RNA-linker. +AP: RNA was treated with Alkaline Phosphatase, then ligated to RNA-linker, then, cDNA synthesis was performed with gene specific primer.

### Increased $Co^{2+}$ toxicity in the presence of an additional plasmid-encoded *coaR* copy

Fig. S2 shows the growth behavior of the two different *Synechocystis* strains used for the dose-response assay under different  $Co^{2+}$  concentrations. While the control strain containing the unmodified pSHDY plasmid shows decreased growth at 30  $\mu M$   $CoCl_2$  (Fig. S2 A), the strain encoding an additional *coaR* copy (pSHDY  $P_{coaT}$ :mVenus) already shows severe growth defects at 10  $\mu M$   $CoCl_2$  (Fig. S2 B).

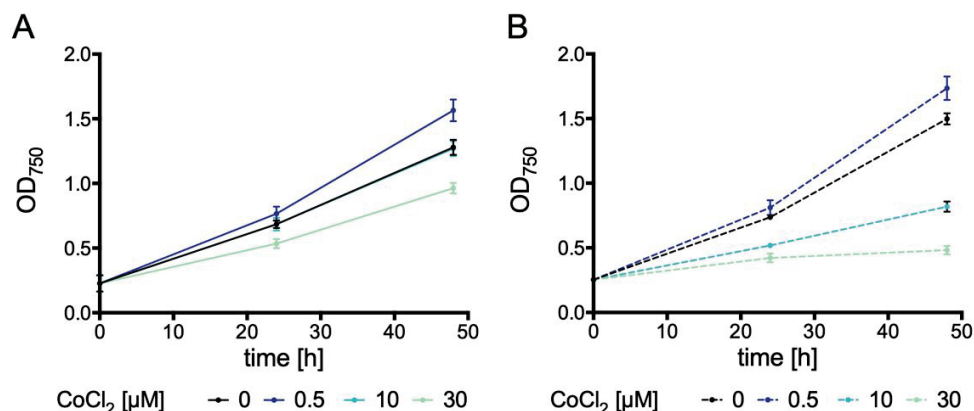


**Fig. S2: Growth of control strain and P<sub>coaT</sub>:mVenus strain in different Co<sup>2+</sup> concentrations.**  
 A: Cobalt-dependent growth behavior of *Synechocystis* with unmodified pSHDY over time.  
 B: Cobalt-dependent growth behavior of *Synechocystis* with pSHDY P<sub>coaT</sub>:mVenus over time.  
 Optical density was measured at 750 nm.

### Evaluation of chemical crosstalk among single promoter constructs

In order to investigate inducer specificity, each single promoter construct was also induced with all possible combinations of inducers.

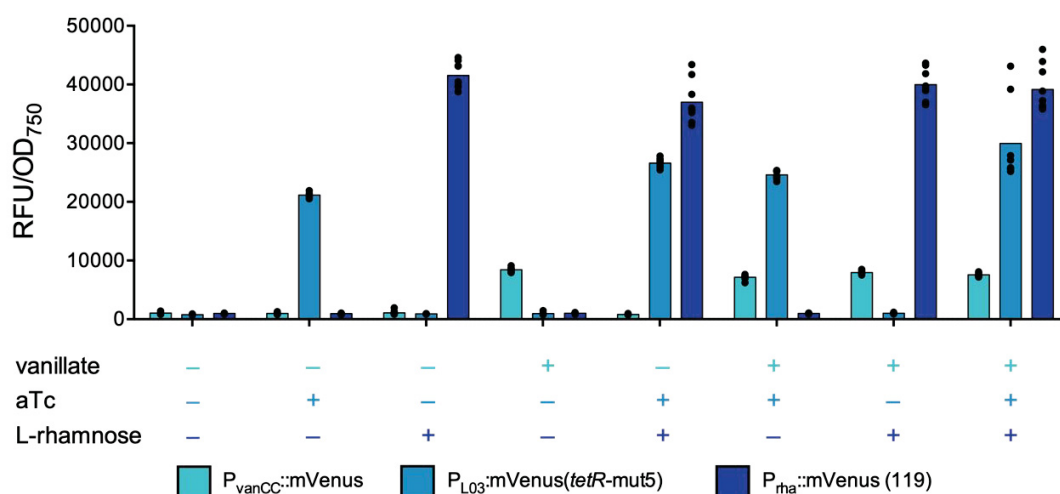
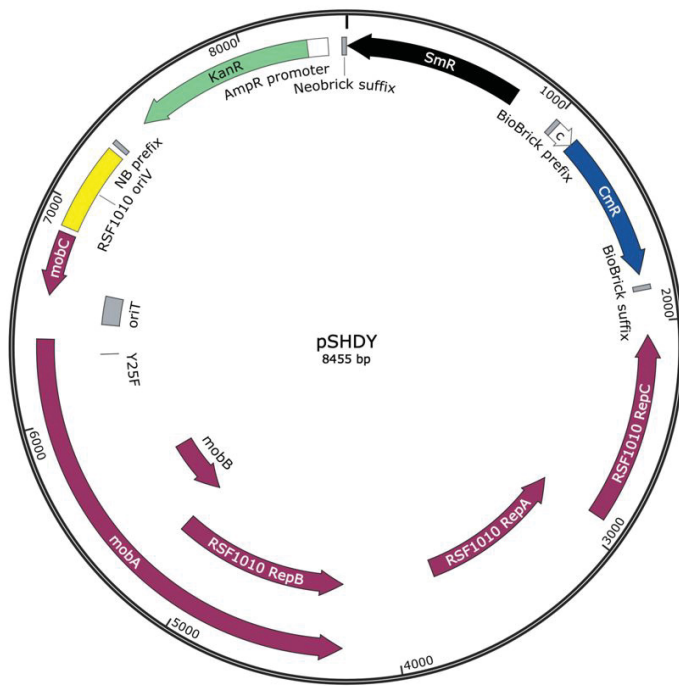


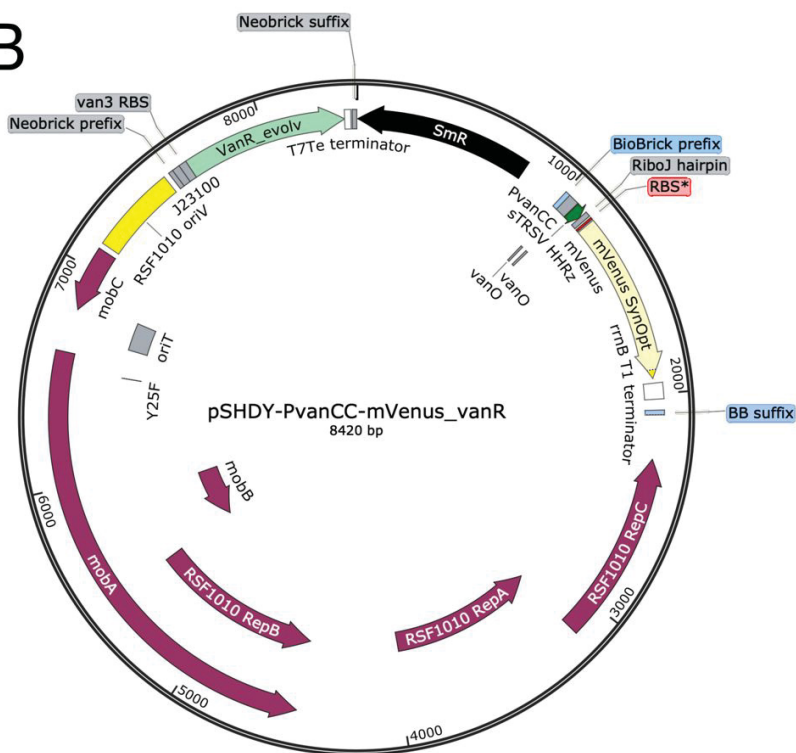
**Fig. S3: Evaluation of chemical crosstalk between different promoter constructs and inducers.**  
 Each separate promoter construct was induced with the different chemical inducers or combinations thereof.

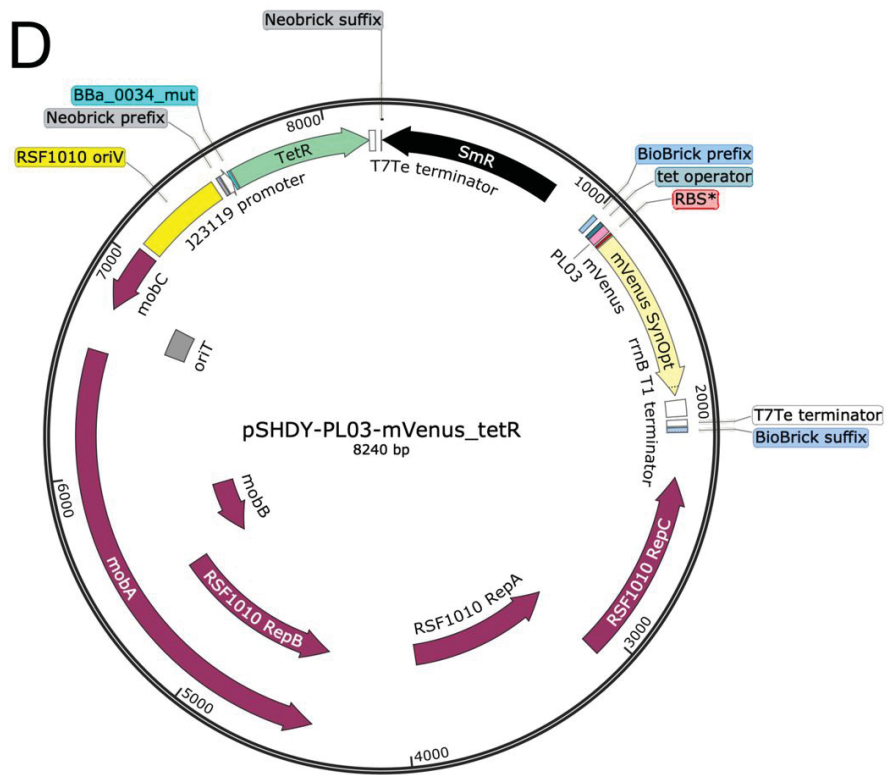
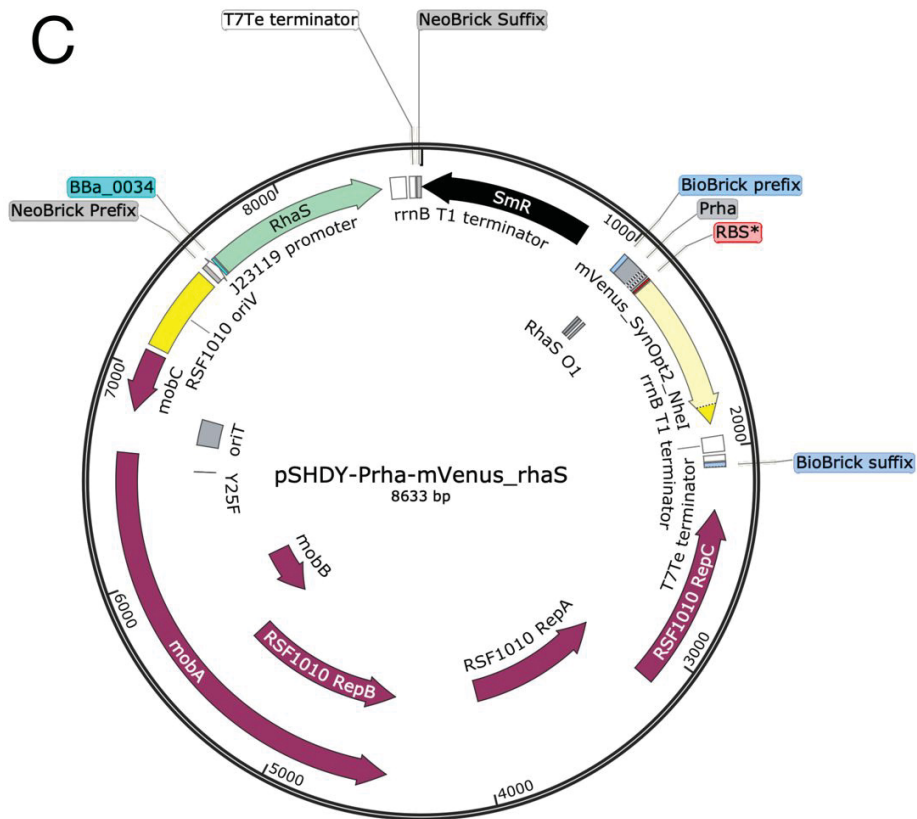
Three biological replicates each were cultured in BG11 + inducer (10 mM rhamnose, 1 mM vanillate or 1 μM aTc or combinations thereof, marked by a + when present or a - when absent) and fluorescence and OD<sub>750</sub> were measured in a microplate reader after 24 h.

A



B





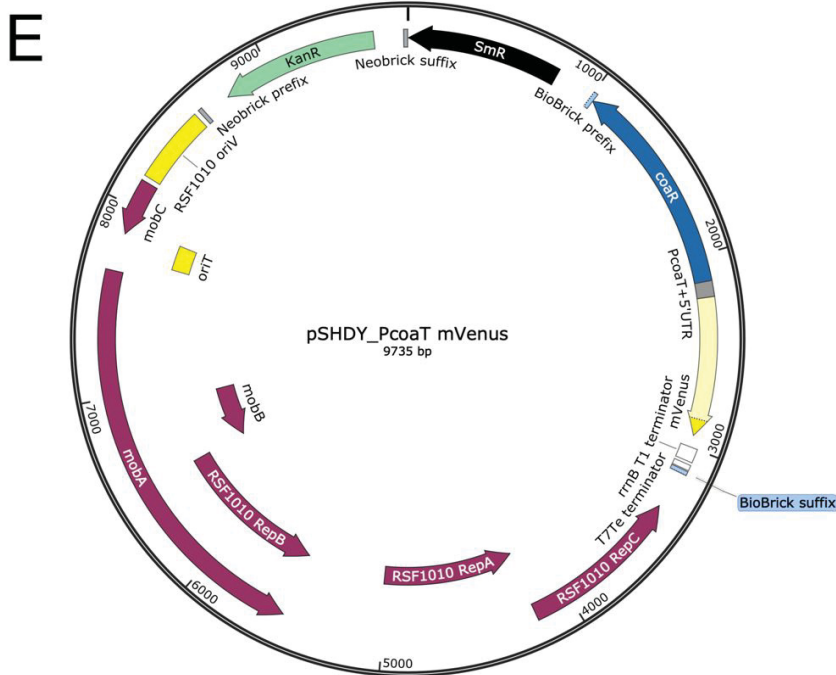


**Fig. S4: Maps of vectors used.**

**A:** pSHDY **B:** pSHDY\_P<sub>vanCC</sub>:mVenus-P<sub>J23100</sub>:vanR **C:** pSHDY\_P<sub>rha</sub>:mVenus-P<sub>J23119</sub>:rhaS **D:** pSHDY\_P<sub>L03</sub>:mVenus-P<sub>J23119</sub>:tetR-mut5 **E:** pSHDY\_P<sub>coaT</sub>:mVenus. Plasmid maps were created using SnapGene.

### Changes of the characteristic vanillate absorption spectra over time

Since vanillate has a characteristic absorption spectrum<sup>1</sup>, we investigated whether this changed over time. We therefore conducted culturing experiments in our incubators, supplementing either BG11 medium only, or *Synechocystis* culture carrying the empty vector only with either 0.1 mM vanillate solved in 100 % ethanol, or an equivalent volume of 100 % ethanol. Indeed, our preliminary results show that the absorption spectrum of vanillate in the supernatant of the *Synechocystis* culture changes, with the two absorption peaks shifting towards 300 nm (Fig. S5). The temporal behavior of this shift is consistent with the loss of signal observed in the fluorescence experiments. In contrast, this does not occur in BG11 only, suggesting chemical stability both in light and over time.

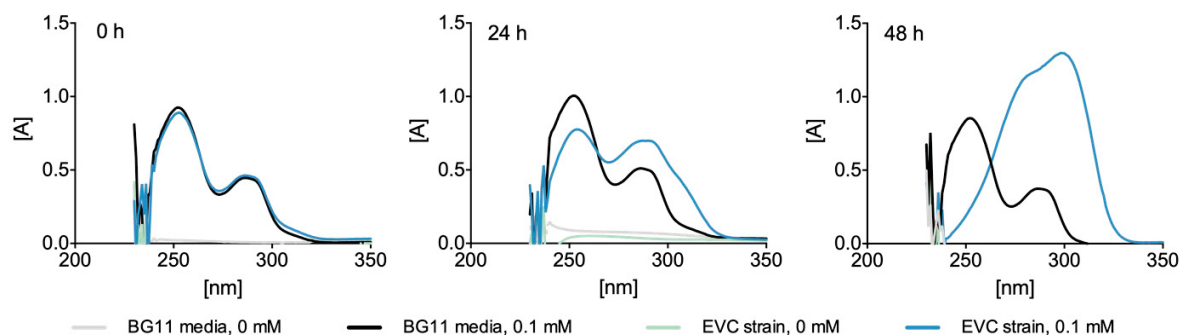


**Fig. S5: Absorption spectra of culture supernatants supplemented with different concentrations of vanillate.**

BG11 media (grey, black) or *Synechocystis* carrying the empty vector was supplemented with 0.1 mM vanillate or an equivalent volume of 100 % ethanol and incubated over time. 1 mL culture volume was sampled and centrifuged, and the absorption spectra of the supernatants were measured 0 h (left), 24 h (middle) and 48 h (right) post-induction, using UV-cuvettes. No absorbance was detected in any sample at wavelengths above 350 nm.



## Supplementary References

- (1) Robbins, R. J. (2003) Phenolic acids in foods: An overview of analytical methodology. *J. Agric. Food Chem.* *51*, 2866–2887.
- (2) Meyer, A. J., Segall-Shapiro, T. H., Glassey, E., Zhang, J., and Voigt, C. A. (2019) *Escherichia coli* “Marionette” strains with 12 highly optimized small-molecule sensors. *Nat Chem. Biol.* *15*, 196–204.
- (3) Heidorn, T., Camsund, D., Huang, H.-H., Lindberg, P., Oliveira, P., Stensjö, K., and Lindblad, P. (2011) Synthetic biology in cyanobacteria engineering and analyzing novel functions. *Methods Enzymol.* *497*, 539–579.
- (4) Kelly, C. L., Taylor, G. M., Hitchcock, A., Torres-Méndez, A., and Heap, J. T. (2018) A Rhamnose-Inducible System for Precise and Temporal Control of Gene Expression in Cyanobacteria. *ACS Synth. Biol.* *7*, 1056–1066.
- (5) Huang, H.-H., and Lindblad, P. (2013) Wide-dynamic-range promoters engineered for cyanobacteria. *J. Biol. Eng.* *7*, 1–11.
- (6) Zhou, J., Zhang, H., Meng, H., Zhu, Y., Bao, G., Zhang, Y., Li, Y., and Ma, Y. (2014) Discovery of a super-strong promoter enables efficient production of heterologous proteins in cyanobacteria. *Sci. Rep.* *4*, 235–6.

# Supplementary File 3: Mathematical Modeling of Induced Gene Expression

## Induced Gene Expression with Inducer Half-Life

Since experimental data suggest that a majority of mRNAs and proteins are degraded with a first-order decay rate,<sup>?</sup> the time-dependent amount of fluorescence protein can be characterized by the following first-order rate equation.<sup>?,?</sup>

$$\frac{dy(t)}{dt} = y'(t) = \alpha(t) - \beta y(t) \quad (1)$$

$$\begin{aligned} \beta &= \mu + \delta_P \\ \alpha(t) &= \ell + v \frac{I^n}{I^n + K^n} \\ I(t) &= I_0 e^{-\delta t} \end{aligned}$$

Here,  $\beta$  describes the decay rate (or half-life, with  $t_{1/2} = \frac{\log 2}{\beta}$ ), including culture growth rate  $\mu$  and AVS-tagged protein degradation rate  $\delta_P$ , and  $y(t)$  represents the time-dependent protein concentration.  $\alpha$  expresses the promoter activity,<sup>?</sup> with the basal ("leaky") transcription rate  $\ell$ , maximal induced transcription rate  $v$ , half-maximal inducer concentration  $K$  and number of inducer binding sites  $n$ . The inducer concentration at time  $t$  is given by  $I(t)$ , with the initial inducer concentration  $I_0$  and inducer degradation rate  $\delta$ .

It is assumed that the inducer half-life  $t_{1/2} = \frac{\log 2}{\delta}$  is not affected by metabolism, and that the measured fluorescence per OD is linearly related to protein concentration,  $f_{\text{OD}} \sim y(t)$ .

It has to be noted, that normally the protein degradation rate  $\delta_P$  cannot easily be estimated from the time-course microarray experiments. In our case, it was estimated from the rhamnose time-course experiment, where the degradation rate was approximated from a linear fit of the step-down.

## Induced Transcription with Constant Inducer Concentration

The inhomogenous linear first order differential equation for constant inducer concentration:

$$y'(t) + \beta y(t) = \alpha \quad (1)$$

is solved by addition of a particular solution  $y_p = \frac{\alpha}{\beta}$  of the inhomogenous equation and the general solution  $y_h = Ce^{-\beta t}$  of the homogenous form of the equation with  $\alpha = 0$ . Assuming an initial condition  $y(0) = y_0$ , the integration constant  $C$  can be described as  $C = y_0 - \frac{\alpha}{\beta}$ , and leads to the solution:

$$y(t) = y_0 e^{-\beta t} + \frac{\alpha}{\beta} (1 - e^{-\beta t}) . \quad (2)$$

## Induced Transcription with Inducer Half-Life

In this case the factor  $\alpha$  itself is a function of time  $t$ :

$$y'(t) + \beta y(t) = \alpha(t). \quad (3)$$

By use of the "Variation of Constants" method, where the constant  $C$  of the solution of the homogenous equation  $y_h = Ce^{-\beta t}$  is replaced by a function  $f(t)$ , substitution in eq. 3 leads to:

$$f(t) = \int \alpha(t) e^{\beta t} dt + C$$

Integration of  $f(t)$  with the more complex activation function  $\alpha(t)$  gives:

$$\alpha(t) = \ell + v \frac{(I_0 e^{-\delta t})^n}{(I_0 e^{-\delta t})^n + K^n}$$

$$f(t) = \frac{e^{\beta t}}{\beta} \left( {}_2F_1 \left( 1, \frac{\beta}{n\delta}; \frac{\beta}{n\delta} + 1; -e^{n\delta t} \frac{K^n}{I_0^n} \right) v + \ell \right) + C. \quad (4)$$

The term  ${}_2F_1(a, b; c; z)$  represents the gaussian or ordinary hypergeometric function. Substituting eq. 4 in  $y(t) = f(t)e^{-\beta t}$ , and solving for  $y(0) = y_0$  leads to the solution:

$$y(t) = \frac{e^{-\beta t}}{\beta} \left[ \beta y_0 - \ell - v \left( {}_2F_1 \left( 1, \frac{\beta}{n\delta}; \frac{\beta}{n\delta} + 1; \frac{K^n}{I_0^n} \right) \right) + e^{\beta t} \left( \ell + v \left( {}_2F_1 \left( 1, \frac{\beta}{n\delta}; \frac{\beta}{n\delta} + 1; -e^{n\delta t} \frac{K^n}{I_0^n} \right) \right) \right) \right]. \quad (5)$$

In our case  ${}_2F_1 \left( 1, \frac{\beta}{n\delta}; \frac{\beta}{n\delta} + 1; \frac{K^n}{I_0^n} \right) \approx 1$ , therefore eq. 5 can be simplified to:

$$y(t) = \frac{e^{-\beta t}}{\beta} \left[ e^{\beta t} + \beta y_0 - \ell - v \left( \ell + v {}_2F_1 \left( 1, \frac{\beta}{\delta n}; \frac{\beta}{\delta n} + 1; -e^{\delta n t} \frac{K^n}{I_0^n} \right) \right) \right]. \quad (6)$$

Table 1: **Fit Parameters** For both promoters  $I_0$  was set to 500  $\mu mol$ ,  $\mu$  to 0.033 [ $h^{-1}$ ] and  $\delta_p$  to 0.064 [ $h^{-1}$ ],  $\beta$  equals  $\mu + \delta_p$ .

Promoter	Parameters			Fitted Parameters		
	$y_0$ [ $\mu mol$ ]	$n$	$\ell$ [ $h^{-1}$ ]	$v$ [ $h^{-1}$ ]	$K$ [ $\mu mol$ ]	$\delta$ [ $h^{-1}$ ]
$P_{\text{vanCC}}$	0.0	4	0.0	696.2	96.3	0.031
$P_{\text{L03}}$	500.0	2	14.5	3562.2	101.9	0.068

## References

- (1) Munchel, S. E., Shultzaberger, R. K., Takizawa, N., and Weis, K. (2011) Dynamic profiling of mRNA turnover reveals gene-specific and system-wide regulation of mRNA decay. *Mol. Biol. Cell* 22, 2787–2795.
- (2) Cacace, F., Paci, P., Cusimano, V., Germani, A., and Farina, L. (2012) Stochastic Modeling of Expression Kinetics Identifies Messenger Half-Lives and Reveals Sequential Waves of Co-ordinated Transcription and Decay. *PLoS Comput. Biol.* 8, e1002772.
- (3) Stefan, D., Pinel, C., Pinhal, S., Cinquemani, E., Geiselman, J., and de Jong, H. (2015) Inference of Quantitative Models of Bacterial Promoters from Time-Series Reporter Gene Data. *PLoS Comput. Biol.* 11, e100402.
- (4) Bhaskaran, S., Umesh, P., and Nair, A. (2015) Hill Equation in Modeling Transcriptional Regulation. In *Systems and Synthetic Biology* (Singh, V., and Dhar, P., Eds.), pp 77-92, Springer, Dordrecht.

## 3 Manuscript II

### 3.1 Author's contributions

M. Dietsch\*, A. Behle\*, P. Westhoff, and I. M. Axmann, "Metabolic engineering of *Synechocystis* sp. PCC 6803 for the photoproduction of the sesquiterpene valencene," *Metab. Eng. Commun.*, vol. 13, p. e00178, Dec. 2021, doi: 10.1016/j.mec.2021.e00178

\* Shared first authorship.

M.D: Conceptualization, Investigation, Methodology, Writing - Original Draft, Writing - Review & Editing, Visualization, Data Curation. A.B: Conceptualization, Investigation, Writing - Original Draft, Writing - Review & Editing, Visualization, Data Curation. P.W: Methodology, Data Curation. I.M.A: Supervision, Writing- Reviewing and Editing.

Study design: 25%

Experimental contribution: 40%

Data analysis: 60%

Manuscript preparation: 70%

### 3.2 Metabolic engineering of *Synechocystis* sp. PCC 6803 for the photoproduction of the sesquiterpene valencene



Contents lists available at ScienceDirect

## Metabolic Engineering Communications

journal homepage: [www.elsevier.com/locate/mec](http://www.elsevier.com/locate/mec)Metabolic engineering of *Synechocystis* sp. PCC 6803 for the photoproduction of the sesquiterpene valenceneMaximilian Dietsch<sup>a,1</sup>, Anna Behle<sup>a,1</sup>, Philipp Westhoff<sup>b</sup>, Ilka M. Axmann<sup>a,\*</sup><sup>a</sup> Institute for Synthetic Microbiology, Department of Biology, Heinrich Heine University Düsseldorf, Düsseldorf, Germany<sup>b</sup> Plant Metabolism and Metabolomics Laboratory, Cluster of Excellence on Plant Sciences (CEPLAS), Heinrich Heine University Düsseldorf, D-40001, Düsseldorf, Germany

## ARTICLE INFO

## Keywords:

Metabolic engineering  
Cyanobacteria  
Synechocystis  
Valencene  
Sesquiterpene

## ABSTRACT

Cyanobacteria are extremely adaptable, fast-growing, solar-powered cell factories that, like plants, are able to convert carbon dioxide into sugar and oxygen and thereby produce a large number of important compounds. Due to their unique phototrophy-associated physiological properties, i.e. naturally occurring isoprenoid metabolic pathway, they represent a highly promising platform for terpenoid biosynthesis. Here, we implemented a carefully devised engineering strategy to boost the biosynthesis of commercially attractive plant sesquiterpenes, in particular valencene. Sesquiterpenes are a diverse group of bioactive metabolites, mainly produced in higher plants, but with often low concentrations and expensive downstream extraction. In this work we successfully demonstrate a multi-component engineering approach towards the photosynthetic production of valencene in the cyanobacterium *Synechocystis* sp. PCC 6803. First, we improved the flux towards valencene by markerless genomic deletions of *shc* and *sqs*. Secondly, we downregulated the formation of carotenoids, which are essential for viability of the cell, using CRISPRi on *crtE*. Finally, we intended to increase the spatial proximity of the two enzymes, *ispA* and *CnVS*, involved in valencene formation by creating an operon construct, as well as a fusion protein. Combining the most successful strategies resulted in a valencene production of 19 mg/g DCW in *Synechocystis*. In this work, we have devised a useful platform for future engineering steps.

## 1. Introduction

Cyanobacteria are known for their unique ability of oxygenic photosynthesis among bacteria. Thus, they are becoming increasingly important in biotechnological applications and for generating sustainable energy. Unlike plants, cyanobacteria can be cultivated in huge salt water basins, even in desert regions, solely with sunlight and CO<sub>2</sub> from the air or from connected power plants and, thus, do not compete with agricultural land and food production. Furthermore, extraction of plant secondary metabolites has proven to be inefficient, as it has yielded only small amounts of the desired products thus far. Here, cyanobacteria represent excellent candidates for the expression of plant biosynthetic genes and gene clusters due to their ancestral relationship to plant chloroplasts. In recent years, continuous efforts have been put into developing industrially viable strains of cyanobacteria for the sustainable production of various fine chemicals, secondary metabolites, and other compounds (Jodlbauer et al., 2021; Liu et al., 2021). Advances in

synthetic microbiology and increasing availability of new genetic tools for this important group of organisms enable even more innovative solutions.

In terms of structural diversity, terpenoids comprise an extremely versatile class of compounds. Naturally, the terpenoid backbones in cyanobacteria are generated via the methyl-erythritol-phosphate (MEP-) pathway, which produces the central terpenoid precursors IPP and DMAPP. By subsequent addition of another precursor, GPP (C10), the precursor for monoterpenes, FPP (C15) the precursor for sesquiterpenes and triterpenes, such as hopanoids, and GGPP (C20), the precursor for di- and tetraterpenes, to which the carotenoids belong, are generated. One prominent example for natural sesquiterpene production is geosmin found in several Cyanobacteria species, which is responsible for the characteristic earthy smell in water bodies (Lee et al., 2017). Sesquiterpenes are especially convenient for the heterologous production in microorganisms because they are often volatile, eliminating the necessity for costly extraction methods and downstream processing.

\* Corresponding author.

E-mail address: [ilka.axmann@hhu.de](mailto:ilka.axmann@hhu.de) (I.M. Axmann).<sup>1</sup> These authors contributed equally to this work.<https://doi.org/10.1016/j.mec.2021.e00178>

Received 2 March 2021; Received in revised form 5 July 2021; Accepted 22 July 2021

Available online 13 August 2021

2214-0301/© 2021 The Author(s). Published by Elsevier B.V. on behalf of International Metabolic Engineering Society. This is an open access article under the

CC BY license (<http://creativecommons.org/licenses/by/4.0/>).

Naturally, they are often found in plants, where they may function as defensive agents against predators. In industry, sesquiterpenes are used as flavor and fragrance additives and have been successfully produced in numerous microbial hosts, with very different yields.

The first metabolic engineering efforts for the production of sesquiterpenoids were made in *Escherichia coli* (*E. coli*), where amorphadiene, the precursor of the antimalarial drug artemisinin, was produced via heterologous expression of the complete mevalonate pathway from the yeast *Saccharomyces cerevisiae* (*S. cerevisiae*) (Newman et al., 2006). Using a combination of metabolic engineering and a two-phase cultivation system, a total yield of ~0.5 g/L product was achieved. This product titer was even further improved by the introduction of metabolically more active enzymes, as well as an improved growth media composition (Tsuruta et al., 2009).

*S. cerevisiae*, as well as other fungal species, has also successfully been applied for the production of sesquiterpenes such as valencene. Similar to previous efforts, enhancing the flux through the native isoprenoid biosynthesis pathway by overexpressing each gene had an advantageous effect on valencene product yield. In addition, by repressing essential genes that normally diverted some of the FPP precursor away from the desired product, valencene yield increased even more. The highest product yield in yeast, ~540 mg/L valencene, was again achieved by a combination of genetic engineering and optimization of media composition and cultivation (Chen et al., 2019). Recently, the corn smut fungus *Ustilago maydis* was explored as a microbial production host for sesquiterpenes, due to previous successes in biotechnological applications using this host (Lee et al., 2020).

Another strategy to increase the utilization of precursors towards desired products instead of native off-target pathways is to increase the spatial proximity of two sequential enzymes. In yeast, this was achieved by fusing FPP-synthase, encoded by *erg20*, with the heterologous sesquiterpene synthase, producing germacrene A in one case, and patchoulol in another (Albertsen et al., 2011; Chen et al., 2019).

This method of creating a chimeric enzyme showed success, with all fusion variants leading to an overall increase in product yield. In another study, heterologous production of carotenoids was achieved through bi- and tridomain fusion proteins, further demonstrating the importance of spatial proximity in metabolic pathways (Rabeharindranto et al., 2019).

Photoautotrophic bacteria, cyanobacteria in particular, have shown promising results in terms of production (Angermayr et al., 2015). Since they are natural terpene producers, they are excellent candidate chassis for metabolic engineering. In terms of product yield, they were able to compete with heterologous hosts under standard laboratory conditions. For example, the two sesquiterpenoids bisabolene and patchoulol were produced under high density conditions, yielding ~179.4 mg/L and 17.3 mg/L, respectively (Dienst et al., 2020). Another study showed successful production of various triterpenes from one key precursor in *Rhodobacter capsulatus* and *Synechocystis* sp. PCC 6803 (*Synechocystis* hereafter), indicating efficient exploitation of the native terpene pathway of photosynthetic organisms through genetic engineering (Loeschcke et al., 2017). Here, we present a multi-component approach towards the photosynthetic production of valencene. First, we applied metabolic engineering to generate a strain with a more favorable flux towards the precursor FPP by markerless genomic deletions. Secondly, we used CRISPRi to downregulate the formation of carotenoids, which are essential for viability of the cell. Finally, we applied two strategies to increase the spatial proximity of the two enzymes involved in valencene formation by creating an operon construct, as well as a fusion protein to increase the flux from FPP to the final precursor, valencene. This work successfully demonstrates heterologous production of the sesquiterpene valencene in the cyanobacterium *Synechocystis* using different engineering approaches.

## 2. Material & methods

### 2.1. Plasmid and strain construction

A detailed list of all relevant genetic modules and information regarding their origin, is provided in the Supporting Information (Table S2).

The previously published pSHDY-Prha-mVenus\_rhaS (Behle et al., 2020) (Addgene #137662) was slightly modified by excising the spectinomycin resistance cassette and replacing it with a nourseothricin resistance cassette, thereby creating an alternative plasmid we termed pSNDY.

Synthetic, codon-optimized genes were synthesized by IDT. Relevant genetic components were amplified and fused using overlap extension PCR when necessary, (dx.doi.org/10.17504/protocols.io.psndnde).

and integrated into the pSNDY backbone, either via Gibson assembly (dx.doi.org/10.17504/protocols.io.n9xdh7n), or using restriction/ligation cloning.

Plasmids were transferred to *Synechocystis* sp. PCC 6803 wild-type using triparental mating (dx.doi.org/10.17504/protocols.io.psndnde).

pMD19T-psba1-Ppsba2-dCas9-SpR was a gift from Paul Hudson (Addgene plasmid # 73220; <http://n2t.net/addgene:73220>; RRID: Addgene\_73220).

### 2.2. Culture conditions

For pre-culturing and growth experiments, *Synechocystis* was cultivated in BG11 medium (Stanier et al., 1979). Standard cultivation was performed at 30 °C with 150 rpm shaking and continuous illumination of ~80 µE m<sup>-2</sup> s<sup>-1</sup>. Aeration was ensured by continuous shaking and CO<sub>2</sub> enriched air (0.5%). Whenever necessary, appropriate antibiotics were added to the different strains. Pre-culturing was performed in 100 ml baffle-free Erlenmeyer shaking flasks with 20 ml cell suspension for three days. After adjusting all different strains on the OD growth experiments were performed after one additional day of pre-culturing. For this, 4 ml cultures were incubated in 6-well plates for 48 h with a start OD<sub>750</sub> of 0.5 in biological triplicates. To avoid loss of the volatile product valencene, cultures were overlaid with 20 % dodecane.

### 2.3. Biomass measurements (DCW, OD, spectra)

Optical density and whole cell spectra measurements were performed in the SpEcoRd 200 plus and diluted if necessary. To determine the cell dry weight (CDW) 2–3.5 ml cell culture was pelleted for 3 min at maximum speed. After washing the pellet with PBS buffer, the pellet was resuspended in ~50 µl water and transferred to a pre-weighed PCR tube, where it was dried at 60° overnight prior to weighing.

### 2.4. Microscopy

Cells were analyzed phenotypically using the bright field setting of a Zeiss AxioScope.A1, under 400-fold magnification.

### 2.5. Pigment quantification

0.2–0.5 ml of each culture was sampled after 48 h at the end of the growth experiment. The sample was centrifuged for 5 min at 14,000 g and 4 °C. The supernatant was discarded and the pellet resuspended in 100 µl water. The samples were frozen at –20 °C until further processing. 900 µl of 100% methanol was added and the sample was mixed by vortexing. After incubation with gentle shaking for 30 min at 4 °C, the sample was centrifuged at 14,000 g for 5 min. The supernatant was transferred to a cuvette and the absorbance spectrum was measured from 400 nm to 750 nm. The absorbance spectra were divided by the OD<sub>750</sub> or CDW and the amount of chlorophyll *a* in the sample was quantified by the absorbance maximum of chlorophyll *a* at 665 nm

( $A_{665\text{nm}}$ ) using following equation (Lichtenthaler and Buschmann, 2001):

$$2.6. \text{ Chlorophyll content } [\mu\text{g/ml}] = 12.66 \mu\text{g/ml} * A_{665 \text{ nm}}$$

The amount of carotenoids in the sample was quantified by the absorbance maximum of the sum of carotenoids at 470 nm ( $A_{470\text{nm}}$ ) and a correction term considering absorbance of chlorophyll *a* at 470 nm (*c* (Chl *a*): concentration of chlorophyll *a* in the sample) using the following equation:

$$\text{Carotenoid content } [\text{mg/ml}] = (1000 \mu\text{g/ml} * A_{470 \text{ nm}} - 1.91 * c (\text{Chl})) / 225.$$

### 2.7. RNA extraction & qRT-PCR

RNA extraction was performed according to (Pinto et al., 2009). Briefly, 0.2–1 ml cell culture was collected and pelleted for 3 min at maximum speed at 4 °C. After discarding the supernatant, the pellet was resuspended with 0.5 ml PGTX and incubated at 95 °C for 5 min. After cooling on ice, 350  $\mu\text{l}$  chloroform/isoamyl alcohol were added and the mixture was incubated shaking gently at room temperature for 10 min. To separate the aqueous from organic phases the mixture was centrifuged for 10 min at maximal speed at 4 °C. The upper phase was transferred to a fresh tube and 1 vol chloroform/isoamyl alcohol added. After repeating the centrifugation step the upper phase was again transferred and precipitated with 3 vol of 100 % ethanol sodium acetate at –20 °C overnight. The RNA was pelleted for 30 min at maximum speed and 4 °C, washed twice with 70% ethanol and resuspended in RNase-free water.

RNA was DNaseI-digested using commercial DNaseI from ThermoFisher (EN0525), according to the manufacturer's specifications. DNaseI-digested RNA was phenol/chloroform extracted again to remove the DNaseI.

For cDNA synthesis, the commercial RevertAid RT from ThermoFisher (K1621) was used according to the manufacturer's specifications.

qRT-PCR was performed using the DyNAmo ColorFlash SYBR™ Green qPCR-Kit (ThermoFisher, F416L), according to the manufacturer's specifications.

### 2.8. GC-MS for the quantification of volatile sesquiterpenoids

100  $\mu\text{L}$  dodecane overlay fractions were collected in micro inserts inside 1.5 mL clear glass GC vials. 2  $\mu\text{L}$  of the sample were diluted 1:50 in HPLC grade hexane (Th. Geyer GmbH, Germany) prior to injection. 1  $\mu\text{l}$  of the diluted was injected with an MPS autosampler with automatic liner exchange system in conjunction with a cold injection system (Gerstel) in splitless mode (ramping from 50 °C to 250 °C at 12 °C  $\text{s}^{-1}$ ) into the GC with a helium flow of 1  $\text{ml min}^{-1}$ . Chromatography was performed using a 7890B GC system (Agilent Technologies) with a HP-5MS column with (5%-phenyl)-methylpolysiloxane film (Agilent, 19091S-433, 30 m length, 0.25 mm internal diameter, 0.25  $\mu\text{m}$  film). The oven temperature was held constant at 70 °C for 2 min and then ramped at 12.5 °C  $\text{min}^{-1}$  to 320 °C at which it was held constant for 5 min; resulting in a total run time of 27 min. Metabolites were ionized with an electron impact source at –70 eV and 200 °C source temperature and recorded in a mass range of  $m/z$  60 to  $m/z$  800 at 20 scans per second with a 7200 GC-QTOF (Agilent Technologies) after a solvent delay time of 8 min. Compound identification was conducted via MassHunter Qualitative (v b08.00, Agilent Technologies) by comparison of mass spectra to the NIST14 Mass Spectral Library (<https://www.nist.gov/srd/nist-standard-reference-database-1a-v14>) and validated by retention time comparison with chemical reference substances (Sigma-Aldrich, #06808). Peaks were integrated using MassHunter Quantitative (v b08.00, Agilent Technologies). The concentration was determined via external calibration. The calibration curve was generated with 8 points from 0.1  $\mu\text{M}$  to 20  $\mu\text{M}$  with a quadratic curve fit and 1/ $x$

curve fit weight. After direct measurement of valencene in the dodecane layer, molar concentrations were calculated to mg valencene/L *Synechocystis* culture. To determine whether valencene was lost over time via evaporation or degradation, dodecane with 225  $\mu\text{M}$  valence was measured directly and compared to a dodecane layered cell culture with 225  $\mu\text{M}$  valence and cultivated for 48 h. Technical triplicates were cultured and measured, and there was no significant difference detected between the samples (Fig. S6).

### 2.9. Total protein isolation and Western Blot analysis

Total protein was extracted from cultured and induced *Synechocystis* cultures as described ([dx.doi.org/10.17504/protocols.io.ps6dnhe](https://doi.org/10.17504/protocols.io.ps6dnhe)). Protein concentration was determined according to Lowry et al. using a BSA standard. 20  $\mu\text{g}$  total protein was loaded on an SDS gel, transferred to a PVDF membrane, UV-crosslinked, and the presence of the IspA: CnVS fusion protein, as well as IspA only from the operon construct, was detected using a monoclonal anti-FLAG-M2-alkaline-phosphatase antibody (Sigma, A9469) as primary, and an anti-mouse antibody as the secondary antibody.

## 3. Results & discussion

The central terpenoid pathway in *Synechocystis* starts with IPP and DMAPP, which are derived from the MEP-pathway. A single gene, *crtE*, is responsible for the elongation of terpene precursors towards GPP, FPP, and GGPP (Fig. 1). Next to GGPP, another downstream metabolic product of FPP is squalene, which is converted to hopanoids.

In the following, we demonstrate various strategies to divert metabolic flux towards heterologous sesquiterpenes (Fig. 1, black components), effectively eliminating undesired side products (Fig. 1, gray components).

### 3.1. Modulating the internal precursor pool by genomic gene deletion of squalene synthase and squalene hopane cyclase

In order to divert metabolic flux away from undesired side products and towards farnesyl pyrophosphate (FPP), which is the central precursor for sesquiterpenes (Fig. 1), we applied two strategies. First, we performed markerless deletions of two genes, squalene synthase (*sll0513*, *sqs*), which is responsible for the conversion of FPP to the triterpene squalene, and the gene directly downstream, squalene hopane cyclase (*slr2089*, *shc*), which further converts squalene to hopanoids. A *shc* knock-out was previously performed in order to accumulate squalene, and a 70-fold increase was demonstrated using this deletion mutant (Englund et al., 2014). We hypothesize that an additional *sqs* deletion might lead to an accumulation in FPP in a similar manner. We further improved the initial strain design by performing markerless gene deletions, which are of special interest because resistance cassettes can be recycled, instead of being occupied indefinitely within the genome. Thereby, multiple different alterations in one strain are possible. Each markerless deletion was performed in two sequential steps as previously described (Viola et al., 2014); first, a CmR-sacB cassette, flanked by the neighboring genomic regions and including a partially overlapping fragment thereof, was introduced into wild type *Synechocystis*. By gradually selecting on higher chloramphenicol concentrations, complete genome segregation was achieved. In a second step, counter-selection of segregated clones on solid media containing sucrose, but no chloramphenicol, was carried out, thereby eliminating cells still carrying the CmR-sacB cassette and selecting for a second double-crossover event between the partial overlaps. The schematic genotype of the double mutant is shown in Fig. 2A.

To ensure complete deletion of both genes, the lack of transcripts was verified via qRT-PCR (Table S1) correctly segregated mutants were verified via colony PCR (Fig. S1A).

The fully segregated strain was then compared to the wild type strain

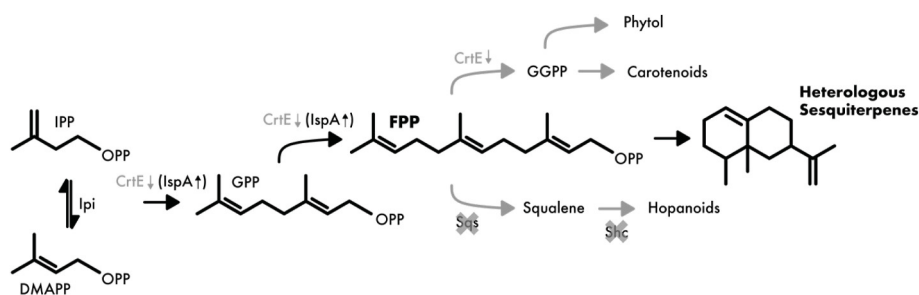


**Fig. 1.** Isoprene pathway from *Synechocystis* with optimizations done in this work. Abbreviations used: IPP = isopentenyl diphosphate; DMAPP = dimethylallyl diphosphate; GPP = geranyl diphosphate; FPP = farnesyl diphosphate; Ipi = isopentenyl diphosphate delta isomerase; CrtE = geranylgeranyl pyrophosphate synthase; Sqs = squalene synthase; Shc = squalene hopene cyclase; IspA = farnesyl diphosphate synthase. Crossed out target = gene deletion. Downward arrow = repression target. Upward arrow = overexpression/rescue.

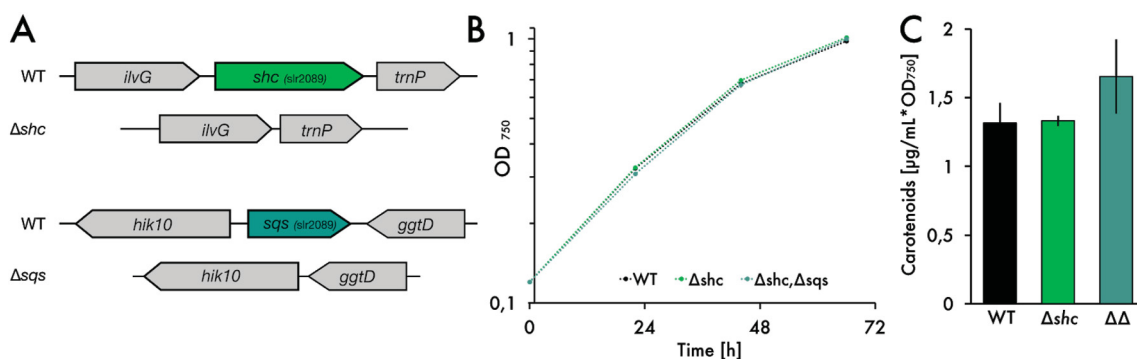


**Fig. 2.** Knockout strategy and growth/pigment analysis of mutants. A: Schematic overview of markerless mutant genotypes. B: Comparison of growth between wild type and mutants. C: Carotenoid content of the three different strains. Results represent the mean of three biological replicates. WT = wild type,  $\Delta shc$  = squalene-hopene-cyclase deletion,  $\Delta\Delta$  = squalene-hopene-cyclase and squalene synthase deletion.

in terms of growth and pigment composition. While there was no discernible difference in growth (Fig. 2B), the double mutant showed a visible shift in carotenoids (Fig. S1 C, D), suggesting an increase in metabolic flux towards the central carotenoid precursor, GGPP, which is derived from FPP (Fig. 1). Upon further investigation via pigment extraction, this observation was confirmed; the double mutant showed an increase in carotenoid content (Fig. 2C). Due to the previously described toxicity of FPP in *E. coli* (Dahl et al., 2013), an enrichment of this intermediate seems implausible and a further conversion to harmless carotenoids seems to be likely.

To test whether this increased carotenoid content could be translated to an increased FPP availability for sesquiterpene production, the wild type and mutant expressing valencene synthase (CnVS) from *Callitropsis nootkatensis* (Beekwilder et al., 2014) under the rhamnose-inducible promoter (Behle et al., 2020) (Fig. 3A) were cultured alongside in 6-well plates for two days. To avoid loss of the volatile product valencene, cultures were overlaid with 20 % dodecane. The dodecane layer was then sampled and quantified directly using GC-MS.

The identification of valencene in all strains was performed by comparing retention time and mass spectra with those of a commercial standard (Fig. S4). In Fig. 3B, the WT expressing CnVS as well as a negative control is shown in the extracted ion chromatogram (m/z 161.12) as an example.

Remarkably, the double mutant showed a ~40% increase in valencene production compared to the wild type (Fig. 3C). In contrast to before (Fig. 2C), the mutant now expressing CnVS did not show an increase in carotenoid content (Fig. 3D). In all likelihood, the excess precursor pool that was diverted towards carotenoid production before was now successfully used by CnVS. Due to the promising production increase in the mutant, we exclusively used the double knockout mutant background for the following experiments.

### 3.2. Enhancing the FPP precursor pool by conditional repression of the essential gene *crtE*

To further exploit the available carotenoid pool, we aimed at reducing the conversion of FPP to GGPP. In *Synechocystis*, a single gene, *crtE*, is responsible for the consecutive condensation of IPP and DMAPP to GPP, FPP and finally to GGPP (Lin et al., 2017), the precursor for diterpenoids, including the chlorophyll phytol tails, and tetraterpenoids, such as carotenoids (Fig. 1A). In contrast, genes from heterotrophic species, such as *ispA* from *E. coli*, only perform these conversions up until FPP (Reiling et al., 2004). Since GGPP-derived pigments are essential for cyanobacterial viability, we decided to reduce *crtE* expression via inducible, dCas9-based CRISPRi, and then introduce a heterologous FPP-synthase to increase the relative amount of FPP compared to GGPP.

We chose an sgRNA from a previously published work to target *crtE* (Yao et al., 2020), as well as the aTc-inducible dCas9 system from Yao et al. (2016) (Fig. 4A).

Interestingly, the qRT-PCR with *crtE*-specific oligonucleotides shows a repression down to <10 % of the wild type level at much lower inducer concentrations of 10 ng/mL aTc, despite a reported >90 % repression at concentrations as low as 100 ng/mL aTc. Notably, the uninduced *crtE*-repression strain already shows a 40 % reduction of gene expression compared to the wild type (Fig. 4B). Consistent with published results, induction with 100 ng/mL aTc shows almost complete repression of *crtE*. While the pigment composition of the uninduced strain resembles the wild type, an aTc-dependent effect on both chlorophyll and carotenoids can be observed (Fig. 2C). General pigmentation is severely affected at 100 ng/mL aTc, whereas only carotenoids are affected at 10 ng/mL aTc. This was further confirmed via pigment extraction (Fig. S2 A). In addition, a severe photoprotective phenotype, where the cells form aggregates, was observed at 100 ng/mL (Fig. 4D). This also occurred at 10 ng/mL aTc, but much less frequent and with smaller clumps (Fig. 4C). Interestingly, when culturing the strains in 6-well plates, OD<sub>750</sub> was almost not affected at all (Fig. S2 B).

It is possible that the slight phenotype observed at 10 ng/mL aTc

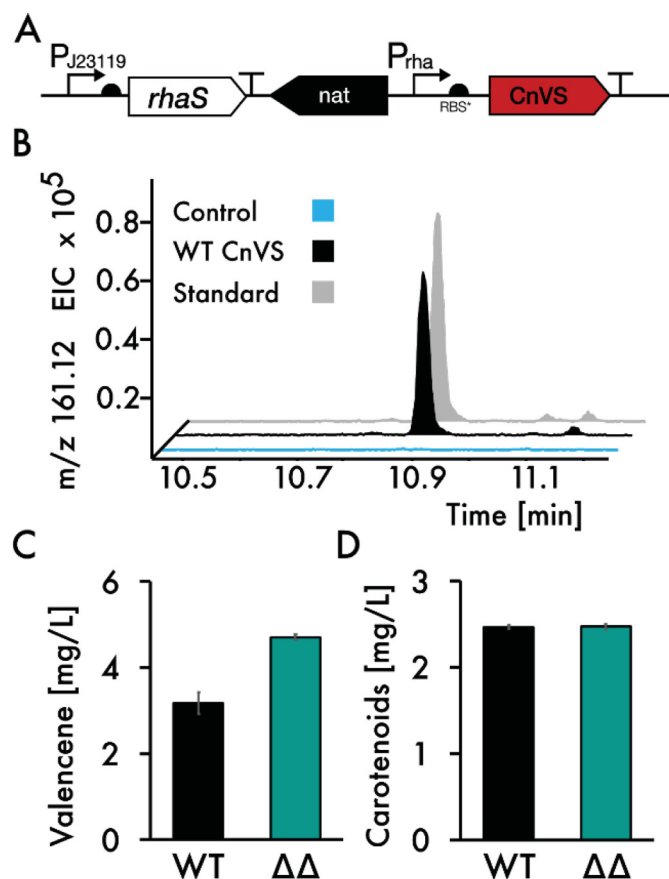


**Fig. 3.** Comparison of productivity between wild type and mutant. A: Construct overview. B: Detection of valencene by GC-MS analysis. Dodecane layer of the engineered *Synechocystis* strain (WT CnVS) after 48 h cultivation with 5  $\mu$ M rhamnose induction, compared with a standard (225  $\mu$ M) and the dodecane layer of the cultivated wild type strain (Extracted ion chromatogram, m/z 161.12). C: Valencene production in wild type (WT) and the  $\Delta$ shc/ $\Delta$ sqs mutant strain ( $\Delta\Delta$ ). D: Carotenoid content in wild type (WT) and the  $\Delta$ shc/ $\Delta$ sqs mutant strain ( $\Delta\Delta$ ). Results represent the mean of three biological replicates.

might become more severe over longer periods of time, since the expression levels appear to be saturated at the lowest concentration used. Likely, this is due to phenotypical changes taking longer than changes in expression. Another possibility is faster repression by higher aTc concentrations, resulting in a higher initial amount of CrE protein at 10 ng/mL aTc compared with 100 ng/mL, which would take longer to be diluted out via cell division. On the other hand, since aTc is light-sensitive, the effect is likely transient and cells may recover from both their phenotype and their carotenoid deficit. Since industrial applications rely on robust strains, ideally without the necessity of adding costly inducer compounds, further fine-tuning might be of interest to achieve a constitutively downregulated *crtE* gene, while still maintaining cell viability and productivity. Since the uninduced control already shows a noticeable decrease in expression, using a stronger promoter for the control of the CRISPRi system might already be sufficient.

Nonetheless, we were able to demonstrate that tuned down-regulation of *crtE* leads to a reduction of carotenoids, while maintaining almost wild type levels of chlorophyll, as well as a wild type-like performance in terms of cell growth, and that by applying this strategy, we likely were able to enhance precursor availability for heterologous biosynthetic pathways upon introduction of alternative prenyltransferases.

### 3.3. Exploiting the carotenoid pool for the production of valencene

Since the newly engineered *crtE* knock-down strain lacks GGPP, but also the desired FPP precursor, we introduced the heterologous *ispA* gene from *E. coli*, which is functionally homologous to *crtE*, but unable to produce GGPP (Reiling et al., 2004).

To favor conversion of IPP and DMAPP towards valencene, we applied two strategies. First, we generated an *ispA*-CnVS protein fusion construct with a GGGGS linker in between to strongly increase proximity between the two enzymes the linker was chosen because it showed the most promising results in previous works (Hu et al., 2017). Second, we cloned the same genes in an operon (Fig. 5A). In the operon case, the enzymes were able to retain their full functions, while still being translated from the same mRNA, thereby optimizing spatial and temporal proximity to each other without potential compromise of function. The constructs were designated *IspA*:CnVS-fus and *IspA*:CnVS-op, respectively. In all variants, heterologous genes were controlled by the strong inducible promoter,  $P_{rha}$ . Fig. 5A outlines the construct design. To verify the production of soluble protein, we included an N-terminal FLAG-tag upstream of *ispA*. Western Blot analysis confirmed the presence of both the chimeric protein in *ispA*:CnVS-fus, as well as *ispA* in *ispA*:CnVS-op (Fig. S3 A). We also included a control with only CnVS to quantify the performance of the enzyme on its own in each background strain.

Cultures were grown as described earlier, and dodecane fractions were sampled after 48 h, before quantifying OD<sub>750</sub> and density-adjusted spectra, as well as sampling for pigment extraction, quantification of dry cell weight (DCW).

As hypothesized, *crtE*-knockdown strains expressing only CnVS performed poorly in terms of valencene production. Induction of *crtE* repression via aTc led to a decrease in both valencene yield and carotenoids. This was expected, since all intermediates within the terpenoid pathway should be affected by a repression of *crtE*.

Coexpression of *ispA* and CnVS, both as an operon and a fusion protein, resulted in an increased amount of valencene. Especially in *IspA*:CnVS-op, production increased by about 3.5-fold compared to the strain expressing only CnVS. The increase in *IspA*:CnVS-fus was less apparent with a 1.7-fold change in valencene.

It is unclear at this point why the protein fusion construct had a smaller effect than the operon construct. Transcript analysis of *ispA* and CnVS in the two strains showed similar expression levels (Fig. S3 B); *ispA* was expressed slightly higher in the operon construct. It is therefore unlikely that different transcript levels play a role in metabolic output, although this might be a hint that it could be beneficial to find the correct balance of expression between all enzymes involved - higher levels of *ispA* lead to higher conversion of IPP and DMAPP toward FPP. The most likely reason for the poorer performance of the fusion protein is therefore a loss in efficiency due to impeded enzyme function or misfolding of the protein. Since other studies showed great promise in this area of research (Daletos and Stephanopoulos, 2020; Wang et al., 2021), it might therefore be interesting to further investigate different protein fusion constructs, for example by switching the order of the enzymes, as well as exploring different protein linkers. While the use of *ispA* in combination with CnVS was briefly described earlier (Matsudaira et al., 2020), we show that this combination of genetic components is even more productive in combination with metabolic engineering of the native pathways in *Synechocystis*, yielding improved levels of valencene. Strikingly, additional *crtE* repression of *ispA*-expressing strains with aTc further increased valencene titer up to 17.6 mg/L and 12.5 mg/L valencene. In contrast, the strains producing more valencene also show a noticeable reduction in carotenoid content, indicating that the pool of the precursors IPP and DMAPP, which are normally diverted towards carotenoid production are now available and successfully used as a substrate by CnVS. This is also consistent with earlier works, in which a common carotenoid precursor was diverted towards production of manoyl oxide (Englund et al., 2015). Surprisingly, despite the reduced

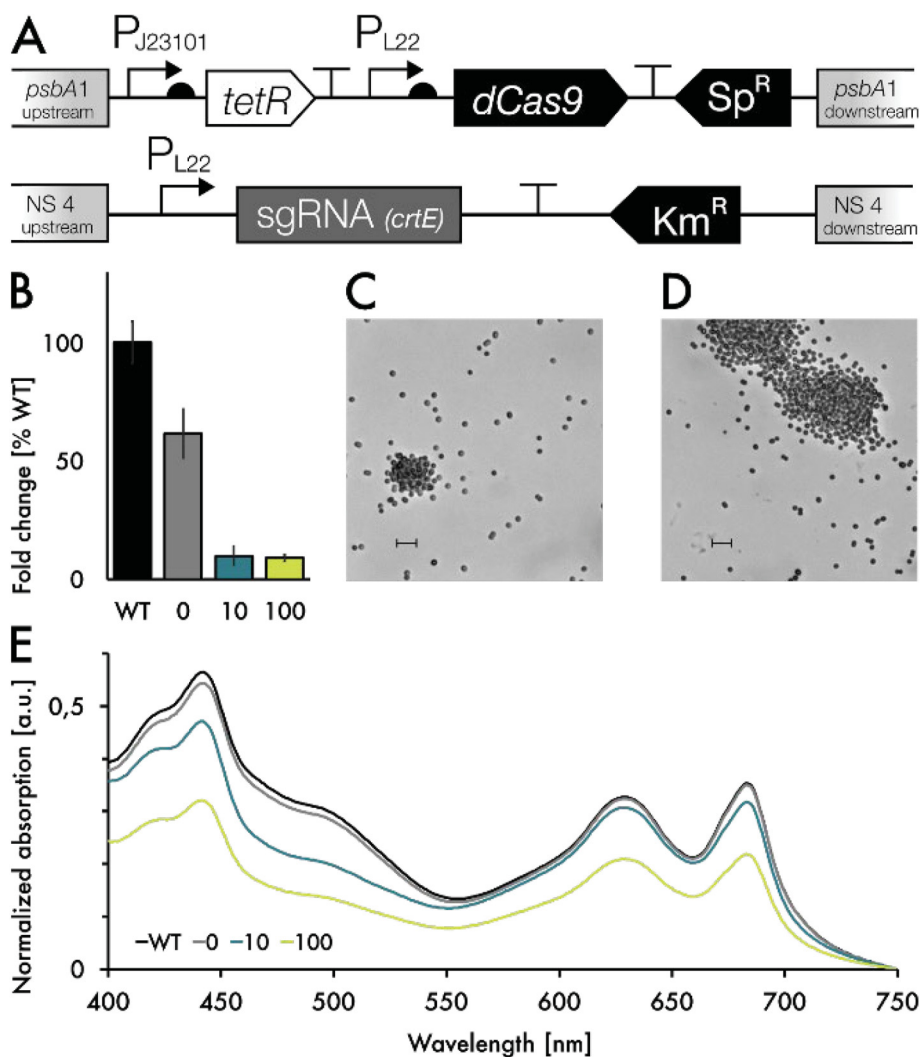


**Fig. 4.** CrtE gene repression in *Synechocystis*. A: Construct overview. B: CRISPRi knockdown of Geranylgeranyl pyrophosphate synthase (CrtE) using the PL22 promoter with 0, 10 and 100 ng/ml anhydrotetracycline (aTc). Transcripts measured by RT-qPCR after 24h of cultivation compared to the induced (100 ng/ml) control strain denoted as WT (containing only dCas9, but no sgRNA). Results represent the mean and standard deviation of three biological replicates and three technical replicates each. C/D: Bright field microscopy picture after 24 h cultivation of the strain with 10 ng/ml (C) or 100 ng/ml (D) aTc induction. Magnification  $\times 400$ , scale bar 10  $\mu\text{m}$ . E: Whole cell absorption spectra analysis. Cultures were adjusted for OD<sub>750</sub> prior for measurement and values were baseline corrected. CrtE reduction leads to a blueish culture color. (For interpretation of the references to color in this figure legend, the reader is referred to the Web version of this article.)

pigment content coupled with the metabolic burden of valencene production, the aTc-induced cells grew remarkably well, reaching an OD<sub>750</sub> of  $\sim 2.5$  compared to uninduced cells, which reached an OD<sub>750</sub> of  $\sim 3$  after 48 h. It is possible that aTc-mediated *crtE*-repression is, in fact, transient due to the light-sensitive properties of aTc, and that after an initial rerouting of the precursor pool towards valencene, the cell returns back to its initial balanced state. While *crtE* was expected to be an essential gene due to carotenoids being an essential part of light harvesting and photoprotection, it remains unclear at this point whether the effect is transient. Nevertheless, the decrease in carotenoid levels clearly shows the expected metabolic effect. It is therefore likely that the introduced genetic alterations function as hypothesized and that a majority of the terpenoid precursor pool is in fact diverted towards valencene production. However, the molar increase in valencene corresponds to roughly three times the amount of FPP that would be made available by the reduction of carotenoids alone. Since the phytol tail of chlorophyll is also derived from GGPP, this is likely partially responsible for the discrepancy. Furthermore, metabolic feedback regulation probably plays an important role, both within the isoprenoid biosynthetic pathway and the carotenoid pathway (Cazzonelli and Pogson, 2010). Since carotenoids are heavily involved in the response to light stress (Llewellyn et al., 2020; Steiger et al., 1999), reduced carotenoid content could lead to the accumulation of ROS, thereby possibly triggering increased flux towards GGPP.

It would be highly interesting to investigate valencene production over time in order to assess whether the generated strain produces stable

metabolic output over a longer amount of time, or whether the cell returns to its pigmented state. We therefore observed the behavior of the best-performing strain,  $\Delta\Delta crtE\downarrow$  IspA:CnVS-op + aTc, over five days. Three replicates were precultured in 30 mL BG11 in non-baffled flasks, induced with 5 mM L-rhamnose and 10 ng/mL aTc, overlaid with 3 mL dodecane, and observed over five days. Fig. S5 shows the volumetric daily production rates of the strain, as well as total valencene accumulation and OD<sub>750</sub>. While the cell density reaches a plateau after four days, valencene is continuously produced. There is a strong depletion of pigments in the production strain (Fig. S5B), both in carotenoid and chlorophyll content. Despite this strong phenotype, the cells appear to retain some level of productivity. However, the pigmentation, as well as the growth halt further indicates that the strain can be further optimized to regain some productivity likely lost due to the loss of photosynthetic efficiency.

The individual yields of each strain in terms of culture volume, dry cell weight (DCW), and cell density are summarized in Table 1.

#### 4. Conclusion & outlook

For the redirection of metabolic flux towards the heterologous production of terpenoids, in this case the sesquiterpene valencene, we identified the native carotenoid pool of *Synechocystis* as a major target. We were able to demonstrate the capability of *Synechocystis* to divert terpene precursors by I. Deletion of native metabolic pathways not essential to the central metabolism, markerless  $\Delta shc$  and  $\Delta sqs$ , II.

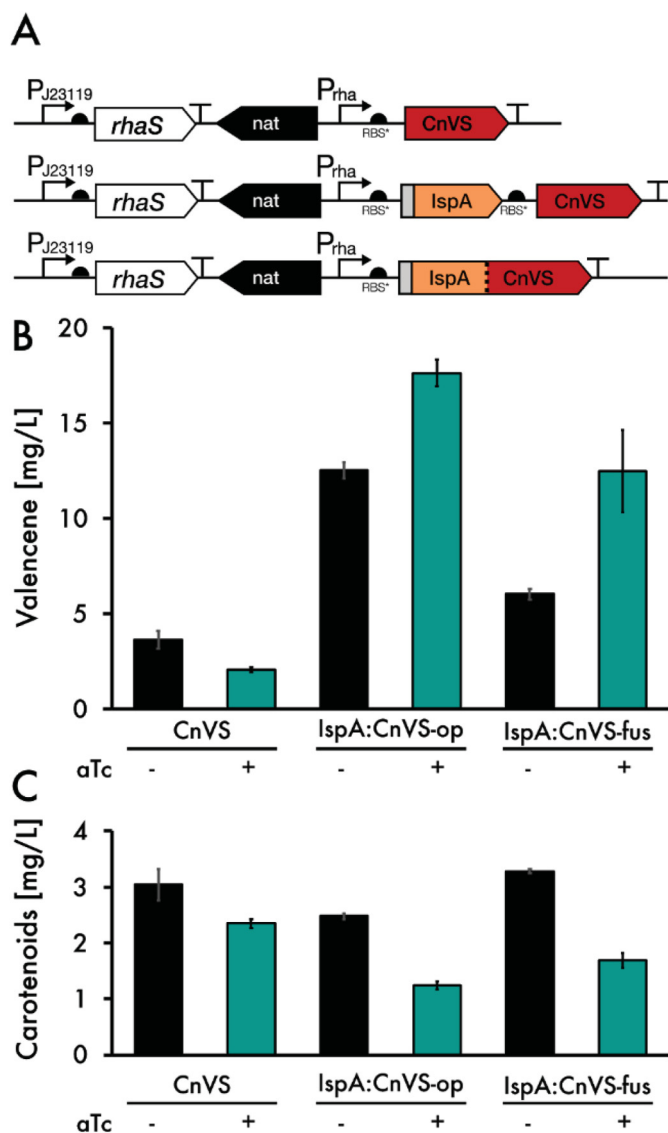


**Fig. 5.** Performance of the *crtE* repressed valence production. A: Construct overview. B: Valencene production in the CnVS, the CnVS-*ispA*-operon and CnVS-*ispA*-fusion strain. All strains are in the  $\Delta \Delta$  and *dCas9/CrtE* sgRNA background. + indicates the induction with 10 ng/ml aTc. Additionally, all strains were induced with 5 mM rhamnose. C: Carotenoid level of strains described. Results represent the mean and standard deviation of three biological replicates.

Conditional gene repression of a major component in the terpenoid pathway, *crtE*, and III. Introduction of heterologous enzymes, *ispA* and CnVS, with functions tailored to the specific production of our target molecule. With these strategies, we were able to successfully overcome some of the native pathway bottlenecks in cyanobacteria, while simultaneously exploiting their native ability of producing terpene compounds. Observing the best-producing strain over time also showed that there is even more potential towards optimization towards a more robust production strain. We believe that this delicate balance between cell viability in terms of conversion of light to energy, but also protection from light stress on the one hand, and improved productivity is an important step towards utilizing these photosynthetic organisms in a more continuous, industrial-scale application. Future studies of long-term effects of metabolic engineering of strains will certainly help improve engineering strategies towards industrially relevant utilization of cyanobacterial chassis.

Furthermore, valencene also serves as an intermediate, which can be

**Table 1**

Individual valencene production performance of strains investigated in this work. Downward arrow represents CRISPRi-mediated repression.  $\Delta \Delta$  represents the  $\Delta shc, \Delta sqs$  double mutant. All values shown represent the mean  $\pm$  the standard deviation of three biological replicates.

Strain	Genotype	Genes expressed from plasmid	Yield [mg/L]	Yield [mg/gDCW]	Yield [mg/OD <sub>750</sub> ]
WT	Non-motile wild type	-	n.d.	n.d.	n.d.
	Synechocystis sp. PCC 6803				
$\Delta shc, \Delta sqs$	$\Delta shc, \Delta sqs$	-	n.d.	n.d.	n.d.
$\Delta \Delta crtE \downarrow$	$\Delta shc, \Delta sqs, \Delta psbA1 :: crtE \downarrow$	-	n.d.	n.d.	n.d.
WT CnVS	-	CnVS	3.2 ± 0.25	4.5 ± 0.43	1.7 ± 0.13
$\Delta \Delta$ CnVS	$\Delta shc, \Delta sqs$	CnVS	4.7 ± 0.06	6.4 ± 0.52	2.4 ± 0.06
$\Delta \Delta crtE \downarrow$ CnVS-aTc	$\Delta shc, \Delta sqs, crtE \downarrow$	CnVS	3.6 ± 0.47	3.7 ± 0.42	1.5 ± 0.18
$\Delta \Delta crtE \downarrow$ CnVS + aTc	$\Delta shc, \Delta sqs, crtE \downarrow$	CnVS	2.0 ± 0.12	2.3 ± 0.18	0.9 ± 0.06
$\Delta \Delta crtE \downarrow$ CnVS-op-aTc	$\Delta shc, \Delta sqs, crtE \downarrow$	ispA, CnVS (operon)	12.5 ± 0.44	9.8 ± 0.54	3.9 ± 0.12
$\Delta \Delta crtE \downarrow$ CnVS-op + aTc	$\Delta shc, \Delta sqs, crtE \downarrow$	ispA, CnVS (operon)	17.6 ± 0.71	19.0 ± 0.62	7.1 ± 0.14
$\Delta \Delta crtE \downarrow$ CnVS-fus-aTc	$\Delta shc, \Delta sqs, crtE \downarrow$	ispA, CnVS (fusion)	6.0 ± 0.27	4.9 ± 0.25	1.9 ± 0.08
$\Delta \Delta crtE \downarrow$ CnVS-fus + aTc	$\Delta shc, \Delta sqs, crtE \downarrow$	ispA, CnVS (fusion)	12.5 ± 2.15	12.6 ± 2.18	5.0 ± 0.84

converted to nootkatone via cytochrome P450 enzymes (CYPs). CYPs that function as monooxygenases are found in many plant species, often membrane-bound and dependent on the availability of oxygen and NADPH. In terms of functionality, cyanobacteria might be especially suitable for the application of engineered CYPs: They already contain endogenous cytochromes P450, for which oxygen and NADPH are readily available via photosynthetic activity, while this can be a limiting factor in heterotrophs.

## Funding

This project was financially supported by the CLIB-Competence Centre Biotechnology (CKB) funded by the European Regional Development Fund ERDF (34.EFRE-0300096).

## Declaration of competing interest

The authors declare that they have no known competing financial interests or personal relationships that could have appeared to influence the work reported in this paper.

## Author statement

Maximilian Dietsch: Conceptualization, Investigation, Methodology, Writing - Original Draft, Writing - Review & Editing, Visualization, Data Curation. Anna Behle: Conceptualization, Investigation, Writing - Original Draft, Writing - Review & Editing, Visualization, Data Curation. Philipp Westhoff: Methodology, Data Curation. Ilka M. Axmann: Supervision, Writing - Reviewing and Editing.

## Acknowledgements

Metabolite analyses were supported by the CEPLAS Plant

Metabolism and Metabolomics laboratory, which is funded by the Deutsche Forschungsgemeinschaft (DFG, German Research Foundation) under Germany's Excellence Strategy – EXC-2048/1 – project ID 390686111. We acknowledge the excellent technical assistance by E. Klemp for GC-MS measurements.

We appreciate the help of Thomas Drepper, Oliver Klaus and Arsenij Kokorin with discussion and technical advice.

We thank Paul Hudson for providing us with the dCas9 plasmid, Nicolas Schmelling for critical comments on the manuscript, Dennis Dienst for helpful advice on cultivation issues and Jungho Lee for providing us with the Nourseothricin resistance gene.

## Appendix A. Supplementary data

Supplementary data to this article can be found online at <https://doi.org/10.1016/j.mec.2021.e00178>.

## References

- Albertsen, L., Chen, Y., Bach, L.S., Rattleff, S., Maury, J., Brix, S., Nielsen, J., Mortensen, U.H., 2011. Diversion of flux toward sesquiterpene production in *Saccharomyces cerevisiae* by fusion of host and heterologous enzymes. *Appl. Environ. Microbiol.* 77, 1033–1040.
- Angermayr, S.A., Gorchs Rovira, A., Hellingwerf, K.J., 2015. Metabolic engineering of cyanobacteria for the synthesis of commodity products. *Trends Biotechnol.* 33, 352–361.
- Beekwilder, J., van Houwelingen, A., Cankar, K., van Dijk, A.D.J., de Jong, R.M., Stoop, G., Bouwmeester, H., Achkar, J., Sonke, T., Bosch, D., 2014. Valencene synthase from the heartwood of Nootka cypress (*Callitropsis nootkatensis*) for biotechnological production of valencene. *Plant Biotechnol. J.* 12, 174–182.
- Behle, A., Saake, P., Germann, A.T., Dienst, D., Axmann, I.M., 2020. Comparative dose–response analysis of inducible promoters in cyanobacteria. *ACS Synth. Biol.* 9, 843–855.
- Cazzonelli, C.I., Pogson, B.J., 2010. Source to sink: regulation of carotenoid biosynthesis in plants. *Trends Plant Sci.* 15, 266–274.
- Chen, H., Zhu, C., Zhu, M., Xiong, J., Ma, H., Zhuo, M., Li, S., 2019. High production of valencene in *Saccharomyces cerevisiae* through metabolic engineering. *Microb. Cell Factories* 18, 195.
- Dahl, R.H., Zhang, F., Alonso-Gutierrez, J., Baidoo, E., Batth, T.S., Redding-Johanson, A.M., Petzold, C.J., Mukhopadhyay, A., Lee, T.S., Adams, P.D., et al., 2013. Engineering dynamic pathway regulation using stress-response promoters. *Nat. Biotechnol.* 31, 1039–1046.
- Daletos, G., Stephanopoulos, G., 2020. Protein engineering strategies for microbial production of isoprenoids. *Metab. Eng. Commun.* 11, e00129.
- Dienst, D., Wichmann, J., Mantovani, O., Rodrigues, J.S., Lindberg, P., 2020. High density cultivation for efficient sesquiterpenoid biosynthesis in *Synechocystis* sp. PCC 6803. *Sci. Rep.* 10, 5932.
- Englund, E., Pattanaik, B., Ubhayasekera, S.J.K., Stensjö, K., Bergquist, J., Lindberg, P., 2014. Production of squalene in *Synechocystis* sp. PCC 6803. *PLoS One* 9, e90270.
- Englund, E., Andersen-Ranberg, J., Miao, R., Hamberger, B., Lindberg, P., 2015. Metabolic engineering of *Synechocystis* sp. PCC 6803 for production of the plant diterpenoid manoyl oxide. *ACS Synth. Biol.* 4, 1270–1278.
- Hu, Y., Zhou, Y.J., Bao, J., Huang, L., Nielsen, J., Krivoruchko, A., 2017. Metabolic engineering of *Saccharomyces cerevisiae* for production of germacrene A, a precursor of beta-elemene. *J. Ind. Microbiol. Biotechnol.* 44, 1065–1072.
- Jodlbauer, J., Rohr, T., Spadiut, O., Mihovilovic, M.D., Rudroff, F., 2021. Biocatalysis in green and blue: cyanobacteria. *Trends Biotechnol.*, S0167779920303346
- Lee, J., Rai, P.K., Jeon, Y.J., Kim, K.-H., Kwon, E.E., 2017. The role of algae and cyanobacteria in the production and release of odorants in water. *Environ. Pollut.* 227, 252–262.
- Lee, J., Hilgers, F., Loeschke, A., Jaeger, K.-E., Feldbrügge, M., 2020. *Ustilago maydis* serves as a novel production host for the synthesis of plant and fungal sesquiterpenoids. *Front. Microbiol.* 11, 1655.
- Lichtenthaler, H.K., Buschmann, C., 2001. Chlorophylls and carotenoids: measurement and characterization by UV-VIS spectroscopy. *Curr. Protoc. Food Anal. Chem.* 1, F4.3.1–F4.3.8.
- Lin, P.-C., Saha, R., Zhang, F., Pakrasi, H.B., 2017. Metabolic engineering of the pentose phosphate pathway for enhanced limonene production in the cyanobacterium *Synechocystis* sp. PCC 6803. *Sci. Rep.* 7.
- Liu, Y., Cruz-Morales, P., Zargar, A., Belcher, M.S., Pang, B., Englund, E., Dan, Q., Yin, K., Keasling, J.D., 2021. Biofuels for a sustainable future. *Cell*, S0092867421000957.
- Llewellyn, C.A., Airs, R.L., Farnham, G., Greig, C., 2020. Synthesis, regulation and degradation of carotenoids under low level UV-B radiation in the filamentous cyanobacterium *Chlorogloeopsis fritschii* PCC 6912. *Front. Microbiol.* 11, 163.
- Loeschke, A., Dienst, D., Wewer, V., Hage-Hülsmann, J., Dietsch, M., Kranz-Finger, S., Hüren, V., Metzger, S., Urlacher, V.B., Gigolashvili, T., et al., 2017. The photosynthetic bacteria *Rhodobacter capsulatus* and *Synechocystis* sp. PCC 6803 as new hosts for cyclic plant triterpene biosynthesis. *PLoS One* 12, e0189816.
- Matsudaira, A., Hoshino, Y., Uesaka, K., Takatani, N., Omata, T., Usuda, Y., 2020. Production of glutamate and stereospecific flavors, (S)-linalool and (+)-valencene, by *Synechocystis* sp. PCC6803. *J. Biosci. Bioeng.* 130, 464–470.
- Newman, J.D., Marshall, J., Chang, M., Nowroozi, F., Paradise, E., Pitera, D., Newman, K.L., Keasling, J.D., 2006. High-level production of amorpha-4,11-diene in a two-phase partitioning bioreactor of metabolically engineered *Escherichia coli*. *Biotechnol. Bioeng.* 95, 684–691.
- Pinto, F., Thapper, A., Sontheim, W., Lindblad, P., 2009. Analysis of current and alternative phenol based RNA extraction methodologies for cyanobacteria. *BMC Mol. Biol.* 10, 79.
- Rabeharindranto, H., Castaño-Cerezo, S., Lautier, T., Garcia-Alles, L.F., Treitz, C., Tholey, A., Truan, G., 2019. Enzyme-fusion strategies for redirecting and improving carotenoid synthesis in *S. cerevisiae*. *Metab. Eng. Commun.* 8, e00086.
- Reiling, K.K., Yoshikuni, Y., Martin, V.J.J., Newman, J., Bohlmann, J., Keasling, J.D., 2004. Mono and diterpene production in *Escherichia coli*. *Biotechnol. Bioeng.* 87, 200–212.
- Stanier, R.Y., Deruelles, J., Rippka, R., Herdman, M., Waterbury, J.B., 1979. Generic assignments, strain histories and properties of pure cultures of cyanobacteria. *Microbiology* 111, 1–61.
- Steiger, S., Schäfer, L., Sandmann, G., 1999. High-light-dependent upregulation of carotenoids and their antioxidative properties in the cyanobacterium *Synechocystis* PCC 6803. *J. Photochem. Photobiol., B* 52, 14–18.
- Tsuruta, H., Paddon, C.J., Eng, D., Lenihan, J.R., Horning, T., Anthony, L.C., Regentin, R., Keasling, J.D., Renninger, N.S., Newman, J.D., 2009. High-level production of amorpha-4,11-diene, a precursor of the antimalarial agent artemisinin, in *Escherichia coli*. *PLoS One* 4, e4489.
- Viola, S., Rühle, T., Leister, D., 2014. A single vector-based strategy for marker-less gene replacement in *Synechocystis* sp. PCC 6803. *Microb. Cell Factories* 13, 4.
- Wang, X., Pereira, J.H., Tsutakawa, S., Fang, X., Adams, P.D., Mukhopadhyay, A., Lee, T.S., 2021. Efficient production of oxidized terpenoids via engineering fusion proteins of terpene synthase and cytochrome P450. *Metab. Eng.* 64, 41–51.
- Yao, L., Cengic, I., Anfelt, J., Hudson, E.P., 2016. Multiple gene repression in cyanobacteria using CRISPRi. *ACS Synth. Biol.* 5, 207–212.
- Yao, L., Shabestary, K., Björk, S.M., Asplund-Samuelsson, J., Joensson, H.N., Jahn, M., Hudson, E.P., 2020. Pooled CRISPRi screening of the cyanobacterium *Synechocystis* sp. PCC 6803 for enhanced industrial phenotypes. *Nat. Commun.* 11, 1666.

# Metabolic engineering of *Synechocystis* sp. PCC 6803 for the photoproduction of the sesquiterpene valencene

Maximilian Dietsch<sup>1\*</sup>, Anna Behle<sup>1\*</sup>, Philipp Westhoff<sup>2</sup>, Ilka M. Axmann<sup>1</sup>

<sup>1</sup>Institute for Synthetic Microbiology, Department of Biology, Heinrich Heine University Düsseldorf, Düsseldorf, Germany.

<sup>2</sup>Plant Metabolism and Metabolomics Laboratory, Cluster of Excellence on Plant Sciences (CEPLAS), Heinrich Heine University Düsseldorf, D-40001 Düsseldorf, Germany

\*These authors contributed equally to this work

## Supporting Information

Fig. S1: Supplementary information on the markerless mutants  $\Delta shc$  and  $\Delta shc, \Delta sqs$ .

Fig. S2: Pigment quantification and growth behavior of the *crtE* knock-down strain.

Fig. S3: Western Blot and qRT-PCR analysis of IspA:CnVS fusion vs. operon strains.

Fig. S4: Mass spectra comparison of samples with reference

Fig. S5: Physiological changes and valencene production in  $\Delta\Delta crtE \downarrow$  IspA:CnVS-op +aTc.

Fig. S6: Quantification of possible valencene loss via evaporation or degradation

Supplementary Table S1: Cq values for *shc* and *sqs* in WT and knock-out strains.

Supplementary Table S2: Detailed descriptions and sequences of all relevant genetic modules used in this work.

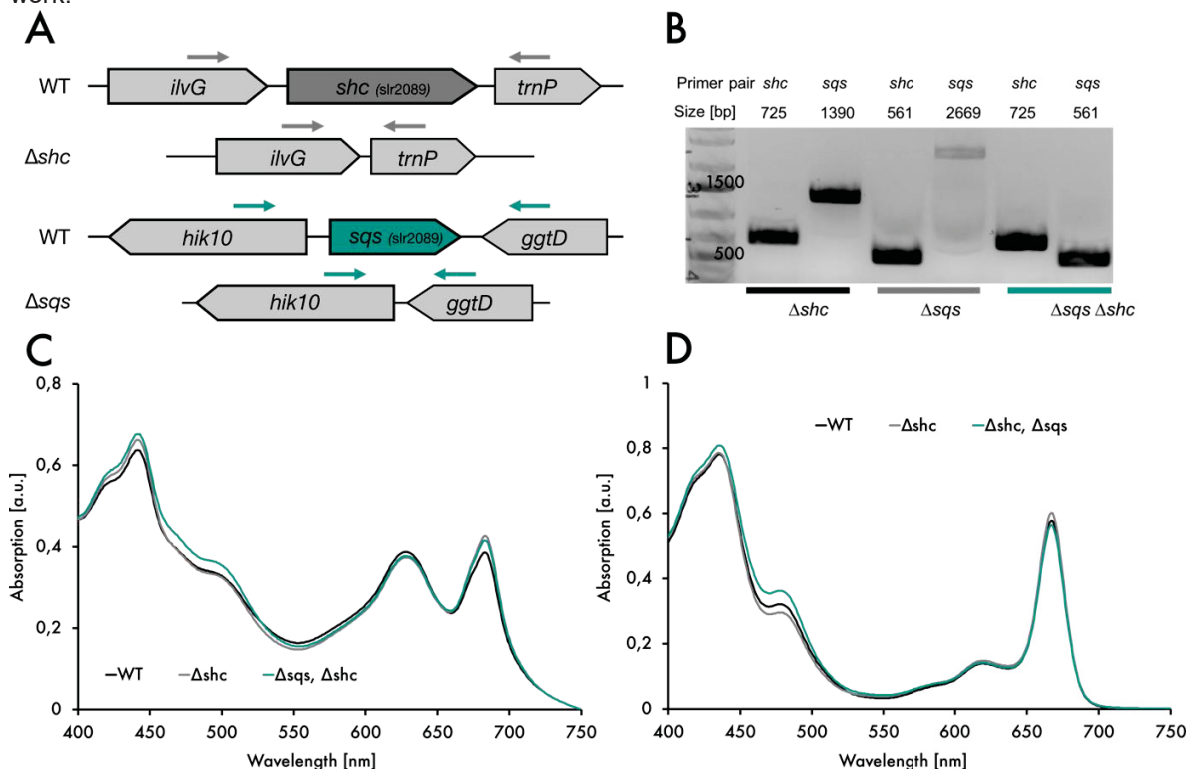


Fig. S1: Supplementary information on the markerless mutants  $\Delta shc$  and  $\Delta shc, \Delta sqs$ .

A: Schematic overview of markerless mutant genotypes. Arrows denote primers used for colony PCR.

B: PCR analysis of single and double mutant strains using oligonucleotides that bind outside of the affected area. Primer pair and expected sizes are shown above. Thermo 1kb+ ladder was used as size standard. C: Whole cell spectra of WT,  $\Delta shc$  and double mutant. Spectra were baseline-corrected by subtracting the absorption at 750 nm. D: Spectra of methanol-extracted cells from WT,  $\Delta shc$  and double mutant strains.

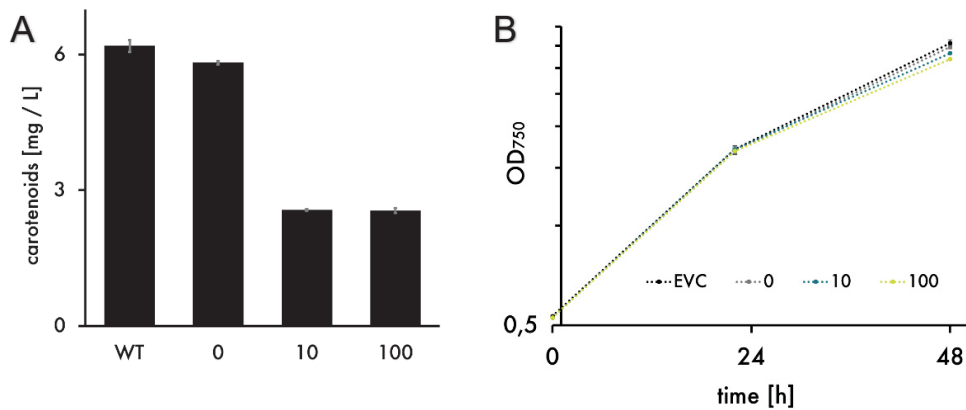
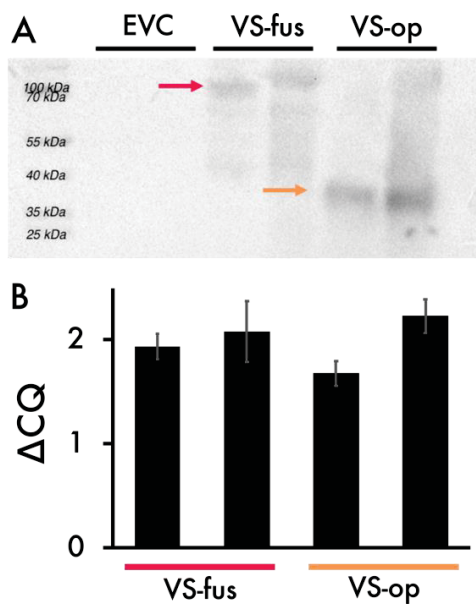


Fig. S2: Pigment quantification and growth behavior of the *crtE* knock-down strain.

A: Carotenoid content of  $\Delta shc$ ,  $\Delta sqs$  mutant expressing dCas9 only (WT) compared to  $\Delta shc$ ,  $\Delta sqs$  mutant expressing both dCas9 and the *crtE* sgRNA, induced with 0, 10, and 100 ng/mL aTc. Carotenoids were quantified as described in Material & Methods, section 2.5. B: Growth behavior of aforementioned strains.



Primers *ispA* *CnVS* *ispA* *CnVS*

Fig. S3: Western Blot and qRT-PCR analysis of IspA:CnVS fusion vs. operon strains. A: Western Blot analysis of IspA:CnVS protein fusion (VS-fus) and IspA:CnVS operon (VS-op). The fusion protein N-FLAG-IspA-CnVS corresponds to a size of ~105 kDa, while N-FLAG-IspA in the operon construct corresponds to about ~35 kDa. B:  $\Delta CQ$  values of qRT-PCR performed on both strains using either *ispA* or *CnVS* primers, as denoted below.  $\Delta CQ$  values were calculated by subtracting the CQ value of the housekeeping gene *rnpB* from each CQ value. A higher  $\Delta CQ$  value corresponds to a lower transcript amount.

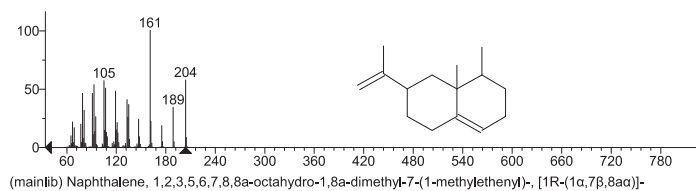
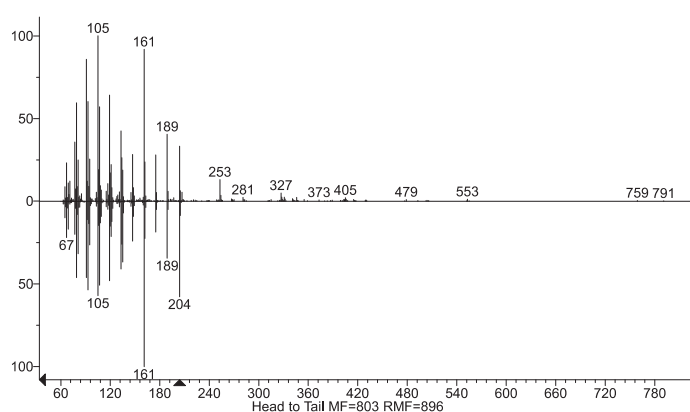
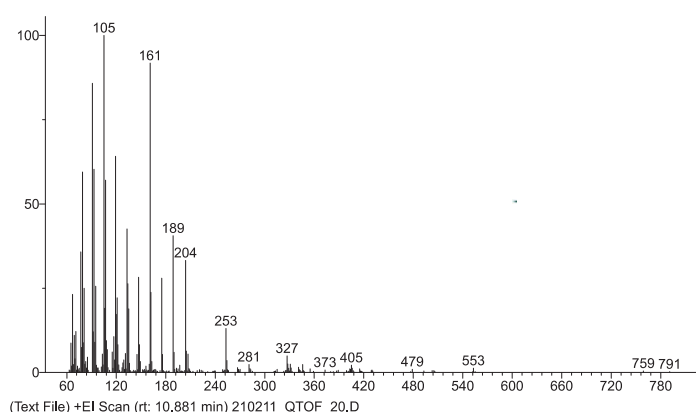


Fig. S4: Mass spectra comparison of samples with reference.  
 Top: Mass spectra of wild type expressing CnVS. Bottom: Reference mass spectra of (+)-valencene. Middle: Direct comparison of top and bottom spectra.

Table S1: Cq values for *shc* and *sqs* in WT and knock-out strains.  
 Values represent the mean and standard deviation of three biological replicates. Cq values were obtained via qRT-PCR. Sample values above 30 were defined as not containing any template.

Strain	Target gene	Cq value
Wild type	<i>sqs</i>	21.2 ± 0.3
	<i>shc</i>	21.8 ± 0.2
$\Delta shc$	<i>sqs</i>	21.1 ± 0.2
	<i>shc</i>	33.4 ± 0.6
$\Delta shc; \Delta sqs$	<i>sqs</i>	31.5 ± 0.8
	<i>shc</i>	35.5 ± 1.2
No template control	<i>sqs</i>	34.4
	<i>shc</i>	n. def.

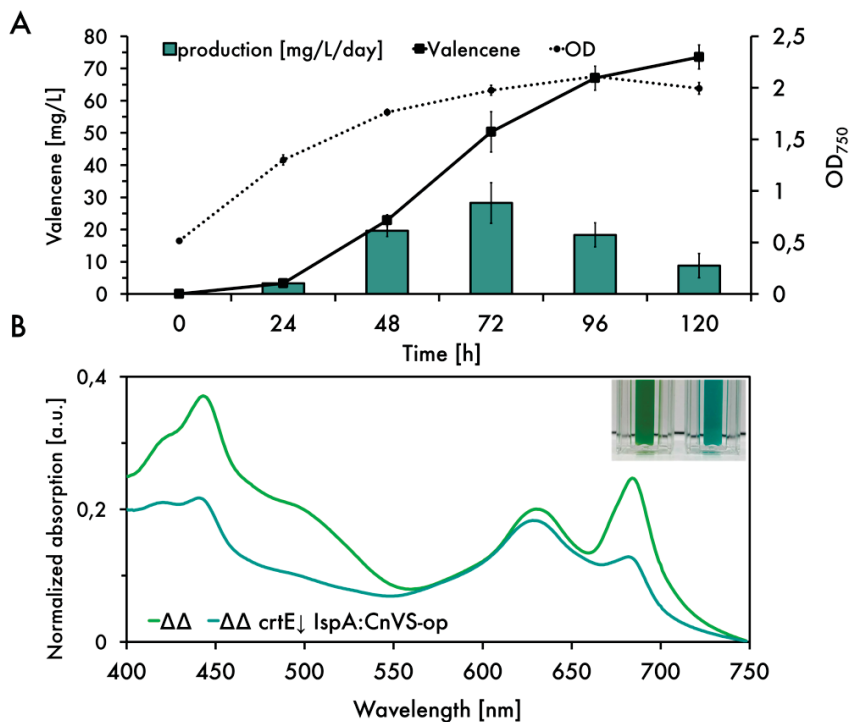


Fig. S1: Physiological changes and valencene production in  $\Delta\Delta crtE\downarrow IspA:CnVS-op +aTc$ . The strain was cultured in biological triplicates over five days in shake flasks overlaid with 10% dodecane. The dodecane layer, as well as the culture, were sampled daily for valencene quantification and cell density ( $OD_{750}$ ), respectively. A: Volumetric accumulation of valencene (square symbols, continuous line) and cell density (round symbols, dotted line). The volumetric production per day is shown as blue bars, corrected for the sample removed each day. B: Whole cell spectra of double mutant (green) and  $\Delta\Delta crtE\downarrow IspA:CnVS-op +aTc$  (blue) after 120 h cultivation. Spectra were baseline-corrected by subtracting the absorption at 750 nm. An image of the cuvettes is embedded for better visualization of the color difference (left: double mutant, right:  $\Delta\Delta crtE\downarrow IspA:CnVS-op +aTc$ ).

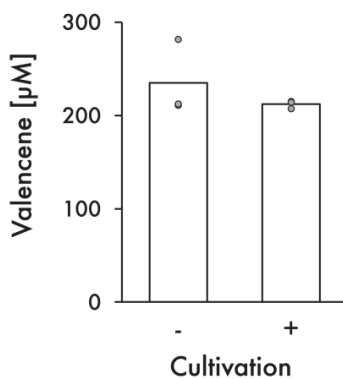


Fig. S2: Quantification of possible valencene loss via evaporation or degradation. A dodecane sample containing 225  $\mu M$  valencene was used to overlay a *Synechocystis* wild type culture, which was grown for 48 h in technical triplicates. Both the initial sample (-) and the sample recovered from the culture (+) was measured and compared. The bars represent the mean of the three technical replicates, each of which is shown in grey. No significant difference was observed (t-test,  $P=0.39$ ).



## Supplementary References

Behle, Anna, Pia Saake, Anna T. Germann, Dennis Dienst, und Ilka M. Axmann. „Comparative Dose–Response Analysis of Inducible Promoters in Cyanobacteria“. *ACS Synthetic Biology* 9, Nr. 4 (17. April 2020): 843–55. <https://doi.org/10.1021/acssynbio.9b00505>.

Hu, Yating, Yongjin J. Zhou, Jichen Bao, Luqi Huang, Jens Nielsen, und Anastasia Krivoruchko. „Metabolic Engineering of *Saccharomyces Cerevisiae* for Production of Germacrene A, a Precursor of Beta-Elemene“. *Journal of Industrial Microbiology & Biotechnology* 44, Nr. 7 (Juli 2017): 1065–72. <https://doi.org/10.1007/s10295-017-1934-z>.

Wiegard, Anika, Anja K. Dörrich, Hans-Tobias Deinzer, Christian Beck, Annegret Wilde, Julia Holtzendorff, und Ilka M. Axmann. „Biochemical Analysis of Three Putative KaiC Clock Proteins from *Synechocystis* Sp. PCC 6803 Suggests Their Functional Divergence“. *Microbiology* 159, Nr. Pt\_5 (1. Mai 2013): 948–58. <https://doi.org/10.1099/mic.0.065425-0>.

Yao, Lun, Kiyun Shabestary, Sara M. Björk, Johannes Asplund-Samuelsson, Haakan N. Joensson, Michael Jahn, und Elton P. Hudson. „Pooled CRISPRi Screening of the Cyanobacterium *Synechocystis* Sp PCC 6803 for Enhanced Industrial Phenotypes“. *Nature Communications* 11, Nr. 1 (Dezember 2020): 1666. <https://doi.org/10.1038/s41467-020-15491-7>.

## 4 Manuscript III

### 4.1 Author's contributions

Anna Behle\*, Maximilian Dietsch\*, Louis Goldschmidt, Wandana Murugathas, David Brandt, Tobias Busche, Jörn Kalinowski, Oliver Ebenhöf, Ilka M. Axmann, Rainer Machné "Uncoupling of the Diurnal Growth Program by Artificial Genome Relaxation in *Synechocystis* sp. PCC 6803," Aug. 2021. Submitted to bioRxiv, doi: 10.1101/2021.07.26.453758

Submitted to Nucleic Acids Research, in revision

\* Shared first authorship.

M.D: Conceptualization, Investigation, Methodology, Writing – Original Draft, Writing – Review & Editing, Data Curation. A.B: Conceptualization, Investigation, Methodology Writing – Original Draft, Writing – Review & Editing, Data Curation. P.W: Methodology, Data Curation. L.G: Methodology, Visualization, Software, Data Curation. W.M: Investigation. D.B: Investigation. T.B: Investigation, Data Curation, Formal Analysis. J.K: Supervision, Resources. O.E: Supervision, Writing – Original Draft, Writing – Review & Editing, Resources, Funding acquisition. I.M.A: Supervision, Writing – Original Draft, Writing – Reviewing and Editing, Resources. R.M: Conceptualization, Methodology, Software, Validation, Formal Analysis, Data Curation, Writing – Original Draft, Writing – Review & Editing, Visualization, Supervision, Project Administration, Funding acquisition.

Study design: 30%

Experimental contribution: 30%

Data analysis: 10%

Manuscript preparation: 10%

## 4.2 Uncoupling of the Diurnal Growth Program by Artificial Genome Relaxation in *Synechocystis* sp. PCC 6803

# Uncoupling of the Diurnal Growth Program by Artificial Genome Relaxation in *Synechocystis* sp. PCC 6803

Anna Behle<sup>1,2,\*</sup>, Maximilian Dietsch<sup>1,\*</sup>, Louis Goldschmidt<sup>3</sup>, Wandana Murugathas<sup>1</sup>, David Brandt<sup>4</sup>, Tobias Busche<sup>4</sup>, Jörn Kalinowski<sup>4</sup>, Oliver Ebenhöf<sup>3</sup>, Ilka M. Axmann<sup>1</sup>, Rainer Machne<sup>1,3,#</sup>

1: Institut f. Synthetische Mikrobiologie, Heinrich-Heine Universität Düsseldorf, Universitätsstrasse 1, 40225 Düsseldorf, Germany,

2: Photanol B.V, Science Park 406, 1098 XH Amsterdam, The Netherlands

3: Institut f. Quantitative u. Theoretische Biologie, Heinrich-Heine Universität Düsseldorf, Universitätsstrasse 1, 40225 Düsseldorf, Germany

4: Centrum für Biotechnologie (CeBiTec), Universität Bielefeld, Universitätsstrasse 27, 33615 Bielefeld, Germany

\* AB and MD contributed equally, # correspondance to RM, machne@hhu.de

## Abstract

In cyanobacteria DNA supercoiling varies over the diurnal light/dark cycle and is integrated with temporal programs of transcription and replication. We manipulated DNA supercoiling in *Synechocystis* sp. PCC 6803 by CRISPRi-based knock-down of gyrase subunits and overexpression of topoisomerase I (TopoI), and characterized the phenotypes. Cell division was blocked, most likely due to inhibition of genomic but not plasmid DNA replication. Cell growth continued to 4-5x of the wildtype cell volume, and metabolic flux was redirected towards glycogen in the TopoI overexpression strain. TopoI induction initially lead to down-regulation of GC-rich and up-regulation of AT-rich genes. The response quickly bifurcated and four diurnal co-expression cohorts (dawn, noon, dusk and night) all responded differently, in part with a circadian ( $\approx 24$  h) pattern. A GC-rich region  $\sim 50$  bp of transcription start sites is differentially enriched in these four cohorts. We suggest a model where energy- and gyrase-gated transcription of growth genes at the dark/light transition (dawn) generates DNA supercoiling which then facilitates DNA replication and initiates the diurnal transcriptome program.

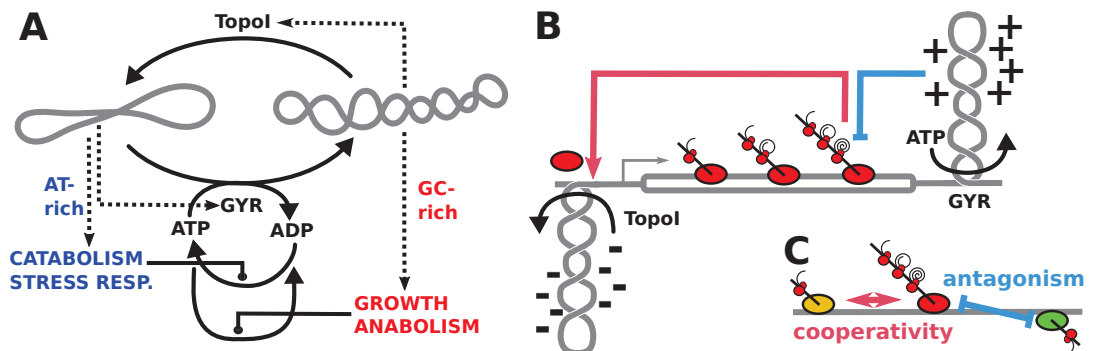


**Figure 1. DNA Supercoiling & Transcription: Homeostasis and *Twin-Domain* Models.** **A:** Global homeostasis of supercoiling by direct feedback on expression of topoisomerases (GYR: Gyrase holoenzyme; TopoI: topoisomerase I) and GC-rich anabolic/growth genes and AT-rich catabolic and stress-response genes. **B:** Transcription-dependent supercoiling downstream (positive) and upstream (negative) of an RNA or DNA polymerase, widely known as the *twin-domain* model. Gyrase-activity downstream can prevent polymerase stalling and induce transcriptional bursts while Topoisomerase I activity upstream prevents R-loop formation. **C:** The torsional stress exerted by transcription can lead to long-distance cooperative and antagonistic effects, and gene order on the chromosome can underlie temporal programs of gene expression.

## Introduction

*In vivo*, the DNA double helix exists in a torsionally strained and underwound state, often denoted as “negative DNA supercoiling”. A homeostatic feedback system of DNA supercoiling is coupled to differential expression of large gene groups in many different bacterial species [1, 2, 3, 4, 5, 6]. The general picture (Fig. 1A) is that DNA supercoiling is high during times of high metabolic flux, such as during exponential growth, and required to express rRNA and GC-rich growth genes and allow for DNA replication [7]. The ATP/ADP ratio has direct effects on DNA supercoiling [8, 9, 10]. Supercoiling would allow an analog modulation of transcription factor and polymerase binding [11] and thereby qualifies as a potential mechanism for the long known and recently re-discovered monotonous relation of rRNA and growth gene expression with growth rate [12, 13, 14]. However, the relation of RNA transcription and DNA replication to DNA supercoiling is mutual and complex [7]. According to the twin-domain model of transcription-dependent supercoiling (Fig. 1B), negative supercoiling accumulates upstream and positive supercoiling downstream of polymerases [15], leading to cooperative and antagonistic long-range effects between transcription loci [16] (Fig. 1C). Strong transcriptional activity requires downstream activity of gyrase to set the elongation rate and avoid polymerase stalling [17, 18, 19] and upstream activity of topoisomerase I (TopoI) to avoid R-loop formation and genome instability [20, 21]. Such cooperative long-range effects can underpin temporal expression programs; locally in the *leu* operon [22, 23] and globally as a spatio-temporal gradient along origin-terminus axis of the *Escherichia coli* (*E. coli*) genome [24].

In cyanobacteria, this system forms an integral part of the diurnal (light/dark cycles) changes in metabolism and transcription, and is integrated with the output of the cyanobacterial circadian clock [25, 3]. Supercoiling of chloroplast genomes, the endosymbiotic descendants of cyanobacteria, was observed to fluctuate with the diurnal light/dark (LD) cycle [26], and plants encode for gyrase enzymes [27]. Cyanobacteria themselves traverse through a well defined transcriptional program during diurnal LD cycles in several species [28, 29, 30, 31]. Mori and Johnson first suggested [32] that diurnal DNA supercoiling may be involved in the genome-wide nature of diurnal transcription in cyanobacteria. Genome compaction was found to fluctuate with LD cycles in *Synechococcus elongatus* PCC 7942 [33], and an endogenous plasmid showed diurnal fluctuations of DNA supercoiling [25]. The temporal transcriptome program during entrained circadian cycles correlated with plasmid supercoiling states and depended on gyrase activity [3]. In *Synechocystis* sp. PCC 6803 (hereafter abbreviated as *Synechocystis*), cold, heat and salt stress all lead to similar changes in the transcriptome and all were enhanced by treatment with the gyrase inhibitor novobiocin (NB) [4]. Gene groups with coherent response to stress and NB overlapped significantly with diurnal co-expression cohorts [34]. Supercoiling of the endogenous plasmid pCA2.4\_M increased within 30 min after the transition to light phase, and continuously decreased during 12 h and further during a prolonged 24 h dark phase [35]<sup>1</sup>.

In this work, we manipulate DNA supercoiling in *Synechocystis* by inducible overexpression [36] and CRISPRi-based knock-down [37] of the key genes involved in modulation of supercoiling: topoisomerase I (gene: *topA*), and gyrase (subunit genes: *gyrA* and *gyrB*). We can confirm both, the homeostasis and transcription-dependent supercoiling models in *Synechocystis*. All manipulations that should decrease supercoiling lead to a strong pleiotropic phenotype, where cell division is blocked but cell volume growth continues. Especially *topA* over-expression induces overflow metabolism and glycogen production, and uncouples the diurnal transcription program. Metabolism and transcriptome appear to be locked in a state between late night and early day.

## Results and Discussion

### Artificial Genome Relaxation Blocks Division but not Growth

**Manipulation of Gyrase and Topoisomerase Expression.** To study DNA supercoiling in *Synechocystis*, we used the dCas9-mediated CRISPR-interference system [37] to repress (knock-down) transcription of topoisomerase I (gene *topA*, slr2058), and gyrase subunits *gyrA* (slr0417) and *gyrB* (slr2005), or *gyrA* and *gyrB*

<sup>1</sup>\*\*\* ref. [35] is a preprint by our group at bioRxiv: <https://doi.org/10.1101/2021.07.26.453679> \*\*\*

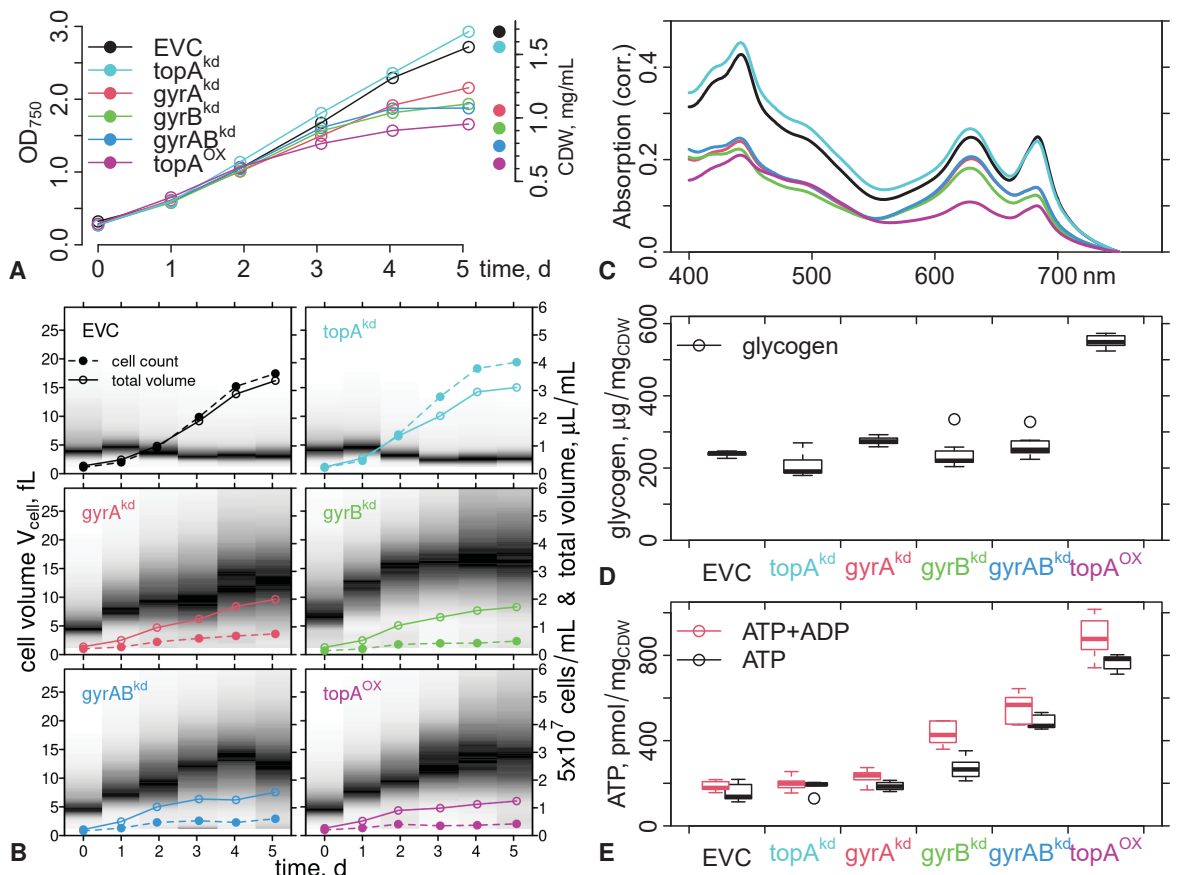


**Figure 2. Batch Culture Endpoint Measurements.** Overexpression and knock-down strains of this study where grown for 5 days in BG11 medium supplemented with all required antibiotics, and all inducers for the plasmid constructs in each experiment (100 ng/mL aTc, 1 mM L-rhamnose). **A:** The optical density at 750 nm ( $OD_{750}$ ) was measured daily and cell dry weight (CDW) determined directly after the last measurement on day 5. **B:** The cell volume distribution was measured daily in the CASY cell counter and plotted as a gray-scale gradient (black: more cells at this volume). **C:** Absorption spectra after the harvest on day 5. See Figure S1B for spectra at inoculation time. The absorption at 750 nm was subtracted from each spectrum. **D:** Glycogen content at harvest time was determined by a colorimetric assay after harvest, and boxplots of 18 technical replicates (3 samples, each measured 3x in 2 assays) are shown. **E:** ATP and ATP+ADP contents at harvest time were determined by a luciferase-based assay, and boxplots of six technical replicates (3 samples and 2 measurements) are shown.

simultaneously, yielding strains named  $\langle \text{gene} \rangle^{\text{KD}}$ . Additionally, we constructed a tunable expression plasmid pSNDY [36] where a copy of the native *Synechocystis topA* is under the control of a rhamnose-inducible promoter, strain  $\text{topA}^{\text{OX}}$  (Tab. S1). All six strains were induced with anhydro-tetracycline (aTc) and rhamnose and cultured for five days, then harvested for quantification of cell dry weight, ATP, glycogen, and plasmid supercoiling. Reverse transcription quantitative PCR (RT-qPCR) verified the functionality of our inducible genetic constructs (Fig. S1A). All knockdown strains showed an abundance reduction to 8%–15% of the wild-type level, and *topA* induction was  $\approx 30$  fold. We also measured all three transcripts in all strains and observed compensatory upregulation and downregulation of the non-manipulated supercoiling enzymes, a first verification of the homeostatic control model in *Synechocystis*.

47  
48  
49  
50  
51  
52  
53  
54  
55

**Cell Volume Growth, Adenosine and Glycogen Content.** Initially, all cultures showed comparable growth (Fig. 2A). After three days all strains except topA<sup>KD</sup> grew slower than the EVC; and topA<sup>OX</sup> showed the strongest growth defect. The cell dry weight (CDW) at harvest time correlated with the final OD<sub>750</sub> of the cultures (Fig. 2A), but was relatively higher for the EVC and topA<sup>KD</sup> strains. Cell volume distributions of the EVC and topA<sup>KD</sup> strains showed a transient small increase ( $\approx 10\%$ ) on the first day of cultivation and were stable thereafter (Fig. 2B). In contrast, cell volumes of the gyr<sup>kd</sup> and topA<sup>OX</sup> strains increased over time, from 4 fL–5 fL to 12 fL–15 fL after four days of cultivation. Total cell numbers increased only slightly. Thus, strains where gyrase subunits were knocked down or topoisomerase I overexpressed showed inhibition of cell division but not of cell growth. Pigmentation was strongly affected. Cultures of the topA<sup>OX</sup> strain appeared pale and gyr<sup>kd</sup> strains blue, compared to their uninduced state and to EVC. Absorption spectra (Fig. 2C, S1B) confirmed an overall decrease of all pigments in topA<sup>OX</sup>. The gyr<sup>kd</sup> strains showed a stronger decrease at chlorophyll-specific wavelengths than at phycocyanin-specific wavelengths, explaining their blue appearance.

All knock-down strains showed glycogen levels similar to the EVC, with 25 % of the total CDW (Fig. 2D), which is consistent with literature values for the wild type [38]. In contrast, topA<sup>OX</sup> showed more than twice as much glycogen with 55 % of CDW. Values of up to 60 % are reported for nitrogen-starved cells [39, 40]. The topA<sup>OX</sup> strain accumulated more than four times as much ATP+ADP as the EVC (Fig. 2E). gyrB<sup>kd</sup> and gyrAB<sup>kd</sup> accumulated about twice as much ATP+ADP as the EVC; topA<sup>KD</sup> and gyrA<sup>kd</sup> showed no difference to the EVC control. Thus, the strains repressing the ATPase subunit of gyrase, gyrB<sup>kd</sup> and gyrAB<sup>kd</sup>, had slightly elevated levels of ATP+ADP.

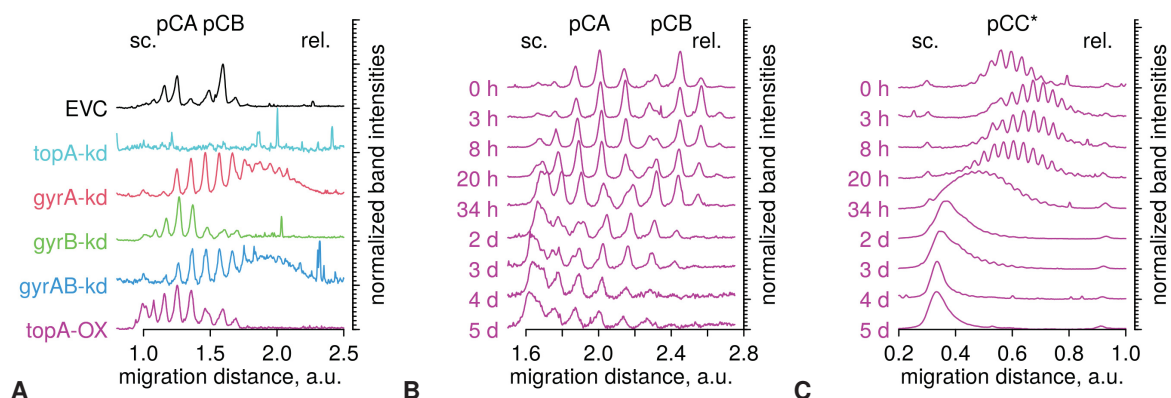


**Figure 3. Plasmid Supercoiling.** **A:** Baseline-corrected electropherograms from CQ agarose gels (Fig. S1D) of samples from the cultures shown in Figure 2, taken at harvest time (5 d). At  $20 \mu\text{g mL}^{-1}$  CQ, originally (*in vivo*) more relaxed (rel.) plasmids migrate further (higher migration distance) than more negatively supercoiled (sc.) plasmids [35]<sup>2\*\*\*</sup>. Two distinct plasmid topoisomer distributions can be distinguished in the EVC, and we assume the less far migrated bands to correspond to the longer plasmid pCA2.4\_M, and the further migrated bands to the shorter plasmid pCB2.4\_M. **B:** same as (A) but samples taken as a time series from the topA<sup>OX</sup> strain, induced with rhamnose at 0 d (Fig. S2). **C:** as (B) but for a population of topoisomers from a larger plasmid which could be separated by running the gel longer than the gel analyzed in (A). We tentatively assign these bands to the endogenous plasmid pCC5.2\_M, based on its relative migration distance.

**Plasmid Hyper-Supercoiling in the topA<sup>OX</sup> Strain.** Agarose gel electrophoresis in the presence of chloroquine (CQ) was used to analyze plasmid supercoiling at harvest time (5 d) of the batch cultures, and interpreted as outlined previously [35]<sup>2</sup>. The gels show three sets of topoisomer bands (Fig. S1D). These likely stem from the three annotated small plasmids of *Synechocystis*, pCA2.4\_M, pCB2.4\_M and pCC5.2\_M. Electropherograms of the two smaller plasmids indicate that only strains gyrA<sup>kd</sup> and gyrAB<sup>kd</sup> showed plasmid relaxation (Fig. 3A). In the gyrB<sup>kd</sup> and topA<sup>OX</sup> strains plasmids appeared to have a higher level of DNA supercoiling. We could not extract plasmids from the topA<sup>KD</sup> strain. Increased plasmid supercoiling in topA<sup>OX</sup> could result

<sup>2\*\*\*</sup> ref. [35] is a preprint by our group at bioRxiv: <https://doi.org/10.1101/2021.07.26.453679> \*\*\*

from a long-term adaptation and compensatory up-regulation of gyrase subunits. We thus tested plasmid supercoiling as a time series after inoculation in fresh medium with and without the inducer (Fig. S2). The gel run time was increased to also separate topoisomers of pCC5.2\_M. All three plasmids were more relaxed (less negative supercoiling) after 3 h of growth (Fig. 3B,C). Already after 8 h the trend had reversed, and at 20 h plasmids were more supercoiled than at time 0 h and in the uninduced control time series (Fig. S2E). Then plasmids became further supercoiled to an extent where topoisomers were not separable anymore.

**Reduction of rRNA Abundances in  $gyr^{kd}$  Strains.** To test effects on transcription, we selected three strains,  $gyrA^{kd}$ ,  $gyrB^{kd}$  and  $topA^{OX}$ , and the EVC for RNA-seq analysis. Strains were grown in triplicate and harvested for flow cytometry, RNA extraction and RNA-seq analysis 5 d after induction and 3 d after a culture dilution step (Fig. S3A). Flow cytometry confirms the growth phenotype (Fig. 4A, S4): forward scatter (FSC) was increased in all strains, and most in  $topA^{OX}$ . Side scatter (SSC) additionally revealed two cell populations in  $topA^{OX}$  which could reflect 8-shaped cells in division. Total nucleic acid content increased with cell size. Total RNA composition and the relative abundances of rRNA and mRNA were analyzed by capillary gel electrophoresis (Fig. S3B,C, S5). Ribosomal RNA species were strongly reduced in the  $gyrA^{kd}$  and  $gyrB^{kd}$  strains and less reduced in  $topA^{OX}$  (Fig. 4B), except for the 600 bp fragment of the 23S rRNA (Fig. S6C).

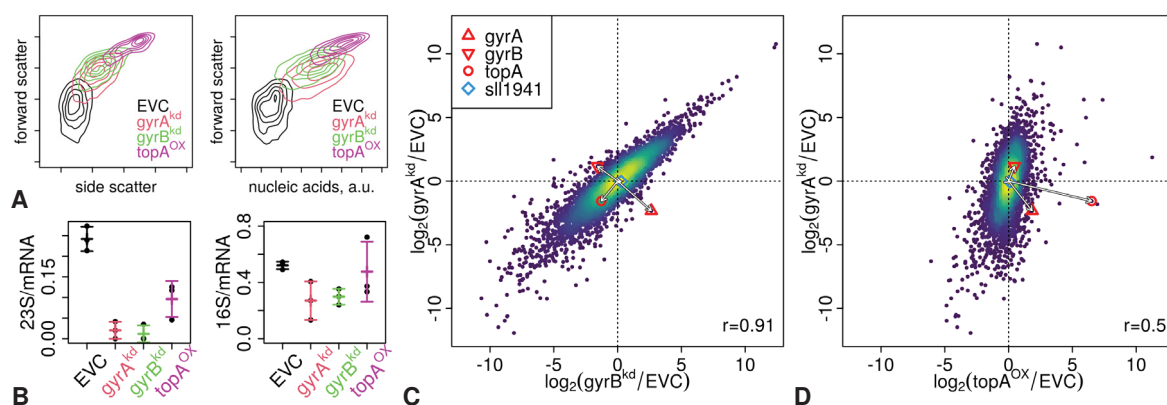


**Figure 4. rRNA and mRNA Abundances in Induced Strains.** **A:** Flow Cytometry confirms the cell growth phenotype. The natural logarithms of forward scatter, side scatter and nucleic acid stain Syto9 were calculated and 2D distributions plotted as contour plots; see Figure S4 for all data and details. **B:** Relative abundances of the unfragmented 23S (B) and the 16S (C) rRNA species were calculated from the electropherograms of capillary gel electrophoresis of extracted RNA (Fig. S5). Figure S6 shows all rRNA species. Mean and standard deviation of the three replicates are indicated as error bars. **C & D:** Relative expression changes of coding genes were derived as the  $\log_2$  ratio of RPKM normalized read-counts in the induced over-expression or knock-down strains to values in the control strain (EVC) and compared between the three different strains by 2D histograms (yellow: highest and purple: lowest local density of genes). The Pearson correlations ( $r$ ) are indicated in the bottom right corner. **C:**  $gyrA^{kd}$  (y-axis) vs.  $gyrB^{kd}$  (x-axis) strains. **D:**  $gyrA^{kd}$  (y-axis) vs.  $topA^{OX}$  (x-axis). The induction/repression and the homeostatic responses of  $gyrA$ ,  $gyrB$  and  $topA$  are highlighted by arrows from the origin to indicate the direction of change. The gene *sll1941* is a homolog or paralog of  $gyrA$  (blue diamond) and its transcript showed no response in either experiment.

**Consistent Changes in mRNA Abundances & Homeostatic Regulation of Supercoiling Enzymes.** The same RNA samples were further processed (rRNA species depleted) and sequenced on the Illumina platform, and transcript abundances relative to the EVC evaluated with DESeq2 [41]. All strains showed overall similar expression changes, but the extent was lower in  $topA^{OX}$  (Fig. 4C,D). However, this difference could also just reflect normalization effects by the decreased rRNA content in the gyrase knock-downs. In all strains the targeted manipulation was still observable at harvest times (arrows in Fig. 4C,D), *i.e.*,  $gyrA$  transcripts

were reduced in  $gyrA^{kd}$ ,  $gyrB$  transcripts in  $gyrB^{kd}$  and  $topA$  transcripts were increased in  $topA^{OX}$ . The non-manipulated genes showed the compensatory response expected from homeostatic regulation, *i.e.*,  $topA$  was repressed in both  $gyr^{kd}$  strains, and all non-manipulated gyrase subunits were induced in all experiments. In contrast, the  $sll1941$  gene, annotated either as a second gyrase A subunit or as the topoisomerase IV ParC subunit, showed no response in either experiment.

## Overexpression of $topA$ Uncouples Diurnal Co-expression Cohorts

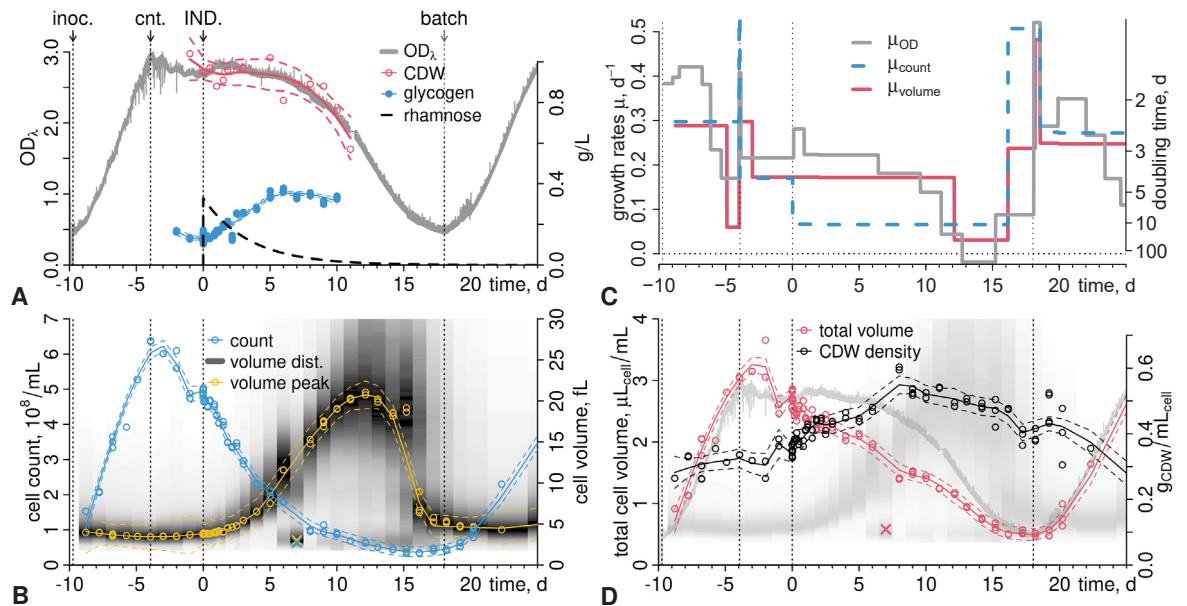


**Figure 5. Pulsed Induction in Continuous Culture.** **A:** Photobioreactor growth of the  $topA^{OX}$  strain (1 L BG11 medium, 0.5%  $\text{CO}_2$ , illumination  $\approx 90 \mu\text{mol m}^{-2} \text{s}^{-1}$  per  $\text{OD}_{750}$ ). Optical density was recorded online ( $\text{OD}_\lambda$ ) and post-calibrated to offline  $\text{OD}_{750}$ . The arrows indicate *inoc.*: inoculation; *cnt.*: onset of continuous culture (rate  $\phi = 0.01 \text{ h}^{-1}$ ); *IND.*: induction of  $topA$  by pulse-addition of rhamnose to 2 mM ( $0.33 \text{ g L}^{-1}$ ) at time 0; and *batch*: switch-off of dilution. The dashed black line is the theoretical wash-out curve of rhamnose ( $\text{g L}^{-1}$ ). Cell dry weight (CDW,  $\text{g L}^{-1}$ , red) and glycogen content ( $\text{g L}^{-1}$ , blue) of the culture were measured at the indicated times (points), and LOESS regressions are shown (solid lines) with 95% confidence intervals (dashed lines). **B:** Cell numbers (blue points) and volume distributions (gray scale) were recorded daily, and at higher resolution after induction, with the CASY cell counter. The peaks of the cell volume distributions are shown as yellow points. LOESS regressions with 95% confidence intervals are shown as lines. One outlier of the CASY measurement (x) was due to cell lysis during a washing step and was not included for regression. **C:** growth rates  $\mu$  were calculated by local (piecewise) linear regressions of the  $\text{OD}_\lambda$  (A), and cell count (B) and total cell volume (D) measurements and subtraction of the culture dilution rate (Fig. S9). **D:** The total cell volume ( $V_{total}$ ) was calculated by integrating the single cell volume distributions in (B), and the CDW density was calculated by dividing the  $\text{OD}_\lambda$  signal, calibrated to the CDW measurements (A, Fig. S8C), by  $V_{total}$ .

**Transient Increase in Cell Volume and Density.** To study the dynamic response to transient  $topA$  induction, the  $topA^{OX}$  strain was grown in a Lambda Minifor bioreactor (Fig. S7) with continuous (online) monitoring of turbidity ( $\text{OD}_\lambda$ , Fig. S8A,B). Continuous culture dilution was initiated at  $\text{OD}_\lambda \approx 2.9$  and with dilution rate  $\phi \approx 0.24 \text{ d}^{-1}$ . The culture stabilized around  $\text{OD}_\lambda \approx 2.7$ . Notably a subtle  $\approx 24 \text{ h}$  pattern of  $\text{OD}_\lambda$  was observed in both, batch and pre-induction continuous growth phases. Then rhamnose was injected to 2 mM to induce overexpression of  $topA$ . The  $topA$  transcript was upregulated to  $\approx 45$ -fold over the pre-induction

level within 4 h, as measured by RT-qPCR and confirmed by RNA-seq (Fig. S11) and decreased slowly over the course of the experiment. The  $OD_{\lambda}$  initially increased for 1 d post-induction, then slowly decreased. Cell dry weight (CDW) measurements were noisy but matched the  $OD_{\lambda}$  signal over the sampled period (Fig. 5A, S8C). In contrast, cell numbers started to decrease immediately, and cell volumes increased (Fig. 5B). We calculated growth rates of  $OD_{\lambda}$ , cell numbers and the total cell volume (Fig. 5C, S9). Cell division was not completely blocked but severely reduced to a division time of  $\approx 10$  d ( $\mu_{\text{count}} \approx 0.07 \text{ d}^{-1}$ ). Total cell volume growth was much less affected and remained stable ( $\mu_{\text{volume}} \approx 0.18 \text{ d}^{-1}$ ) throughout continuous culture operation until 12 d post-induction. Thus, artificial *topA* overexpression blocked cell division but not cell volume growth.  $OD_{\lambda}$  growth remained highest ( $\mu_{OD} \approx 0.23 \text{ d}^{-1}$ ) and stable over the first 5 d–6 d. In parallel, glycogen content increased to about 35%–40% of the CDW (Fig. 5A). We further noticed that sampled cells started to sediment much faster, indicating increased intracellular density. By calibrating the  $OD_{\lambda}$  signal to the CDW measurements (Fig. S8C) and dividing by the total cell volume we can estimate a CDW density and this value also increased over time from 0.3 to 0.5  $\text{g}_{\text{DCW}}/\text{mL}_{\text{cell}}$  (Fig. 5D). This range is consistent with data from *E. coli* [42, 43]. However, the CDW per  $OD_{750}$  was relatively lower for the enlarged strains in the endpoint measurement (Fig. 2A), and thus, the calibration to  $OD_{\lambda}$  may overestimate true CDW density. The enlarged cells also became increasingly fragile: in the CASY cell counter data a small population of varying intensity appeared at  $<2$  fL. This peak was highest at 7 d (outlier x in Fig. 5B), where cells were lysed during centrifugation in a washing step. The washing step was skipped thereafter, and the peak of small cells (dead or fragmented) remained small but increased towards the end of the continuous culture.

Maximal cell volumes  $>20$  fL were reached 10 d–15 d post-induction. From day 14 a population of smaller cells,  $\approx 7.5$  fL, appeared. On 16 d this population was the majority, and cell volume further decreased to 5 fL. Cell pigmentation recovered and the culture appeared greener again. We then switched off dilution, and the culture resumed growth, although at lower growth rates than pre-induction.

**Upregulation of Plasmid & Growth Genes, Downregulation of Photosynthesis Genes.** Samples for total RNA analysis and RNA-seq were taken 1 d and 0.5 h before induction, and then over the next 25 d in decreasing temporal resolution to roughly capture three time-scales of the response. Coding gene transcript abundances were calculated, the resulting time series clustered (Fig. 6A, S12), clusters sorted along significant overlaps with diurnal cohorts (Fig. 6C), and functional annotation enrichments (CyanoBase “categories”: Fig. 6B, S14A; gene ontology: Fig. S15) calculated. Cluster 2 (red) comprises the majority of the ribosomal protein category, enzymes of RNA and DNA synthesis, amino acid biosynthesis and the ATP synthase. Transcript abundances increased slightly over the three days after induction, with a notable circadian ( $\approx 24$  h) pattern. Cluster 3 (yellow) comprises the majority of photosynthesis-related genes, including the two photosystems. Its transcript abundances decreased continuously. The remaining clusters showed less clear functional profiles. Clusters 1 (green) and 4 (blue) were enriched in genes with unknown function, and cluster 4 strongly enriched with transposase genes. Gene Ontology analysis additionally shows enrichments with 7 of 8 genes annotated with “DNA polymerase activity” and 60 “DNA binding” proteins (Fig. S15). Both clusters 1 and 4 showed decreased transcript abundances on the first day post-induction, then only cluster 4 increased steeply. Cluster 1 transcripts showed a subtle circadian pattern, peaking anti-phase to cluster 2 transcripts. Cluster 6 (cyan) showed a similar profile to cluster 4 and comprises transcripts that showed the strongest abundance increase. Both clusters 4 and 6, were strongly enriched for plasmid-encoded genes (Fig. S16), and both also contained significant fractions of the ribosomal protein category. Cluster 5 (gray) showed decreased abundances but had the least change over time, was slightly enriched with “hypothetical”, “Hydrogenase” and “plasma membrane” gene annotations.

**Clusters Reflect Co-expression Cohorts.** Next, we compared the time series clustering from *topA*<sup>OX</sup> and the endpoint transcript abundances from the *topA*<sup>OX</sup> and *gyr*<sup>kd</sup> strains with previously characterized co-expression cohorts (Fig. 6D). Prakash *et al.* clustered genes into three groups by their response to salt, heat and cold stress, each with or without the gyrase inhibitor novobiocin (NB) [4]. Zavrel *et al.* measured protein abundances at different growth rates in constant light conditions and presented 7 clusters [14] which we summarized into cohorts upregulated or downregulated with growth rate, with a complex response and stable proteins without growth rate-dependence. Saha *et al.* and Lehmann *et al.* analyzed transcriptome



experiment enrichment profiles. Cluster 1 is enriched with proteins of unknown function. In both, stress and growth experiments, we found only enrichments in the NA classes, ie. the original papers did not report values. However, in the diurnal data set we found enrichment with genes clusters that peak at noon or after noon. We denote this cohort as UK/dusk (unknown function, expressed at dusk). The remaining clusters 5, 4 and 6 all show weak functional enrichments. Only cluster 4 is enriched with transposase genes, DNA polymerase and other DNA binding proteins. All of them, and strongest in cluster 4, show weak enrichment with transcript cohorts that peak during the dark phase. Cluster 6 is enriched in the late night cohort in the diurnal data set, and further shows some overlaps in enrichment with the RB/dawn cohort, thus closing the (diurnal) cycle of expression. We tentatively label cluster 4 as the DNA/night cohort and cluster 6 as plasmids.

To compare the time series with the endpoint transcriptome data, we calculated t-test profiles of all clusters (red/blue squares in Fig. 6D and S13). RB/dawn, PS/noon and UK/dusk showed consistent behavior in all strains, although at lower t-values for the gyrase knock-downs. DNA/night and plasmids, both enriched with plasmid genes, were upregulated only in topA<sup>OX</sup> but not in the gyr<sup>kd</sup> strains. Transcripts of the large cluster 5, which showed the weakest response in the time series, were upregulated only in the gyr<sup>kd</sup> strains. Likewise, the diurnal co-expression cohorts from ref. [44] (Fig. S17)) all show subtle but notable differences between the strains, only PS/noon was consistently downregulated.

**Uncoupling the Diurnal Program at Dawn.** Genes with supercoiling-activated transcription were found to be GC-rich in both upstream non-coding and coding regions of several species, and *vice versa*, supercoiling-repressed genes are AT-rich [1, 3, 45, 6]. Thus, we aligned nucleotide sequences of all genes from the main chromosome at their start codons (ATG), calculated average nucleotide content in moving windows for each cluster, and performed a statistical enrichment test (cumulative hypergeometric distribution) at each position (Fig. 6E). The up-regulated RB/dawn cohort and the down-regulated PS/noon cohort are GC-rich downstream and upstream of the start codon. The UK/dusk (downregulated) and DNA/night cohorts (upregulated) are AT-rich. Zooming in to the immediate response after induction shows that the response of the co-expression cohorts switches within the first h post-induction (Fig. 6C). The immediate response is consistent with data from other species. Transcript abundances of both GC-rich cohorts, RB/dawn and PS/noon, decreased, while those of the AT-rich UK/dusk and DNA/night cohorts increased. Already 1 h post-induction, the two GC-rich and two AT-rich cohorts have bifurcated. Transcript abundances of RB/dawn increased while those of PS/noon continue to decrease. Similarly, the AT-rich UK/dusk transcripts now decreased while DNA/night transcripts continued to increase in abundance.

**Transcription Unit Promoter Structure: A GC-rich Discriminator.** To analyze actual promoter structures we mapped the coding genes on previously described transcription units (TU) [46], calculated average temporal abundance profiles of TUs, and clustered TU profiles by *k*-means using the average profiles of the gene-based clustering as cluster centers (Fig. S23). TU were then aligned at their transcription start sites (TSS) and again average nucleotide content profiles of clustered TU calculated (Fig. 6E). Downstream of the TSS the general differences in GC/AT content were similar to those of start codon-aligned coding genes, albeit with lower statistical power. TSS alignment reveals a distinct GC-rich peak at ca. -50 bp. This peak corresponded better to the mid-term trend of transcript abundances. Cohorts that were upregulated within the first 3 d post-induction (DNA/night and RB/dawn) had a higher, and downregulated cohorts (PS and UK/dusk) had the lowest GC-content at this putative “discriminator” position.

**Genes of Interest.** In Figures S18–S22, we analyze transcript abundances of a few specific gene sets: circadian clock genes (*kai*), response regulators, sigma factors, and photosynthesis and metabolic genes. However, these patterns are hard to interpret, due to the unknown function of upregulated genes and differential regulation of paralogs and enzyme complex subunits. In short: most *kai* genes were down-regulated, while *kaiC3* is upregulated with RB/dawn, followed by *kaiB2* and *kaiC2* from 3 d (Fig. 7A, S18A). KaiC3 is required for chemoheterotrophic growth in constant darkness [47]. The response regulator *rpaB* is downregulated, and *rpaA* slightly upregulated (Fig. S18B). Of the tested regulators, only *pmgA* is strongly upregulated over the first three days, with the diurnal pattern of the RB/dawn cohort. Sigma factors of unknown function [48], *sigH*→*segl*,

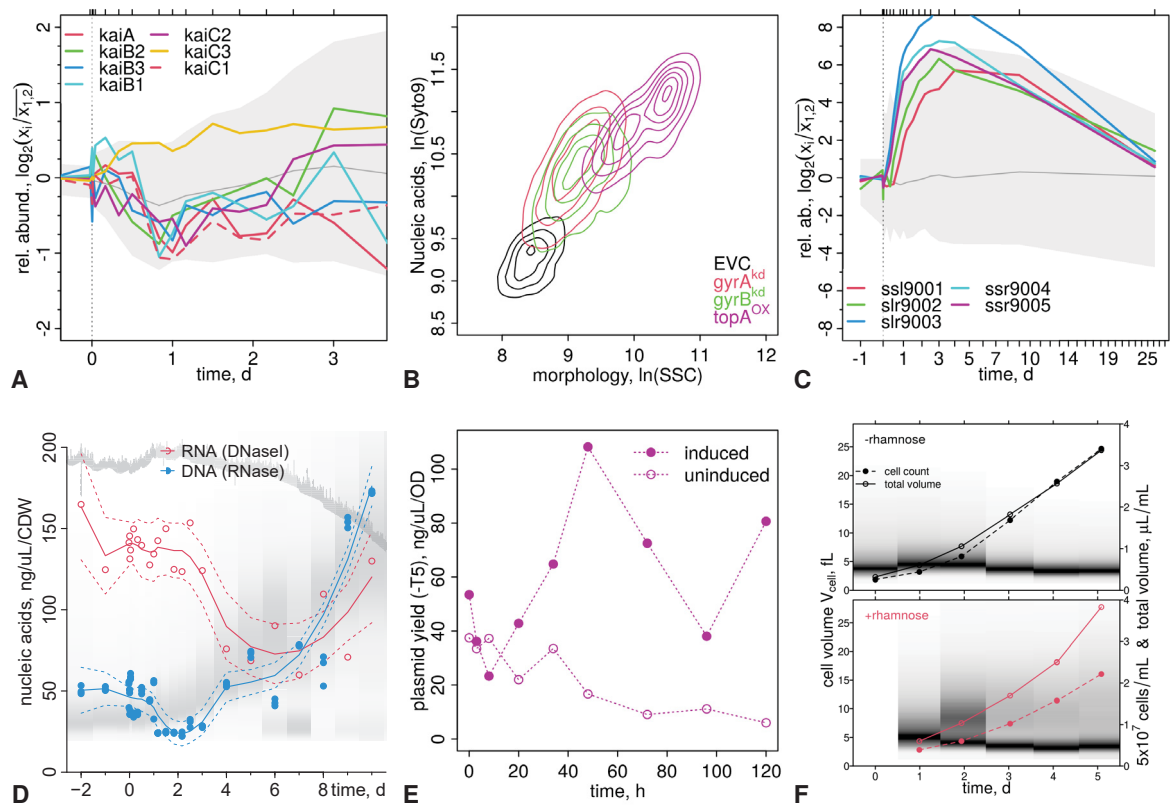


**Figure 7. Explaining the Phenotype?** **A:** Relative transcript abundances of the Kai circadian clock genes in the *topA<sup>OX</sup>* time series, only *kaiC3* is upregulated over the first three days post-induction. The gray background shows the 92.5% and 7.5% quantiles of all data as a reference. **B:** Flow cytometry of batch culture endpoint samples, as Fig. 4A but for nucleic acid content (Syto9 marker) vs. the side scatter signal, an indicator of cell morphological features. **C:** Relative transcript abundances (as in (A)) of genes from the plasmid pCC5.2\_M. **D:** RNA and DNA extraction yields in the *topA<sup>OX</sup>* time series experiment, divided by the  $\text{OD}_{\lambda}$  signal calibrated to CDW.  $\text{OD}_{\lambda}$  and cell volume distributions (Fig. 5A,B) are shown (gray) as reference. Lines show a LOESS regression with 95% confidence interval. **E:** Plasmid extraction yields in the plasmid supercoiling time series (Fig. 3) from the induced and uninduced cultures. **F:** Cell volume and count development after re-induction of cells isolated after harvest from the *topA<sup>OX</sup>* time series experiment in fresh BG11 medium.

were upregulated until 3 d; the stress factor *sigB* is up-regulated only at 10 d (Fig. S18C), where cells are enlarged. Photosystem, phycobilisome, and carboxysome genes are predominantly downregulated (Fig. S19–S20). In contrast, RuBisCo and genes of the carbon concentrating mechanisms are predominantly upregulated over the first three days (Fig. S21). The glycogen degrading enzyme *glgP1* was strongly downregulated; glucose-1-phosphate adenylyltransferase *glgC* was upregulated, and glycogen debranching enzymes *glgX1/X2* peaked at 3 d (Fig. S22A). NAD synthesis genes are generally upregulated, and we find strong differential response of certain subunits of the NADH dehydrogenase (Fig. S22B,C). Together with the upregulation of the redox and photomixotrophic growth regulator *pgmA* [49], these responses point to changes in redox metabolism. The thioredoxin *trxM1* is strongly down-regulated, and *trxA* has only a short and low peak at 2 d–3 d (Fig. S22D).

**Reversible Inhibition of DNA Replication Explains the Growth Phenotype.** Manipulation of DNA supercoiling has highly pleiotropic effects, and can also interfere with DNA replication and lead to DNA damage [50]. Here, we observed a block of division while cell growth continued. Could an inhibition of genome replication be

involved? In endpoint RNA-seq experiments relative rRNA abundances were decreased but the total nucleic acid content (Syto-9 stain) increased with cell size and morphology (Fig. 4A, 7B, S4). To differentiate nucleic acids, we extracted RNA and DNA from the topA<sup>OX</sup> time series experiment (Fig. 7C). DNA extraction yields per CDW were lower while RNA yield was constant over the three days post-induction. From 4 d post-induction DNA yield increased steeply and surpassed RNA yields. This could be due to increased genome or plasmid copy numbers. The transcript abundances from all plasmid-derived genes became high at this time (Fig. 7D, S16). Plasmid DNA extraction yields from the topA<sup>OX</sup> plasmid supercoiling time series increased strongly in the induced but not the control culture, but this bias was lost when treating with the T5 exonuclease to remove all linear or nicked circular DNA (Fig. 7E, S2B,C). Large plasmids and the genome are easily nicked during the extraction procedure. Thus, the most parsimonious explanation for the division block phenotype is impaired DNA replication of the genome, while plasmid copy numbers increased during the late stages of cell volume growth. A block of genome replication could be due to permanent DNA damage. The volume growth and division block phenotype was reversible. All strains recovered readily when re-inoculated in fresh medium without the inducer (Fig. S1C). In the continuous culture experiment, cells recovered as the inducer was washed out (Fig. 5A). Re-inoculation with and without inducer showed that in some cells our constructs remained intact and induced cells again grew in volume, while other cells were refractive to induction, and overgrew the division-blocked cells (Fig. 7E, S10). Thus, we conclude that the putative block in genome DNA replication was not due to irreversible and lethal genome damage.

## Conclusion

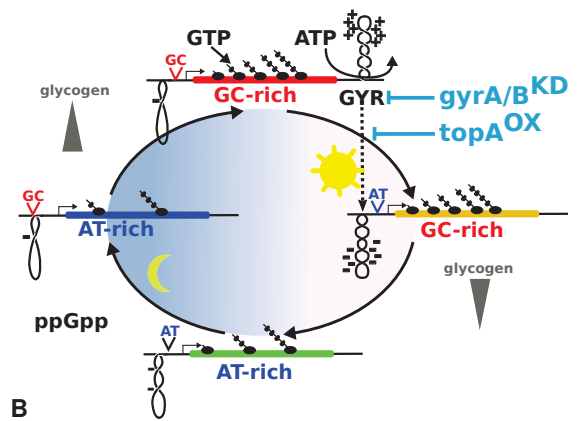
We presented a comprehensive characterization of DNA supercoiling effects in *Synechocystis*. Several models of the role of this regulatory system in bacterial cell biology can be confirmed in this species. The enzymes directly responsible for supercoiling are under homeostatic control [55]. Increased gyrase levels and transcription conspire to hyper-supercoil plasmids in the topA<sup>OX</sup> strain, in agreement with the twin-domain model of transcription-dependent supercoiling [15, 56]. Differential transcription of GC-rich and AT-rich genes [1, 3, 45, 6] was observed immediately (5 min–20 min) after induction of *topA* over-expression. Already after 60 min the pattern had changed. The compensatory upregulation of gyrase and other regulatory mechanisms, such as the ppGpp mediated repression of day time transcription [53], may underlie this quick bifurcation of the response. A GC-rich discriminator –50 bp upstream of TSS could be involved. Large gene cohorts developed similarly over the first three days post-induction, and these revealed a tight link to the diurnal transcription program, consistent with results from *Synechococcus elongatus* PCC 7942 [3].

Cooperative and antagonistic long-range effects of transcription *via* local accumulation and diffusion of DNA torsional strain [16] underlies temporal expression sequences in operons [22, 23], and genome-wide along the origin-terminus axis during *E. coli* growth phases [24]. We suggest a simple model of supercoiling-mediated cooperativity (Fig. 8), where energy-driven transcription of ribosomal RNA and growth genes around dawn (RB/dawn) requires downstream gyrase activity. This process would generate the supercoiling required for both, transcription of the GC-rich PS/noon genes and DNA replication between dawn and noon [57]. This coupling is affected differently by our interventions, and reflected in the subtly different response of diurnal cohorts in the three strains (Fig. 6B). In the gyrase knock-downs it is directly inhibited, resulting in drastic reduction of rRNA abundances (Fig. 4B). In the *topA* overexpression experiments the gyrase genes were upregulated and downstream gyrase activity could locally be enhanced. Globally, the high abundance of topoisomerase I would constantly remove accumulated negative supercoiling. In all strains, the supercoiling required for the onset of the program beyond dawn gene expression could not be generated: DNA replication is blocked, and transcripts of the PS/noon and UK/dusk cohorts are downregulated. The overall decreased genomic supercoiling level results in up-regulation of night-specific transcripts, including *kaiC3*, a homolog of the circadian clock gene and required for heterotrophic growth in constant darkness [47]. The cells overall appear “stuck” between night and dawn states. Next, our strains and interventions should be studied in this natural diurnal context, that is, in cultures grown in regular day/light cycles, and interference initiated at different times of the cycle. Our tunable induction/repression constructs could further be combined in one strain, topA<sup>OX</sup>+gyr<sup>kd</sup>, to avoid adaptive effects of gyrase overexpression. This would allow better and tunable external control of DNA supercoiling and the transcriptional response. Finally, we note that topoisomerase

strain	volume	ATP	glyc.	rRNA	plasmid sc.
topA <sup>KD</sup>	↓	-	-	n.a.	n.a.
gyrA <sup>KD</sup>	↑	-	-	↓↓	↓
gyrB <sup>KD</sup>	↑	↑	-	↓↓	↓
gyrAB <sup>KD</sup>	↑	↑	-	n.a.	(↑)
topA <sup>OX</sup>	↑	↑	↑	(↓)	↑↑

cohort	init.	late	function	GC	discr.
2/RB/dawn	↓	↑	growth	↑	↑
3/PS/noon	↓	↓	photosynt.	↑	↓
1/UK/dusk	↑	↓	unknown	↓	↓
4/DNA/night	↑	↑	replication	↓	(↑)

**A**



**B**

**Figure 8. Summary and Model.** **A:** Summary tables of physiological characteristics of the tested strains (top) and the co-expression cohorts observed after topA<sup>OX</sup> induction (bottom). The top table indicates changes in cell volume, ATP+ADP, glycogen, rRNA content and plasmid supercoiling. The bottom table summarizes enriched properties of the co-expression cohorts (clusters): the initial and late response of transcript abundances, functional enrichments, overall GC content and the presence of a putative GC-rich discriminator at -50 bp upstream of the TSS. **B:** Development of an Integrative Model: at dawn energy from photosynthesis becomes available, allowing for transcription of GC-rich growth genes (RB/dawn), gyrase activity downstream of these genes can gate their transcription, e.g. tune bursting frequency [51] or set the elongation rate [52]. This is inhibited in the gyrase knock-downs and not inhibited or even enhanced through gyrase upregulation in the topA over-expression experiments. The combination of transcription and gyrase activity leads to genome-wide increase in negative supercoiling. The accumulated torsional strain can then be channeled into transcription of the second GC-rich cohort, PS/noon. This latter process is inhibited in all strains. In normal conditions topoisomerase I could then be involved in resolving R-loops [20] that may have been generated by the dawn/noon program. During night-metabolism ppGpp signaling [53] activates the night transcription program, at low levels of transcription [31], and supercoiling globally decreases. Clock-mediated glycogen mobilization at the end of the night [54] could kick-start the RB/dawn program already before onset of light [44].

I overexpression caused an increase of cellular glycogen content of up to 60% of the cell dry weight. This phenotype could be exploited in biotechnological applications, e.g. for synthesis of high value products or directly as a fermentation substrate for yeast [40].

## Data Availability

The clustering and time series data from the topA<sup>OX</sup> strain (both as raw abundances in TPM and as the log<sub>2</sub> ratios to the mean of two pre-induction values, as plotted in this manuscript), and endpoint measurements (log<sub>2</sub> ratio of abundances in the gyrA<sup>KD</sup>, gyrB<sup>KD</sup> and topA<sup>OX</sup> strains to the EVC strain) are available as Datatable\_S1.tsv.

\*\*\* The raw sequencing reads will be made available at an appropriate facility (SRA) upon publication. \*\*\*

## Funding

RM was funded by the *Deutsche Forschungsgemeinschaft* (DFG), grants AX 84/4-1 & STA 850/30-1 (COILseq) and EXC-2048/1–project ID 390686111 (CEPLAS). MD, DB and TB were financially supported by the CLIB Competence Centre Biotechnology (CKB) funded by the European Regional Development Fund ERDF (EFRE-0300096 and EFRE-0300095).

---

## Acknowledgments

The parental strain *Synechocystis* sp. PCC 6803, encoding aTc-inducible dCas9, and the *gyrB*<sup>kd</sup> strain were a gift from P. Hudson and L. Yao. We are grateful to Nic Schmelling for critical discussion of the manuscript.

## Materials and Methods

### Strains and Plasmids

The *Synechocystis* parent strain used for all genetic alterations was kindly provided by Dr. Lun Yao and Dr. Paul Hudson, and based on a strain they had obtained from Dr. Martin Fulda (Göttingen, Germany). It contains a TetR cassette, as well as dCas9 under the promoter PL<sub>22</sub>, inducible with anhydrotetracycline (aTc), at the genomic insertion site *psbA1*. Construction of this strain was described in ref. [37]. For overexpression of genes in *Synechocystis*, relevant genes were directly PCR-amplified from the *Synechocystis* genome, fused to the rhamnose-inducible promoter [36] *via* overlap extension PCR, and integrated into a modified variant of the conjugative vector pSHDY containing a nourseothricin resistance instead of spectinomycin, termed pSNDY. The vector backbone also contained the activator *rhaS* from [36]. Lun Yao and Paul Hudson further provided a strain with *gyrB*-targeting sgRNA. For the construction of the additional sgRNA constructs, sgRNA sequences were designed using CHOPCHOP [58], constructed *via* overlap extension PCR and integrated into the vector designed by [37] (Addgene #73224), which inserts into the *slr0230* site of the *Synechocystis* genome. Integrative sgRNA plasmids were integrated *via* transformation. Briefly, 10 mL of exponentially grown culture was concentrated to 250  $\mu$ L, 1  $\mu$ g–2  $\mu$ g of pure plasmid was added and the mixture was incubated up to 5 h before plating the entire mixture on BG11 plates. After drying the plates, agar was underlaid with 300  $\mu$ L of 1 mg mL<sup>-1</sup> kanamycin stock using a sterile spatula, thereby forming a diffusion gradient. After 1-2 weeks of incubation at 30 °C with the lid facing upward, isolated green colonies were carefully transferred to a fresh plate. Over time, positive clones were gradually shifted to higher concentrations of kanamycin (*i.e.*, 4, 8, 12, 20, 40  $\mu$ g mL<sup>-1</sup> final concentration in the plate). Complete segregation of mutants was ensured *via* colony PCR. Replicative vectors were introduced into the dCas9 background strain *via* conjugation as described ([dx.doi.org/10.17504/protocols.io.ftpbnnm](https://doi.org/10.17504/protocols.io.ftpbnnm)). Clones were selected using nourseothricin (Jena Bioscience, #AB-102L) at a final concentration of 50  $\mu$ g mL<sup>-1</sup> and verified *via* colony PCR.

### Culture Conditions

**Batch Culture Conditions.** Plates were freshly streaked before liquid cultivation. In the case of nourseothricin, liquid cultures were maintained with 25  $\mu$ g mL<sup>-1</sup> while solid media was supplemented with 50  $\mu$ g mL<sup>-1</sup>. Spectinomycin and Kanamycin were supplemented at concentrations of 20  $\mu$ g mL<sup>-1</sup> and 25  $\mu$ g mL<sup>-1</sup>, respectively. For pre-culturing and growth experiments, *Synechocystis* strains were cultivated in BG11 medium [59]. Cultivation was performed at 30 °C with 150 rpm shaking and continuous illumination of  $\approx 80 \mu\text{mol m}^{-2} \text{s}^{-1}$  (16 % setting in Infors HT). Aeration was ensured by continuous shaking and CO<sub>2</sub> enriched air (0.5 %) in an Infors HT multitron chamber. Pre-culturing was performed in 100 mL baffle-free Erlenmeyer shaking flasks with 20 mL cell suspension for three days. After adjusting all different strains to the same OD<sub>750</sub>  $\approx 0.4$ , growth experiments were performed after one additional day of pre-culturing. For this, 30 mL cultures were incubated in Erlenmeyer shaking flasks for 5 days with a start OD<sub>750</sub>  $\approx 0.25$  in biological triplicates.

### Continuous Culture, Online Measurements and Calculations

Continuous culture was performed in a Lambda Photobioreactor and with additional measurement and control devices (Fig. S7) in BG11 medium, supplemented with the required antibiotics, at culture volume  $V_\ell = 1 \text{ L}$ , aeration with 1 L min<sup>-1</sup> of CO<sub>2</sub>-enriched (0.5 %) air, agitation by the Lambda fish-tail mixing system at 5 Hz, temperature control at 30 °C, and pH 8, with 0.5 M NaOH and 0.5 M H<sub>2</sub>SO<sub>4</sub> as correction solutions. After equilibration to these conditions the reactor was inoculated to a start OD<sub>750</sub>  $\approx 0.5$ , from 100 mL pre-culture.

White light from the Lambda LUMO module was initially increased as a ramp from 42 to 250 photons, then kept constant, and manually decreased to maintain light intensity approximately at  $\sim 90 \mu\text{mol m}^{-2} \text{s}^{-1}$  per  $\text{OD}_{750}$  (Fig. S8F). After the switch to batch culture light was again increased in ramp from 70 to  $250 \mu\text{mol m}^{-2} \text{s}^{-1}$ . For evaporation control and continuous culture, the total weight of the reactor setup was kept constant using the built-in Lambda reactor mass control module and automatic addition of fresh culture medium through the feed pump. In batch mode this controls for evaporation of medium. Continuous culture was performed by setting the waste pump to a fixed speed.

**Calibrations of Measured & Controlled Data.** The Lambda Photobioreactor (Fig. S7) was equipped with online monitoring of dissolved  $\text{O}_2$  and pH, and additional monitoring of optical density by a DasGip OD4 module and monitoring of offgas  $\text{O}_2$  and  $\text{CO}_2$  concentrations and the weights of feed and pH control bottles by Arduino-based custom-built data loggers (Fig. S7). The signal from the OD4 probe was calibrated to offline  $\text{OD}_{750}$  measurements (Fig. S8A-B). For normalizations of glycogen measurements by biomass and for estimation of the biomass density of cells ( $g_{\text{DCW}}/\text{mL}_{\text{cell}}$ , Fig. 5D) a LOESS regression of the  $\text{OD}_\lambda$  signal was calibrated to CDW (Fig. S8C-D). The Lambda LUMO light module consists of a strip of white LEDs and was calibrated to light intensity in  $\mu\text{mol m}^{-2} \text{s}^{-1}$  with a Licor light meter (LI-250A) with a spherical sensor bulb (LI-193) (Fig. S8E-F).

**Calculation of Dilution and Growth Rates.** All rates were calculated as slopes of measured data using piecewise linear segmentation [60], implemented in the CRAN R package `dpseg` (version 0.1.2) [61] (Fig. S9A-D). Growth rates were then calculated as the difference between slopes of measured biomass rate changes ( $\text{OD}_\lambda$ , CASY cell counts) and the culture dilution rate corrected for evaporation loss, see Figure S9E-F for details. Cell volume growth rate was calculated as the rate of change of the peaks of the CASY cell volume distributions.

## Biomass & Metabolite Measurements

**Cell Dry Weight Measurement.** To determine the cell dry weight (CDW) 5 mL cell culture was filtered through a pre-dried and pre-weighed cellulose acetate membrane (pore size  $0.45 \mu\text{m}$ ) using a filtering flask. After that the membrane was dried at  $50^\circ\text{C}$  for 24 h and weighed after cooling. 5 mL of filtered and dried growth medium served as a blank.

**Optical Density  $\text{OD}_{750}$  and Absorption Spectra.** The optical density ( $\text{OD}_{750}$ ) and absorbance spectra were measured on a Specord200 Plus (Jena Bioscience) dual path spectrometer, using BG11 as blank and reference. Samples were appropriately diluted with BG11 before measuring. All  $\text{topA}^{\text{OX}}$  time series samples were diluted 1:4 before recording  $\text{OD}_{750}$ . For absorbance spectra the  $\text{OD}_{750}$  was adjusted to 0.5 and the absorbances at 750 nm were subtracted from each spectrum.

**Cell Count and Size Distributions.** To determine the cell count 10  $\mu\text{L}$  cyanobacteria culture, pre-diluted for  $\text{OD}_{750}$  measurement, were dispensed in 10 mL CASYton and measured with a Schaefer CASY Cell Counter (Modell TTC) using a diameter  $45 \mu\text{m}$  capillary. Cell size was recorded in the diameter range  $0 \mu\text{m}$ – $10 \mu\text{m}$ . Each sample was measured with 400  $\mu\text{L}$  in triplicate runs.

Analysis of the raw data was performed in R. Counted events in the CASY are a mix of live cells, dead cells, cell debris and background signals. Only counts with diameter  $d > 1.5 \mu\text{m}$  and  $d < 5 \mu\text{m}$  were considered for the time series experiment (Fig. 5B) while a lower cutoff  $d > 1.25 \mu\text{m}$  was used for the endpoint measurements (Fig. 2C) to avoid cutting the distribution of the slightly smaller  $\text{topA}^{\text{KD}}$  cells. Since *Synechocystis* cells are spherical, the cell volumes were calculated from the reported cell diameters  $d$  as  $V_{\text{cell}} = \left(\frac{d}{2}\right)^3 \pi \frac{4}{3}$ .

**Glycogen Measurement.** To determine the glycogen content, 0.5 mL of cell culture was harvested into reaction vessels that had been pre-cooled on ice. After centrifugation at maximum speed for 5 min at  $4^\circ\text{C}$  the pellets were flash-frozen in liquid nitrogen and stored at  $-80^\circ\text{C}$  until further processing. To start the

glycogen extraction, the pellet was resuspended in 400  $\mu$ L KOH (30% w/v) and incubated at 95 °C for 2 h. For precipitation, 1200  $\mu$ L ice cold ethanol was added and the mixture was incubated at –20 °C overnight. After centrifugation at 4 °C for 10 min at 10 000 g, the pellet was washed once with 70 % ethanol and again with pure ethanol. Afterwards the pellets were dried in a Concentrator Plus speed-vac (Eppendorf) for 20 min at 60 °C. Then the pellet was resuspended in 1 mL 100 mM sodium acetate (pH 4.5) supplemented with amyloglucosidase powder (Sigma-Aldrich, 10115) at a final concentration of 35 U/mL. For enzymatic digestion samples were incubated at 60 °C for 2 h. For the spectrometric glycogen determination the Sucrose/D-Glucose Assay Kit from Megazyme (K-SUGL) was applied according to the manufacturer's specifications, but omitting the fructosidase reaction step and scaling down the total reaction volume to 850  $\mu$ L. Absorbance at 510 nm was measured using a BMG Clariostar photospectrometer.

**ATP and ADP Measurement.** 2 mL tubes were preloaded with 250  $\mu$ L of buffer BI (3 M HClO<sub>2</sub>, 77 mM EDTA). 1 mL culture sample was added, briefly vortexed and incubated on ice for 15 min. 600  $\mu$ L of BII (1 M KOH, 0.5 M KCl, 0.5 M Tris) were added, vortexed and incubated on ice for 10 min. After centrifugation at 0 °C for 10 min at 12 000 g, samples were flash-frozen in liquid nitrogen and stored at –80 °C until further processing. Extracts were thawed on ice and centrifuged again at 0 °C for 10 min at 12 000 g. 200  $\mu$ L samples were added either to 320  $\mu$ L of BIII/PEP (100 mM HEPES, 50 mM MgSO<sub>4</sub> x 7H<sub>2</sub>O, adjusted to pH 7.4 with NaOH, and 1.6 mM phosphoenolpyruvate (Sigma-Aldrich, 860077) for ATP quantification or BIII/PEP+PK (BIII/PEP with 2 U/ $\mu$ L pyruvate kinase (Sigma-Aldrich, P1506) for ATP + ADP quantification, and incubated for 30 min at 37 °C. All samples were heat-inactivated at 90 °C for 10 min. For luminescence-based quantification, the Invitrogen ATP determination kit was used (ThermoFisher: A22066). 10  $\mu$ L of each PEP or PEP+PK-treated sample was loaded in a white 96 well plate with solid bottom and kept on ice until the reaction was started. The luciferase master mix was scaled down in volume, and 90  $\mu$ L of master mix was added to each well. Luminescence was recorded using a BMG Clariostar. ATP concentrations were calculated using a standard curve with commercially available ATP stock solution (Invitrogen).

**Flow Cytometry and Analysis** Samples were fixed in 4 % para-formaldehyde in 1xPBS (phosphate buffered saline), washed three times in 1xPBS, and stained with the SYTO9 green fluorescent nucleic acid stain from the LIVE/DEAD kit (thermo) according to manufacturer's instructions. The flow cytometric measurements were taken at the FACS Facility at the Heinrich-Heine University (Dipl.-Biol. Klaus L. Meyer) using a BD FACSAria III. Forward scatter (FSC) and side-scatter (SSC) were recorded. Syto9 was measured with a 530/30 nm filter, and chlorophyll fluorescence was measured with 695/40 nm filter. For each sample 10,000 events (cells, debris and background) were recorded.

Data was exported in .fcs format, parsed and analyzed using the `flowCore` R package [62], and plotted using functions from our in-house `segmentTools` R package.

## DNA and Plasmid Extraction Agarose Gels

**DNA Extraction.** To isolate the DNA, 1 mL culture was centrifuged at maximum speed for 10 min at 4 °C, flash-frozen in liquid nitrogen and stored at –80 °C. After thawing, the samples were then resuspended in 1 mL 1x TE buffer by pipetting up and down and 100  $\mu$ L lysozyme (50 mg/mL stock solution) was added, inverted, and incubated for 1 h at 37 °C. Then 10  $\mu$ L Proteinase K (20 mg/mL stock solution) and 100  $\mu$ L 20 % SDS were added to the samples and incubated at 37 °C for 20 h. The lysed cell suspension was completely transferred to Phasemaker Tubes (ThermoFisher: A33248) and one volume of phenol/chloroform/isoamyl alcohol was added to each tube. The two resulting phases were thoroughly mixed and then separated by centrifugation for 10 min at maximal speed at 4 °C and the upper (nucleic acid-containing) phase transferred to a new tube. This was mixed with 100 ng/ $\mu$ L RNase A and incubated for 15 min at 37 °C for RNA degradation. Followed by the addition of 1 volume of chloroform/isoamyl alcohol, the centrifugation step was repeated. The upper phase was again transferred and precipitated with 1 volume 2-propanol at –20 °C over night. After centrifugation at maximal speed and 4 °C for 10 min to pellet the DNA, the supernatant was discarded. The pellet was washed twice with 500  $\mu$ L ice-cold 70 % EtOH and centrifuged for 10 min at maximal speed at 4 °C.

After drying the pellets at room temperature, the pellets were dissolved in 30  $\mu\text{L}$  water and the concentration was determined *via* Nanodrop (Thermo Scientific NanoDrop 2000c) .

**Plasmid Extraction.** 20 mL of cell culture were mixed with 20 mL of undenatured 99.5% ethanol, pre-cooled to  $-80^\circ\text{C}$ , in 50 mL centrifuge tubes and stored at  $-80^\circ\text{C}$  until processing. After thawing on ice, the supernatant was discarded after centrifugation for 10 min at  $4^\circ\text{C}$  and 4000 g. The QIAprep Spin miniprep kit was used for the following steps and adapted and expanded for individual steps. The cell pellet was resuspended in 250  $\mu\text{L}$  Qiagen P1 solution and transferred to 1.5 mL reaction tubes. Then 50  $\mu\text{L}$  lysozyme solution ( $50\text{ mg mL}^{-1}$ ) was added, mixed, and incubated for 1 h at  $37^\circ\text{C}$ . After the addition of 55  $\mu\text{L}$  of 20% SDS and 3  $\mu\text{L}$  of proteinase K ( $20\text{ mg mL}^{-1}$ ), the reaction mixture was incubated at  $37^\circ\text{C}$  for 16 h. Starting with the alkaline lysis with the Qiagen P2 solution, all further steps according to the QIAprep Spin Miniprep Kit were carried out with amounts that were adjusted to the initial volume. Next, the concentrations and quality (260/280, 230/280 ratio) was determined using the Nanodrop (Thermo Scientific NanoDrop 2000c). The T5 exonuclease (NEB: M0363) was used for removal of linear and open circular DNA according to the manufacturer's protocol and incubated at  $37^\circ\text{C}$  for 30 min. The isolated plasmid DNA was further purified with the QIAprep modules. For this, 5 volumes of the PB buffer were added to 1 volume of DNA solution. All subsequent steps were carried out using the QIAprep Spin miniprep kit and the plasmid DNA concentration was determined with the Nanodrop.

## Gel Electrophoresis and Analysis

**Chloroquine Agarose Gel Electrophoresis.** Agarose gels with chloroquine diphosphate (CQ, Sigma: C6628-50G, CAS: 50-63-5) were used to determine the relative migration speed of supercoiled topoisomers. A 1.2% agarose gel in 0.5x TBE (Roth: 3061.2) was prepared by heating to boiling. After cooling (hand-warm) CQ was added to  $20\text{ }\mu\text{g mL}^{-1}$  and the mixture poured into the gel chamber. As running buffer served 0.5x TBE buffer with the same CQ concentration as the gel. For each sample, 120 ng DNA was mixed with loading dye and filled up to 30  $\mu\text{L}$  with water. Next, the voltage source was adjusted  $1.8\text{ V cm}^{-1}$ . Gels were run for 20 h–24 h covered in foil to protect from light. Next, the gel was washed two times for 30 min in 250 mL 0.5x TBE buffer to remove the CQ. After that, the gel is stained with 25  $\mu\text{L}$  SYBR Gold (ThermoFisher: S11494) in 225 mL 0.5x TBE buffer for 3 h. Then the CQ agarose gel was imaged by a BioRad Imaging System (ChemiDoc<sup>TM</sup> MP). Washing and staining were also performed light-protected. \*\*\* This method and its calibration are introduced in more detail in our preprint manuscript at [bioRxiv \[35\]](https://doi.org/10.1101/2021.03.11.436888). \*\*\*

**Analysis of Gel Electropherograms.** Electropherograms of agarose gels of plasmids were extracted in ImageJ for each lane. Electropherograms from capillary gel electrophoresis of total RNA samples (Agilent Bioanalyzer) were parsed from exported XML files using the R package `bioanalyzerR` (v 0.7.3, obtained from <https://github.com/jwfoley/bioanalyzerR>) [63]. Electropherograms were then processed in R, using LOESS smoothing and peak detection functions from the `msProcess` R package (version 1.0.7) (<https://cran.r-project.org/web/packages/msProcess/>). A baseline was determined in two steps using the `msSmoothLoess` function. The first step used the full signal and served to determine the coarse positions of peaks. The final baseline was then calculated from the signal after removal of peak values. This baseline was subtracted from the total signal to detect peaks (bands) with the `msPeakSimple` function from `msProcess` and calculate peak areas. For the total RNA analysis, the baseline signal stems from mRNA and rRNA degradation fragments, and was used to calculate ratios of rRNA peak areas to the “baseline” area.

## Transcriptome Analysis: Sampling, RNA Extraction and Sequencing

**RNA Extraction and Processing.** Cellular activity was stopped by adding 1 mL culture directly to 250  $\mu\text{L}$  100% ethanol supplemented with 5% phenol, flash-frozen in liquid nitrogen and stored at  $-80^\circ\text{C}$  until further processing. For RNA extraction, a protocol modified from [64] was used. Briefly, frozen samples were centrifuged at maximum speed at  $4^\circ\text{C}$ . After discarding the supernatant, the pellet was resuspended in 1 mL PGTX and incubated at  $95^\circ\text{C}$  for 5 min. After cooling on ice for 2 min, 700  $\mu\text{L}$  chloroform:isoamyl alcohol

(24:1) were added and the mixture was incubated shaking gently at room temperature for 10 min. The mixture was centrifuged for 10 min at maximal speed at 4 °C. The upper phase was transferred to a fresh tube and 1 volume chloroform:isoamyl alcohol was added. After repeating the centrifugation step, the upper phase was again transferred and precipitated with 3 volumes of 99.5 % ethanol and 1/2 volume 7.5 M ammonium acetate at –20 °C over night. In cases where low RNA concentrations were to be expected, 1 µL RNA-grade glycogen was added to the precipitation mixture. The RNA was pelleted for 30 min at maximum speed and 4 °C, washed twice with 70 % ethanol and resuspended in 30 µL RNase-free water. RNA was DNaseI-digested using commercial DNaseI (ThermoFisher: EN0525), according to the manufacturer's specifications, but using twice the concentration of reaction buffer. DNaseI-digested RNA was phenol/chloroform extracted again to remove the DNaseI. For precipitation after DNaseI-digest, 1/10 volume of 3 M sodium acetate (pH 5.3), was used instead of ammonium acetate.

**Quantitative RT-PCR.** For qRT-PCR, DNaseI-digested RNA was reverse-transcribed to cDNA using the commercial RevertAid RT (ThermoFisher: K1621) according to the manufacturer's specifications in a reaction volume of 20 µL. To the 20 µL reaction, 60 µL RNase-free water was added. Of this cDNA dilution, 2 µL per reaction well were loaded, and 8 µL Master Mix prepared from the DyNAmo ColorFlash SYBR Green qPCR-Kit (ThermoFisher: F416L) were added to each 2 µL cDNA reaction. The thermal cycling conditions were as follows: 7 min at 95 °C, followed by 40 cycles of 5 s at 95 °C and 30 s at 60 °C. Data was recorded after each cycle. RT-negative controls and no-template-controls (distilled water) were included for each run. Each sample was loaded in technical triplicates.

Gene expression changes at indicated time points, usually after induction, were then quantified by the  $\Delta\Delta Ct$  method [65]:

$$\Delta Ct = Ct_{goi} - Ct_{ref} \quad (1)$$

$$\Delta\Delta Ct = \Delta Ct_t - \Delta Ct_{t_0}, \quad (2)$$

where  $Ct_{goi}$  and  $Ct_{ref}$  are the Ct values of a gene of interest (*gyrA*, *gyrB*, *topA*) and of a reference gene (*rpoA*), respectively. The  $\Delta\Delta Ct$  value then compares expression at time points  $t$  after induction with expression at a time point  $t_0$  before induction, and is equivalent to a  $\log_2$  fold change.

**RNAseq: Total RNA Analysis, Library Generation and Sequencing.** RNA quality was evaluated spectrometrically by Trinean Xpose (Gentbrugge, Belgium) and by fragment size distribution on an Agilent 2100 Bioanalyzer with the RNA Nano 6000 kit (Agilent Technologies, Böblingen, Germany). Electropherograms for the endpoint RNAseq samples were exported as XML files for further analysis; see paragraph *Analysis of Gel Electropherograms* for details.

The Illumina Ribo-Zero Plus rRNA Depletion Kit was used to remove the ribosomal RNA molecules from the isolated total RNA. Removal of rRNA was evaluated with the RNA Pico 6000 kit on the Agilent 2100 Bioanalyzer. RNA was free of detectable rRNA. Preparation of cDNA libraries was performed according to the manufacturer's instructions for the TruSeq stranded mRNA kit (Illumina, San Diego, CA, United States). Subsequently, each cDNA library was sequenced on an Illumina NextSeq 500 system (2 x 75 nt PE high output v2.5).

**RNAseq: Read Mapping.** The resulting sequence reads were quality trimmed with Trimmomatic v0.33 [66] using standard setting. The quality trimmed reads were subsequently mapped to coding genes of the *Synechocystis* sp. PCC 6803 reference genome (NC\_000911) including the plasmids pCA2.\_M, pCB2.4.\_M, pCC5.2.\_M, pSYSM, pSYSA, pSYSG and pSYSX (CP003270, CP003271, CP003272, NC\_005229, NC\_005230, NC\_005231, NC\_005232), and the constructed plasmid pSNDY\_Prha\_topA-6\_119rhaS\_20210310 using Bowtie 2 [67].

For the endpoint measurements from batch cultures the  $\log_2$ -fold changes with respect to the controls (EVC) were calculated with the DESeq2 algorithm [41] via the ReadXplorer software version 2.0 [68], based on three replicate measurements for each strain ("M-value"). For the time series read-count data were normalized

by library sizes to the Transcripts Per kilobase Million (TPM) unit. Missing values at individual time points were interpreted as 0 TPM.

## Transcriptome Analysis: Batch and Time-Series Analysis

**Cluster Analysis.** For clustering the time series into co-expressed cohorts, a previously established pipeline was used [69, 70]. Briefly, the time-series of TPM values was  $\text{arcsinh}$ -transformed:

$$x' = \ln \left( |x| + \sqrt{|x|^2 + 1} \right), \quad (3)$$

then the Discrete Fourier Transform (DFT) was calculated:

$$X_k = \sum_{n=0}^{N-1} x'_n e^{-2\pi i \frac{kn}{N}}, \quad k = \{0, \dots, N-1\}, \quad (4)$$

where  $x'_n = \{x'_0, \dots, x'_{N-1}\}$  are the (transformed) expression values at time points  $\{t_0, \dots, t_{N-1}\}$ , and  $X_k$ , the DFT, is a vector of complex numbers representing the decomposition of the original time series into a constant (mean) component (at  $k = 0$ ) and a series of harmonic oscillations around this mean. The input time series  $x_n$  were RNA-seq samples 2 to 16 (from  $-0.5$  h to 72 h around the time of induction at 0 h), *i.e.*, without the first pre-induction time-point and ignoring the two long-term response samples. Components  $k > 1$  were further scaled by the mean of amplitudes at all other components  $k > 1$ :

$$X'_{k>0} = \frac{X_{k>0}}{|X|_{k \neq \{0,k\}}}. \quad (5)$$

Real and imaginary parts of selected components  $X_{k=1, \dots, 6}$  of the DFT were then clustered with the `flowClust` algorithm [71] over cluster numbers  $K = 2, \dots, 10$ . The clustering with the maximal Bayesian Information Criterion, as reported by `flowClust` (Fig. S12A), was selected for further analyses. Data transformation and clustering were performed by the `processTimeseries` and the `clusterTimeseries2` functions of `segmentTier` and `segmentTools` packages, respectively. The resulting clusters were sorted and colored based on the comparison with diurnal co-expression cohorts (Fig. 6 and S17) for informative plots of the subsequent analyses.

**Immediate Response Analysis.** To estimate the immediate transcriptional response to *topA* overexpression (Fig. 6C, bottom panel) the difference of read counts (TPM) between the means of the two pre-induction time points ( $-1$  d,  $-35$  min) and the two post-induction time points (5 min, 20 min) was calculated. Transcripts with negative values were labelled as “down”, with positive values as “up”, and 0 or not available values as “nc”.

**Clustering of Transcription Units.** Average expression was calculated for transcription units (TU) reported by ref. [46] from the expression of coding genes they encompass (*via* the “Sense.tags” column of the original data set). The resulting TU time-series was clustered by *k*-means, using cluster centers from the CDS clustering (Fig. 5) and identical time-series processing. This way protein-coding transcription units could be assigned to the same cluster labels (Fig. S23). Clusters were then sorted by their mean expression peaks, and colored and named according to the diurnal time of their peaks.

**Clustering of Diurnal Transcriptome Data.** Diurnal expression data from [44] were obtained from GEO (GSE79714) and genes summarized as the mean over all associated probes. These expression values were clustered the same as described for the RNA-seq data: all time-series were DFT-transformed and amplitude-scaled DFT components  $X'_{k=1, \dots, 7}$  (eq. 4–5) were clustered with `segmentTier` functions `processTimeseries` and `flowclusterTimeseries`, using the maximal BIC clustering with  $K = 5$  clusters.

---

**Cluster-Cluster Overlap Tests.** Categorical enrichments, *e.g.*, coding gene co-expression cohorts vs. gene annotations, were analyzed by cumulative hypergeometric distribution tests (R's `phyper`) using `segmenTools`'s `clusterCluster` function and the `clusterAnnotation` wrapper for GO and protein complex analysis, which compares overlaps of each pair of two distinct classifications into multiple classes, and stores overlap counts and p-values (enrichment tables) for informative plots (see "Enrichment Profile Plots").

**Enrichment Table Sorting.** For intuitively informative plots the enrichment tables were sorted. Table rows were sorted along the other dimension (table columns) such that all categories enriched above a certain threshold  $p_{\text{sort}}$  in the first column cluster are moved to the top, and, within, sorted by increasing p-values. Next, the same sorting is applied to all remaining row clusters for the second column cluster, and so on until the last column cluster. Remaining row clusters are either plotted unsorted below a red line or removed. This is especially useful to visualize enrichment of functional categories along the temporal program of co-expression cohorts, *e.g.*, Figure 6B. This sorting is implemented in `segmenTools`' function `sortOverlaps`.

**Cluster t-Test Profiles.** To compare clusters (co-expression cohorts) with numerical data, here the  $\log_2$  fold-changes of transcript abundances in induced `gyrkd` and `topAOX` strains, we developed the `segmenTools`' function `clusterProfile`. For each cluster a two-sided t-test was performed (R base function `t.test`, incl. Welch approximation for different sample sizes), comparing the distribution of values of the cluster with all other values. The reported *t* statistic and the *p*-value were stored for each test. The resulting t-test profile was stored for informative plots (see "Enrichment Profile Plots").

**Enrichment Profile Plots.** The results of cluster enrichment tests (cluster-cluster overlap tests and t-test profiles) were visualized as colored table plots (*e.g.* Fig. 6B, C), using `segmenTools`' function `plotOverlaps`. For the categorical overlap tests, the total counts of overlapping pairs are plotted as text, and for t-test profiles the rounded *t* statistic. The text color is black or white based on a p-value cutoff  $p_{\text{txt}}$  (as indicated).

The field background colors scale with  $\log_2(p)$  of the reported p-values, where the full color corresponds to a minimal p-value  $p_{\text{min}}$  cutoff (as indicated). For categorical enrichment tests the full color is black and other colors are selected from a gradient to white. For numerical tests, the sign of the *t* statistic is used to determine a color to indicate the direction of change: red for negative values (downregulated) and blue for positive values (upregulated).

**Motif Scan and DNA Structure Analysis.** The genome was scanned for short sequence motifs using custom-built R code based on the `str_locate_all` function of the `stringr` R package [72] into a vector of 0 and 1 for each genome position, where 1 indicates occurrence of the motif under consideration. Motif occurrence vectors upstream and downstream of start codons or transcription start sites were extracted from the genome vector and aligned into a matrix (columns: positions around the alignment anchor, rows: all genomic sites under consideration). The occurrence of a motif in all sequences of a cluster were counted at each position *i* in 66 bp windows surrounding the position. Cumulative hypergeometric distribution tests (R's `phyper`) were performed to analyze statistical enrichment or deprivation of a given motif within the 66 bp window of all genes in a cluster vs. the same window in all genes in the total analyzed set (all clustered and aligned sequences), and the p-values  $p_i$  at position *i* stored. In the resulting plots of the mean position-wise motif occurrence the size of the plotted data point at position *i* was scaled by the enrichment or deprivation p-values to emphasize regions of significant difference (Fig. 6D). The maximal size was determined by the minimum p-value in each test series (Figure panels). The point style (closed or open circles) indicates the directionality of the test (enriched or deprived). The significance points are only shown at every third or tenth position to avoid overlaps.

**Other Data Sources.** Genome sequences and annotation were downloaded from NCBI, see "RNAseq: Read Mapping" for the RefSeq IDs. The gene "categories" annotation was downloaded on 2017-09-23 from CyanoBase [73]: <http://genome.annotation.jp/cyanobase/Synechocystis/genes/category.txt>. Gene Ontology annotation was downloaded from the UniProt database (2021-03-20, organism: 1111708)

[74]. Datasets from other publications were all obtained from the supplemental materials of the indicated publications.

## References

1. B.J. Peter, J. Arsuaga, A.M. Breier, A.B. Khodursky, P.O. Brown, and N.R. Cozzarelli. Genomic transcriptional response to loss of chromosomal supercoiling in *Escherichia coli*. *Genome Biol*, 5(11):R87, 2004.
2. N. Blot, R. Mavathur, M. Geertz, A. Travers, and G. Muskhelishvili. Homeostatic regulation of supercoiling sensitivity coordinates transcription of the bacterial genome. *EMBO Rep*, 7(7):710–715, Jul 2006.
3. V. Vijayan, R. Zuzow, and E.K. O’Shea. Oscillations in supercoiling drive circadian gene expression in cyanobacteria. *Proc Natl Acad Sci U S A*, 106(52):22564–22568, Dec 2009.
4. J.S. Prakash, M. Sinetova, A. Zorina, E. Kupriyanova, I. Suzuki, N. Murata, and D.A. Los. DNA supercoiling regulates the stress-inducible expression of genes in the cyanobacterium *Synechocystis*. *Mol Biosyst*, 5(12):1904–1912, Dec 2009.
5. A.G. de la Campa, M.J. Ferrandiz, A.J. Martin-Galiano, M.T. Garcia, and J.M. Tirado-Velez. The transcriptome of *Streptococcus pneumoniae* induced by local and global changes in supercoiling. *Front Microbiol*, 8:1447, 2017.
6. M.J. Szafran, M. Gongerowska, T. Malecki, M. Elliot, and D. Jakimowicz. Transcriptional response of *Streptomyces coelicolor* to rapid chromosome relaxation or long-term supercoiling imbalance. *Front Microbiol*, 10:1605, 2019.
7. C.J. Dorman. DNA supercoiling and transcription in bacteria: a two-way street. *BMC Mol Cell Biol*, 20(1):26, Jul 2019.
8. L.S. Hsieh, R.M. Burger, and K. Drlica. Bacterial DNA supercoiling and [ATP]/[ADP] changes associated with a transition to anaerobic growth. *J Mol Biol*, 219(3):443–450, Jun 1991.
9. M. van Workum, S.J. van Dooren, N. Oldenburg, D. Molenaar, P.R. Jensen, J.L. Snoep, and H.V. Westerhoff. DNA supercoiling depends on the phosphorylation potential in *Escherichia coli*. *Mol Microbiol*, 20(2):351–360, Apr 1996.
10. J.L. Snoep, C.C. van der Weijden, H.W. Andersen, H.V. Westerhoff, and P.R. Jensen. DNA supercoiling in *Escherichia coli* is under tight and subtle homeostatic control, involving gene-expression and metabolic regulation of both topoisomerase I and DNA gyrase. *Eur J Biochem*, 269(6):1662–1669, Mar 2002.
11. A.A. Travers, G. Muskhelishvili, and J.M. Thompson. DNA information: from digital code to analogue structure. *Philos Transact A Math Phys Eng Sci*, 370(1969):2960–2986, Jun 2012.
12. M. Schaechter, O. Maaløe, and N.O. Kjeldgaard. Dependency on medium and temperature of cell size and chemical composition during balanced growth of *Salmonella typhimurium*. *J Gen Microbiol*, 19(3):592–606, Dec 1958.
13. M. Scott, C.W. Gunderson, E.M. Mateescu, Z. Zhang, and T. Hwa. Interdependence of cell growth and gene expression: origins and consequences. *Science*, 330(6007):1099–1102, Nov 2010.
14. T. Zavrel, M. Faizi, C. Loureiro, G. Poschmann, K. Stuhler, M. Sinetova, A. Zorina, R. Steuer, and J. Cervený. Quantitative insights into the cyanobacterial cell economy. *Elife*, 8, Feb 2019.
15. L.F. Liu and J.C. Wang. Supercoiling of the DNA template during transcription. *Proc Natl Acad Sci U S A*, 84(20):7024–7027, Oct 1987.
16. S. Kim, B. Beltran, I. Irnov, and C. Jacobs-Wagner. Long-distance cooperative and antagonistic RNA polymerase dynamics via DNA supercoiling. *Cell*, 179(1):106–119.e16, Sep 2019.
17. N.S. Rovinskiy, A.A. Agbleke, O.N. Chesnokova, and N.P. Higgins. Supercoil levels in *E. coli* and *Salmonella* chromosomes are regulated by the C-terminal 35(-)38 amino acids of GyrA. *Microorganisms*, 7(3), Mar 2019.
18. J. Ma, L. Bai, and M.D. Wang. Transcription under torsion. *Science*, 340(6140):1580–1583, Jun 2013.
19. D. Sutormin, N. Rubanova, M. Logacheva, D. Ghilarov, and K. Severinov. Single-nucleotide-resolution mapping of DNA gyrase cleavage sites across the *Escherichia coli* genome. *Nucleic Acids Res*, 47(3):1373–1388, Feb 2019.
20. M. Drolet, S. Broccoli, F. Rallu, C. Hraiky, C. Fortin, E. Masse, and I. Baaklini. The problem of hypernegative supercoiling and R-loop formation in transcription. *Front Biosci*, 8:d210–21, Jan 2003.
21. W. Ahmed, C. Sala, S.R. Hegde, R.K. Jha, S.T. Cole, and V. Nagaraja. Transcription facilitated

- genome-wide recruitment of topoisomerase I and DNA gyrase. *PLoS Genet*, 13(5):e1006754, May 2017.
22. H.Y. Wu and M. Fang. DNA supercoiling and transcription control: a model from the study of suppression of the leu-500 mutation in *Salmonella typhimurium* topA- strains. *Prog Nucleic Acid Res Mol Biol*, 73:43–68, 2003.
  23. X. Zhi, S. Dages, K. Dages, Y. Liu, Z.C. Hua, J. Makemson, and F. Leng. Transient and dynamic DNA supercoiling potentially stimulates the leu-500 promoter in *Escherichia coli*. *J Biol Chem*, 292(35):14566–14575, Sep 2017.
  24. P. Sobetzko, M. Glinkowska, A. Travers, and G. Muskhelishvili. DNA thermodynamic stability and supercoil dynamics determine the gene expression program during the bacterial growth cycle. *Mol Biosyst*, Mar 2013.
  25. M.A. Woelfle, Y. Xu, X. Qin, and C.H. Johnson. Circadian rhythms of superhelical status of DNA in cyanobacteria. *Proc Natl Acad Sci U S A*, 104(47):18819–18824, Nov 2007.
  26. M.L. Salvador, U. Klein, and L. Bogorad. Endogenous fluctuations of DNA topology in the chloroplast of *Chlamydomonas reinhardtii*. *Mol Cell Biol*, 18(12):7235–7242, Dec 1998.
  27. M.K. Wall, L.A. Mitchenall, and A. Maxwell. *Arabidopsis thaliana* DNA gyrase is targeted to chloroplasts and mitochondria. *Proc Natl Acad Sci U S A*, 101(20):7821–7826, May 2004.
  28. H. Ito, M. Mutsuda, Y. Murayama, J. Tomita, N. Hosokawa, K. Terauchi, C. Sugita, M. Sugita, T. Kondo, and H. Iwasaki. Cyanobacterial daily life with Kai-based circadian and diurnal genome-wide transcriptional control in *Synechococcus elongatus*. *Proc Natl Acad Sci U S A*, 106(33):14168–14173, Aug 2009.
  29. J.R. Waldbauer, S. Rodrigue, M.L. Coleman, and S.W. Chisholm. Transcriptome and proteome dynamics of a light-dark synchronized bacterial cell cycle. *PLoS One*, 7(8):e43432, 2012.
  30. R. Lehmann, R. Machné, J. Georg, M. Benary, I. M. Axmann, and R. Steuer. How cyanobacteria pose new problems to old methods: challenges in microarray time series analysis. *BMC Bioinformatics*, 14(1):133, Apr 2013.
  31. C. Beck, S. Hertel, A. Rediger, R. Lehmann, A. Wiegard, A. Kolsch, B. Heilmann, J. Georg, W.R. Hess, and I.M. Axmann. Daily expression pattern of protein-encoding genes and small noncoding RNAs in *Synechocystis* sp. strain PCC 6803. *Appl Environ Microbiol*, 80(17):5195–5206, Sep 2014.
  32. T. Mori and C.H. Johnson. Circadian programming in cyanobacteria. *Semin Cell Dev Biol*, 12(4):271–278, Aug 2001.
  33. R.M. Smith and S.B. Williams. Circadian rhythms in gene transcription imparted by chromosome compaction in the cyanobacterium *Synechococcus elongatus*. *Proc Natl Acad Sci U S A*, 103(22):8564–8569, May 2006.
  34. R. Lehmann, R. Machné, and H. Herzel. The structural code of cyanobacterial genomes. *Nucleic Acids Res*, 42(14):8873–8883, Oct 2014.
  35. Salima Rüdiger, Anne Rediger, Adrian Kölsch, Dennis Dienst, Ilka Maria Axmann, and Rainer Machné. Plasmid supercoiling decreases during the dark phase in cyanobacteria: a clarification of the interpretation of chloroquine-agarose gels. *bioRxiv*, 2021.
  36. A. Behle, P. Saake, A.T. Germann, D. Dienst, and I.M. Axmann. Comparative dose-response analysis of inducible promoters in cyanobacteria. *ACS Synth Biol*, 9(4):843–855, Apr 2020.
  37. L. Yao, I. Cengic, J. Anfelt, and E.P. Hudson. Multiple gene repression in cyanobacteria using CRISPRi. *ACS Synth Biol*, 5(3):207–212, Mar 2016.
  38. R. Damrow, I. Maldener, and Y. Zilliges. The multiple functions of common microbial carbon polymers, glycogen and PHB, during stress responses in the non-diazotrophic cyanobacterium *Synechocystis* sp. PCC 6803. *Front Microbiol*, 7:966, 2016.
  39. T. Hasunuma, F. Kikuyama, M. Matsuda, S. Aikawa, Y. Izumi, and A. Kondo. Dynamic metabolic profiling of cyanobacterial glycogen biosynthesis under conditions of nitrate depletion. *J Exp Bot*, 64(10):2943–2954, Jul 2013.
  40. K.B. Mollers, D. Cannella, H. Jorgensen, and N.U. Frigaard. Cyanobacterial biomass as carbohydrate and nutrient feedstock for bioethanol production by yeast fermentation. *Biotechnol Biofuels*, 7:64, 2014.
  41. M.I. Love, W. Huber, and S. Anders. Moderated estimation of fold change and dispersion for RNA-seq data with DESeq2. *Genome Biol*, 15(12):550, 2014.
  42. S.B. Zimmerman and S.O. Trach. Estimation of macromolecule concentrations and excluded volume effects for the cytoplasm of *Escherichia coli*. *J Mol Biol*, 222(3):599–620, Dec 1991.
  43. Enno R. Oldewurtel, Yuki Kitahara, Baptiste Cordier, Gizem Özbaykal, and Sven van Teeffelen. Bacteria control cell volume by coupling cell-surface expansion to dry-mass growth. *bioRxiv*, 2019.
  44. R. Saha, D. Liu, A. Hoynes-O’Connor, M. Liberton, J. Yu, M. Bhattacharyya-Pakrasi, A. Balassy,

- F. Zhang, T.S. Moon, C.D. Maranas, and H.B. Pakrasi. Diurnal regulation of cellular processes in the cyanobacterium *Synechocystis* sp. strain PCC 6803: Insights from transcriptomic, fluxomic, and physiological analyses. *MBio*, 7(3), 2016.
45. M.J. Ferrandiz, A.J. Martin-Galiano, J.B. Schwartzman, and A.G. de la Campa. The genome of *Streptococcus pneumoniae* is organized in topology-reacting gene clusters. *Nucleic Acids Res*, 38(11):3570–3581, Jun 2010.
  46. M. Kopf, S. Klahn, I. Scholz, J.K. Matthiessen, W.R. Hess, and B. Voss. Comparative analysis of the primary transcriptome of *Synechocystis* sp. PCC 6803. *DNA Res*, 21(5):527–539, Oct 2014.
  47. A. Wiegard, C. Kobler, K. Oyama, A.K. Dorrich, C. Azai, K. Terauchi, A. Wilde, and I.M. Axmann. *Synechocystis* KaiC3 displays temperature- and KaiB-dependent ATPase activity and is important for growth in darkness. *J Bacteriol*, 202(4), Jan 2020.
  48. A. Srivastava, M.L. Summers, and R. Sobotka. Cyanobacterial sigma factors: Current and future applications for biotechnological advances. *Biotechnol Adv*, 40:107517, May 2020.
  49. Y. Nishijima, Y. Kanasaki, H. Yoshikawa, T. Ogawa, K. Sonoike, Y. Nishiyama, and Y. Hihara. Analysis of spontaneous suppressor mutants from the photomixotrophically grown pmgA-disrupted mutant in the cyanobacterium *Synechocystis* sp. PCC 6803. *Photosynth Res*, 126(2-3):465–475, Dec 2015.
  50. K.S. Jeong, Y. Xie, H. Hiasa, and A.B. Khodursky. Analysis of pleiotropic transcriptional profiles: a case study of DNA gyrase inhibition. *PLoS Genet*, 2(9):e152, Sep 2006.
  51. S. Chong, C. Chen, H. Ge, and X.S. Xie. Mechanism of transcriptional bursting in bacteria. *Cell*, 158(2):314–326, Jul 2014.
  52. N. Rovinskiy, A.A. Agbleke, O. Chesnokova, Z. Pang, and N.P. Higgins. Rates of gyrase supercoiling and transcription elongation control supercoil density in a bacterial chromosome. *PLoS Genet*, 8(8):e1002845, 2012.
  53. A.M. Puszynska and E.K. O'Shea. ppGpp controls global gene expression in light and in darkness in *S. elongatus*. *Cell Rep*, 21(11):3155–3165, Dec 2017.
  54. S.A. Angermayr, P. van Alphen, D. Hasdemir, G. Kramer, M. Iqbal, W. van Grondelle, H.C. Hoefsloot, Y.H. Choi, and K.J. Hellingwerf. Culturing *Synechocystis* sp. strain PCC 6803 with N<sub>2</sub> and CO<sub>2</sub> in a diel regime reveals multiphase glycogen dynamics with low maintenance costs. *Appl Environ Microbiol*, 82(14):4180–4189, Jul 2016.
  55. R. Menzel and M. Gellert. Regulation of the genes for *E. coli* DNA gyrase: homeostatic control of DNA supercoiling. *Cell*, 34(1):105–113, Aug 1983.
  56. M. Drolet, X. Bi, and L.F. Liu. Hypernegative supercoiling of the DNA template during transcription elongation *in vitro*. *J Biol Chem*, 269(3):2068–2074, Jan 1994.
  57. A. Werner, C.D. Broeckling, A. Prasad, and C.A.M. Peebles. A comprehensive time-course metabolite profiling of the model cyanobacterium *Synechocystis* sp. PCC 6803 under diurnal light:dark cycles. *Plant J*, 99(2):379–388, Jul 2019.
  58. K. Labun, T.G. Montague, M. Krause, Y.N. Torres Cleuren, H. Tjeldnes, and E. Valen. CHOPCHOP v3: expanding the CRISPR web toolbox beyond genome editing. *Nucleic Acids Res*, 47(W1):W171–W174, Jul 2019.
  59. Rosmarie Rippka, Josette Deruelles, John B. Waterbury, Michael Herdman, and Roger Y. Stanier. Generic assignments, strain histories and properties of pure cultures of cyanobacteria. *Journal of General Microbiology*, 111(1):1–61, 1979.
  60. Richard Bellman. On the approximation of curves by line segments using dynamic programming. *Communications of the ACM*, 4(6):284, 1961.
  61. Rainer Machné and Peter F. Stadler. *dpseg: Piecewise Linear Segmentation by Dynamic Programming*, 2020. R package version 0.1.2.
  62. B. Ellis, P. Haaland, F. Hahne, N. Le Meur, N. Gopalakrishnan, J. Spidlen, M. Jiang, and G. Finak. *flowCore: Basic structures for flow cytometry data*, 2019. R package version 1.48.1.
  63. Joseph Foley. *bioanalyzeR: Analysis of Agilent electrophoresis data*, 2021. R package version 0.7.3.
  64. F.L. Pinto, A. Thapper, W. Sontheim, and P. Lindblad. Analysis of current and alternative phenol based RNA extraction methodologies for cyanobacteria. *BMC Mol Biol*, 10:79, Aug 2009.
  65. K.J. Livak and T.D. Schmittgen. Analysis of relative gene expression data using real-time quantitative PCR and the  $2^{-\Delta\Delta C_T}$  method. *Methods*, 25(4):402–408, Dec 2001.
  66. A.M. Bolger, M. Lohse, and B. Usadel. Trimmomatic: a flexible trimmer for illumina sequence data. *Bioinformatics*, 30(15):2114–2120, Aug 2014.
  67. B. Langmead and S.L. Salzberg. Fast gapped-read alignment with Bowtie 2. *Nat Methods*, 9(4):357–359, Mar 2012.
  68. R. Hilker, K.B. Stadermann, O. Schwengers, E. Anisiforov, S. Jaenicke, B. Weisshaar, T. Zimmermann,

- 
- and A. Goesmann. ReadXplorer 2 – detailed read mapping analysis and visualization from one single source. *Bioinformatics*, 32(24):3702–3708, Dec 2016.
69. R. Machné and D.B. Murray. The yin and yang of yeast transcription: elements of a global feedback system between metabolism and chromatin. *PLoS One*, 7(6):e37906, 2012.
  70. R. Machné, D.B. Murray, and P.F. Stadler. Similarity-based segmentation of multi-dimensional signals. *Sci Rep*, 7(1):12355, Sep 2017.
  71. K. Lo, F. Hahne, R.R. Brinkman, and R. Gottardo. flowClust: a Bioconductor package for automated gating of flow cytometry data. *BMC Bioinformatics*, 10:145, 2009.
  72. Hadley Wickham. *stringr: Simple, Consistent Wrappers for Common String Operations*, 2019. R package version 1.4.0.
  73. T. Fujisawa, R. Narikawa, S.I. Maeda, S. Watanabe, Y. Kanesaki, K. Kobayashi, J. Nomata, M. Hanaoka, M. Watanabe, S. Ehira, E. Suzuki, K. Awai, and Y. Nakamura. CyanoBase: a large-scale update on its 20th anniversary. *Nucleic Acids Res*, 45(D1):D551–D554, Jan 2017.
  74. UniProt Consortium. UniProt: the universal protein knowledgebase in 2021. *Nucleic Acids Res*, 49(D1):D480–D489, Jan 2021.
  75. S. Sakata, N. Mizusawa, H. Kubota-Kawai, I. Sakurai, and H. Wada. Psb28 is involved in recovery of photosystem II at high temperature in *Synechocystis* sp. PCC 6803. *Biochim Biophys Acta*, 1827(1):50–59, Jan 2013.
  76. J. Fu and X. Xu. The functional divergence of two glgP homologues in *Synechocystis* sp. PCC 6803. *FEMS Microbiol Lett*, 260(2):201–209, Jul 2006.

## Supplementary Information for Behle, Dietsch, *et al.*: Uncoupling of the Diurnal Growth Program by Artificial Genome Relaxation in *Synechocystis* sp. PCC 6803

Strain name	Chromosomal genotype	Plasmid
EVC	P <sub>L22</sub> :dCas9	pSNDY (EVC)
<i>gyrA</i> <sup>kd</sup>	P <sub>L22</sub> :dCas9; P <sub>L22</sub> :sgRNA <sub><i>gyrA</i></sub>	pSNDY (EVC)
<i>gyrB</i> <sup>kd</sup>	P <sub>L22</sub> :dCas9; P <sub>L22</sub> :sgRNA <sub><i>gyrB</i></sub>	pSNDY (EVC)
<i>gyrAB</i> <sup>kd</sup>	P <sub>L22</sub> :dCas9; P <sub>L22</sub> :sgRNA <sub><i>gyrA</i></sub> ; P <sub>L22</sub> :sgRNA <sub><i>gyrB</i></sub>	pSNDY (EVC)
<i>topA</i> <sup>KD</sup>	P <sub>L22</sub> :dCas9; P <sub>L22</sub> :sgRNA <sub><i>topA</i></sub>	pSNDY (EVC)
<i>topA</i> <sup>OX</sup>	P <sub>L22</sub> :dCas9	pSNDY P <sub>J23119</sub> : <i>rhaS</i> ; P <sub><i>rha</i></sub> : <i>topA</i>

**Table S1. Construction of strains investigated in this work.** The parental strain for all strains listed here (*Synechocystis* sp. PCC 6803 encoding aTc-inducible dCas9) was a gift from P. Hudson and L. Yao [37], and is based on a strain they had obtained from Dr. Martin Fulda (Göttingen, Germany). It contains a TetR cassette, as well as dCas9 under the promoter P<sub>L22</sub>, inducible with anhydrotetracycline (aTc), at the genomic insertion site psbA1. Lun Yao and Paul Hudson further provided a strain with *gyrB*-targeting sgRNA. For the construction of the additional sgRNA constructs, sgRNA sequences (Tab. S2) were designed using CHOPCHOP [58], constructed *via* overlap extension PCR and integrated into the vector designed by [37] (Addgene ID 73224), which inserts into the *slr0230* site of the *Synechocystis* genome. The sgRNA plasmids were integrated *via* transformation. Briefly, 10 mL of exponentially grown culture was concentrated to 250  $\mu$ L, 1  $\mu$ g–2  $\mu$ g of pure plasmid was added and the mixture was incubated up to 5 h before plating the entire mixture on BG11 plates. After drying the plates, agar was underlaid with 300  $\mu$ L of 1 mg mL<sup>-1</sup> kanamycin stock using a sterile spatula, thereby forming a diffusion gradient. After 1-2 weeks of incubation at 30 °C with the lid facing upward, isolated green colonies were carefully transferred to a fresh plate. Over time, positive clones were gradually shifted to higher concentrations of kanamycin (4, 8, 12, 20, 40  $\mu$ g mL<sup>-1</sup> final concentration in the plate). Complete segregation of mutants was ensured *via* colony PCR. For rhamnose-inducible overexpression, the coding sequence of *slr2058* (*topA*) was integrated into pSHDY P<sub>J23119</sub>:*rhaS*; P<sub>*rha*</sub>:*mVenus* (Addgene ID 137662) [36] in place of *mVenus* *via* Gibson assembly. Both this new construct and pSHDY (Addgene ID 137661) were further modified by exchanging the spectinomycin resistance cassette with the nourseothricin cassette, resulting in pSNDY P<sub>J23119</sub>:*rhaS*; P<sub>*rha*</sub>:*topA* and pSNDY (EVC), respectively. Replicative vectors were introduced into the dCas9 background strain *via* conjugation as described ([dx.doi.org/10.17504/protocols.io.ftpbnnm](https://doi.org/10.17504/protocols.io.ftpbnnm)). Clones were selected using nourseothricin (Jena Bioscience, #AB-102L) at a final concentration of 50  $\mu$ g mL<sup>-1</sup> and verified *via* colony PCR.

Gene	sgRNA Sequence
<i>gyrA</i>	TCAGTCATGCAATTACTCCA
<i>gyrB</i>	CTGGCTTCAACCCATCCCGTGCAT
<i>topA</i>	GATAGTGCGGGCTTTAGTGG

**Table S2. sgRNA Sequences.** sgRNA sequences for CRISPRi-based knockdown strains (Tab. S1) were designed using CHOPCHOP [58].

Gene	Direction	Sequence
<i>gyrA</i>	forward	GAAC TTTGGCTCCGTGGATAA
	reverse	GCCTCAATGTCCCGCAATAA
<i>gyrB</i>	forward	TGCCCCGTAAGCGCAATAA
	reverse	ATTCTGGGTCCGGTACTTTAAC
<i>topA</i>	forward	AGACCGGGAAGGAGAAAGTA
	reverse	CGAATGGCTTCCTGGGTAAT
<i>rpoA</i>	forward	CCATGAGTTCGCCACTATTCT
	reverse	GGCTGATCGGTGTAGCTTT

**Table S3. RT-qPCR Primers.** Primers used for RT-qPCR of the indicated genes were designed using the IDT PrimerQuest tool (<https://eu.idtdna.com/pages/tools/primerquest>).

Name	RefSeq ID
genome	NC_000911
pCA2.4_M	CP003270
pCB2.4_M	CP003271
pCC5.2_M	CP003272
pSYSM	NC_005229
pSYSA	NC_005230
pSYSG	NC_005231
pSYSX	NC_005232
pSNDY P <sub>J23119</sub> : <i>rhaS</i> ; P <sub>rha</sub> : <i>topA</i>	*** submit ***

**Table S4. Genome and Plasmid Sequences for RNA-seq Mapping.** RefSeq IDs of the genome and plasmid sequences of *Synechocystis* used for mapping of the RNA-seq reads. \*\*\* pSNDY will be submitted to genbank before publication. \*\*\*

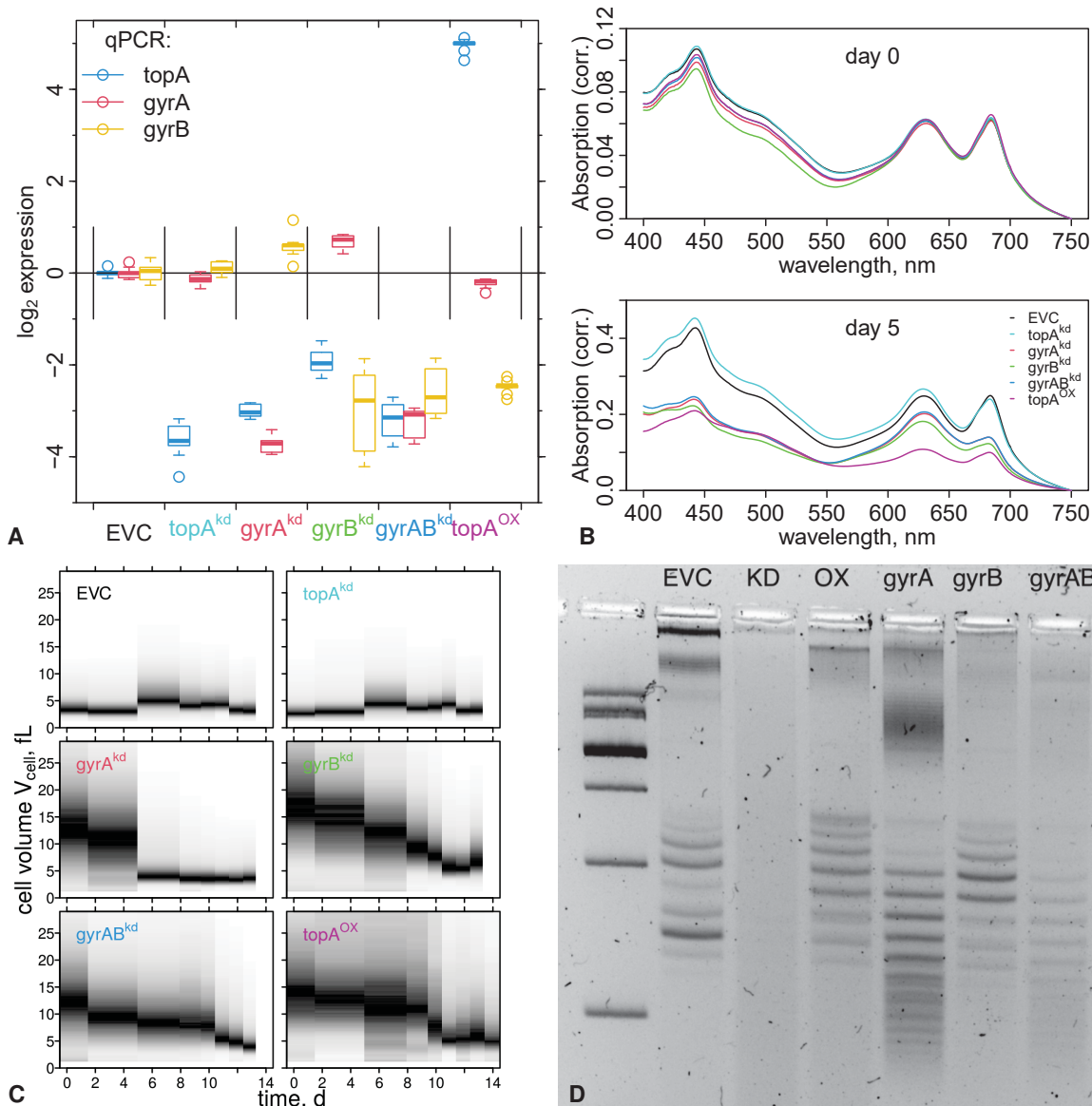


**Figure S1. Batch Culture Endpoint Measurements.** See Figure 2 for details. **A:** RT-qPCR results using *rpoA* as reference gene. Boxplots of 9 technical replicates (3 samples, each measured 3x). **B:** Absorption spectra at inoculation and harvest times. **C:** Recovery without inducer: all cultures were re-inoculated in fresh BG11 with antibiotics but without the inducers (aTc and rhamnose) and the cell size distributions measured at indicated time points. **D:** Chloroquine-agarose gels (1.2% agarose, 0.5x TBE and  $20 \mu\text{g mL}^{-1}$  CQ) of plasmids extracted at harvest time (5 d).

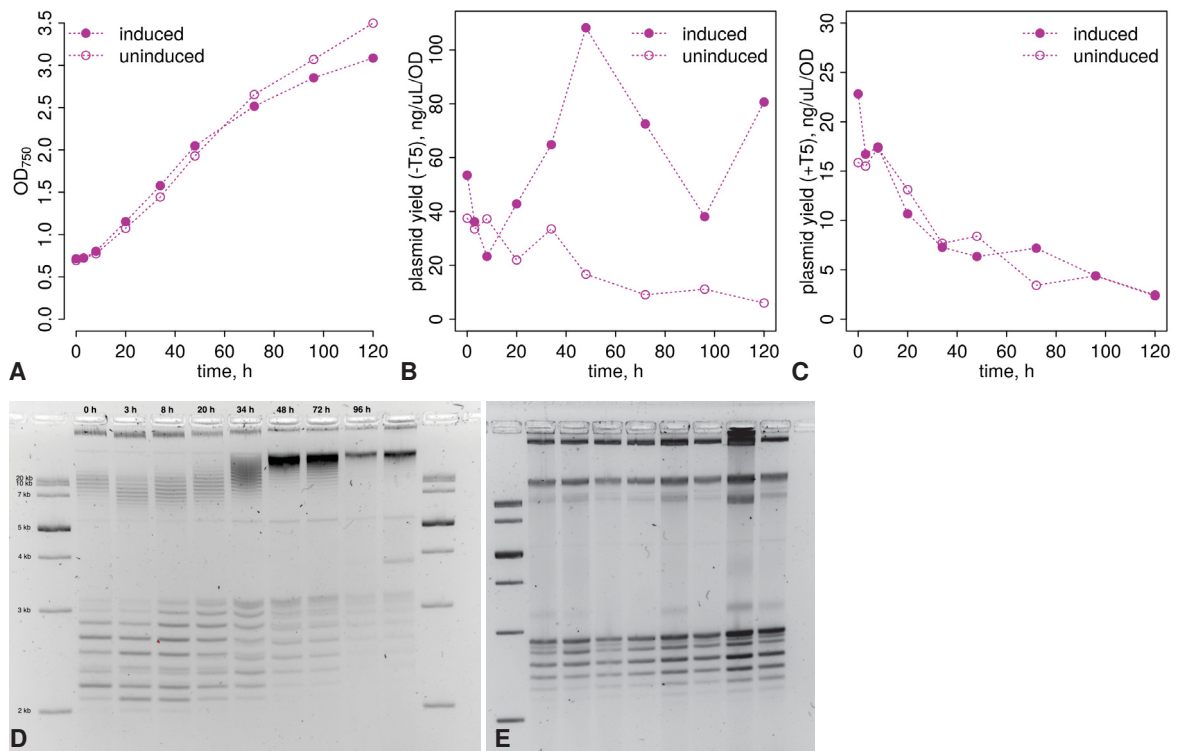


**Figure S2. Plasmid Supercoiling Gels.** **A:** Growth curves of  $\text{topA}^{\text{OX}}$  strain, induced with 1 mM rhamnose at time 0 h and uninduced control. A starter culture was split into 8 cultures at 0 h, each harvested at the indicated time points for  $\text{OD}_{750}$  measurement and plasmid extraction. **B & C:** Yields of plasmid extraction over time, each normalized to the  $\text{OD}_{750}$  (A), and before (B) and after (C) treatment with the T5 exonuclease to remove all non closed circular DNA. **D & E:** Chloroquine-agarose gels (1.2% agarose, 0.5x TBE and  $20 \mu\text{g mL}^{-1}$  CQ) of plasmids extracted from  $\text{topA}^{\text{OX}}$  strain cultures (A), induced (B) and uninduced (C). Note that only the gel of the induced culture (B) was run for a longer time (XYZ) to get a better separation of topoisomers of the pCC5.5\_M plasmid. Samples are ordered by sampling times (see A) from left to right on both gels. The 120 h sample is missing in (E).

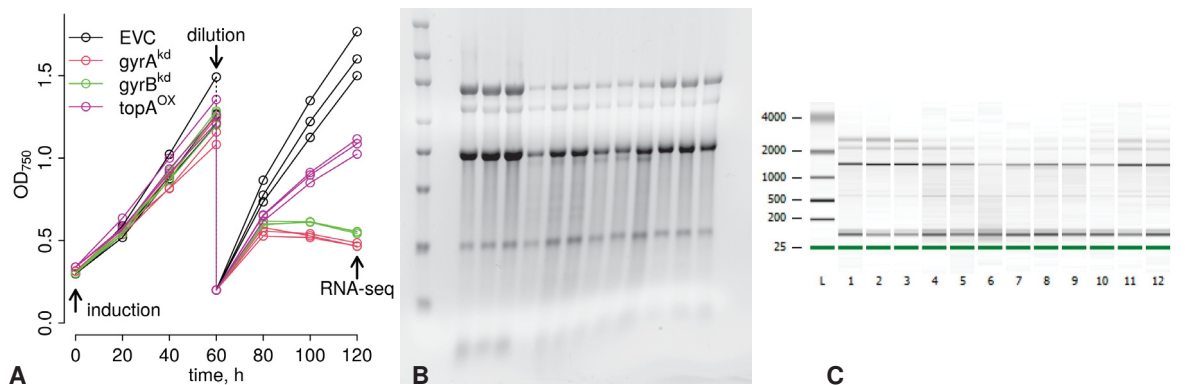


**Figure S3. Growth Curves & RNA Extraction for RNA-seq Experiment.** **A:** Growth curves of triplicate cultures (split upon induction at 0 d). **B & C:** Total RNA compositions were analysed by a formaldehyde-agarose gel (B, 500 ng RNA per well) and by capillary gel electrophoresis (Agilent Bioanalyzer); electropherograms of these samples were analyzed for Figures 4, S5 and S6. Sample lane order are identical in (B) and (C) and comprise of triplicates from EVC (lanes 1-3),  $\text{gyrA}^{\text{kd}}$  (lanes 4-6),  $\text{gyrB}^{\text{kd}}$  (lanes 7-9) and  $\text{topA}^{\text{OX}}$  (lanes 10-12).

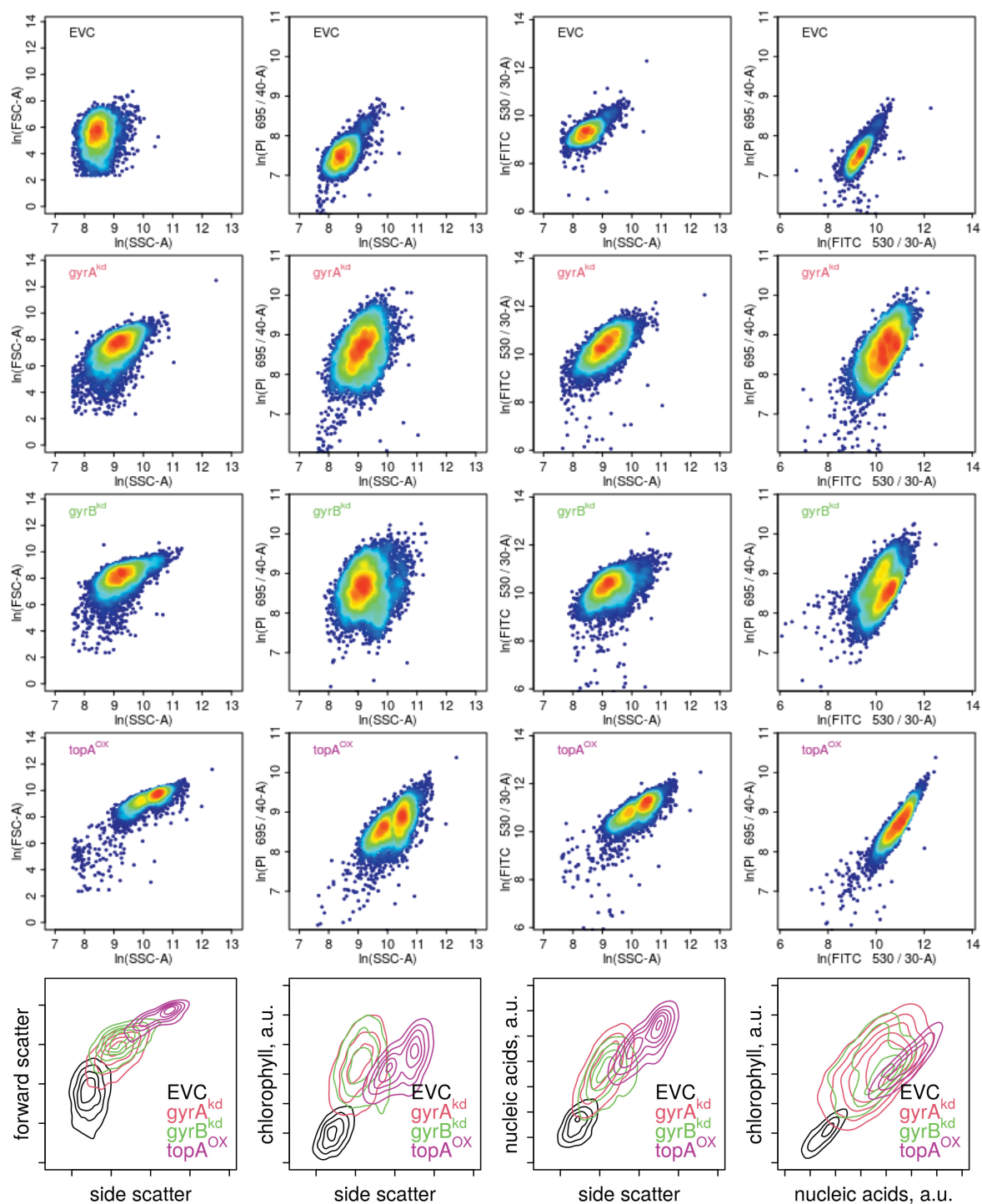


**Figure S4. Flow Cytometry.** Cells from the cultures used for RNA-seq and total RNA analysis (Fig. 4) were fixed in para-formaldehyde and stained with Syto-9, a nucleic acid fluorescence marker, and analyzed by flow cytometry. The data was gated by the side scatter signal ( $\text{SSC-A} > 2000$ ) and the forward scatter signal ( $\text{FSC-A} > 10$ ) to filter debris and background signals. Forward scatter (FSC-A) is proportional to cell size, side scatter (SSC-A) reflects cytoplasmic granularity and morphology; the FITC fluorescence channel (530/30 nm) excites the Syto-9 stain, and the PI channel (695/40 nm) excites chlorophyll. The natural logarithm ( $\ln$ ) of all data was plotted. Colors reflect local density (red: high, blue: low). The bottom panels show a zoom into the data, comparing the two strains with the most extreme values, EVC and  $\text{topA}^{\text{ox}}$  (white: high local density).

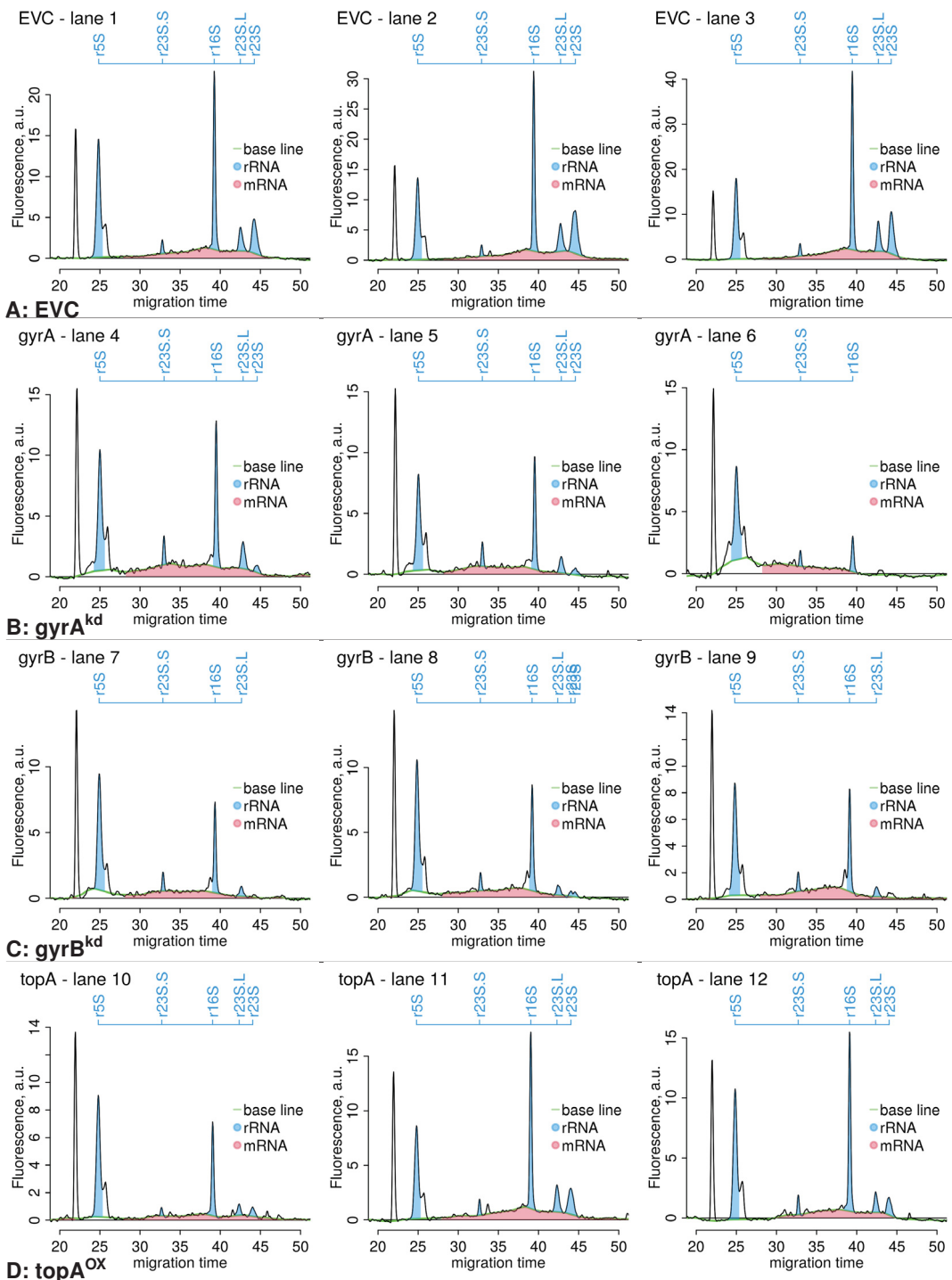


**Figure S5. Total RNA Electropherogram Analysis.** Electropherograms of the capillary gel electrophoresis (Fig. 4A), exported as XML files from the 2100 Bioanalyzer software. **A–D:** are each the triplicate samples for the indicated strain. Samples are the same as shown on the formaldehyde-agarose gel in Figure S3B and subsequently used for RNAseq analysis (Fig. 4B,C). Data was parsed into R with `bioanalyzer` (v 0.7.3) [63]. Baseline and peak detection and quantification were performed in R, see Methods paragraph *Analysis of Gel Electropherograms* for details. The areas of the blue peaks were further analyzed as relative rRNA species abundances (see top axis annotation). r23S.S and r23S.L are short and long fragments of the 23S rRNA typically seen in *Synechocystis*, the other peaks were assigned to 5S, 16S and (full length) 23S rRNA. The red area under the baseline (green) and > 200 bp was used as relative mRNA abundance for the ratios in Figure 4B,C and S6. The 200 nt length cut-off was based on the size calibration to the RNA ladder lane as reported by the `bioanalyzer` parser. The peak on the left is the 25 nt lower size marker.

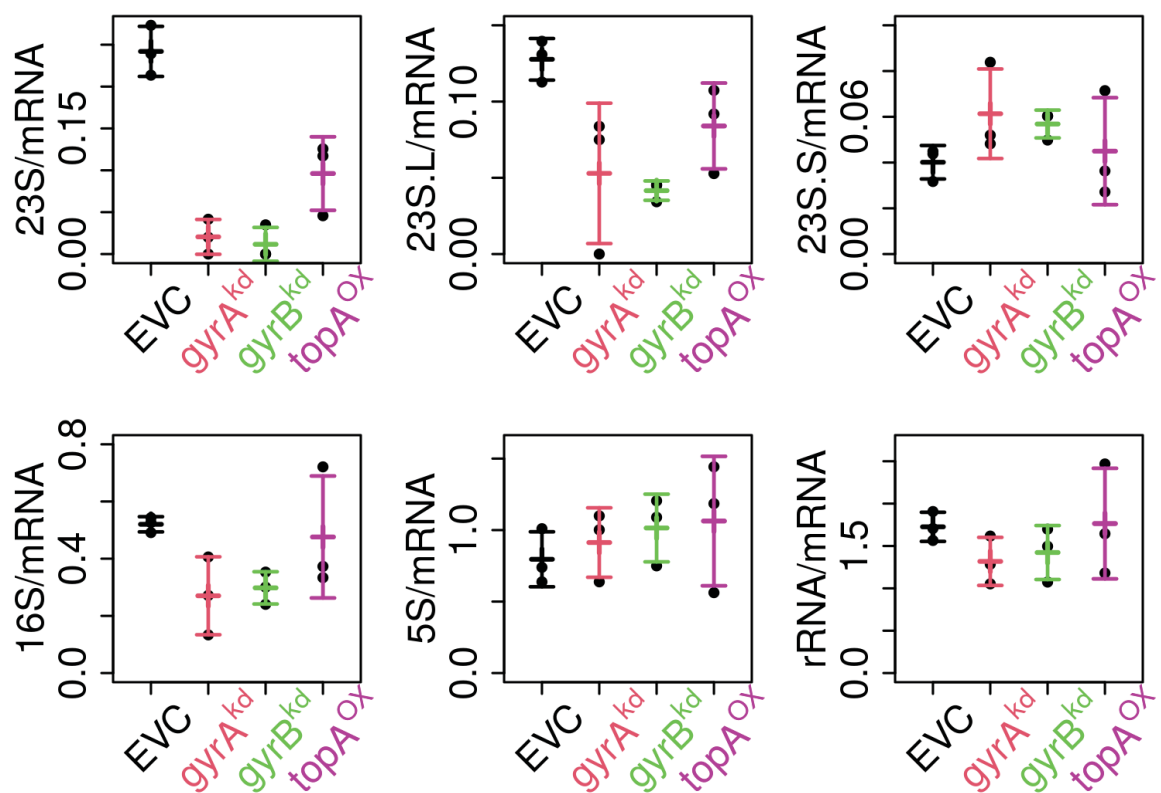


**Figure S6. rRNA vs. mRNA: Relative Abundances.** Ratios of the indicated rRNA peak areas to the baseline (mRNA) area, the blue and red areas in Figure S5, respectively. The error bars indicate the mean and standard deviation of the three replicates.

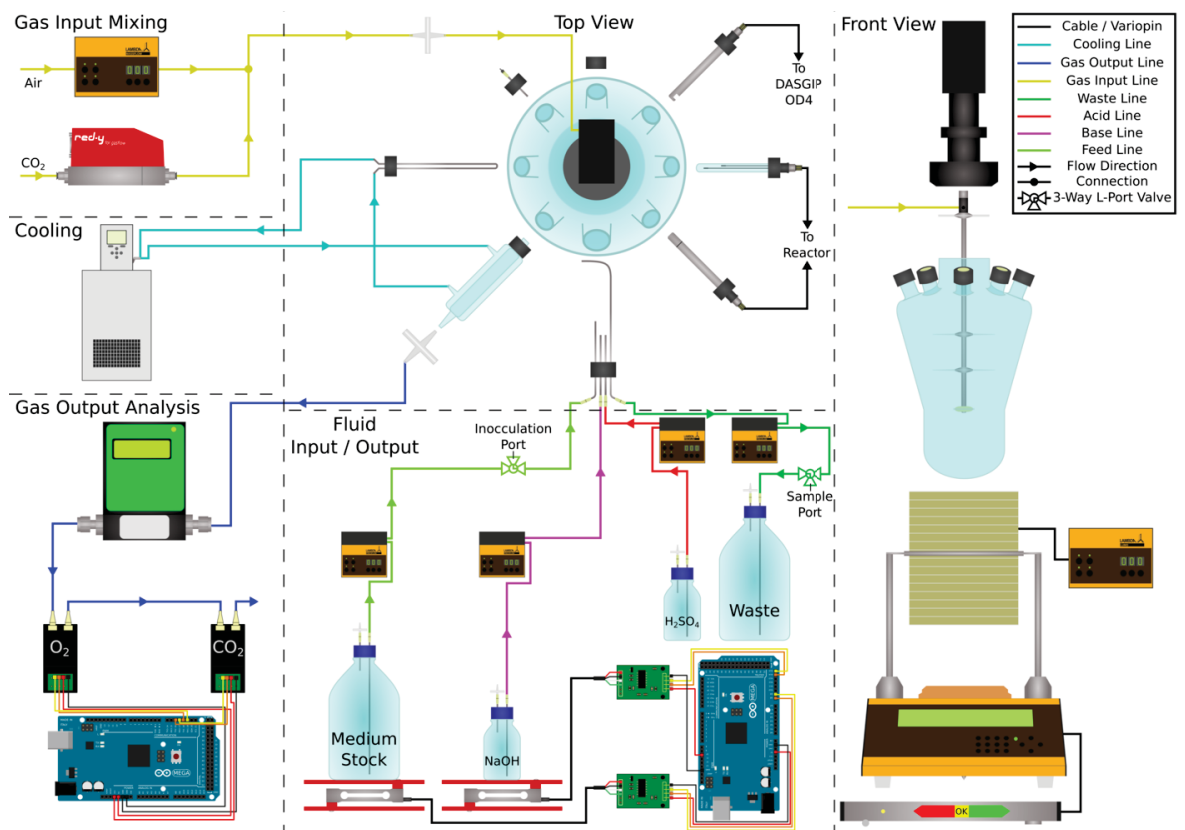


**Figure S7. Photobioreactor Setup.** A schematic overview of the cultivation setup showing the Lambda minifor bioreactor in front and top-down views alongside its external components and custom expansions. The gas input mixture is generated by a Lambda MASSFLOW 5000 gas flow controller and a Voegtlin red-y smart controller, which regulate the flow of compressed air and CO<sub>2</sub> respectively. This input gas mixture is then introduced into the cultivation vessel via the sparger at the end of the agitation unit. The offgas condenser as well as the reactor's cooling finger are part of a water cooling circuit which is regulated by a Lauda Eco Silver thermostat set to 16 °C. An Aalborg Massflow Meter monitors the flow rate of the culture's offgas before it is led through a custom microcontroller-based gas sensor array in order to evaluate its O<sub>2</sub> and CO<sub>2</sub> content. The reactor actively regulates the culture's pH and temperature values by controlling its heating compartment as well as the Lambda Preciflow peristaltic pumps which are attached to NaOH and H<sub>2</sub>SO<sub>4</sub> stock bottles, each 0.5 M. Additional culture parameters are monitored by a dissolved O<sub>2</sub> probe attached to the reactor and an OD4 probe connected to a DASGIP OD4 device. An additional set of peristaltic pumps is attached to the culture's medium stock and waste containers in order to control the reactor's volume and medium turnover. The reactor weighting module enables the system to operate under chemostatic conditions. This is achieved by manually configuring the medium feed peristaltic pump at a constant speed in order to achieve a desired medium turnover rate while automatically regulating the waste pump speed to keep the total reactor weight constant. Additionally, a custom microcontroller-based scale setup is monitoring the weight of both the medium and NaOH stock bottles, which allows for the calculation of medium and base pump rates from the recorded data. The culture's illumination is provided by the Lambda LUMO modules, an LED strip fitted around the cultivation vessel.

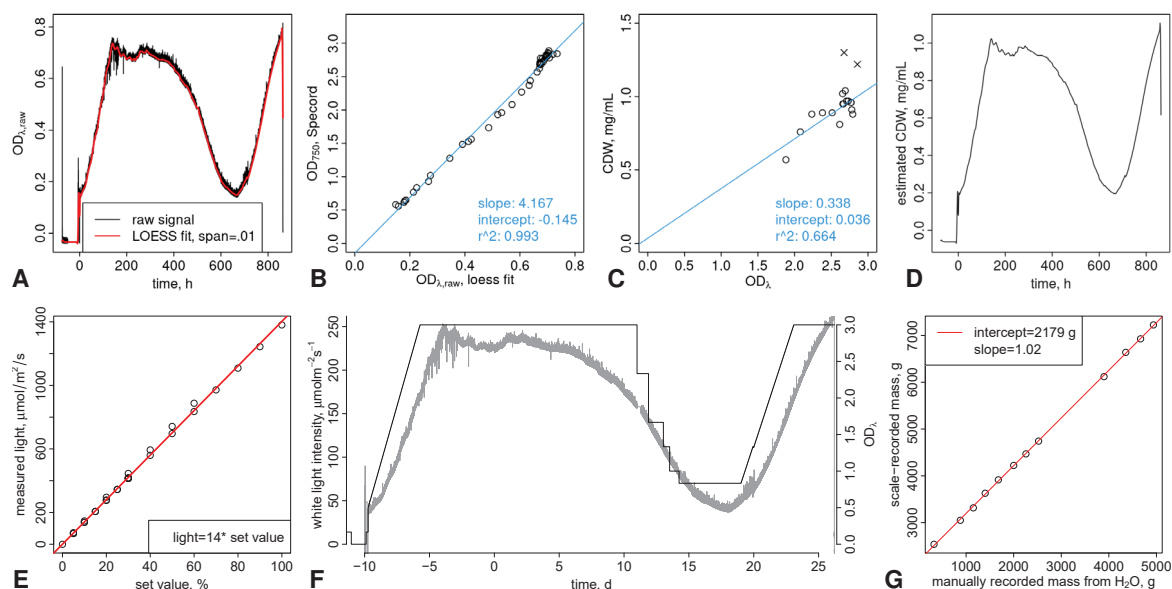


**Figure S8. Calibrations.** **A:** LOESS regression ( $R_{\text{loess}}$ ) of the raw signal (resolution ca. 1 sec) from the DasGip OD4 module ( $OD_{\lambda, \text{raw}}$ ). **B:** calibration of the LOESS fit of the  $OD_{\lambda, \text{raw}}$  signal to offline  $OD_{750 \text{ nm}}$  by linear regression ( $R_{lm}$ ). The calibrated signal is used throughout the document and denoted  $OD_{\lambda}$ . **C:** calibration cell dry weight (CDW) to the  $OD_{\lambda}$  signal. Data points marked by X were removed as outliers. **D:** the LOESS fit of the OD4 signal was then used to estimate CDW for all time points. **E:** calibration of the Lambda LUMO light module with a Licor light meter (LI-250A) with a spherical sensor bulb (LI-193). **F:** time-series of set and calibrated (white) light intensities (black line, left y-axis) compared to the  $OD_{\lambda}$  time-series (gray line, right axis). The light intensity was manually adjusted to avoid high-light stress in the culture during biomass decrease: light was initially increased as a ramp from 42 to 250 photons, then kept constant, and manually decreased to maintain light intensity approximately at  $\sim 90 \mu\text{mol m}^{-2} \text{s}^{-1}$  per  $OD_{750}$ . After the switch to batch culture light was again increased from 70 to  $250 \mu\text{mol m}^{-2} \text{s}^{-1}$ . **G:** The Arduino-based scales were calibrated prior to the experiment (not shown). During the experiment the liquid level on the 5L feed bottle was marked regularly, and the mass of water filled to these marked was recorded on a benchtop scale (Kern) after the experiment to test consistent performance. The recorded mass was reproduced sufficiently well (red line: linear regression): the intercept of the linear regression corresponds to the mass of the empty feed bottle and the slope was  $\approx 1$ . Since the manual marks on the bottle are more error prone than the pre-calibration, we did not re-calibrate the data but relied on the recorded mass for calculation of the dilution rate.

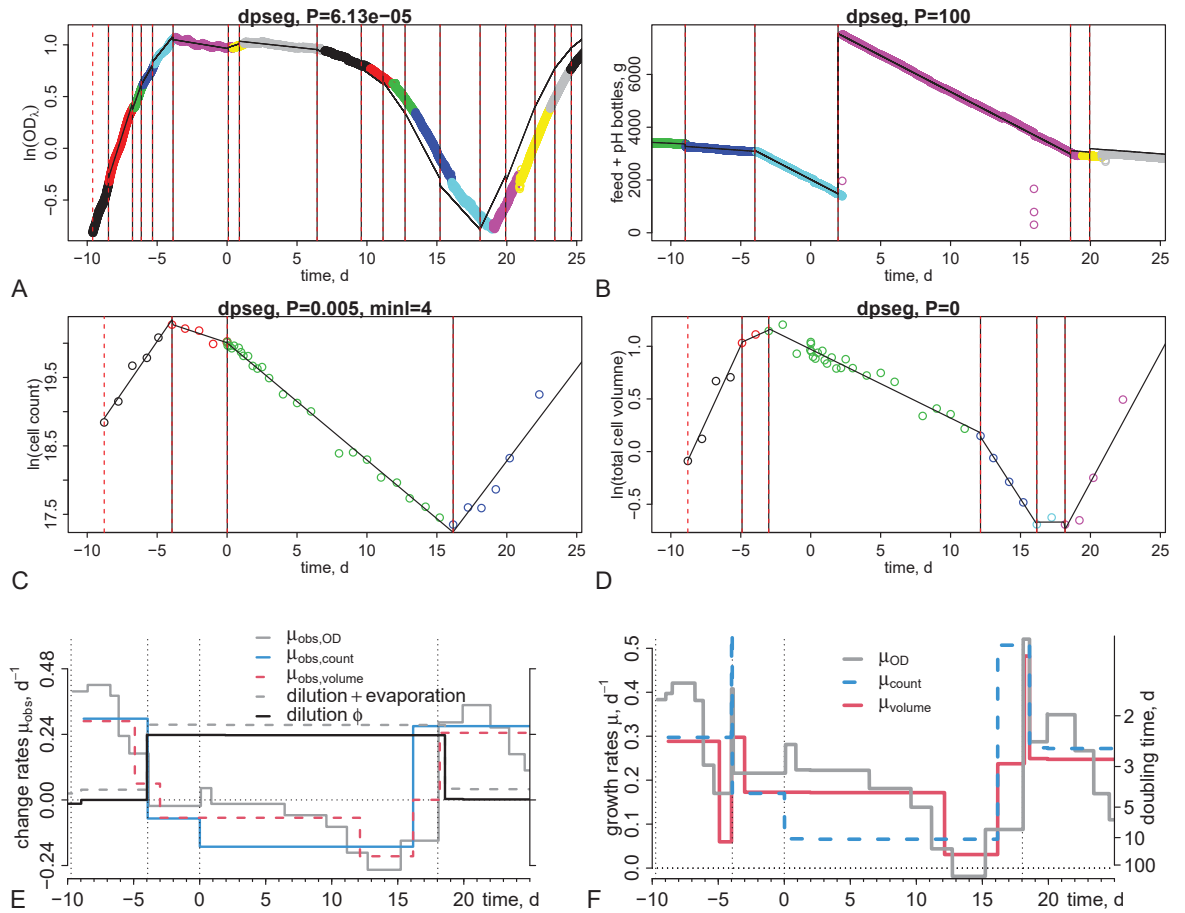


**Figure S9. Calculation of Dilution and Growth Rates.** All rates were calculated from the slopes of measured data (or of their natural logarithms as indicated) using piecewise linear segmentation with the R package `dpseg`. The plots in **A-D** were generated by `dpseg` and the vertical lines indicate borders of the piecewise segments, and the used penalty parameter  $P$  is shown in the plot title on the top axis. The minimal segment length parameter `minl` was only used in (C). **A**: the calibrated  $OD_\lambda$  signal (1 sec resolution) was smoothed with a moving average and window size 15 and interpolated at 300 sec intervals. **B**: sum of the recorded weights of edium feed and pH control bottle weight; outliers (faulty measurements or bottle changes) were removed and data interpolated at 300 sec intervals. **C**: the total cell count for each CASY measurement, single measurements and means of technical duplicates. **D**: the total cell volume, calculated as the integral of the single cell volume distribution, for each CASY measurement, single measurements and means of technical duplicates. **E**: Observed rates. The (negative) slopes of the summed bottle weight changes (B) reflect the amounts added to the reactor culture by the Lambda reactor mass control system, assuming 1 g/mL density. The total culture dilution rate (dashed gray line, “dilution + evaporation”) is obtained by division by the culture volume ( $V_\ell = 1$  L). The liquid loss by evaporation is seen at times before onset of continuous culture (time -4 d) and is subtracted to obtain the actual dilution rate  $\phi$  (black line). The slopes of the change of the natural logarithms of the  $OD_\lambda$  signal (A), the total integrated cell volume (B), and the cell counts (C) are the observed change rates  $\mu_{\text{obs,OD}}$  (gray line),  $\mu_{\text{obs,volume}}$  (red line) and  $\mu_{\text{obs,count}}$  (blue line), respectively. **F**: The culture growth rates  $\mu_{\text{OD}}$  (gray line) and  $\mu_{\text{count}}$  (blue line) and  $\mu_{\text{volume}}$  (red line) were calculated as the difference between observed change rates and the culture dilution rate:  $\mu = \mu_{\text{obs}} - \phi$ .

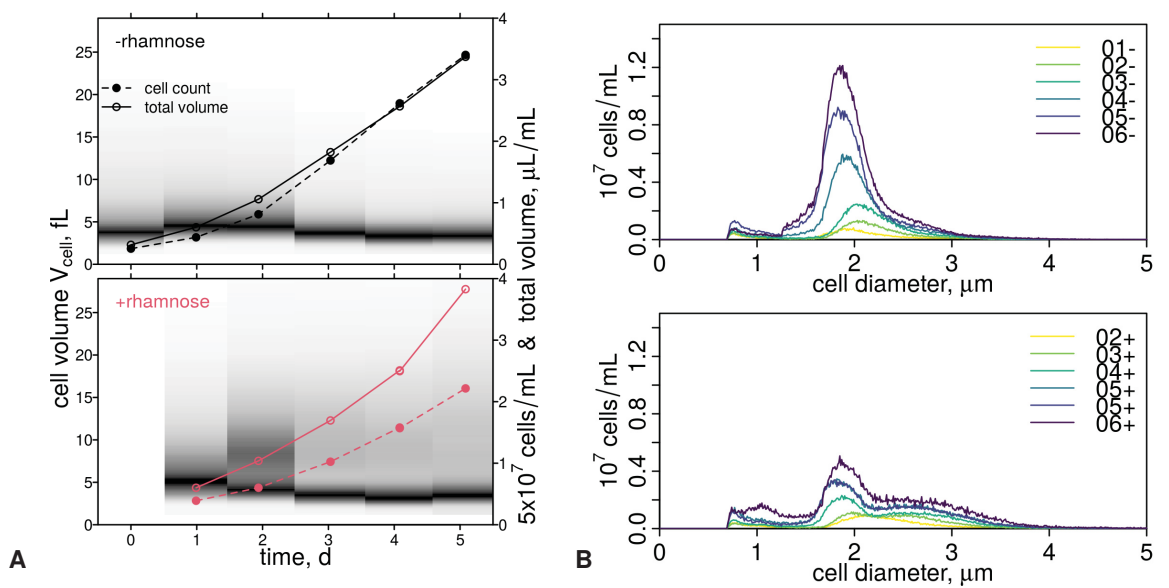


**Figure S10. Re-Induction of Bioreactor Time-Series Cultures.** After harvest, cells from the bioreactor timeseries experiment (strain  $\text{topA}^{\text{OX}}$ ) were spun down, washed and re-inoculated in fresh BG11 with antibiotics and without (top panels, -rhamnose) or with (bottom panels, +rhamnose) in shake flasks (batch culture), and cell count and volume distribution measured daily with the CASY cell counter. **A:** cell volume distributions as gray-scale (left axis) and cell count and total cell volume with open and closed points (right y-axis). **B:** Distributions of the cell diameter as reported by the CASY cell counter and from which cell volumes were calculated. Cells grew normally without further  $\text{topA}^{\text{OX}}$  induction and showed the initial transient volume increase that was observed in all experiments without induced volume growth (e.g. EVC and  $\text{topA}^{\text{KD}}$  in Fig. 2B and Fig. S1C). After re-induction of  $\text{topA}^{\text{OX}}$ , only a fraction of cells again showed in increase in cell volume.

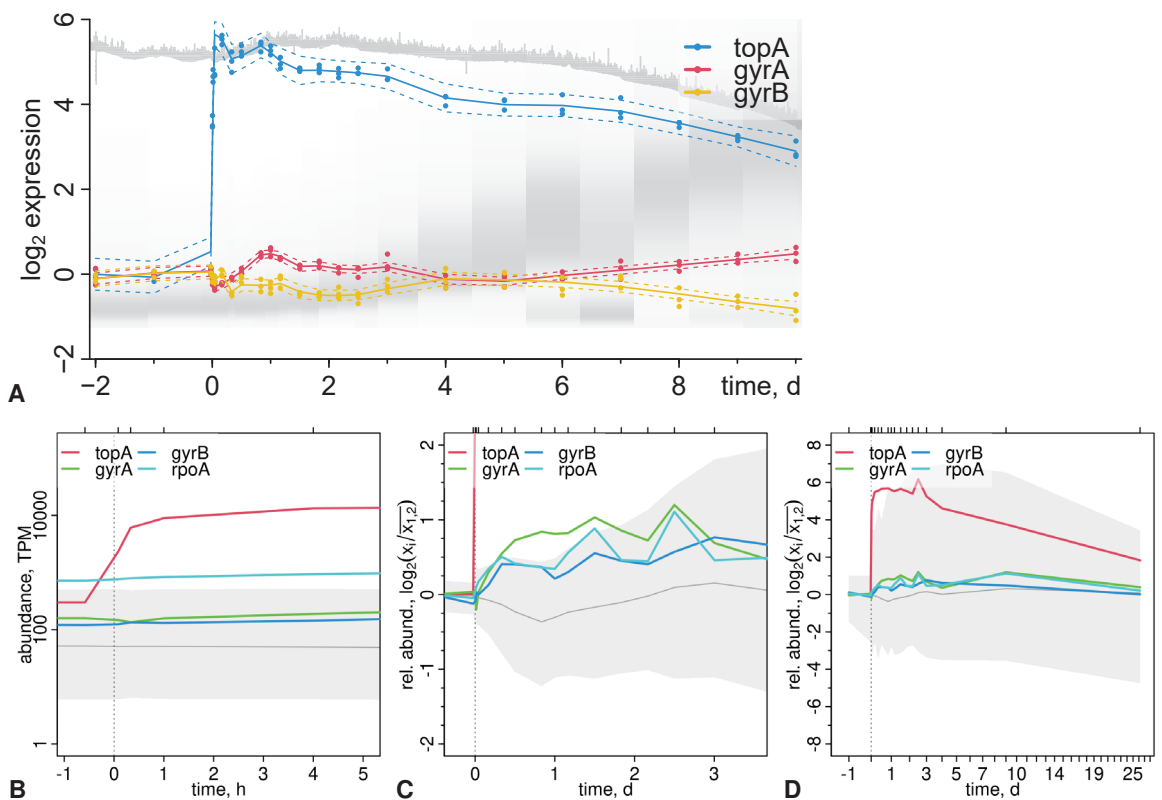


**Figure S11. RT-qPCR vs. RNA-seq.** **A:** The *topA*, *gyrA* and *gyrB* genes were also measured by RT-qPCR using *rpoA* as a reference “house-keeping” gene. **B-D:** The tested genes and the house-keeping gene in the RNA-seq data at different x-axis zoom levels and for raw TPM read-count data in (B) and  $\log_2$ -fold change over the mean of the two pre-induction samples (C, D). Notably, *rpoA* expression in RNA-seq data increases with a periodic pattern and this should have affected the RT-qPCR measurements. Considering this, the RT-qPCR and RNA-seq data are consistent: *gyrA* initially decreases and *gyrB* increases (< 1 h); later (< 3 d) *gyrA* increases more (than *rpoA*) and *gyrB* less (than *rpoA*); followed by a phase of roughly equal expression (4-5 d) and again bifurcation of expression values (> 6 d).

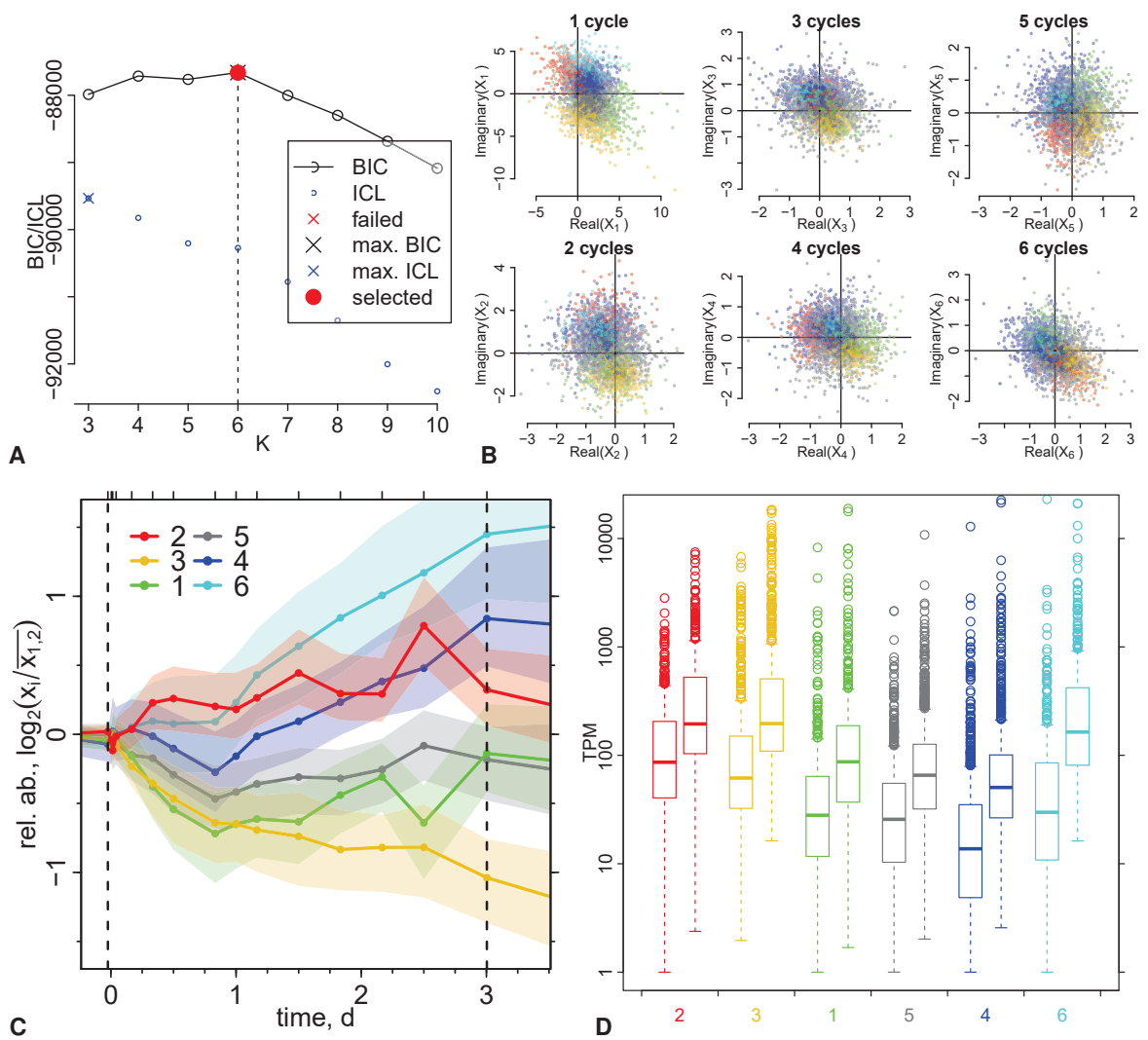


**Figure S12. Clustering & Total Read-Count Distribution.** **A:** Bayesian Information Content (BIC) as reported by `flowClust` for clustering of selected scaled components  $X'_{k=1,\dots,6}$  of the Discrete Fourier Transform (DFT) of the `arcsinh`-transformed TPM data over varying number of cluster centers ( $K$ ). The maximal BIC was reached for a classification into  $K = 6$  distinct clusters (co-expression cohorts). This clustering was chosen for further analysis. **B:** real and imaginary parts of the DFT that were used for clustering (R package `flowClust` [71]). Colors already indicate the final cluster assignments of each transcript at  $K = 6$  (A). **C:** Cluster medians (solid lines) of the relative transcript abundances (rel. abund.). For each transcript the  $\log_2$  of the ratio of read-counts at time points  $i$  to mean of the two samples before induction ( $i = 1, 2$ , at  $-1$  d and  $-1$  h) was calculated (points indicate the sampling time points  $i$ ). The transparent ranges indicate the 25% and 75% quantiles of each cluster. Only the time points within to two vertical lines were used for clustering. **D:** Cluster-wise distributions (boxplots) of minimal (left) and maximal (right) read-count values (TPM) of each transcripts.

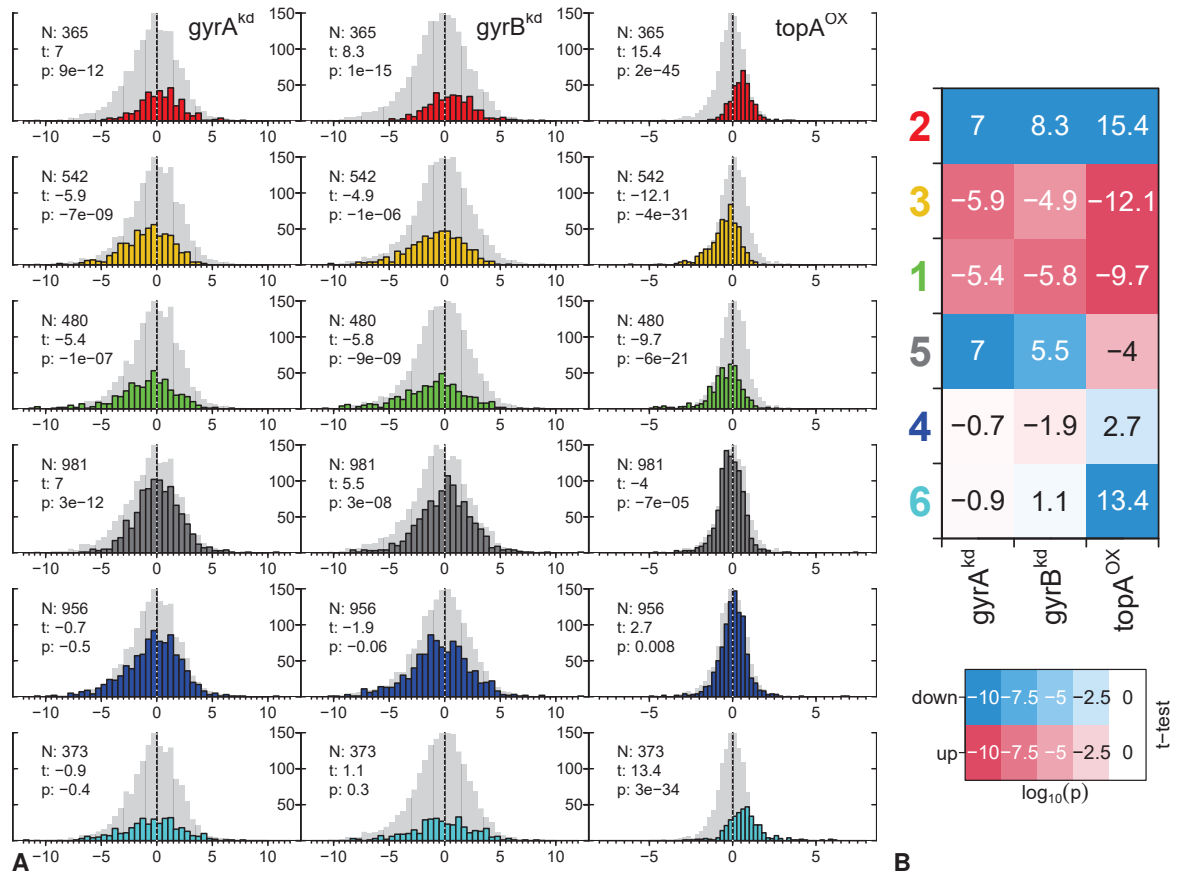


**Figure S13. Co-Expression Cohorts in the Endpoint RNA-seq and Construction of t-Test Profiles. A:** Distributions of the  $\log_2$  fold-change of transcript abundances in the three strain endpoint experiment for each of the co-expression clusters derived from the *topA<sup>ox</sup>* time series data. The gray background shows the distribution of all other transcripts. The y-axis are the counts for the colored distributions, while the gray background distributions are densities (without axis). For each cluster a t-test was performed (base R function `t.test`) against all transcripts not in the cluster, and the cluster sizes  $n$ , and the  $t$ -values and the  $p$ -values from each test are shown in each plot. The total number of transcripts with expression values were 3676 for *gyrA<sup>kd</sup>* and *gyrB<sup>kd</sup>*, and 3680 for *topA<sup>ox</sup>*. **B:** A t-test profile plot is constructed from the t-test results in (A). A negative  $t$ -value indicates that the tested cluster transcripts have a lower mean abundance than all other transcripts and this is indicated by a red color field, the rounded  $t$ -value is shown in the fields; blue indicates a positive  $t$ -value and higher mean abundance. The  $p$ -value is converted to a transparency value for the red and blue colors (along a color palette from red/blue to white), such that the full color is reached for  $p \leq p_{\min}$ , and for higher  $p$ -values the transparency scales with  $\log_2(p)$ . Both, for visibility of the text and to indicate an additional  $p$ -value cut-off the text ( $t$ -values) is plotted in white if  $p \leq p_{\text{text}}$ . The bottom legend shows 5  $p$ -values (text:  $\log_{10}(p)$ ) and the resulting field and text colors. Here  $p_{\min} = 10^{-10}$  and  $p_{\text{text}} = 10^{-5}$ .

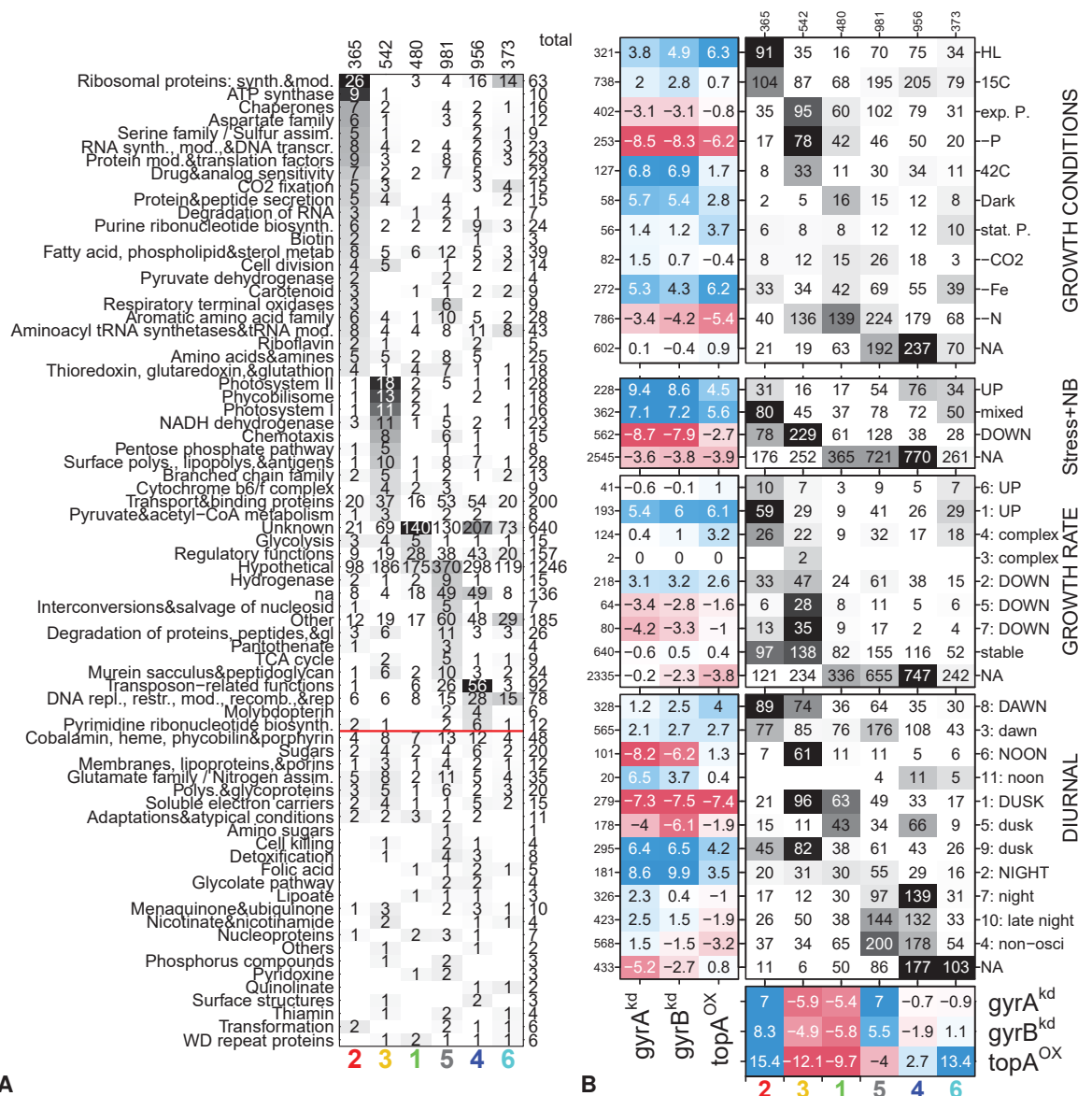


**Figure S14. CyanoBase Category Analysis of Co-Expressed Cohorts. A:** Sorted enrichment profile of functional category annotations as in Figure 5E (colored with  $p_{\min} = 10^{-10}$  and  $p_{\text{text}} = 10^{-5}$ ) but sorted at  $p_{\text{sort}} = 0.1$ . All categories below the red line had only  $p > p_{\text{sort}}$  and are unsorted. Some abbreviations of the original annotation terms are used for readability of the plot: synth. - synthesis, mod. - modification, repl. - replication, transcr. - transcription, recomb. - recombination, restr. - restriction, s. - saccharides, assim. - assimilation, & - and. **B:** Overlap enrichment and t-test profiles with clusterings as Figure 6C but for additional gene classifications from other publications; from top to bottom: experimental GROWTH CONDITIONS with maximal expression of transcription units from Kopf *et al.* [46], stress and novobiocin (Stress + NB) treatment (same as in Fig. 6C) from ref. [4], the original non-collapsed clustering of protein abundance level response to GROWTH RATE from Zavrel *et al.* [14], and a clustering of a DIURNAL transcriptome data set from the supplemental material of Lehmann *et al.* [34].

	365	542	480	981	956	373	total
structural constituent of ribosome	25	2	2	14	13	56	
translation	25	2	2	15	14	62	
rRNA binding	17	1	2	8	7	35	
proton-transporting ATP synthase activity, rotational mechanism	3	1	1	2	1	8	
cytoplasm	55	34	26	80	63	285	
cytosolic small ribosomal subunit	9	1	1	2	1	14	
ATP binding	53	43	28	61	71	292	
cytosol	43	30	18	58	47	220	
plasma membrane proton-transporting ATP synthase complex	6	1				7	
cytosolic large ribosomal subunit	10			4	6	20	
ATP synthesis coupled proton transport	5					5	
proton-transporting ATP synthase complex, coupling factor F <sub>0</sub>	5					5	
chaperone cofactor-dependent protein refolding	5		1			6	
GTP binding	12	5	2	9	2	35	
tRNA binding	10	1	1	3	4	21	
RNA binding	12	3	1	3	1	21	
unfolded protein binding	7	3	1	3	2	15	
proton-transporting ATP synthase complex, catalytic core F <sub>1</sub>	4	1				5	
DNA-directed 5'-3' RNA polymerase activity	4			1		5	
transcription, DNA-templated	4			1		5	
protein transport by the Sec complex	4					4	
protein targeting	4					4	
GTPase activity	8	5	3	3	3	22	
mRNA binding	1	2	1	1	2	7	
protein folding	5	5	1	2		13	
threonine biosynthetic process	4	1	1		1	7	
response to heat	4			1		5	
carotenoid biosynthetic process	3			1		4	
ribosome	6		2	1	5	14	
carboxysome	5	1		2	2	10	
protein transport	4	1	1	2	1	9	
RNA processing	3			2		5	
RNA processing	3			2		5	
ribosomal small subunit assembly	3				2	5	
intracellular protein transmembrane transport	3	1				4	
translation elongation factor activity	3	1				4	
metal ion binding	33	43	21	61	38	221	
glycogen debranching enzyme activity	2					2	
cytochrome complex	2					2	
cell envelope Sec protein transport complex	2					2	
cytoplasmic translation	2					2	
GroEL-GroES complex	2					2	
NAD metabolic process	2					2	
NADP biosynthetic process	2					2	
translational elongation	2					2	
'de novo' CTP biosynthetic process	2					2	
CTP biosynthetic process	2					2	
plasma membrane-derived thylakoid membrane	63	13	11	2		90	
photosynthesis	41	11	14	3	6	75	
plasma membrane-derived thylakoid photosystem II	1	19	2	2		24	
integral component of membrane	60	148	64	125	129	499	
inorganic phosphate transmembrane transporter activity	7					7	
phycobilisome	3	13	1	2	2	21	
quinone binding	3	12	2	4	3	25	
protein-chromophore linkage	1	15	4	5	3	28	
photosystem II reaction center	1	8	1	1	1	12	
photosynthesis, light reaction	9	1	1	1	1	13	
NADH dehydrogenase (ubiquinone) activity	7	1	4	1	1	14	
electron transporter, transferring electrons within the cyclic electron transport pathway of photosynthesis	7	1	1	1	1	11	
plasma membrane-derived photosystem I	5					5	
phosphate ion binding	4					4	
phosphate ion transmembrane transport	4					4	
iron ion binding	3	4	4	11	4	26	
photosynthetic electron transport in photosystem II	5	1	1			7	
photosystem I	1	5	1			7	
metalloendopeptidase activity	4	10		7	1	22	
efflux transmembrane transporter activity	4			1		5	
photosynthetic electron transport chain	4					4	
nitrate assimilation	4			1		5	
heme binding	3	9	6	2	2	22	
ATPase-coupled phosphate ion transmembrane transporter activity	3					3	
oxidoreductase activity, acting on the CH-CH group of donors, iron-sulfur protein as acceptor	3					3	
photosynthesis, dark reaction	7	19	12	17	9	64	
outer membrane-bounded periplasmic space	4					4	
light-independent chlorophyll biosynthetic process	4					4	
photosystem II	4	1	1			6	
oxygen evolving activity	4	1	1			6	
NADP binding	3	7	1	2	3	17	
electron transfer activity	5	12	3	12	4	36	
NOT ANNOTATED	49	123	223	313	838	1355	
histidine phosphotransfer kinase activity	1	8	3	3	3	18	
monosaccharide binding	1	3	3	3	3	13	
protein autophosphorylation	2	8	4	3	3	20	
protein disulfide oxidoreductase activity	1	4	1	1	1	7	
protein-disulfide reductase activity	1	3				4	
chemotaxis	1	1		7	1	10	
plasma membrane transposase activity	31	45	20	77	48	230	
transposition, DNA-mediated	4			4	22	26	
DNA binding	13	10	12	34	20	149	
DNA-directed DNA polymerase activity	1					1	
endonuclease activity	1	2	1		10	16	
defense response to virus	1		3		9	13	
maintenance of CRISPR repeat elements	1				5	6	
exodeoxyribonuclease V complex	1				1	2	
single-stranded DNA helicase activity	1				3	4	
siderophore uptake transmembrane transporter activity	1				3	4	
5'-3' DNA helicase activity	1				3	4	
type I site-specific deoxyribonuclease activity	1				3	4	
ribosomal large subunit assembly	2				1	3	
DNA modification	2				1	3	

**Figure S15. GO Analysis of Co-Expressed Cohorts.** Sorted enrichment profile as in Figures 5E and S14A (colored with  $p_{\min} = 10^{-10}$  and  $p_{\text{ext}} = 10^{-5}$ ) but for Gene Ontology (GO) terms, downloaded from the UniProt database (2021-03-20, organism: 1111708). Rows are cut and sorted along columns at  $p_{\text{sort}} = 0.01$ .

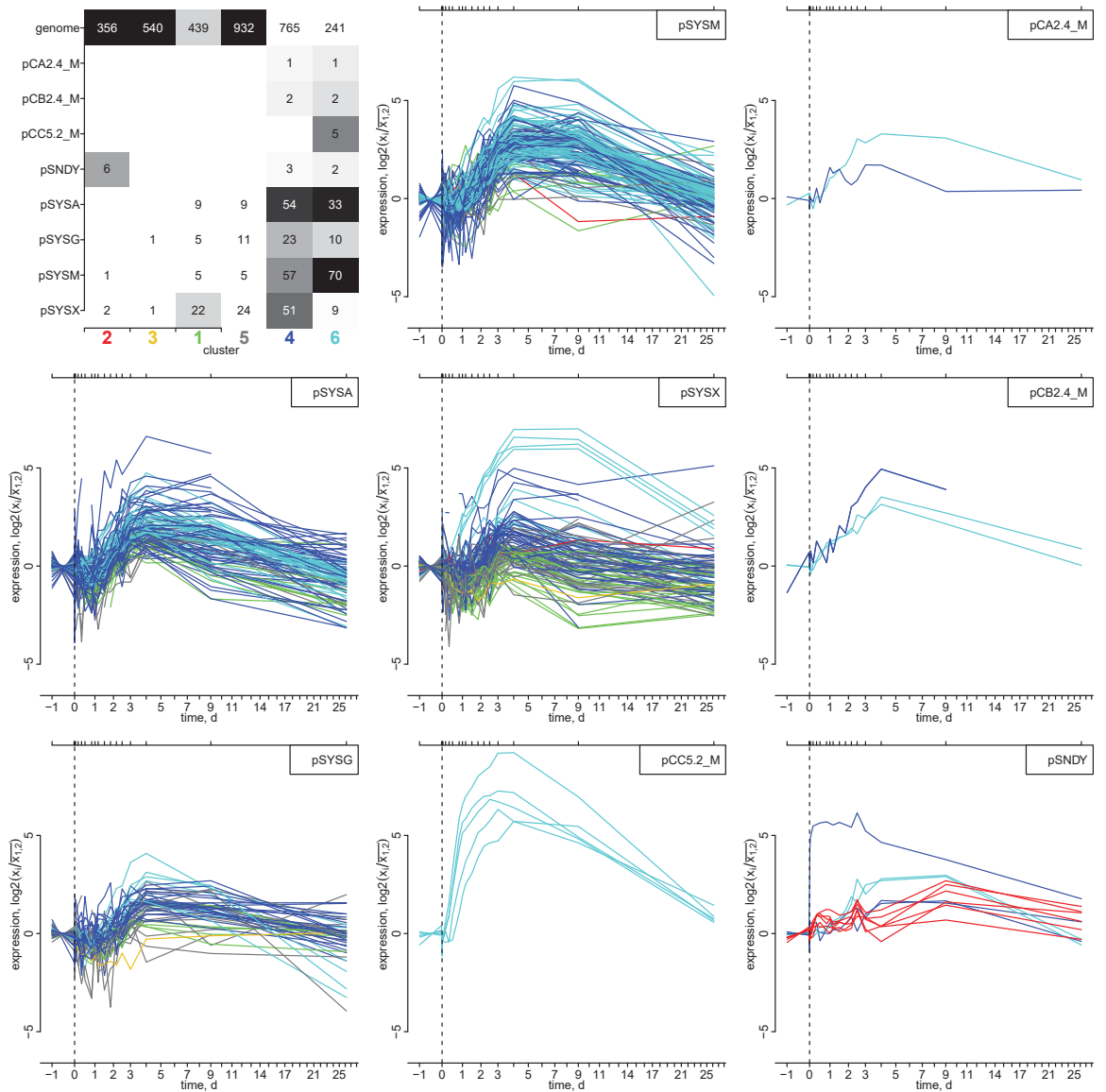


**Figure S16. Transcriptome Time Series - Plasmids.** Top left panel: Enrichment profile of time series clusters with the locations on the chromosome, one of the seven endogenous plasmids, or our construct pSNDY [36] (Table S1). All other panels show the temporal transcript abundance profiles for the coding genes of each plasmid (see top right legends for plasmid names); each transcript is colored according to its cluster label.

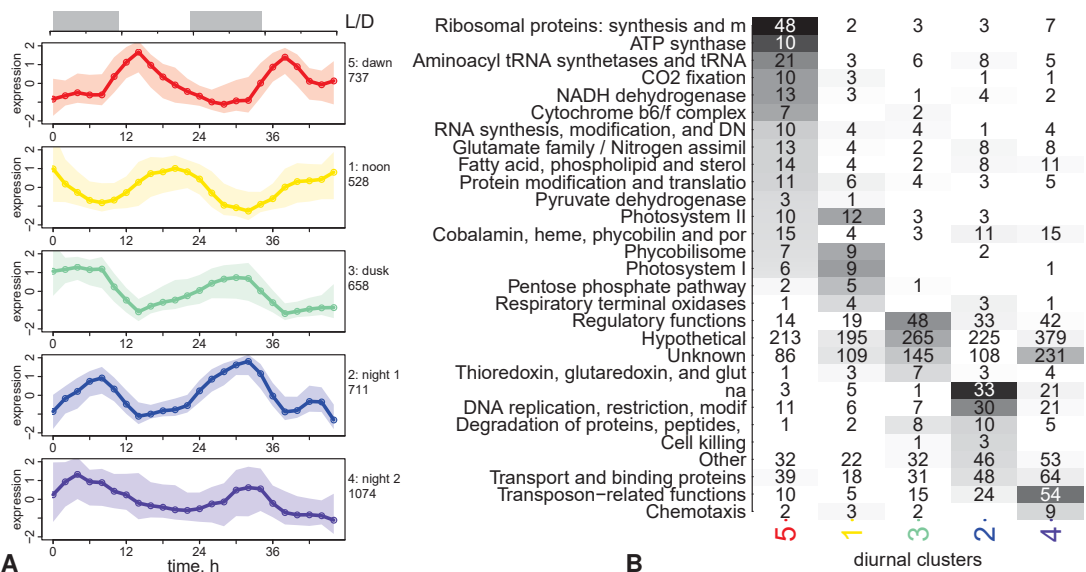


**Figure S17. Diurnal Co-Expression Cohorts.** Clustering of diurnal transcriptome data from ref. [44] into 5 co-expression cohorts, see Methods for details. **A:** Cluster medians of the normalized (to mean 0) expression values with an additional moving average over 3 samples. Transparent ranges show the 10% and 90% quantiles, *i.e.* they encompass 80% of all values in a cluster. Cluster labels and sizes (number of genes) are indicated on the right y-axis. The gray and white bars on the top indicate dark and light phases of the experiment. **B:** Enrichment profiles of co-expressed cohorts with CyanoBase functional categories as for Figure 5E (colored with  $p_{\min} = 10^{-10}$  and  $p_{\text{text}} = 10^{-5}$ ), but cut and sorted at  $p_{\text{sort}} = 0.05$ .

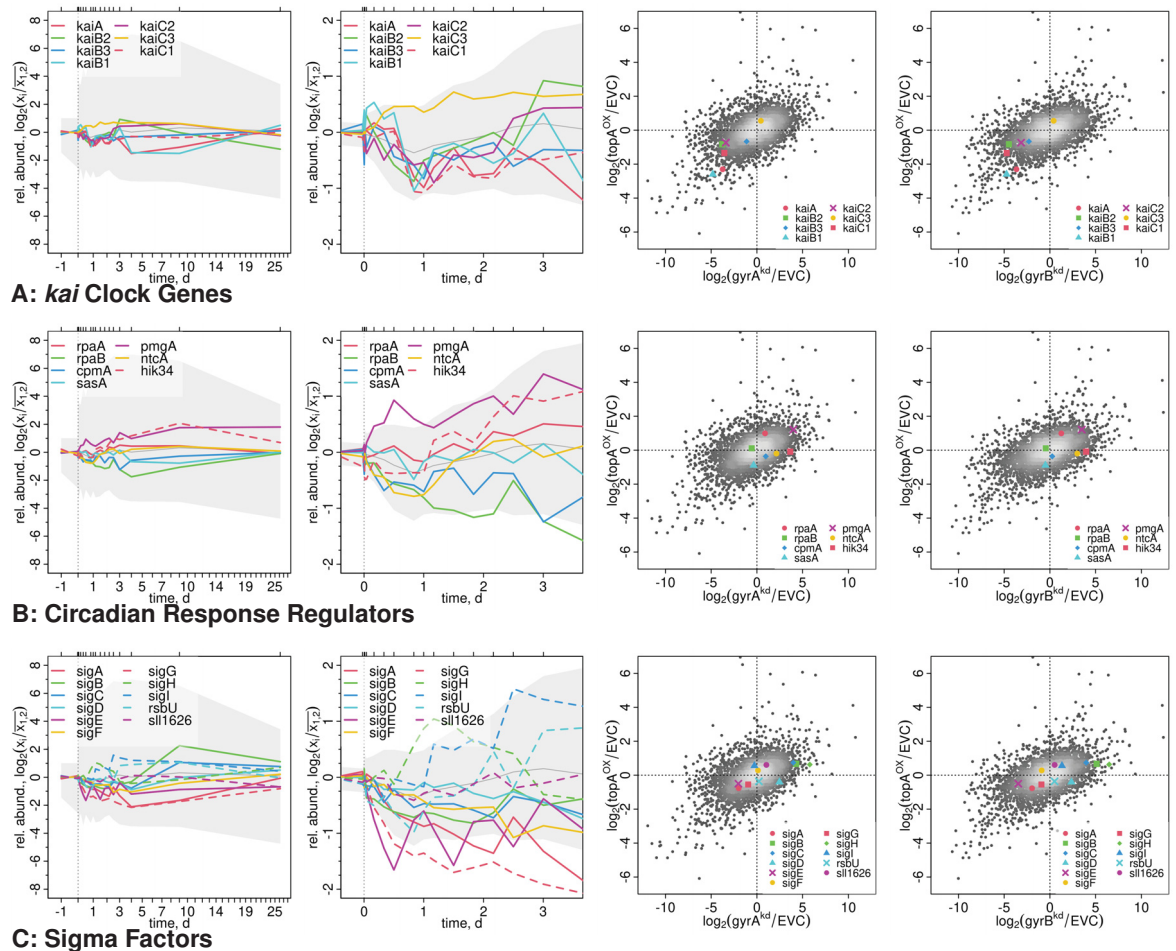


**Figure S18. Genes of Interest: Regulators.** Transcript abundance profiles of a selected groups of genes; from left to right: the full time-course, a zoom on the first three days, and expression changes with respect to the EVC in the endpoint experiments (as in Fig. 4D,E). The gray background in the time series plots shows the 92.5% and 7.5% quantiles of all data as a reference, the gray dots in the endpoint experiments are all other genes and the gray scale indicates local density. Some genes with strong response are specifically mentioned in the following. **A, Clock Genes:** During the first half day post-induction *kaiB1* was upregulated, then quickly downregulated with most other *kai* genes. Only *kaiC3* was upregulated, reflecting the pattern of the RB/*dawn* cohort, and then remained slightly overexpressed until the last sampled time point. At 3 d *kaiB2* and *kaiC2* were upregulated. **B, Signaling:** The circadian clock output regulator *rpaA* was only slightly upregulated, while its paralog *rpaB* was downregulated. **C, Sigma Factors:** Most sigma factors [48] were downregulated, except for the group 3/4 factors *sigH*, peaking at 1 d, followed by *sigI* (2 d–3 d), and a late peak (10 d, when cells were already enlarged) of the group 2 and stress-response sigma factor *sigB*.

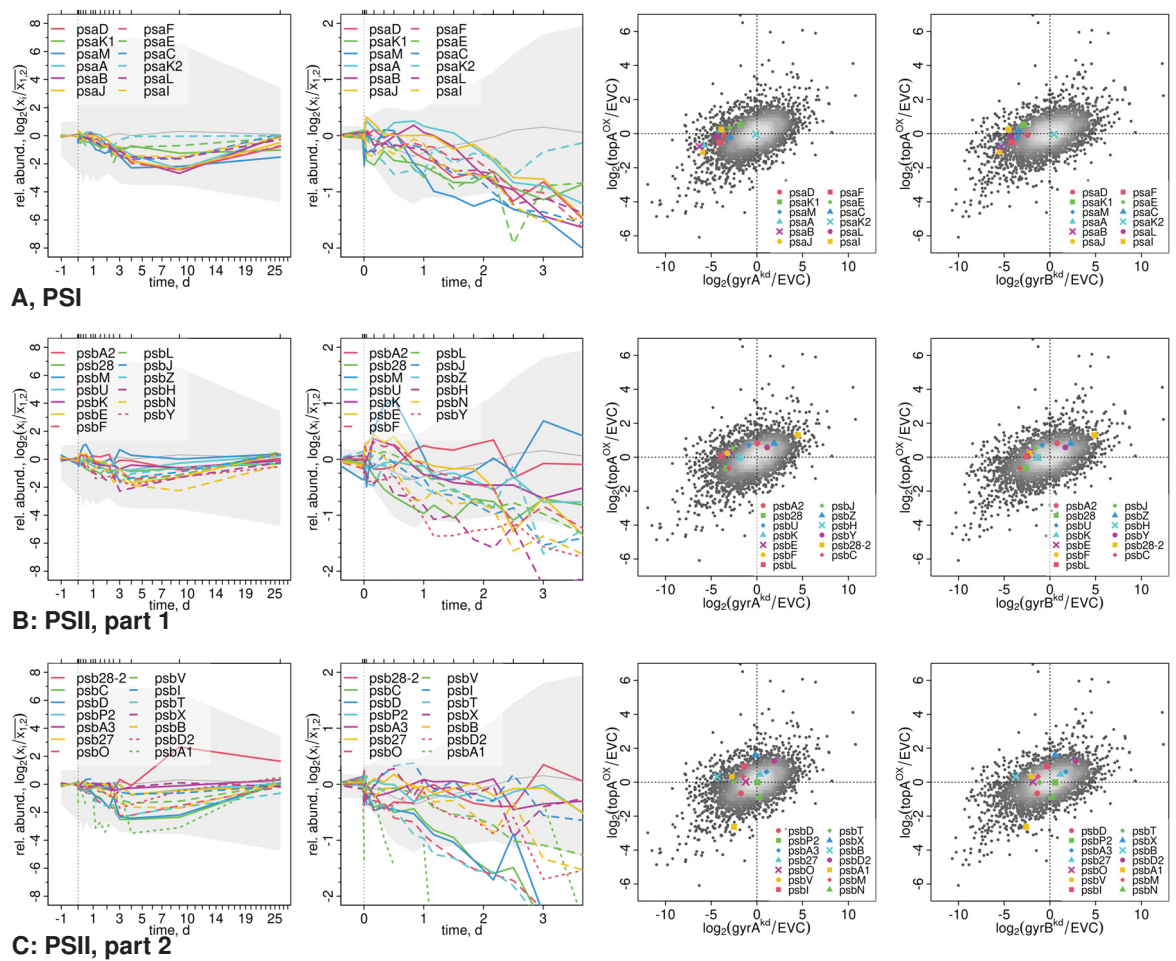


**Figure S19. Genes of Interest: Photosystem I & II.** As Figure S18 but for genes encoding for the photosystems. **A:** Photosystem I genes. **B/C:** Photosystem II genes; *psb28-2*: photosystem II reaction center protein Psb28 homologue, extrinsic protein of photosystem II, *psb28-1* but not *psb28-2* was required in PSII recovery after high-light [75].

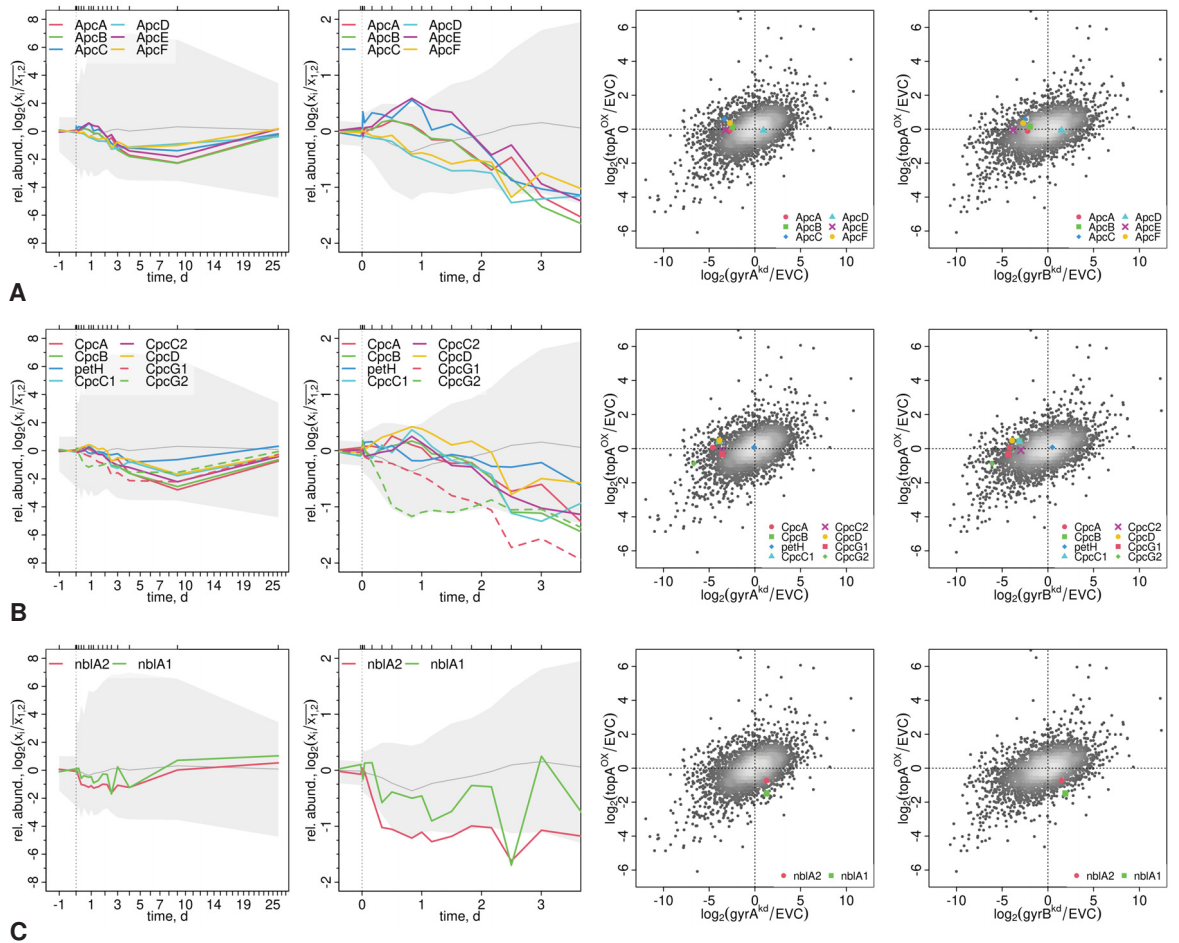


**Figure S20. Genes of Interest: Phycobilisome.** As Figure S18 but for genes encoding for the phycobilisome. Phycobilisome genes were downregulated in all experiments, except for the topA<sup>OX</sup> endpoint measurements (right panels).

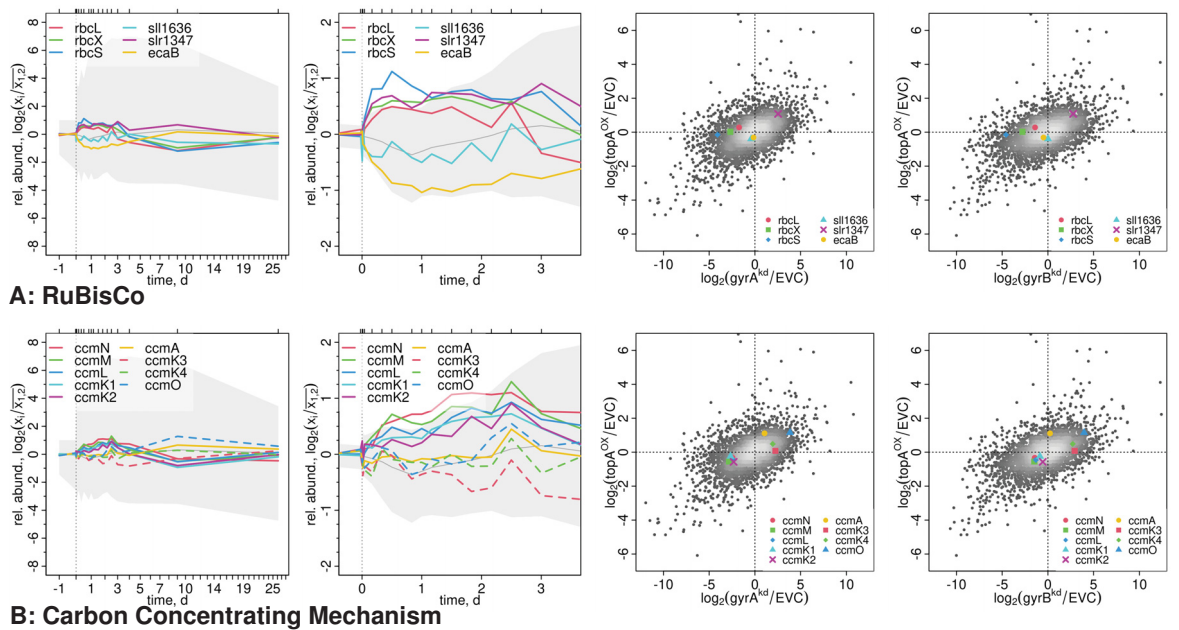


**Figure S21. Genes of Interest: RuBisCo, Carbon Concentrating Mechanism.** As Figure S18 but for genes encoding for RuBisCo and carbon concentrating mechanisms. **A, RuBisCo:** large and small subunits of RuBisCo (*rbcL/S*) and the assembly factor (*rbcX*) were all upregulated. *ecaB*: carbonic anhydrase; *slr1347*: carbonic anhydrase; *sl1636*: gamma carbonic anhydrase. One carbonic anhydrase *slr1347* was upregulated, while the other two were downregulated. **B:** genes of the carbon concentrating mechanism (CCM).

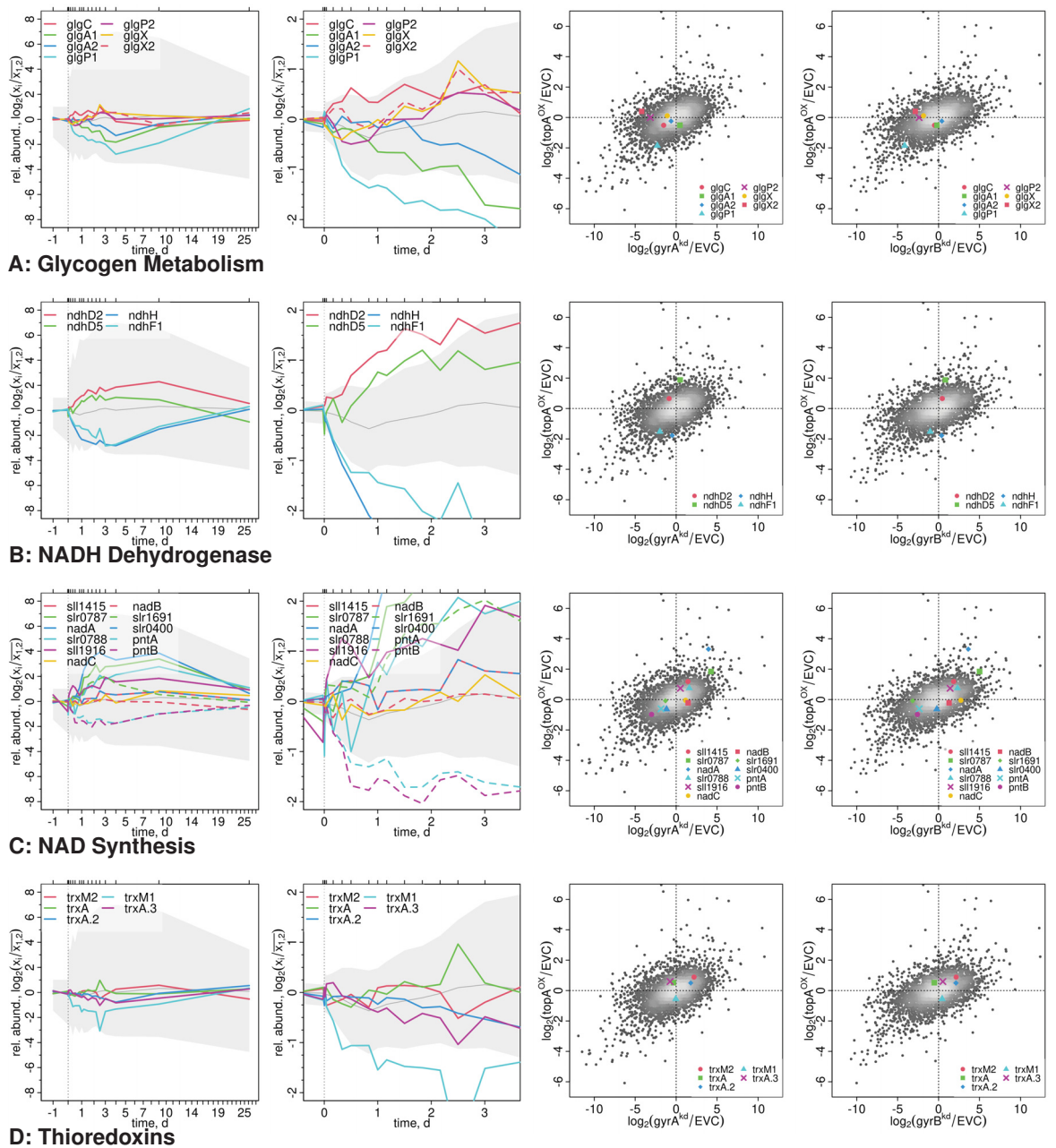


**Figure S22. Genes of Interest: Metabolism.** As Figure S18 but for genes that encode for metabolic enzymes/pathways. **A, Glycogen:** The glycogen degrading enzyme *glgP1* [76] was strongly downregulated, but *glgP2* upregulated at 3 d. The glucose-1-phosphate adenylyltransferase *glgC* was upregulated with the RB/*dawn* cohort, but both glycogen synthase genes, *glgA/A2*, were downregulated. The glycogen debranching enzymes, *glgX/X2*, were both upregulated at 3 d. **B, NADH dehydrogenase:** selected genes from the NADH dehydrogenase complex that showed a strong response, notably, only in the *topA<sup>OX</sup>* strain but not the *gyr<sup>kd</sup>* strains; their annotations are *ndhD2* (*slr1291*): electron transfer from NADH to plastoquinone; *ndhD5* (*slr2007*): Na-proton antiporter; *ndhH/ndhF1* (*slr0261/slr0844*): NAD(P)H-quinone oxidoreductase subunit H (chain 7) and chain 5. Notably, a knock-out of *pgmA* had impaired growth in photomixotrophic conditions, with frequent revertant mutations in NADH dehydrogenase subunits [49]. **C, NAD metabolism:** *nadA* (*sll0622*): quinolinate synthase genes involved in NAD metabolism, *pntA/B* (*slr1239/slr1434*): transhydrogenase, transfers H from NADPH to NAD. **D, Thioredoxins:** The thioredoxin *trxM1* is strongly down-regulated, while *trxA* has a short peak at 2 d–3 d.

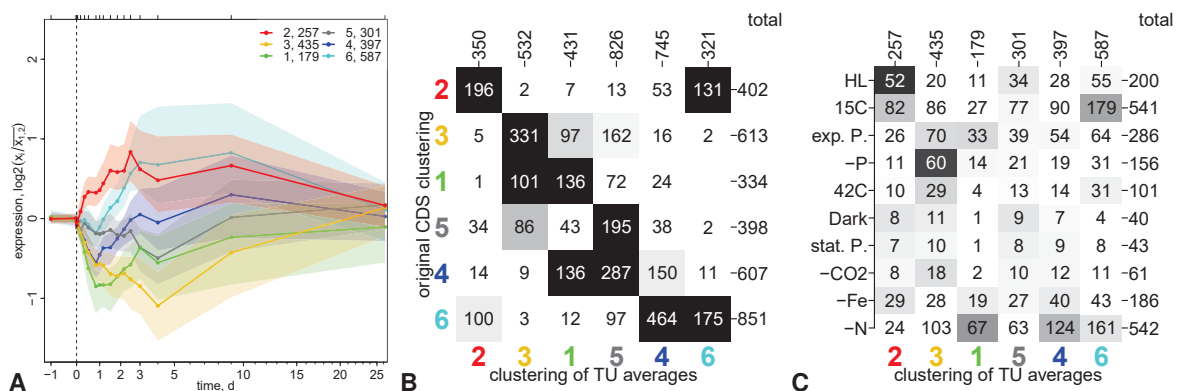


**Figure S23. Transcription Start Site Analysis.** **A:** Clustering of transcription units (TU) defined by [46]. Average expression was calculated for all TU from the expression of coding genes they encompass (via the “Sense.tags” column of the original data set), and the resulting TU time-series was clustered by k-means, using cluster centers from the CDS clustering (Fig. 5) and identical time-series processing. **B:** enrichment profile of the original CDS clustering (y-axis) with the TU-based re-clustering; colored with  $p_{\min} = 10^{-10}$  and  $p_{\text{text}} = 10^{-5}$  and with the original order. **C:** enrichment profile of the time-series clusters with the original TU classification by condition of maximal expression (column “Max.cond.”) by [46]; colored with  $p_{\min} = 10^{-10}$  and  $p_{\text{text}} = 10^{-5}$  but using the original orders. Note, that many CDS were re-assigned to different clusters but the overall pattern is reproduced.

## 5 Conclusions and Future Perspectives

Human development has been impacted immensely by scientific progress. While natural human curiosity has always impacted individual scientists, the demands of an ever-changing society have also factored into scientific innovation.

More recently, major threats to humankind have directly impacted research. One prime example for this is the recent pandemic brought on by SARS-CoV-2. In an effort to prevent further spreading, existing technologies were improved to enable rapid PCR- and antigen-based testing. Additionally, new technologies such as the development of mRNA vaccines were able to prevent numerous hospitalizations and, likely, deaths.

Another major challenge has been the management of resources, more specifically how to replace and recycle finite resources in a sustainable way<sup>92</sup>. Alongside, the threat of climate change has also contributed to this development, as fossil fuels, major contributors to climate change, fall into the category of finite resources<sup>93</sup>.

Science and technology will likely need to focus on overcoming fossil-fuel consuming processes in the long term, and microbial production hosts have been identified as one of the major solutions. As natural and efficient consumers of CO<sub>2</sub>, cyanobacteria provide a promising platform for future circular bioeconomies<sup>94,95</sup>. Additionally, with regard to arable land becoming more limited due to the climate crisis<sup>96,97</sup>, the need for continuous research on photosynthetic organisms is becoming more apparent. In order to achieve these challenging goals, it is important to understand as many of the intricate details present in cyanobacterial hosts as possible.

In this work, a number of different genetic tools were investigated in a comparative manner. Using a fluorophore as read-out, inducible promoters were assessed on their temporal and dose-dependent response, as well as their orthogonality with respect to inducer molecules. They were then compared to one another and a number of reference constitutive promoters to determine their relative strength. Overall, the three promoters P<sub>rha</sub>, P<sub>L03</sub> and P<sub>vanCC</sub> were deemed successful, with the vanillate-inducible promoter being tested for the first time ever in this fashion.

In order to demonstrate the value and feasibility of these tools, two of them were then successfully applied in an attempt to engineer *Synechocystis* for the production of valencene. This proved especially useful to distinguish the effects of different

engineering steps. Another useful detail was being able to use CRISPRi to block transcription of an essential pathway, in this case the pathway leading towards formation of carotenoids. This would not have been possible by simple knock-out mutation, but it shows the scope of what is technically possible beyond the confines of essentiality. Alongside *in silico* flux analysis, metabolomics-based approaches will guide future engineering of chemical production in cyanobacteria<sup>98,99</sup>, enabling the construction of more metabolically balanced and robust strains.

Next to the absolutely essential components of photosynthesis, there are other global regulatory mechanisms present in all bacteria, playing an important role in microbial growth. One of these underlying mechanisms is DNA supercoiling, which has been studied in cyanobacteria, but not in a targeted genetic study thus far.

In accordance with the previous project, inducible CRISPRi was used to repress essential genes responsible for introducing negative supercoiling. In addition, one of the more robust promoter candidates was used to drive expression of topoisomerase I, which is responsible for DNA relaxation in an extensive continuous culture time-series. This strategy enabled an in-depth analysis of changes in physiology, expression patterns and morphology.

As we are transitioning into the systems era of research, precise control of cellular processes is becoming even more imperative. One example is high-throughput screening of cyanobacterial strains, which has not been developed yet to the same extent as for hosts such as *E. coli*. Through targeted evolution, as well as computer-aided, predictive design, production strains can be optimized far beyond rational design<sup>100,101</sup>.

Overall, this work laid the foundation for the advancement of cyanobacterial research both in applied and basic research. The generation of comparable data on available and new genetic tools in cyanobacteria will positively impact other laboratories and projects in the future.

## 6 References from Chapters 1. and 5.

- (1) Kelly, J. R.; Rubin, A. J.; Davis, J. H.; Ajo-Franklin, C. M.; Cumbers, J.; Czar, M. J.; de Mora, K.; Glielberman, A. L.; Monie, D. D.; Endy, D. Measuring the Activity of BioBrick Promoters Using an in Vivo Reference Standard. *J. Biol. Eng.* **2009**, *3* (1), 4. <https://doi.org/10.1186/1754-1611-3-4>.
- (2) Jessop-Fabre, M. M.; Sonnenschein, N. Improving Reproducibility in Synthetic Biology. *Front. Bioeng. Biotechnol.* **2019**, *7*. <https://doi.org/10.3389/fbioe.2019.00018>.
- (3) Elowitz, M. B.; Leibler, S. A Synthetic Oscillatory Network of Transcriptional Regulators. *Nature* **2000**, *403* (6767), 335–338. <https://doi.org/10.1038/35002125>.
- (4) Gardner, T. S.; Cantor, C. R.; Collins, J. J. Construction of a Genetic Toggle Switch in *Escherichia Coli*. *Nature* **2000**, *403* (6767), 339–342. <https://doi.org/10.1038/35002131>.
- (5) Weinstock, M. T.; Heseck, E. D.; Wilson, C. M.; Gibson, D. G. *Vibrio natriegens* as a Fast-Growing Host for Molecular Biology. *Nat. Methods* **2016**, *13* (10), 849–851. <https://doi.org/10.1038/nmeth.3970>.
- (6) Hoff, J.; Daniel, B.; Stukenberg, D.; Thuronyi, B. W.; Waldminghaus, T.; Fritz, G. *Vibrio natriegens*: An Ultrafast-Growing Marine Bacterium as Emerging Synthetic Biology Chassis. *Environ. Microbiol.* **2020**, *22* (10), 4394–4408. <https://doi.org/10.1111/1462-2920.15128>.
- (7) Hoffart, E.; Grenz, S.; Lange, J.; Nitschel, R.; Müller, F.; Schwentner, A.; Feith, A.; Lenfers-Lücker, M.; Takors, R.; Blombach, B. High Substrate Uptake Rates Empower *Vibrio natriegens* as Production Host for Industrial Biotechnology. *Appl. Environ. Microbiol.* **83** (22), e01614-17. <https://doi.org/10.1128/AEM.01614-17>.
- (8) Stanton, B. C.; Nielsen, A. A. K.; Tamsir, A.; Clancy, K.; Peterson, T.; Voigt, C. A. Genomic Mining of Prokaryotic Repressors for Orthogonal Logic Gates. *Nat. Chem. Biol.* **2014**, *10* (2), 99–105. <https://doi.org/10.1038/nchembio.1411>.
- (9) Meyer, A. J.; Segall-Shapiro, T. H.; Glassey, E.; Zhang, J.; Voigt, C. A. *Escherichia Coli* “Marionette” Strains with 12 Highly Optimized Small-Molecule Sensors. *Nat. Chem. Biol.* **2019**, *15* (2), 196–204. <https://doi.org/10.1038/s41589-018-0168-3>.
- (10) Li, S.; Sun, T.; Xu, C.; Chen, L.; Zhang, W. Development and Optimization of Genetic Toolboxes for a Fast-Growing Cyanobacterium *Synechococcus elongatus* UTEX 2973. *Metab. Eng.* **2018**, *48*, 163–174. <https://doi.org/10.1016/j.ymben.2018.06.002>.
- (11) Dalia, T. N.; Hayes, C. A.; Stolyar, S.; Marx, C. J.; McKinlay, J. B.; Dalia, A. B. Multiplex Genome Editing by Natural Transformation (MuGENT) for Synthetic Biology in *Vibrio natriegens*. *ACS Synth. Biol.* **2017**, *6* (9), 1650–1655. <https://doi.org/10.1021/acssynbio.7b00116>.
- (12) Flombaum, P.; Gallegos, J. L.; Gordillo, R. A.; Rincón, J.; Zabala, L. L.; Jiao, N.; Karl, D. M.; Li, W. K. W.; Lomas, M. W.; Veneziano, D.; Vera, C. S.; Vrugt, J. A.; Martiny, A. C. Present and Future Global Distributions of the Marine Cyanobacteria *Prochlorococcus* and *Synechococcus*. *Proc. Natl. Acad. Sci. U. S. A.* **2013**, *110* (24), 9824–9829. <https://doi.org/10.1073/pnas.1307701110>.
- (13) Pikuta, E. V.; Hoover, R. B.; Tang, J. Microbial Extremophiles at the Limits of Life. *Crit. Rev. Microbiol.* **2007**, *33* (3), 183–209. <https://doi.org/10.1080/10408410701451948>.
- (14) López-Archilla, A. I.; Moreira, D.; López-García, P.; Guerrero, C. Phytoplankton Diversity and Cyanobacterial Dominance in a Hypereutrophic Shallow Lake with Biologically

- Produced Alkaline PH. *Extrem. Life Extreme Cond.* **2004**, *8* (2), 109–115. <https://doi.org/10.1007/s00792-003-0369-9>.
- (15) Ponce-Toledo, R. I.; Deschamps, P.; López-García, P.; Zivanovic, Y.; Benzerara, K.; Moreira, D. An Early-Branching Freshwater Cyanobacterium at the Origin of Plastids. *Curr. Biol. CB* **2017**, *27* (3), 386–391. <https://doi.org/10.1016/j.cub.2016.11.056>.
- (16) Branco dos Santos, F.; Du, W.; Hellingwerf, K. J. *Synechocystis*: Not Just a Plug-Bug for CO<sub>2</sub>, but a Green *E. coli*. *Front. Bioeng. Biotechnol.* **2014**, *2*, 36. <https://doi.org/10.3389/fbioe.2014.00036>.
- (17) Adir, N.; Bar-Zvi, S.; Harris, D. The Amazing Phycobilisome. *Biochim. Biophys. Acta BBA - Bioenerg.* **2020**, *1861* (4), 148047. <https://doi.org/10.1016/j.bbabi.2019.07.002>.
- (18) Santos-Merino, M.; Torrado, A.; Davis, G. A.; Röttig, A.; Bibby, T. S.; Kramer, D. M.; Ducat, D. C. Improved Photosynthetic Capacity and Photosystem I Oxidation via Heterologous Metabolism Engineering in Cyanobacteria. *Proc. Natl. Acad. Sci.* **2021**, *118* (11). <https://doi.org/10.1073/pnas.2021523118>.
- (19) Orr, D. J.; Pereira, A. M.; da Fonseca Pereira, P.; Pereira-Lima, Í. A.; Zsögön, A.; Araújo, W. L. Engineering Photosynthesis: Progress and Perspectives. *F1000Research* **2017**, *6*, 1891. <https://doi.org/10.12688/f1000research.12181.1>.
- (20) Stanier, R. Y.; Kunisawa, R.; Mandel, M.; Cohen-Bazire, G. Purification and Properties of Unicellular Blue-Green Algae (Order Chroococcales). *Bacteriol. Rev.* **1971**, *35* (2), 171–205. <https://doi.org/10.1128/br.35.2.171-205.1971>.
- (21) Kaneko, T.; Sato, S.; Kotani, H.; Tanaka, A.; Asamizu, E.; Nakamura, Y.; Miyajima, N.; Hirosawa, M.; Sugiura, M.; Sasamoto, S.; Kimura, T.; Hosouchi, T.; Matsuno, A.; Muraki, A.; Nakazaki, N.; Naruo, K.; Okumura, S.; Shimpo, S.; Takeuchi, C.; Wada, T.; Watanabe, A.; Yamada, M.; Yasuda, M.; Tabata, S. Sequence Analysis of the Genome of the Unicellular Cyanobacterium *Synechocystis* Sp. Strain PCC6803. II. Sequence Determination of the Entire Genome and Assignment of Potential Protein-Coding Regions (Supplement). *DNA Res. Int. J. Rapid Publ. Rep. Genes Genomes* **1996**, *3* (3), 185–209. <https://doi.org/10.1093/dnares/3.3.185>.
- (22) Raymond, J.; Swingle, W. D. Phototroph Genomics Ten Years On. *Photosynth. Res.* **2008**, *97* (1), 5. <https://doi.org/10.1007/s11120-008-9308-z>.
- (23) Imamura, S.; Asayama, M. Sigma Factors for Cyanobacterial Transcription. *Gene Regul. Syst. Biol.* **2009**, *3*, 65–87. <https://doi.org/10.4137/grsb.s2090>.
- (24) Ruffing, A. M.; Kallas, T. Editorial: Cyanobacteria: The Green *E. coli*. *Front. Bioeng. Biotechnol.* **2016**, *4*, 7. <https://doi.org/10.3389/fbioe.2016.00007>.
- (25) Albers, S. C.; Gallegos, V. A.; Peebles, C. A. M. Engineering of Genetic Control Tools in *Synechocystis* Sp. PCC 6803 Using Rational Design Techniques. *J. Biotechnol.* **2015**, *216*, 36–46. <https://doi.org/10.1016/j.jbiotec.2015.09.042>.
- (26) Kim, W. J.; Lee, S.-M.; Um, Y.; Sim, S. J.; Woo, H. M. Development of SyneBrick Vectors As a Synthetic Biology Platform for Gene Expression in *Synechococcus elongatus* PCC 7942. *Front. Plant Sci.* **2017**, *8*. <https://doi.org/10.3389/fpls.2017.00293>.
- (27) Markley, A. L.; Begemann, M. B.; Clarke, R. E.; Gordon, G. C.; Pfleger, B. F. Synthetic Biology Toolbox for Controlling Gene Expression in the Cyanobacterium *Synechococcus* Sp. Strain PCC 7002. *ACS Synth. Biol.* **2015**, *4* (5), 595–603. <https://doi.org/10.1021/sb500260k>.
- (28) Ma, A. T.; Schmidt, C. M.; Golden, J. W. Regulation of Gene Expression in Diverse Cyanobacterial Species by Using Theophylline-Responsive Riboswitches. *Appl.*

- Environ. Microbiol.* **2014**, *80* (21), 6704–6713. <https://doi.org/10.1128/AEM.01697-14>.
- (29) Huang, H.-H.; Lindblad, P. Wide-Dynamic-Range Promoters Engineered for Cyanobacteria. *J. Biol. Eng.* **2013**, *7* (1), 10. <https://doi.org/10.1186/1754-1611-7-10>.
- (30) Higo, A.; Isu, A.; Fukaya, Y.; Hisabori, T. Efficient Gene Induction and Endogenous Gene Repression Systems for the Filamentous Cyanobacterium *Anabaena* Sp. PCC 7120. *Plant Cell Physiol.* **2016**, *57* (2), 387–396. <https://doi.org/10.1093/pcp/pcv202>.
- (31) Yao, L.; Shabestary, K.; Björk, S. M.; Asplund-Samuelsson, J.; Joensson, H. N.; Jahn, M.; Hudson, E. P. Pooled CRISPRi Screening of the Cyanobacterium *Synechocystis* Sp PCC 6803 for Enhanced Industrial Phenotypes. *Nat. Commun.* **2020**, *11* (1), 1666. <https://doi.org/10.1038/s41467-020-15491-7>.
- (32) Khlebnikov, A.; Risa, Ø.; Skaug, T.; Carrier, T. A.; Keasling, J. D. Regulatable Arabinose-Inducible Gene Expression System with Consistent Control in All Cells of a Culture. *J. Bacteriol.* **2000**, *182* (24), 7029–7034.
- (33) Romano, E.; Baumschlager, A.; Akmeriç, E. B.; Palanisamy, N.; Houmani, M.; Schmidt, G.; Öztürk, M. A.; Ernst, L.; Khammash, M.; Di Ventura, B. Engineering AraC to Make It Responsive to Light Instead of Arabinose. *Nat. Chem. Biol.* **2021**, *17* (7), 817–827. <https://doi.org/10.1038/s41589-021-00787-6>.
- (34) Cao, Y.-Q.; Li, Q.; Xia, P.-F.; Wei, L.-J.; Guo, N.; Li, J.-W.; Wang, S.-G. AraBAD Based Toolkit for Gene Expression and Metabolic Robustness Improvement in *Synechococcus elongatus*. *Sci. Rep.* **2017**, *7* (1), 18059. <https://doi.org/10.1038/s41598-017-17035-4>.
- (35) Immethun, C. M.; DeLorenzo, D. M.; Focht, C. M.; Gupta, D.; Johnson, C. B.; Moon, T. S. Physical, Chemical, and Metabolic State Sensors Expand the Synthetic Biology Toolbox for *Synechocystis* Sp. PCC 6803: New Sensors for *Synechocystis* ' Toolbox. *Biotechnol. Bioeng.* **2017**, *114* (7), 1561–1569. <https://doi.org/10.1002/bit.26275>.
- (36) Kelly, C. L.; Taylor, G. M.; Hitchcock, A.; Torres-Méndez, A.; Heap, J. T. A Rhamnose-Inducible System for Precise and Temporal Control of Gene Expression in Cyanobacteria. *ACS Synth. Biol.* **2018**, *7* (4), 1056–1066. <https://doi.org/10.1021/acssynbio.7b00435>.
- (37) Ruegg, T. L.; Pereira, J. H.; Chen, J. C.; DeGiovanni, A.; Novichkov, P.; Mutalik, V. K.; Tomaleri, G. P.; Singer, S. W.; Hillson, N. J.; Simmons, B. A.; Adams, P. D.; Thelen, M. P. Jungle Express Is a Versatile Repressor System for Tight Transcriptional Control. *Nat. Commun.* **2018**, *9* (1), 3617. <https://doi.org/10.1038/s41467-018-05857-3>.
- (38) Nozzi, N. E.; Atsumi, S. Genome Engineering of the 2,3-Butanediol Biosynthetic Pathway for Tight Regulation in Cyanobacteria. *ACS Synth. Biol.* **2015**, *4* (11), 1197–1204. <https://doi.org/10.1021/acssynbio.5b00057>.
- (39) Dexter, J.; Armshaw, P.; Sheahan, C.; Pembroke, J. T. The State of Autotrophic Ethanol Production in Cyanobacteria. *J. Appl. Microbiol.* **2015**, *119* (1), 11–24. <https://doi.org/10.1111/jam.12821>.
- (40) Ducat, D. C.; Way, J. C.; Silver, P. A. Engineering Cyanobacteria to Generate High-Value Products. *Trends Biotechnol.* **2011**, *29* (2), 95–103. <https://doi.org/10.1016/j.tibtech.2010.12.003>.
- (41) Wang, B.; Eckert, C.; Maness, P.-C.; Yu, J. A Genetic Toolbox for Modulating the Expression of Heterologous Genes in the Cyanobacterium *Synechocystis* Sp. PCC 6803. *ACS Synth. Biol.* **2018**, *7* (1), 276–286. <https://doi.org/10.1021/acssynbio.7b00297>.
- (42) Koch, M.; Bruckmoser, J.; Scholl, J.; Hauf, W.; Rieger, B.; Forchhammer, K. Maximizing PHB Content in *Synechocystis* Sp. PCC 6803: A New Metabolic Engineering Strategy

- Based on the Regulator PirC. *Microb. Cell Factories* **2020**, *19* (1), 231. <https://doi.org/10.1186/s12934-020-01491-1>.
- (43) Sánchez, O.; Diestra, E.; Esteve, I.; Mas, J. Molecular Characterization of an Oil-Degrading Cyanobacterial Consortium. *Microb. Ecol.* **2005**, *50* (4), 580–588. <https://doi.org/10.1007/s00248-005-5061-4>.
- (44) Furmaniak, M. A.; Misztak, A. E.; Franczuk, M. D.; Wilmotte, A.; Waleron, M.; Waleron, K. F. Edible Cyanobacterial Genus *Arthrospira*: Actual State of the Art in Cultivation Methods, Genetics, and Application in Medicine. *Front. Microbiol.* **2017**, *8*, 2541. <https://doi.org/10.3389/fmicb.2017.02541>.
- (45) Abramson, B. W.; Kachel, B.; Kramer, D. M.; Ducat, D. C. Increased Photochemical Efficiency in Cyanobacteria via an Engineered Sucrose Sink. *Plant Cell Physiol.* **2016**, *57* (12), 2451–2460. <https://doi.org/10.1093/pcp/pcw169>.
- (46) Liu, X.; Sheng, J.; Iii, R. C. Fatty Acid Production in Genetically Modified Cyanobacteria. *Proc. Natl. Acad. Sci.* **2011**, *108* (17), 6899–6904. <https://doi.org/10.1073/pnas.1103014108>.
- (47) Angermayr, S. A.; Paszota, M.; Hellingwerf, K. J. Engineering a Cyanobacterial Cell Factory for Production of Lactic Acid. *Appl. Environ. Microbiol.* **2012**, *78* (19), 7098–7106. <https://doi.org/10.1128/AEM.01587-12>.
- (48) Osanai, T.; Shirai, T.; Iijima, H.; Nakaya, Y.; Okamoto, M.; Kondo, A.; Hirai, M. Y. Genetic Manipulation of a Metabolic Enzyme and a Transcriptional Regulator Increasing Succinate Excretion from Unicellular Cyanobacterium. *Front. Microbiol.* **2015**, *6*. <https://doi.org/10.3389/fmicb.2015.01064>.
- (49) Carrieri, D.; Broadbent, C.; Carruth, D.; Paddock, T.; Ungerer, J.; Maness, P.-C.; Ghirardi, M.; Yu, J. Enhancing Photo-Catalytic Production of Organic Acids in the Cyanobacterium *Synechocystis* Sp. PCC 6803  $\Delta$ glgC, a Strain Incapable of Glycogen Storage. *Microb. Biotechnol.* **2015**, *8* (2), 275–280. <https://doi.org/10.1111/1751-7915.12243>.
- (50) Dittmann, E.; Gugger, M.; Sivonen, K.; Fewer, D. P. Natural Product Biosynthetic Diversity and Comparative Genomics of the Cyanobacteria. *Trends Microbiol.* **2015**, *23* (10), 642–652. <https://doi.org/10.1016/j.tim.2015.07.008>.
- (51) Martínez-Núñez, M. A.; López, V. E. L. y. Nonribosomal Peptides Synthetases and Their Applications in Industry. *Sustain. Chem. Process.* **2016**, *4* (1), 13. <https://doi.org/10.1186/s40508-016-0057-6>.
- (52) Lindberg, P.; Park, S.; Melis, A. Engineering a Platform for Photosynthetic Isoprene Production in Cyanobacteria, Using *Synechocystis* as the Model Organism. *Metab. Eng.* **2010**, *12* (1), 70–79. <https://doi.org/10.1016/j.ymben.2009.10.001>.
- (53) Loeschcke, A.; Dienst, D.; Wewer, V.; Hage-Hülsmann, J.; Dietsch, M.; Kranz-Finger, S.; Hüren, V.; Metzger, S.; Urlacher, V. B.; Gigolashvili, T.; Kopriva, S.; Axmann, I. M.; Drepper, T.; Jaeger, K.-E. The Photosynthetic Bacteria *Rhodobacter Capsulatus* and *Synechocystis* Sp. PCC 6803 as New Hosts for Cyclic Plant Triterpene Biosynthesis. *PLOS ONE* **2017**, *12* (12), e0189816. <https://doi.org/10.1371/journal.pone.0189816>.
- (54) Dienst, D.; Wichmann, J.; Mantovani, O.; Rodrigues, J. S.; Lindberg, P. High Density Cultivation for Efficient Sesquiterpenoid Biosynthesis in *Synechocystis* Sp. PCC 6803. *Sci. Rep.* **2020**, *10* (1), 5932. <https://doi.org/10.1038/s41598-020-62681-w>.
- (55) Lin, P.-C.; Pakrasi, H. B. Engineering Cyanobacteria for Production of Terpenoids. *Planta* **2019**, *249* (1), 145–154. <https://doi.org/10.1007/s00425-018-3047-y>.

- (56) Ambati, R. R.; Gogisetty, D.; Aswathanarayana, R. G.; Ravi, S.; Bikkina, P. N.; Bo, L.; Yuepeng, S. Industrial Potential of Carotenoid Pigments from Microalgae: Current Trends and Future Prospects. *Crit. Rev. Food Sci. Nutr.* **2019**, *59* (12), 1880–1902. <https://doi.org/10.1080/10408398.2018.1432561>.
- (57) Saini, D. K.; Pabbi, S.; Shukla, P. Cyanobacterial Pigments: Perspectives and Biotechnological Approaches. *Food Chem. Toxicol.* **2018**, *120*, 616–624. <https://doi.org/10.1016/j.fct.2018.08.002>.
- (58) Kallio, P.; Kugler, A.; Pyytövaara, S.; Stensjö, K.; Allahverdiyeva, Y.; Gao, X.; Lindblad, P.; Lindberg, P. Photoautotrophic Production of Renewable Ethylene by Engineered Cyanobacteria: Steering the Cell Metabolism towards Biotechnological Use. *Physiol. Plant.* **2021**. <https://doi.org/10.1111/ppl.13430>.
- (59) Kamravamanesh, D.; Kiesenhofer, D.; Fluch, S.; Lackner, M.; Herwig, C. Scale-up Challenges and Requirement of Technology-Transfer for Cyanobacterial Poly (3-Hydroxybutyrate) Production in Industrial Scale. *Int. J. Biobased Plast.* **2019**, *1* (1), 60–71. <https://doi.org/10.1080/24759651.2019.1688604>.
- (60) Takenaka, H.; Yamaguchi, Y. Commercial-Scale Culturing of Cyanobacteria: An Industrial Experience. In *Cyanobacteria*; John Wiley & Sons, Ltd, 2014; pp 293–301. <https://doi.org/10.1002/9781118402238.ch18>.
- (61) Qiang, H.; Zarmi, Y.; Richmond, A. Combined Effects of Light Intensity, Light-Path and Culture Density on Output Rate of *Spirulina platensis* (Cyanobacteria). *Eur. J. Phycol.* **1998**, *33* (2), 165–171. <https://doi.org/10.1080/09670269810001736663>.
- (62) Bhandari, R.; Sharma, P. K. High-Light-Induced Changes on Photosynthesis, Pigments, Sugars, Lipids and Antioxidant Enzymes in Freshwater (*Nostoc Spongiaeforme*) and Marine (*Phormidium Corium*) Cyanobacteria. *Photochem. Photobiol.* **2006**, *82* (3), 702–710. <https://doi.org/10.1562/2005-09-20-RA-690>.
- (63) Rajvanshi, M.; Gautam, K.; Manjre, S.; Krishna Kumar, G. R.; Kumar, C.; Govindachary, S.; Dasgupta, S. Stoichiometrically Balanced Nutrient Management Using a Newly Designed Nutrient Medium for Large Scale Cultivation of *Cyanobacterium Aponinum*. *J. Appl. Phycol.* **2019**, *31* (5), 2779–2789. <https://doi.org/10.1007/s10811-019-01851-4>.
- (64) Johnson, T. J.; Jahandideh, A.; Isaac, I. C.; Baldwin, E. L.; Muthukumarappan, K.; Zhou, R.; Gibbons, W. R. Determining the Optimal Nitrogen Source for Large-Scale Cultivation of Filamentous Cyanobacteria. *J. Appl. Phycol.* **2017**, *29* (1), 1–13. <https://doi.org/10.1007/s10811-016-0923-3>.
- (65) Mascarelli, A. L. Algae: Fuel of the Future? *Environ. Sci. Technol.* **2009**, *43* (19), 7160–7161. <https://doi.org/10.1021/es902509d>.
- (66) Hays, S. G.; Yan, L. L. W.; Silver, P. A.; Ducat, D. C. Synthetic Photosynthetic Consortia Define Interactions Leading to Robustness and Photoproduction. *J. Biol. Eng.* **2017**, *11*. <https://doi.org/10.1186/s13036-017-0048-5>.
- (67) Weiss, T. L.; Young, E. J.; Ducat, D. C. A Synthetic, Light-Driven Consortium of Cyanobacteria and Heterotrophic Bacteria Enables Stable Polyhydroxybutyrate Production. *Metab. Eng.* **2017**, *44*, 236–245. <https://doi.org/10.1016/j.ymben.2017.10.009>.
- (68) Karunanithi, P. S.; Zerbe, P. Terpene Synthases as Metabolic Gatekeepers in the Evolution of Plant Terpenoid Chemical Diversity. *Front. Plant Sci.* **2019**, *10*.
- (69) Loza-Tavera, H. Monoterpenes in Essential Oils. Biosynthesis and Properties. *Adv. Exp. Med. Biol.* **1999**, *464*, 49–62. [https://doi.org/10.1007/978-1-4615-4729-7\\_5](https://doi.org/10.1007/978-1-4615-4729-7_5).

- (70) Canonico, M.; Konert, G.; Crepin, A.; Šedivá, B.; Kaňa, R. Gradual Response of Cyanobacterial Thylakoids to Acute High-Light Stress-Importance of Carotenoid Accumulation. *Cells* **2021**, *10* (8), 1916. <https://doi.org/10.3390/cells10081916>.
- (71) Chaves, J. E.; Melis, A. Biotechnology of Cyanobacterial Isoprene Production. *Appl. Microbiol. Biotechnol.* **2018**, *102* (15), 6451–6458. <https://doi.org/10.1007/s00253-018-9093-3>.
- (72) Gao, X.; Gao, F.; Liu, D.; Zhang, H.; Nie, X.; Yang, C. Engineering the Methylerythritol Phosphate Pathway in Cyanobacteria for Photosynthetic Isoprene Production from CO<sub>2</sub>. *Energy Environ. Sci.* **2016**, *9* (4), 1400–1411. <https://doi.org/10.1039/C5EE03102H>.
- (73) Lin, P.-C.; Saha, R.; Zhang, F.; Pakrasi, H. B. Metabolic Engineering of the Pentose Phosphate Pathway for Enhanced Limonene Production in the Cyanobacterium *Synechocystis* Sp. PCC 6803. *Sci. Rep.* **2017**, *7* (1), 17503. <https://doi.org/10.1038/s41598-017-17831-y>.
- (74) Rodrigues, J. S.; Lindberg, P. Metabolic Engineering of *Synechocystis* Sp. PCC 6803 for Improved Bisabolene Production. *Metab. Eng. Commun.* **2020**, *12*, e00159. <https://doi.org/10.1016/j.mec.2020.e00159>.
- (75) Formighieri, C.; Melis, A. Sustainable Heterologous Production of Terpene Hydrocarbons in Cyanobacteria. *Photosynth. Res.* **2016**, *130* (1–3), 123–135. <https://doi.org/10.1007/s11120-016-0233-2>.
- (76) López-Hernández, J. F.; García-Alamilla, P.; Palma-Ramírez, D.; Álvarez-González, C. A.; Paredes-Rojas, J. C.; Márquez-Rocha, F. J. Continuous Microalgal Cultivation for Antioxidants Production. *Molecules* **2020**, *25* (18), 4171. <https://doi.org/10.3390/molecules25184171>.
- (77) Yao, J.; Wang, J.; Ju, Y.; Dong, Z.; Song, X.; Chen, L.; Zhang, W. Engineering a Xylose-Utilizing *Synechococcus elongatus* UTEX 2973 Chassis for 3-Hydroxypropionic Acid Biosynthesis under Photomixotrophic Conditions. *ACS Synth. Biol.* **2022**. <https://doi.org/10.1021/acssynbio.1c00364>.
- (78) Li, X.; Liang, Y.; Li, K.; Jin, P.; Tang, J.; Klepacz-Smółka, A.; Ledakowicz, S.; Daroch, M. Effects of Low Temperature, Nitrogen Starvation and Their Combination on the Photosynthesis and Metabolites of *Thermosynechococcus* E542: A Comparison Study. *Plants Basel Switz.* **2021**, *10* (10), 2101. <https://doi.org/10.3390/plants10102101>.
- (79) Georg, J.; Dienst, D.; Schürgers, N.; Wallner, T.; Kopp, D.; Stazic, D.; Kuchmina, E.; Klähn, S.; Lokstein, H.; Hess, W. R.; Wilde, A. The Small Regulatory RNA SyR1/PsrR1 Controls Photosynthetic Functions in Cyanobacteria. *Plant Cell* **2014**, *26* (9), 3661–3679. <https://doi.org/10.1105/tpc.114.129767>.
- (80) Rübsam, H.; Kirsch, F.; Reimann, V.; Erban, A.; Kopka, J.; Hagemann, M.; Hess, W. R.; Klähn, S. The Iron-Stress Activated RNA 1 (IsaR1) Coordinates Osmotic Acclimation and Iron Starvation Responses in the Cyanobacterium *Synechocystis* Sp. PCC 6803. *Environ. Microbiol.* **2018**, *20* (8), 2757–2768. <https://doi.org/10.1111/1462-2920.14079>.
- (81) Pattanayak, G. K.; Phong, C.; Rust, M. J. Rhythms in Energy Storage Control the Ability of the Cyanobacterial Circadian Clock to Reset. *Curr. Biol. CB* **2014**, *24* (16), 1934–1938. <https://doi.org/10.1016/j.cub.2014.07.022>.
- (82) Postow, L.; Crisona, N. J.; Peter, B. J.; Hardy, C. D.; Cozzarelli, N. R. Topological Challenges to DNA Replication: Conformations at the Fork. *Proc. Natl. Acad. Sci.* **2001**, *98* (15), 8219–8226. <https://doi.org/10.1073/pnas.111006998>.

- (83) Kim, S.; Beltran, B.; Irnov, I.; Jacobs-Wagner, C. Long-Distance Cooperative and Antagonistic RNA Polymerase Dynamics via DNA Supercoiling. *Cell* **2019**, *179* (1), 106–119.e16. <https://doi.org/10.1016/j.cell.2019.08.033>.
- (84) Naughton, C.; Avlonitis, N.; Corless, S.; Prendergast, J. G.; Mati, I. K.; Eijk, P. P.; Cockroft, S. L.; Bradley, M.; Ylstra, B.; Gilbert, N. Transcription Forms and Remodels Supercoiling Domains Unfolding Large-Scale Chromatin Structures. *Nat. Struct. Mol. Biol.* **2013**, *20* (3), 387–395. <https://doi.org/10.1038/nsmb.2509>.
- (85) Kouzine, F.; Gupta, A.; Baranello, L.; Wojtowicz, D.; Ben-Aissa, K.; Liu, J.; Przytycka, T. M.; Levens, D. Transcription-Dependent Dynamic Supercoiling Is a Short-Range Genomic Force. *Nat. Struct. Mol. Biol.* **2013**, *20* (3), 396–403. <https://doi.org/10.1038/nsmb.2517>.
- (86) Liu, L. F.; Wang, J. C. Supercoiling of the DNA Template during Transcription. *Proc. Natl. Acad. Sci. U. S. A.* **1987**, *84* (20), 7024–7027. <https://doi.org/10.1073/pnas.84.20.7024>.
- (87) Ahmed, W.; Menon, S.; Karthik, P. V. D. N. B.; Nagaraja, V. Autoregulation of Topoisomerase I Expression by Supercoiling Sensitive Transcription. *Nucleic Acids Res.* **2016**, *44* (4), 1541–1552. <https://doi.org/10.1093/nar/gkv1088>.
- (88) Tadesse, S.; Graumann, P. L. Differential and Dynamic Localization of Topoisomerases in *Bacillus Subtilis*. *J. Bacteriol.* **2006**, *188* (8), 3002–3011. <https://doi.org/10.1128/JB.188.8.3002-3011.2006>.
- (89) Szafran, M. J.; Gongerowska, M.; Małeck, T.; Elliot, M.; Jakimowicz, D. Transcriptional Response of *Streptomyces coelicolor* to Rapid Chromosome Relaxation or Long-Term Supercoiling Imbalance. *Front. Microbiol.* **2019**, *10*, 1605. <https://doi.org/10.3389/fmicb.2019.01605>.
- (90) Prakash, J. S. S.; Sinetova, M.; Zorina, A.; Kupriyanova, E.; Suzuki, I.; Murata, N.; Los, D. A. DNA Supercoiling Regulates the Stress-Inducible Expression of Genes in the Cyanobacterium *Synechocystis*. *Mol. Biosyst.* **2009**, *5* (12), 1904–1912. <https://doi.org/10.1039/B903022k>.
- (91) Vijayan, V.; Zuzow, R.; O’Shea, E. K. Oscillations in Supercoiling Drive Circadian Gene Expression in Cyanobacteria. *Proc. Natl. Acad. Sci. U. S. A.* **2009**, *106* (52), 22564–22568. <https://doi.org/10.1073/pnas.0912673106>.
- (92) Speirs, J.; McGlade, C.; Slade, R. Uncertainty in the Availability of Natural Resources: Fossil Fuels, Critical Metals and Biomass. *Energy Policy* **2015**, *87*, 654–664. <https://doi.org/10.1016/j.enpol.2015.02.031>.
- (93) Höök, M.; Tang, X. Depletion of Fossil Fuels and Anthropogenic Climate Change—A Review. *Energy Policy* **2013**, *52*, 797–809. <https://doi.org/10.1016/j.enpol.2012.10.046>.
- (94) Prabha, S.; Vijay, A. K.; Paul, R. R.; George, B. Cyanobacterial Biorefinery: Towards Economic Feasibility through the Maximum Valorization of Biomass. *Sci. Total Environ.* **2022**, *814*, 152795. <https://doi.org/10.1016/j.scitotenv.2021.152795>.
- (95) Mitra, M.; Mishra, S. Multiproduct Biorefinery from *Arthrospira* Spp. towards Zero Waste: Current Status and Future Trends. *Bioresour. Technol.* **2019**, *291*, 121928. <https://doi.org/10.1016/j.biortech.2019.121928>.
- (96) Zhang, X.; Cai, X. Climate Change Impacts on Global Agricultural Land Availability. *Environ. Res. Lett.* **2011**, *6* (1), 014014. <https://doi.org/10.1088/1748-9326/6/1/014014>.

- (97) Borrelli, P.; Robinson, D. A.; Panagos, P.; Lugato, E.; Yang, J. E.; Alewell, C.; Wuepper, D.; Montanarella, L.; Ballabio, C. Land Use and Climate Change Impacts on Global Soil Erosion by Water (2015-2070). *Proc. Natl. Acad. Sci.* **2020**, *117* (36), 21994–22001. <https://doi.org/10.1073/pnas.2001403117>.
- (98) Kato, Y.; Inabe, K.; Hidese, R.; Kondo, A.; Hasunuma, T. Metabolomics-Based Engineering for Biofuel and Bio-Based Chemical Production in Microalgae and Cyanobacteria: A Review. *Bioresour. Technol.* **2022**, *344*, 126196. <https://doi.org/10.1016/j.biortech.2021.126196>.
- (99) Hasunuma, T.; Matsuda, M.; Kondo, A. Improved Sugar-Free Succinate Production by *Synechocystis* sp. PCC 6803 Following Identification of the Limiting Steps in Glycogen Catabolism. *Metab. Eng. Commun.* **2016**, *3*, 130–141. <https://doi.org/10.1016/j.meteno.2016.04.003>.
- (100) Seok, J. Y.; Yang, J.; Choi, S. J.; Lim, H. G.; Choi, U. J.; Kim, K.-J.; Park, S.; Yoo, T. H.; Jung, G. Y. Directed Evolution of the 3-Hydroxypropionic Acid Production Pathway by Engineering Aldehyde Dehydrogenase Using a Synthetic Selection Device. *Metab. Eng.* **2018**, *47*, 113–120. <https://doi.org/10.1016/j.ymben.2018.03.009>.
- (101) Arnold, F. H. Directed Evolution: Bringing New Chemistry to Life. *Angew. Chem. Int. Ed Engl.* **2018**, *57* (16), 4143–4148. <https://doi.org/10.1002/anie.201708408>.

## 7 List of scientific contributions

### Scientific articles

1. Comparative dose-response analysis of inducible promoters in cyanobacteria. (ACS Synthetic Biology, 9:4, 843-855, April 2020)
2. Metabolic engineering of *Synechocystis* sp. PCC 6803 for the photoproduction of the sesquiterpene valencene (Metabolic Engineering Communications, 13:178, August 2021)
3. Uncoupling of the Diurnal Growth Program by Artificial Genome Relaxation in *Synechocystis* sp. PCC 6803 (bioRxiv, August 2021)

### Book chapters

1. pSHDY: A valuable tool for genetic engineering of cyanobacteria (Methods in Molecular biology: Plant Synthetic Biology, Springer Nature, February 2022)

### Other articles

1. Induzierbare Promotoren für Cyanobakterien. (Biospektrum 5/21)

### Conference presentations

1. pSHDY: An optimized expression platform for fluorescence-based reporter systems in *Synechocystis* sp. PCC 6803 (Cyano 2017, Düsseldorf)
2. New gene regulatory tools to improve synthetic biology in *Synechocystis* sp. PCC 6803 (VAAM 2019, Mainz)

### Conference posters

1. Building a reporter system for sRNA interaction studies in cyanobacteria (Cyano 2017, Düsseldorf)
2. Reengineering of a synthetic toehold switch for posttranscriptional activation of gene expression in *Synechocystis* sp. PCC 6803 (VAAM 2018, Wolfsburg)
3. Supercoiling-mediated changes in gene expression (Cyano 2018, Freiburg)
4. Comparative analysis of inducible promoters in *Synechocystis* sp. PCC 6803 (Cyano 2019, Tübingen)
5. Characterization of a vanillate inducible promoter in *Synechocystis* sp. PCC 6803 (Cyano 2019, Tübingen)
6. Manipulation of *Synechocystis* sp. PCC 6803 on a whole-genome scale (VAAM 2020, Leipzig)

## 8 Acknowledgements

Als allererstes möchte ich Ilka Axmann danken. Ilka, vielen Dank, für die Möglichkeit, in deinem Labor meine Doktorarbeit anfertigen zu dürfen und im Rahmen dessen so viele Teilprojekte auf die Beine zu stellen. Auch für die Möglichkeit, viele Konferenzen zu besuchen und zwei Jahre in Folge iGEM zu machen will ich mich herzlich bedanken. Dank dir bin ich eine selbstständige Wissenschaftlerin geworden – Du hattest immer ein offenes Ohr, und durch deine lockere Art war die Arbeitsatmosphäre auch super angenehm. Ich denke, ich hätte es nicht besser treffen können!

Weiterhin danke ich Julia Frunzke für die Zweitbetreuung meiner Arbeit, und das damit einhergehende Interesse.

Rainer, ohne dich wäre ich vermutlich nie dazu gekommen den Coil zu hacken. Ich danke dir für deinen Enthusiasmus und dein bodenloses Fachwissen während unserer zahlreichen Diskussionen, und dafür, dass du mit uns am Ball geblieben bist.

Ich danke außerdem unseren Kooperationspartnern - Philipp Westhoff, Paul Hudson, Lun Yao, David Brandt, Tobias Busche, Jörg Kalinowski, und Oliver Ebenhöf – ganz herzlich für die hervorragende Zusammenarbeit und die tollen Publikationen, die dadurch entstanden sind.

Dennis, für deine Mentorenschaft möchte ich mich ganz herzlich bedanken. Nicht nur während der Masterarbeit, sondern weit darüber hinaus, hattest du immer ein offenes Ohr für Fragen zu Cyanos oder RNA oder Terpenen. Es war mir eine Freude mit dir zusammenzuarbeiten.

Herr Grützmacher, dank Ihnen bin ich überhaupt erst auf die Idee gekommen, Biologie zu studieren. Vielen Dank, dass Sie mich gefordert und gefördert haben.

I would like to thank Danny Ducat and Beronda Montgomery for introducing me to the fabulous world of cyanobacteria. Your excellent guidance has contributed substantially to the fact that I am where I am today.

Eric Young and Josh MacCready, thank you both so much for supervising me at MSU. I had the best time, and learned to really love the lab during my stay with you.

Ein herzliches Dankeschön gebührt auch den zahlreichen Studierenden, die ich während des Doktors (mit-)betreuen durfte. Trevor, Michelle, Miriam, Pia, Daniela, Wandana und Kai – eure harte Arbeit spiegelt sich auch in dieser wider. Vielen Dank euch allen für eine tolle Zusammenarbeit und eure Unterstützung.

Vielen Dank natürlich an die gesamte AG Axmann 2015 – 2022 für das beste Arbeitsklima und die schöne Zeit mit zahlreichen Kuchen und Grillabenden. Ich werde euch vermissen! Ich danke der iGEM 2019 Truppe, besonders Katharina und Melanie, für das coole Projekt, die Nachtschichten, und die unvergessliche Zeit in Boston.

Kai und Max, für viele Spiel- und Quatschabende und die frühmorgendlichen Deeptalks, vor allem während der Lockdowns, danke ich euch von Herzen.

Vielen Dank an die achtarmigen Orgler, Nik, Lutz, Nic und Max für viele köstliche Feierabendbiere und das beste Doktorandenbüro.

Ein besonderer Dank geht an dich, Kai, für deine langjährige Freundschaft und viel Spaß und Schabernack mit und ohne Gewandung.

Natürlich danke ich auch meiner Familie, für die Unterstützung und Ermutigung über die Jahre.

Zu guter Letzt danke ich Max. Vielen Dank für die vielen Nacht- und Wochenendschichten die du mir versüßt hast, und für deine Gesellschaft während des gesamten Doktors, der ohne dich sterbenslangweilig gewesen wäre. Ich mag die Idee von dir!